# Enteric glial reactivity in intestinal inflammation and colorectal cancer

Doctoral thesis

to obtain a doctorate (PhD)

from the Faculty of Medicine

of the University of Bonn

**Linda Schneider**

from Kirchen, Germany

2025

Written with authorization of

the Faculty of Medicine of the University of Bonn

First reviewer: Prof. Dr. rer. nat. Sven Wehner

Second reviewer: Prof. Dr. med. Nicolas Schlegel

Day of oral examination: May 20, 2025

From the Clinic and Policlinic for general, visceral, thoracic and vascular surgery

## Table of content

**List of abbreviations** ..... **5**

**Animal testing applications and ethics proposal** ..... **9**

**1. Abstract** ..... **10**

**2. Introduction** ..... **12**

2.1 Enteric glial cells ..... 12

2.1.1 Models to study enteric glial cell biology ..... 13

2.2 Extracellular matrix ..... 13

2.3 Immune-driven intestinal disorders and diseases ..... 15

2.3.1 Acute intestinal inflammation ..... 15

2.3.2 Chronic intestinal inflammation ..... 16

2.3.3 Colorectal cancer ..... 17

2.4 Molecular mechanisms of EGC reactivity in intestinal inflammation and CRC 19

2.5 Intercellular communication of EGCs and immune cells in intestinal inflammation and CRC ..... 20

2.6 Aim of the study ..... 22

2.7 References ..... 24

**3. Publications** ..... **38**

3.1 Publication 1: Schneider L, et al. 2024 - Extracellular matrix substrates differentially influence enteric glial cell homeostasis and immune reactivity ..... 38

3.2 Publication 2: Leven P and Schneider R, et al. 2023 – β-adrenergic signaling triggers enteric glial reactivity and acute enteric gliosis during surgery ..... 54

3.3 Publication 3: Schneider R, et al. 2022 – IL-1-dependent enteric gliosis guides intestinal inflammation and dysmotility and modulates macrophage function ..... 77

3.4 Publication 4: van Baarle L, De Simone V, Schneider L, et al. 2024 – IL-1R signaling drives enteric glia-macrophage interactions in colorectal cancer ..... 93

**4. Discussion** ..... **115**

4.1 Activation of EGCs in acute intestinal inflammation ..... 115

4.2 Potential interactions of different glial activators in the inflammatory environment ..... 119

4.3 IL-1-mediated, tumor-promoting signaling cascade between EGCs and macrophages in colorectal cancer ..... 120

4.4 Clinical translation and potential therapeutic targets ..... 122

4.5 Overall impact ..... 124

4.6 References ..... 126
**5. Acknowledgements ..... 137**
**6. Publications and conference contributions ..... 139**

## List of abbreviations

| | |
|---|---|
| 3’ | 3-prime |
| 6-OHDA | 6-Hydroxydopamine |
| AAV | Adeno-associated virus |
| AKPT | villinCre$^{ER}$ Apc$^{fl/fl}$ Kras$^{G12D/+}$ Trp53$^{fl/fl}$ TrgfbrI$^{fl/fl}$ |
| ANNA1 | Antineuronal nuclear antibody-type 1 |
| ANOVA | Analysis of variances |
| AOM | Azoxymethane |
| AR | Adrenergic receptors |
| ARG1 | Arginase 1 |
| αSMA | alpha-smooth muscle actin |
| ATP | Adenosine triphosphate |
| BM | Bone marrow |
| BMDM | Bone marrow-derived macrophages |
| C1Q | Complement component 1q |
| CAC | Colitis-associated cancer |
| CaCl2 | Calcium chloride |
| CCL | C-C motif chemokine ligand |
| CCR | C-C chemokine receptor type 2 |
| CD | Cluster of differentiation |
| CM | Conditioned medium |
| CMS | Consensus molecular subtype |
| CNS | Central nervous system |
| COAD | Colon adenocarcinoma |
| CRC | Colorectal cancer |
| Cre | Cre recombinase |
| CSF-1 | Colony stimulating factor 1 |
| Cx43 | Connexin-43 |
| CXCL | C-X-C motif chemokine ligand |
| ddH2O | Double-distilled water |
| DEG | Differentially expressed genes |
| DMEM | Dulbecco’s modified Eagle’s medium |
| DSS | Dextran sodium salt |
| DT | Diphtheria toxin |
| DTT | Dithiothreitol |
| ECM | Extracellular matrix |
| EDTA | Ethylenediaminetetraacetic acid |
| EGCs | Enteric glial cells |
| EGF | Epidermal growth factor |
| ELISA | Enzyme-linked immunosorbent assay |
| ENS | Enteric nervous system |

| | |
|---|---|
| FACS | Fluorescence-activated cell sorting |
| FBS | Fetal bovine serum |
| FDR | False discovery rate |
| FFPE | Formalin-fixed paraffin-embedded |
| FGF | Fibroblast growth factor |
| GC | Geometric center |
| GDNF | Glial-derived neurotrophic factor |
| GEO | Gene Expression Omnibus |
| GFAP | Glial fibrillary acidic protein |
| GI | Gastrointestinal |
| GIT | Gastrointestinal transit |
| GO | Gene ontology |
| GPCR | G-protein-coupled receptor |
| HA | Hemagglutinin |
| HBSS | Hanks' balanced salt solution |
| HCl | Hydrochloric acid |
| H-CM | Healthy conditioned medium |
| IBA1 | Ionized calcium-binding adapter molecule 1 |
| IBD | Inflammatory bowel disease |
| i.c. | Intracolonic |
| IFNγ | Interferon-gamma |
| IL | Interleukin |
| IL-1R1 | Interleukin-1 receptor type 1 |
| IM | Intestinal manipulation |
| IOC | Intestinal organotypic culture |
| i.p. | Intraperitoneal |
| JellyOP | Jellyfish opsin |
| KCl | Potassium chloride |
| KI67 | Kiel 67 |
| Lap | Laparotomy |
| LCN2 | Lipocalin 2 |
| LPS | Lipopolysaccharide |
| MAP2 | Microtubule-associated protein 2 |
| M-CSF | Macrophage colony-stimulating factor |
| ME | Muscularis externa |
| ME-Macs | Muscularis externa macrophages |
| MgCl2 | Magnesium chloride |
| Min | Minute |
| MPO | Myeloperoxidase |
| mRNA | Messenger ribonucleic acid |
| NaCl | Sodium chloride |

| | |
|---|---|
| NaHCO3 | Sodium hydrogen carbonate |
| NaH2PO4 | Sodium dihydrogen phosphate |
| NB | Neurobasal |
| NE | Norepinephrine |
| ON | Overnight |
| OS | Overall survival |
| P2X2 | purinergic subtype X2 receptors |
| PBS | Phosphate buffered saline |
| PC | Principal component |
| PCA | Principal component analysis |
| PLO | Poly-L-ornithine |
| PLP1 | Proteolipid protein 1 |
| POI | Postoperative ileus |
| PSD95 | Postsynaptic density protein 95 |
| QC | Quality control |
| qPCR | Quantitative polymerase chain reaction |
| READ | Rectum adenocarcinoma |
| *Ribotag* | HA-tagged Rpl22 subunit of the ribosome |
| RNA | Ribonucleic acid |
| Rpl | Large subunit ribosomal protein |
| rpm | Revolutions per minute |
| RT | Room temperature |
| S100B | S100 calcium-binding protein B |
| scRNAseq | Single-cell RNA sequencing |
| SEM | Standard error of the mean |
| Seq | Sequencing |
| SNS | Sympathetic nervous system |
| SOX10 | SRY-box transcription factor 10 |
| SPP1 | Secreted phosphoprotein 1 |
| STX | Sympathectomy |
| SYN | Synapsin |
| TAMs | Tumor-associated macrophages |
| TCGA | The Cancer Genome Atlas |
| TH | Tyrosine hydroxylase |
| TIMP1 | Tissue inhibitor of metalloproteinases 1 |
| TME | Tumor microenvironment |
| TME-CM | Tumor microenvironment conditioned medium |
| TNBS | 2,4,6-trinitrobenzene sulfonic acid |
| TNFα | Tumor necrosis factor-alpha |
| TNM | Tumor, node, metastasis |
| TUBB3 | β3-tubulin |

| | |
|---|---|
| WGCNA | Weighted gene correlation network analysis |
| WNT | Wingless-related integration site |
| WT | Wild-type |

## Animal testing applications and ethics proposal

Animal experiments performed at the University Hospital Bonn were carried out under German federal law and approved by the appropriate authorities of North-Rhine Westphalia, Germany, under the following file numbers: 81-02.04.2021.A424, 81-02.04.2016.A367, 81-02-04-02018.A221, and 84-02.04.2017.A114.

Collection of samples from surgical patient material at the University Hospital Bonn was approval by the ethics committee of North-Rhine-Westphalia, Germany: Accession number 266_14.

## 1. Abstract

Enteric glial cells (EGCs) are important regulators of gastrointestinal functions in health and disease. Over the last few years, their role in intestinal inflammation and their interplay with the local tissue microenvironment has raised increasing attention. As EGCs can react to various environmental stimuli, such as cytokines and chemokines, and contribute to the inflammatory milieu, it is critical to understand the signaling pathways inducing their reactive phenotype and the resulting actions on their tissue microenvironment. Using primary EGC cultures and glial-specific genetic modifications, we revealed specialized extracellular matrix compositions, the sympathetic nervous system, and interleukin (IL)-1 as important regulators of EGCs' immune functions. Applying brightfield and immunofluorescent imaging and RNA-sequencing, we demonstrated distinct effects of extracellular matrix substrates on EGC primary cultures, pinpointing Matrigel and laminin as superior coating substrates in EGC purity, network formation, and reactivity. Postoperative RNA sequencing results expanded our knowledge about EGC reactivity by identifying the sympathetic nervous system as an early EGC activator during acute intestinal inflammation. Using EGC cultures, we discovered norepinephrine signaling via β-1/2-adrenergic receptors as a responsible inducer of immediate postoperative glial reactivity. Moreover, we used a targeted approach to analyze the effect of the well-known and strong immune activator IL-1 on glial-specific reactivity in acute postoperative intestinal inflammation. Strikingly, glial activation via IL-1 led to increased expression of genes related to 'enteric gliosis' both *in vitro* and in intestinal inflammatory models *in vivo*. Furthermore, glial reactivity correlated with macrophage activation and migration, highlighting EGCs' contribution to the inflammatory microenvironment. Finally, we transferred the insights gained from the acute postoperative intestinal inflammation studies into the field of tumor immunology, representing a chronic inflammatory condition as it occurs in colorectal cancer (CRC). Applying three murine CRC models, including EGC-specific molecular reporters and gene deficiencies, we identified a bidirectional signaling cascade between EGCs and tumor-promoting macrophages in CRC, leading to cancer progression. Unraveling the molecular pathways involved, monocyte-derived IL-1 was identified as an EGC activator via glial IL-1 receptor 1 signaling, triggering the secretion of IL-6 into the tumor microenvironment, which promotes the differentiation of infiltrating monocytes into tumor-promoting $SPP1^{+}$ macrophages.

Together, we highlighted the significance of EGCs in intestinal inflammatory diseases. Identifying the extracellular matrix, the sympathetic nervous system, and IL-1 as crucial regulators of glial biology and immune reactivity, we substantiated our understanding of the molecular pathways involved in EGCs' reactive phenotype. Importantly, IL-1-mediated glial activation was proven essential for glia-macrophage interactions in intestinal inflammation and CRC, underlining EGCs' vital role as immune regulators actively modifying disease outcomes in inflammation-driven intestinal diseases and disorders.

# 2. Introduction

## 2.1 Enteric glial cells

The enteric nervous system (ENS), our so-called “second brain” [1], is part of the peripheral nervous system that autonomously regulates gastrointestinal functions. In the ENS, neurons and glia lay in close proximity to each other [2] and fulfill various roles based on their location, such as regulating muscle contractility, secretion, blood flow, or immune responses [3]. The uniqueness of the ENS originates not only from its widespread functions but also from its size, which is unmatched in the peripheral nervous system [3]. The human ENS has been estimated to consist of ~170 million neurons [4] and up to five times as many glia, dependent on the location [3, 5]. In humans and many other species, enteric glial cells (EGCs) have been shown to outnumber enteric neurons, highlighting their prominence in the ENS [5–7]. Although the interest in EGCs has increased over the last decades, their role in health and disease is still not fully understood.

EGCs are distributed throughout all layers of the gut and either accumulate around enteric neurons in two interconnected plexuses, the myenteric plexus and the submucosal plexus, or around neuronal processes in the muscle and mucosa [8]. They can be divided into subsets based on morphological, regional, and transcriptional characteristics [9–11]. The most common markers used to identify EGCs are SRY-box transcription factor 10 (SOX10) [12], glial fibrillary acidic protein (GFAP) [13], S100 calcium-binding protein B (S100B) [14], and proteolipid protein 1 (PLP1) [15]. However, not all glial subsets express every marker, and their expression levels differ between subsets, with typically four EGC subsets based on morphological and regional properties [9, 16–18]. Additionally, transcriptional data derived from single-cell RNA-sequencing studies postulated new distinctions with up to nine EGC subsets [16–18]. Although it remains open if these transcriptionally different populations come indeed along with heterogeneous functionality, these data at least suggest the potential existence of functionally distinct EGC populations with different reactivity, particularly under inflammatory conditions.

The molecules interfacing with EGCs, such as extracellular matrices, neurotransmitters, cytokines, and chemokines, vary constantly, thereby defining specific tissue microenvironments. These molecular compositions do not only change based on regional

cues during homeostasis but also, importantly, during diseases, where EGCs are important players in regulating inflammatory responses [8]. Being able to sense and respond to such changes during inflammation, i.e., by releasing immune-modulatory mediators themselves, EGCs, together with their targeted cells, actively shape the inflammatory microenvironment and inflammation [8, 19].

### 2.1.1 Models to study enteric glial cell biology

In order to study specific molecular responses of EGCs in homeostasis and disease, several *in vitro* and *in vivo* models have been established. The role of individual molecules or signaling pathways is often investigated *in vivo* by cell-specific genetic modifications achieved by Cre-loxP mice [20]. For EGCs, the common markers SOX10, GFAP, S100B, and PLP1 are often used as genetic drivers of the Cre recombinase, together with loxP sites flanking the molecular targets, resulting in glial-specific reporters or knockouts of the genes of interest. These models have proven valuable, particularly in analyzing the effects of EGCs on their surrounding cells, such as intestinal stem cells [21], B- and T-lymphocyte activation [22], macrophage phenotypes [23], or their communication with neurons [24]. However, prior to testing specific molecular interactions *in vivo*, the first evidence is often collected by *in vitro* assays using cell lines or primary cells. For EGCs, cell lines are very limited, with only a few, such as CRL-2690 [25] or CIK [26] available. Therefore, most *in vitro* studies utilize primary EGC cultures isolated from intestinal tissue, allowing the treatment of those cultures with individual molecules or other cells. Additional transgenic modifications of primary EGCs, i.e., by AAVs [27] or lentiviruses [28], help to unravel glial-specific responses. Thereby, EGC cultures have proven to be an important model for cell-cell, cell-compound, and specific molecular interactions [18, 29].

Consequently, several EGC models, with glial-specific reporter and knockout mouse lines, and *in vitro* studies were included in this thesis.

## 2.2 Extracellular matrix

As EGCs are distributed throughout all layers of the intestine, they will likely receive different inputs from the various tissue microenvironments. Besides intercellular interactions between EGCs and other cells, another important part of their surrounding is

the dynamic extracellular matrix (ECM), which might also impact EGC biology. The intestinal ECM is a complex network of proteins that provides structure, participates in barrier function, and interacts with resident cells [30]. The ECM comprises more than 300 proteins, including collagens, laminins, elastins, and fibronectins [31], and can be divided into two main parts: the basement membrane and the interstitial matrix, based on location and ECM composition. The basement membrane is located directly underneath the epithelial layer. It is composed of non-fibrillary collagens, perlecans, laminins, and nidogens. In contrast, the interstitial matrix is located in the underlying connective tissue and the lamina propria [30] and contains fibrillary collagens, elastins, fibronectins, and proteoglycans [32]. Being highly variable and carefully orchestrated along the crypt-villus axis [33], the ECM is at a constant interplay between homeostasis, ECM-cell interactions, and remodeling for tissue regeneration [32]. Being able to interact with resident cells, ECM compounds have also gained rising interest in the context of intestinal diseases, including inflammation [34] and cancer [35–37]. For instance, in colorectal cancer (CRC), the ECM changes in composition and amount, modifying tumor progression and metastasis [38].

With regard to the ENS, ECM compounds were described to affect ENS development [39]. Also, for intestinal macrophages, which are in close spatial proximity to ENS cells [40], ECM influences on monocyte-to-macrophage differentiation [41] and macrophage phenotypes [42] have been described previously. However, for EGCs, the effect of specific ECM compounds *in vitro* is almost unexplored. Although EGC primary cultures are widely used, there is a broad range of protocols for EGC isolation, media, or coating substrates [29], highlighting the lack of standardization for those cultures. While most of the studies imply ECM compounds as culture substrates, the heterogeneous use of these compounds is substantial and far from standardized. A comparative study previously analyzed the effects of some ECM substrates on neuronal and glial differentiation [43], providing evidence of a direct influence of the ECM on EGC biology *in vitro*. However, a more in-depth characterization of how the various ECM compounds affect primary EGC purity, network formation, and gene expression is missing. Moreover, the potential influence of the ECM on glial reactivity in inflammatory conditions is still unexplored. Therefore, a better understanding of how different ECM substrates affect EGC biology and immune reactivity is needed.

## 2.3 Immune-driven intestinal disorders and diseases

Intestinal inflammation can have several causes, such as infections through viruses, parasites, or bacteria, as well as ischemia, and genetic or environmental factors [44]. However, it can also be an iatrogenic consequence of medical treatment like radiation therapy [45, 46] or surgical trauma [47]. Once the immune reaction and inflammation have been initiated, they are frequently accompanied by acute and chronic clinical symptoms. The acute symptoms range from diarrhea to constipation and include bloody stool, abdominal pain, nausea, vomiting, and fatigue [48–50].

### 2.3.1 Acute intestinal inflammation

Acute intestinal inflammation, including one or more of the abovementioned symptoms, commonly occurs after abdominal surgery. The resulting clinical condition is the so-called postoperative ileus (POI), characterized by temporary motility disturbances reducing the well-being of patients and increasing hospitalization times and, consequently, the medico-economic burden [51, 52]. Despite the consistent improvement of perioperative management and the development of minimal-invasive surgery, POI is still a frequent complication of abdominal surgery. Therefore, unraveling the mechanisms behind acute intestinal inflammation, especially in the early onset, is crucial to finding potential pathways for clinical intervention. To study acute gut inflammation, researchers utilize a mouse model of POI, in which mechanical stimulation (so-called intestinal manipulation (IM)) of the intestine results in reduced gastrointestinal transit, increased infiltration of immune cells, and enhanced levels of proinflammatory cytokines [53, 54]. Over the last decades, several studies have focused on cellular mechanisms in acute intestinal inflammation, identifying important players in its disease course, such as mast cells [55–57], T cells [58], or macrophages [59, 60]. Besides the immune cell populations, the innervation of the gut also plays its part in POI development, as shown by the beneficial effects of parasympathetic activation via vagus nerve stimulation in rodents [61–63] and humans [64]. Similarly, disruption of sympathetic signaling, the counterpart of the parasympathetic nervous system, ameliorates intestinal inflammation [65] and directly induces anti-inflammatory pathways in muscularis macrophage [66]. Additionally, enteric neurons were described as important mediators of macrophage activation in acute intestinal inflammation [67]. Likewise, reactive EGCs were associated with POI progression [68, 69]. However, the exact

mechanism of how EGCs impact the initiation of acute intestinal inflammation, how the ENS changes during inflammation, and how this affects immune cell infiltration is not well understood.

### 2.3.2 Chronic intestinal inflammation

When an acute intestinal inflammation is not properly controlled, it can develop into a chronic form, with recurrent inflammation cycles. Chronic inflammation can have several causes, including but not limited to genetic susceptibility, environmental factors, or altered reactions to the host microbiome [70–72]. The most prominent examples of chronic gut inflammation are inflammatory bowel diseases (IBD), whose etiology is still not fully understood. The two most prominent forms of IBD are Crohn's disease and ulcerative colitis [73]. Although both forms come with comparable symptoms, they differ in the affected area, tissue penetration, and pathophysiology, with Crohn's disease affecting any part of the gastrointestinal tract by transmural inflammation, while ulcerative colitis causes inflammation of the mucosal layer only in the colon and rectum [74]. The latter is of particular interest as it is accompanied by a significantly increased risk of CRC development [75]. Mechanistic insights to study whether and how colitis can be prevented or interrupted early during its onset are often gained by murine models [76]. Among those are chemically-induced models, with dextran sodium sulfate (DSS) [76], 2,4,6-trinitrobenzene sulfonic acid (TNBS) [77, 78], or oxazolone [79, 80] being the responsible chemical compounds. Other models utilize adoptive T-cell transfer [81] or genetic interleukin (IL)-10-deficiency [82] to induce experimental colitis in mice [83]. One of the most commonly used models in mice is DSS-induced colitis with DSS administration via drinking water [76, 84]. DSS can be used to study a variety of intestinal inflammatory reactions, as its administration can be adjusted to mimic acute, relapsing, or chronic diseases, such as ulcerative colitis [84]. Several studies utilizing this inflammatory model described the involvement of immune cells, such as macrophages, B cells, T cells [85], enteric neurons [86], and glia [23] in chronic inflammation. Since chronic inflammation is a risk factor for the development of advanced diseases, such as CRC [87], a deeper understanding of the disease course will benefit patients in the context of IBD and beyond.

### 2.3.3 Colorectal cancer

CRC is the third most common type of cancer and the second leading cause of cancer-related deaths worldwide [88]. While new treatment options offer promising 5-year survival rates of up to 90 % for early-stage CRC patients, this number drops drastically to as low as 10 % for patients with advanced or metastatic disease stages [89]. CRC can be distinguished into three subtypes: colitis-associated cancer (CAC), hereditary, and sporadic CRC. While all of them are initiated by single- or multistep mutations, the order of mutational events and the histological tumor manifestation differs [90, 91]. For example, mutations of the oncogene p53 occur early in CAC and late in sporadic CRC, which is reversed for adenomatous polyposis coli (APC) mutations [90]. Moreover, CAC affects middle-aged patients (median age 50 years), while sporadic CRC patients are usually older than 65. Hereditary CRC, on the other hand, can be diagnosed early in life based on genetic screening. Out of these three, sporadic cancer is the most common one and presents up to 70 % of cases.

Mechanistically, genetic or epigenetic alterations initiate CRC, leading to hyperproliferation of epithelial cells and the formation of benign polyps or adenomas, potentially advancing to malignant tumors [92]. These tumors are divided into stages based on size (T) and expansion within the intestinal wall, spread to nearby lymph nodes (N), and metastasis (M) [93]. Based on this TNM score, tumor cells might encounter distinct surroundings, and their tumor microenvironment (TME) changes. The TME is a dynamic composition of various cell types and their ECM, along with signaling molecules that impact both cancerous and non-malignant cells. Thereby, cancer cells are encompassed by a complex network of stromal fibroblasts [94], resident or tumor-infiltrating immune cells [95, 96], and neuronal cells [97–100]. Notably, tumor epithelial cells were described to use neuronal networks as migratory routes in CRC [97]. As cellular migration or infiltration is often causing inflammation, the inflammatory state of the TME is an important factor in CRC. While intestinal inflammation is already present in CAC before tumor formation [101], it presents a major trigger for tumorigenesis in other CRC subtypes [102]. Based on the inflammatory state, two main groups of tumors can be distinguished: immune-hot and immune-cold tumors. Immune-hot tumors are defined as tumors with a strong inflammatory signature [103], a high degree of infiltrating and cytotoxic T cells determined

by the Immunoscore [104], and checkpoint activation [105]. Due to the vast interactions of cancer and immune cells in these “hot” tumors, they are promising targets for immunotherapy. Conversely, immune-cold tumors, defined by weak immune cell recruitment or even immune evasion, present a challenge in classic immunotherapy [106]. Overall, the heterogeneity of CRC tumors underlines the need for a better understanding of their individual biology and the specific TME.

Over the last few years, a rising number of studies focused on the interaction of different cell types of the TME with tumor cells or between themselves and their impact in shaping specific tumor niches. Several murine models have been established to study these cellular interactions in CRC, including genetic, orthotopic, and chemically-induced disease models. The APC model [107], for instance, is a genetic model applied to induce mutation-driven tumor development in mice, resulting in immune-cold tumors [108]. The APC gene is similarly involved in human diseases such as familial adenomatous polyposis and sporadic cancers [109]. Besides, the colonoscopy-guided orthotopic injection of tumor cells into the colonic wall is a way to generate localized tumors [110]. In this model, the immune status of resulting tumors is dependent on the injected cells, such as MC38 [111] or *villin*Cre$^{ER}$*Apc*$^{fl/fl}$*Kras*$^{G12D/+}$*Trp53*$^{fl/fl}$*Trgfbrl*$^{fl/fl}$ (AKPT)-derived cells [112], resulting in immune-hot [113, 114] or immune-cold [115] tumors, respectively. Another commonly used method of murine CRC induction is the azoxymethane (AOM)/DSS model. Herein, the injection of the carcinogenic drug AOM combined with DSS-induced colonic inflammation provokes tumor development [116]. Due to the DSS-induced local inflammation of the colon, this method causes the development of multiple tumors, specifically in the colon, presenting a valuable model for cancer research. Using these murine models, as well as cell culture models and transcriptional analyses of human and murine data, specific cellular pathways have already been identified [117, 118]. Among them, the interaction of cancer-associated fibroblasts and cancer cells was found to drive cancer invasion [119]. Similarly, tumor-infiltrating monocytes [120] and tumor-associated macrophages [121] contributed to tumor progression. Moreover, spatial analysis has identified a tumor-promoting interaction of cancer-associated fibroblasts and an SPP1$^{+}$ macrophage subset [122].

Interestingly, the enteric neuronal network was also described as being involved in CRC development [123]. Enteric neurons present migratory routes for invasive tumor epithelial

cells [97]. This tumoral invasion along nerves is known as perineural invasion and presents an important aspect in several types of cancer [124, 125]. Moreover, bidirectional signaling between neurons and cancer cells has been observed before, and specific neural circuits have been proposed for cancer treatment [126]. As glial cells are in close proximity to enteric neurons [2], are already recognized as key regulators in intestinal inflammation [19], and are part of the CRC TME [127], their contribution to CRC pathophysiology is likely.

### 2.4 Molecular mechanisms of EGC reactivity in intestinal inflammation and CRC

EGCs were known for a long time solely as “neurosupportive” cells. However, they can sense and secrete various signaling molecules, contributing to disease outcomes. In inflammation, they have been described to acquire a so-called “reactive” phenotype, resulting in the secretion of pro- and anti-inflammatory cytokines and chemokines acting on surrounding cell types [128]. Glial-derived immune-modulatory molecules include IL-6 [68, 129], C-C motif chemokine ligand (CCL)-2 [68], C-X-C motif chemokine ligand (CXCL)-10 [130], glial-derived neurotrophic factor (GDNF) [131], nitric oxide [132, 133], and macrophage colony- stimulating factor (M-CSF) [23]. Besides the variety of molecules secreted by reactive EGCs, multiple activators during intestinal inflammatory diseases can induce this phenotypic switch termed ‘enteric gliosis’ [129]. Among them are, for example, lipopolysaccharide (LPS) [134, 135], tumor necrosis factor-alpha (TNFα) [136], extracellular adenosine triphosphate (ATP) [129], or IL-1 [68]. IL-1 presents a strong immune regulator [137]. Several studies have reported IL-1-induced glial activation and the important role of IL-1-activated EGCs in shaping both acute [68, 138] and chronic inflammation [139, 140]. However, their molecular responses contributing to the disease outcomes, as well as their communication with surrounding cell types, need to be better understood.

Besides inflammatory mediators, additional factors shape the intestinal microenvironment. One is the innervation via the sympathetic nervous system (SNS), which regulates gastrointestinal motility in homeostasis and disease. In previous work, our group and others demonstrated the effect of the SNS on macrophage activation in intestinal inflammation [141–143]. The molecular mechanisms that guide SNS-mediated alterations are induced by adrenergic signaling [144], which has been shown to regulate immune cells in a

variety of tissue contexts [145]. For example, adrenergic signaling is involved in maintaining mature natural killer cells in the spleen and bone marrow [146], regulating epithelial proliferation in the intestine [147], or modifying macrophage effector functions upon infection [143] and inflammation [148]. Interestingly, the SNS has been demonstrated to have both proinflammatory and anti-inflammatory effects in arthritis dependent on the disease phase [149], and a similar time-dependent SNS dichotomy was suggested for intestinal inflammation [144]. Importantly, EGCs express adrenergic receptors [150] and can be affected by the SNS, too [151], but so far, little is known about SNS-EGC interactions in intestinal inflammation. Therefore, it is important to address the time-dependent inflammatory reactions in the intestine, with SNS-mediated glial reactivity and glia-macrophage interactions presenting potential regulators.

Furthermore, EGC reactivity has recently been suggested to be involved in CRC, acting pro-tumorigenic [127, 152]. The central role of EGCs in CRC was first evident when Yuan *et al.* showed that glial cell depletion in a CRC mouse model leads to reduced tumor burden [152]. Another study, utilizing *in vitro* cultures and supernatant transfer assays, suggested a bidirectional communication of EGCs with the CRC TME, also implying IL-1 as a potentially important factor for EGC reactivity in CRC [127], similar to acute [68, 138] and chronic inflammation [139, 140]. However, despite these findings highlighting a certain role of EGCs in CRC, there is still a substantial knowledge gap on EGC-CRC TME interactions and the molecular mechanisms involved.

## 2.5 Intercellular communication of EGCs and immune cells in intestinal inflammation and CRC

As a consequence of their reactivity, EGCs release signaling cues for different cell types within the intestine. Besides neurons [153], this also includes intestinal epithelial cells [154], for which EGCs provide WNT ligands, thereby supporting the renewal of the epithelial barrier [21]. Also enteroendocrine cells [155] and immune cells, such as T cells or macrophages [18]

are affected by reactive EGCs. Interactions between EGCs and macrophages were first described in models of acute intestinal inflammation [23, 138]. While Stakenborg *et al.*

uncovered that glial colony stimulating factor-1 (CSF-1) release induces anti-inflammatory macrophage polarization [138], others demonstrated the opposite effect and a proinflammatory phenotype [23]. Interestingly, in the latter study, IL-1β was utilized as the inflammatory trigger for EGCs [23], the first evidence for the interaction of IL-1β-activated EGCs and macrophages in intestinal inflammation. However, in-depth analyses are needed to decipher the intercellular communication between IL-1β-activated EGCs and macrophages and their effects on the inflammatory environment.

The interaction of glial cells and macrophages might be a conserved mechanism in inflammatory diseases, as it is also shown to play a role in different cancer types, previously described for pancreatic ductal adenocarcinoma [156] and lung cancer [157]. However, EGC-macrophage crosstalk in CRC remains undescribed. Nevertheless, EGCs have recently come into focus as crucial players in CRC tumor development [127, 152]. Similarly, tumor-associated macrophages (TAMs) are known as important mediators in the CRC TME and fulfill tumor-promoting functions [121, 158, 159]. Specifically, an $SPP1^{+}$ subtype of TAMs was associated with CRC initiation and progression [160] and was already described in other TME interactions [122, 161]. As both EGCs and macrophages have individually been recognized as key players in CRC, a more in-depth analysis of their potential interactions is needed.

## 2.6 Aim of the study

EGCs, as a major part of the ENS, have been shown to acquire a reactive state during intestinal inflammation. However, the molecular pathways and triggers of EGC activation, the acquired immune modulatory phenotype, and the intercellular communication between reactive EGCs and macrophages are still poorly defined. Given the complexity of intestinal inflammation, I selected specific aspects that, in my view, are important to contribute to a better understanding of EGC biology in inflammation and chose two clinically-relevant disorders to approach these.

Therefore, my PhD thesis addressed the following aims:

**Aim 1:** To specify the effect of different ECM substrates on glial biology and immune reactivity [162].

**Aim 2:** To decipher glial reactivity in the course of acute intestinal inflammation with an unbiased, longitudinal approach [27].

**Aim 3:** To analyze the effect of IL-1, a major cytokine in intestinal inflammation, on EGC reactivity targeting glial IL-1 receptor 1 (IL-1R1) in acute intestinal inflammation [163].

**Aim 4:** To identify the role of glial-IL-1R1 signaling and their interaction with macrophages in CRC [164].

To address **aim 1**, I studied the effect of different ECM substrates on EGC purity, network formation and immune reactivity in EGC primary cultures [162]. Additionally, for **aim 2**, we deciphered EGC reactivity along the course of acute intestinal inflammation in an unbiased approach, identifying adrenergic signaling [27] as an early EGC activator. In **aim 3**, targeting glial-IL-1R1 in intestinal inflammation *in vitro* and *in vivo*, we verified its induction of the EGC phenotypic switch towards a reactive glial cell [163]. In the latter study, we found IL-1R1-induced glial reactivity and glia-macrophage interactions as important signaling pathways in intestinal inflammation [163]. Due to their close spatial association along the intestine and throughout all bowel layers, EGCs and macrophages might also interact in other intestinal inflammatory diseases. Therefore, we proposed a conserved disease-overarching role of glia-macrophage communication that might also affect intestinal tumor immunology in inflammation-triggered CRC. Consequently, we expanded

our knowledge about reactive glia from intestinal inflammation to CRC in **aim 4**, focusing on glial-specific IL-1R1 signaling and their interaction with immune cells in CRC mouse models [164].

Overall, my PhD thesis aimed to refine EGC biology in intestinal inflammation-driven diseases. Herein, I optimized glial cell culture conditions to facilitate standardization and transfer of EGC studies in the future. Moreover, I advanced the knowledge about the molecular pathways of glial reactivity in acute intestinal inflammation and transferred them to the chronic disease CRC, ultimately identifying a complex signaling cascade that drives cancer progression. The findings of these studies yield valuable insights into the molecular mechanisms driving glia-macrophage interactions and provide potential targets for clinical interventions and diagnostics.

## 2.7 References


1. News & Highlights. *Mucosal Immunol*, 2008; 1:328–329. doi:10.1038/mi.2008.25
2. Boesmans W, Martens MA, Weltens N, Hao MM, Tack J, Cirillo C, et al. Imaging neuron-glia interactions in the enteric nervous system. *Front Cell Neurosci*, 2013; 7:183. doi:10.3389/fncel.2013.00183
3. Sharkey KA, Mawe GM. The enteric nervous system. *Physiol Rev*, 2023; 103:1487–1564. doi:10.1152/physrev.00018.2022
4. Michel K, Kuch B, Dengler S, Demir IE, Zeller F, Schemann M. How big is the little brain in the gut? Neuronal numbers in the enteric nervous system of mice, Guinea pig, and human. *Neurogastroenterol Motil*, 2022; 34:e14440. doi:10.1111/nmo.14440
5. Hoff S, Zeller F, Weyhern CW von, Wegner M, Schemann M, Michel K, et al. Quantitative assessment of glial cells in the human and guinea pig enteric nervous system with an anti-Sox8/9/10 antibody. *J Comp Neurol*, 2008; 509:356–371. doi:10.1002/cne.21769
6. Grubišić V, Gulbransen BD. Enteric glia: the most alimentary of all glia. *J Physiol*, 2017; 595:557–570. doi:10.1113/JP271021
7. Gabella G, Trigg P. Size of neurons and glial cells in the enteric ganglia of mice, guinea-pigs, rabbits and sheep. *J Neurocytol*, 1984; 13:49–71. doi:10.1007/BF01148318
8. Santhosh S, Zanoletti L, Stamp LA, Hao MM, Matteoli G. From diversity to disease: unravelling the role of enteric glial cells. *Front Immunol*, 2024; 15:1408744. doi:10.3389/fimmu.2024.1408744
9. Boesmans W, Lasrado R, Vanden Berghe P, Pachnis V. Heterogeneity and phenotypic plasticity of glial cells in the mammalian enteric nervous system. *Glia*, 2015; 63:229–241. doi:10.1002/glia.22746
10. Zeisel A, Hochgerner H, Lönnerberg P, Johnsson A, Memic F, van der Zwan J, et al. Molecular Architecture of the Mouse Nervous System. *Cell*, 2018; 174:999-1014.e22. doi:10.1016/j.cell.2018.06.021
11. Drokhlyansky E, Smillie CS, van Wittenberghe N, Ericsson M, Griffin GK, Eraslan G, et al. The Human and Mouse Enteric Nervous System at Single-Cell Resolution. *Cell*, 2020; 182:1606-1622.e23. doi:10.1016/j.cell.2020.08.003
12. Young HM, Bergner AJ, Müller T. Acquisition of neuronal and glial markers by neural crest-derived cells in the mouse intestine. *J Comp Neurol*, 2003; 456:1–11. doi:10.1002/cne.10448
13. Jessen KR, Mirsky R. Glial cells in the enteric nervous system contain glial fibrillary acidic protein. *Nature*, 1980; 286:736–737. doi:10.1038/286736a0

14. Ferri GL, Probert L, Cocchia D, Michetti F, Marangos PJ, Polak JM. Evidence for the presence of S-100 protein in the glial component of the human enteric nervous system. *Nature*, 1982; 297:409–410. doi:10.1038/297409a0

15. Rao M, Nelms BD, Dong L, Salinas-Rios V, Rutlin M, Gershon MD, et al. Enteric glia express proteolipid protein 1 and are a transcriptionally unique population of glia in the mammalian nervous system. *Glia*, 2015; 63:2040–2057. doi:10.1002/glia.22876

16. Boesmans W, Nash A, Tasnády KR, Yang W, Stamp LA, Hao MM. Development, Diversity, and Neurogenic Capacity of Enteric Glia. *Front Cell Dev Biol*, 2021; 9:775102. doi:10.3389/fcell.2021.775102

17. Guyer RA, Stavely R, Robertson K, Bhave S, Mueller JL, Picard NM, et al. Single-cell multiome sequencing clarifies enteric glial diversity and identifies an intraganglionic population poised for neurogenesis. *Cell Reports*, 2023; 42:112194. doi:10.1016/j.celrep.2023.112194

18. Seguella L, Gulbransen BD. Enteric glial biology, intercellular signalling and roles in gastrointestinal disease. *Nature reviews. Gastroenterology & hepatology*, 2021; 18:571–587. doi:10.1038/s41575-021-00423-7

19. Le Berre C, Naveilhan P, Rolli-Derkinderen M. Enteric glia at center stage of inflammatory bowel disease. *Neurosci Lett*, 2023; 809:137315. doi:10.1016/j.neulet.2023.137315

20. Kim H, Kim M, Im S-K, Fang S. Mouse Cre-LoxP system: general principles to determine tissue-specific roles of target genes. *Lab Anim Res*, 2018; 34:147–159. doi:10.5625/lar.2018.34.4.147

21. Baghdadi MB, Ayyaz A, Coquenlorge S, Chu B, Kumar S, Streutker C, et al. Enteric glial cell heterogeneity regulates intestinal stem cell niches. *Cell Stem Cell*, 2022; 29:86-100.e6. doi:10.1016/j.stem.2021.10.004

22. Chow AK, Grubišić V, Gulbransen BD. Enteric Glia Regulate Lymphocyte Activation via Autophagy-Mediated MHC-II Expression. *Cell Mol Gastroenterol Hepatol*, 2021; 12:1215–1237. doi:10.1016/j.jcmgh.2021.06.008

23. Grubišić V, McClain JL, Fried DE, Grants I, Rajasekhar P, Csizmadia E, et al. Enteric Glia Modulate Macrophage Phenotype and Visceral Sensitivity following Inflammation. *Cell Reports*, 2020; 32:108100. doi:10.1016/j.celrep.2020.108100

24. Ahmadzai MM, Seguella L, Gulbransen BD. Circuit-specific enteric glia regulate intestinal motor neurocircuits. *Proc Natl Acad Sci U S A*, 2021; 118. doi:10.1073/pnas.2025938118

25. Rühl A, Trotter J, Stremmel W. Isolation of enteric glia and establishment of transformed enteroglial cell lines from the myenteric plexus of adult rat. *Neurogastroenterol Motil*, 2001; 13:95–106. doi:10.1046/j.1365-2982.2001.00246.x

26. Zanoletti L, Valdata A, Nehlsen K, Faris P, Casali C, Cacciatore R, et al. Cytological, molecular, cytogenetic, and physiological characterization of a novel immortalized

human enteric glial cell line. *Front Cell Neurosci*, 2023; 17:1170309. doi:10.3389/fncel.2023.1170309

27. Leven P, Schneider R, Schneider L, Mallesh S, Vanden Berghe P, Sasse P, et al. β-adrenergic signaling triggers enteric glial reactivity and acute enteric gliosis during surgery. *J Neuroinflammation*, 2023; 20:255. doi:10.1186/s12974-023-02937-0
28. Laddach A, Chng SH, Lasrado R, Progatzky F, Shapiro M, Erickson A, et al. A branching model of lineage differentiation underpinning the neurogenic potential of enteric glia. *Nat Commun*, 2023; 14:5904. doi:10.1038/s41467-023-41492-3
29. Schonkeren SL, Küthe TT, Idris M, Bon-Frauches AC, Boesmans W, Melotte V. The gut brain in a dish: Murine primary enteric nervous system cell cultures. *Neurogastroenterology Motil*, 2022; 34:e14215. doi:10.1111/nmo.14215
30. Pompili S, Latella G, Gaudio E, Sferra R, Vetuschi A. The Charming World of the Extracellular Matrix: A Dynamic and Protective Network of the Intestinal Wall. *Front Med (Lausanne)*, 2021; 8:610189. doi:10.3389/fmed.2021.610189
31. Hynes RO, Naba A. Overview of the matrisome--an inventory of extracellular matrix constituents and functions. *Cold Spring Harb Perspect Biol*, 2012; 4:a004903. doi:10.1101/cshperspect.a004903
32. Vilardi A, Przyborski S, Mobbs C, Rufini A, Tufarelli C. Current understanding of the interplay between extracellular matrix remodelling and gut permeability in health and disease. *Cell Death Discov*, 2024; 10:258. doi:10.1038/s41420-024-02015-1
33. Rezakhani S, Gjorevski N, Lutolf MP. Extracellular matrix requirements for gastrointestinal organoid cultures. *Biomaterials*, 2021; 276:121020. doi:10.1016/j.biomaterials.2021.121020
34. Vetuschi A, Pompili S, Gaudio E, Latella G, Sferra R. PPAR-γ with its anti-inflammatory and anti-fibrotic action could be an effective therapeutic target in IBD. *Eur Rev Med Pharmacol Sci*, 2018; 22:8839–8848. doi:10.26355/eurrev_201812_16652
35. Crotti S, Piccoli M, Rizzolio F, Giordano A, Nitti D, Agostini M. Extracellular Matrix and Colorectal Cancer: How Surrounding Microenvironment Affects Cancer Cell Behavior? *J Cell Physiol*, 2017; 232:967–975. doi:10.1002/jcp.25658
36. Henke E, Nandigama R, Ergün S. Extracellular Matrix in the Tumor Microenvironment and Its Impact on Cancer Therapy. *Front Mol Biosci*, 2019; 6:160. doi:10.3389/fmolb.2019.00160
37. Kai F, Drain AP, Weaver VM. The Extracellular Matrix Modulates the Metastatic Journey. *Dev Cell*, 2019; 49:332–346. doi:10.1016/j.devcel.2019.03.026
38. Karlsson S, Nyström H. The extracellular matrix in colorectal cancer and its metastatic settling - Alterations and biological implications. *Crit Rev Oncol Hematol*, 2022; 175:103712. doi:10.1016/j.critrevonc.2022.103712

39. Gazquez E, Watanabe Y, Broders-Bondon F, Paul-Gilloteaux P, Heysch J, Baral V, et al. Endothelin-3 stimulates cell adhesion and cooperates with β1-integrins during enteric nervous system ontogenesis. *Sci Rep*, 2016; 6:37877. doi:10.1038/srep37877

40. Muller PA, Koscsó B, Rajani GM, Stevanovic K, Berres M-L, Hashimoto D, et al. Crosstalk between muscularis macrophages and enteric neurons regulates gastrointestinal motility. *Cell*, 2014; 158:300–313. doi:10.1016/j.cell.2014.04.050

41. Li L, Song J, Chuquisana O, Hannocks M-J, Loismann S, Vogl T, et al. Endothelial Basement Membrane Laminins as an Environmental Cue in Monocyte Differentiation to Macrophages. *Front Immunol*, 2020; 11:584229. doi:10.3389/fimmu.2020.584229

42. Jha A, Moore E. Laminin-derived peptide, IKVAV, modulates macrophage phenotype through integrin mediation. *Matrix Biol Plus*, 2024; 22:100143. doi:10.1016/j.mbplus.2024.100143

43. Veríssimo CP, Da Carvalho JS, da Silva FJ, Campanati L, Moura-Neto V, Coelho-Aguiar Jd. Laminin and Environmental Cues Act in the Inhibition of the Neuronal Differentiation of Enteric Glia in vitro. *Front Neurosci*, 2019; 13:914. doi:10.3389/fnins.2019.00914

44. Wehkamp J, Götz M, Herrlinger K, Steurer W, Stange EF. Inflammatory Bowel Disease. *Dtsch Arztebl Int*, 2016; 113:72–82. doi:10.3238/arztebl.2016.0072

45. Dilauro S, Crum-Cianflone NF. Ileitis: when it is not Crohn's disease. *Curr Gastroenterol Rep*, 2010; 12:249–258. doi:10.1007/s11894-010-0112-5

46. Jessurun J. The Differential Diagnosis of Acute Colitis: Clues to a Specific Diagnosis. *Surg Pathol Clin*, 2017; 10:863–885. doi:10.1016/j.path.2017.07.008

47. Sido B, Teklote J-R, Hartel M, Friess H, Büchler MW. Inflammatory response after abdominal surgery. *Best Pract Res Clin Anaesthesiol*, 2004; 18:439–454. doi:10.1016/j.bpa.2003.12.006

48. Vather R, Trivedi S, Bissett I. Defining Postoperative Ileus: Results of a Systematic Review and Global Survey. *Journal of Gastrointestinal Surgery*, 2013; 17:962–972. doi:10.1007/s11605-013-2148-y

49. Levartovsky A, Ovdat T, Barash Y, Ben-Shatach Z, Skinezes Y, Jesin S, et al. Signs and Symptoms of Acute Bowel Inflammation and the Risk of Progression to Inflammatory Bowel Disease: A Retrospective Analysis. *J Clin Med*, 2022; 11. doi:10.3390/jcm11154595

50. Perler BK, Ungaro R, Baird G, Mallette M, Bright R, Shah S, et al. Presenting symptoms in inflammatory bowel disease: descriptive analysis of a community-based inception cohort. *BMC Gastroenterol*, 2019; 19:47. doi:10.1186/s12876-019-0963-7

51. Wolthuis AM, Bislenghi G, Fieuws S, van Buck Overstraeten A de, Boeckxstaens G, D'Hoore A. Incidence of prolonged postoperative ileus after colorectal surgery: a systematic review and meta-analysis. *Colorectal Disease*, 2016; 18:O1-9. doi:10.1111/codi.13210

52. Asgeirsson T, El-Badawi KI, Mahmood A, Barletta J, Luchtefeld M, Senagore AJ. Postoperative ileus: it costs more than you expect. *Journal of the American College of Surgeons*, 2010; 210:228–231. doi:10.1016/j.jamcollsurg.2009.09.028

53. Kalff JC, Carlos TM, Schraut WH, Billiar TR, Simmons RL, Bauer AJ. Surgically induced leukocytic infiltrates within the rat intestinal muscularis mediate postoperative ileus. *Gastroenterology*, 1999; 117:378–387. doi:10.1053/gast.1999.0029900378

54. Kalff JC, Schraut WH, Simmons RL, Bauer AJ. Surgical Manipulation of the Gut Elicits an Intestinal Muscularis Inflammatory Response Resulting in Postsurgical Ileus. *Annals of Surgery*, 1998; 228:652–663. doi:10.1097/00000658-199811000-00004

55. The FO, Bennink RJ, Ankum WM, Buist MR, Busch OR, Gouma DJ, et al. Intestinal handling-induced mast cell activation and inflammation in human postoperative ileus. *Gut*, 2007; 57:33–40. doi:10.1136/gut.2007.120238

56. Jonge WJ de, The FO, van der Coelen D, Bennink RJ, Reitsma PH, van Deventer SJ, et al. Mast cell degranulation during abdominal surgery initiates postoperative ileus in mice. *Gastroenterology*, 2004; 127:535–545. doi:10.1053/j.gastro.2004.04.017

57. Snoek SA, Dhawan S, van Bree SH, Cailotto C, van Diest SA, Duarte JM, et al. Mast cells trigger epithelial barrier dysfunction, bacterial translocation and postoperative ileus in a mouse model. *Neurogastroenterology Motil*, 2012; 24:172. doi:10.1111/j.1365-2982.2011.01820.x

58. Engel DR, Koscielny A, Wehner S, Maurer J, Schiwon M, Franken L, et al. T helper type 1 memory cells disseminate postoperative ileus over the entire intestinal tract. *Nat Med*, 2010; 16:1407–1413. doi:10.1038/nm.2255

59. Wehner S, Behrendt FF, Lyutenski BN, Lysson M, Bauer AJ, Hirner A, et al. Inhibition of macrophage function prevents intestinal inflammation and postoperative ileus in rodents. *Gut*, 2007; 56:176–185. doi:10.1136/gut.2005.089615

60. Farro G, Stakenborg M, Gomez-Pinilla PJ, Labeeuw E, Goverse G, Di Giovangiulio M, et al. CCR2-dependent monocyte-derived macrophages resolve inflammation and restore gut motility in postoperative ileus. *Gut*, 2017; 66:2098–2109. doi:10.1136/gutjnl-2016-313144

61. Hong G-S, Zillekens A, Schneiker B, Pantelis D, Jonge WJ de, Schaefer N, et al. Non-invasive transcutaneous auricular vagus nerve stimulation prevents postoperative ileus and endotoxemia in mice. *Neurogastroenterology Motil*, 2019; 31. doi:10.1111/nmo.13501

62. Stakenborg N, Wolthuis AM, Gomez-Pinilla PJ, Farro G, Di Giovangiulio M, Bosmans G, et al. Abdominal vagus nerve stimulation as a new therapeutic approach to prevent postoperative ileus. *Neurogastroenterology Motil*, 2017; 29. doi:10.1111/nmo.13075

63. Costes L, van der Vliet J, van Bree S, Boeckxstaens GE, Cailotto C. Endogenous vagal activation dampens intestinal inflammation independently of splenic innervation in postoperative ileus. *Autonomic Neuroscience*, 2014; 185:76–82. doi:10.1016/j.autneu.2014.07.006

64. Chapman SJ, Helliwell JA, Naylor M, Tassinari C, Corrigan N, Jayne DG. Noninvasive vagus nerve stimulation to reduce ileus after major colorectal surgery: early development study. *Colorectal Disease*, 2021; 23:1225–1232. doi:10.1111/codi.15561

65. Fukuda H, Tsuchida D, Koda K, Miyazaki M, Pappas TN, Takahashi T. Inhibition of sympathetic pathways restores postoperative ileus in the upper and lower gastrointestinal tract. *J Gastroenterol Hepatol*, 2007; 22:1293–1299. doi:10.1111/j.1440-1746.2007.04915.x

66. Tsuchida Y, Hatao F, Fujisawa M, Murata T, Kaminishi M, Seto Y, et al. Neuronal stimulation with 5-hydroxytryptamine 4 receptor induces anti-inflammatory actions via 7nACh receptors on muscularis macrophages associated with postoperative ileus. *Gut*, 2011; 60:638–647. doi:10.1136/gut.2010.227546

67. Stakenborg N, Labeeuw E, Gomez-Pinilla PJ, Schepper S de, Aerts R, Goverse G, et al. Preoperative administration of the 5-HT4 receptor agonist prucalopride reduces intestinal inflammation and shortens postoperative ileus via cholinergic enteric neurons. *Gut*, 2019; 68:1406–1416. doi:10.1136/gutjnl-2018-317263

68. Stoffels B, Hupa KJ, Snoek SA, van Bree S, Stein K, Schwandt T, et al. Postoperative ileus involves interleukin-1 receptor signaling in enteric glia. *Gastroenterology*, 2014; 146:176-87.e1. doi:10.1053/j.gastro.2013.09.030

69. Sun A, an Hu, Lin J, Wang L, Xie C, Shi Y, et al. Involvement of iNOS-induced reactive enteric glia cells in gastrointestinal motility disorders of postoperative Ileus mice. *Journal of Chemical Neuroanatomy*, 2023; 133:102312. doi:10.1016/j.jchemneu.2023.102312

70. Guan Q. A Comprehensive Review and Update on the Pathogenesis of Inflammatory Bowel Disease. *J Immunol Res*, 2019; 2019:7247238. doi:10.1155/2019/7247238

71. Rogler G, Vavricka S. Exposome in IBD: recent insights in environmental factors that influence the onset and course of IBD. *Inflamm Bowel Dis*, 2015; 21:400–408. doi:10.1097/MIB.0000000000000229

72. Cleynen I, Boucher G, Jostins L, Schumm LP, Zeissig S, Ahmad T, et al. Inherited determinants of Crohn's disease and ulcerative colitis phenotypes: a genetic association study. *Lancet*, 2016; 387:156–167. doi:10.1016/S0140-6736(15)00465-1

73. Hendrickson BA, Gokhale R, Cho JH. Clinical aspects and pathophysiology of inflammatory bowel disease. *Clin Microbiol Rev*, 2002; 15:79–94. doi:10.1128/CMR.15.1.79-94.2002

74. Muzammil MA, Fariha F, Patel T, Sohail R, Kumar M, Khan E, et al. Advancements in Inflammatory Bowel Disease: A Narrative Review of Diagnostics, Management, Epidemiology, Prevalence, Patient Outcomes, Quality of Life, and Clinical Presentation. *Cureus*, 2023; 15:e41120. doi:10.7759/cureus.41120

75. Olén O, Erichsen R, Sachs MC, Pedersen L, Halfvarson J, Askling J, et al. Colorectal cancer in ulcerative colitis: a Scandinavian population-based cohort study. *Lancet*, 2020; 395:123–131. doi:10.1016/S0140-6736(19)32545-0

76. Okayasu I, Hatakeyama S, Yamada M, Ohkusa T, Inagaki Y, Nakaya R. A novel method in the induction of reliable experimental acute and chronic ulcerative colitis in mice. *Gastroenterology*, 1990; 98:694–702. doi:10.1016/0016-5085(90)90290-h

77. Morris GP, Beck PL, Herridge MS, Depew WT, Szewczuk MR, Wallace JL. Hapten-induced model of chronic inflammation and ulceration in the rat colon. *Gastroenterology*, 1989; 96:795–803.

78. Antoniou E, Margonis GA, Angelou A, Pikouli A, Argiri P, Karavokyros I, et al. The TNBS-induced colitis animal model: An overview. *Ann Med Surg (Lond)*, 2016; 11:9–15. doi:10.1016/j.amsu.2016.07.019

79. Boirivant M, Fuss IJ, Chu A, Strober W. Oxazolone colitis: A murine model of T helper cell type 2 colitis treatable with antibodies to interleukin 4. *J Exp Med*, 1998; 188:1929–1939. doi:10.1084/jem.188.10.1929

80. Meroni E, Stakenborg N, Gomez-Pinilla PJ, Hertogh G de, Goverse G, Matteoli G, et al. Functional characterization of oxazolone-induced colitis and survival improvement by vagus nerve stimulation. *PLoS One*, 2018; 13:e0197487. doi:10.1371/journal.pone.0197487

81. Ostanin DV, Bao J, Koboziev I, Gray L, Robinson-Jackson SA, Kosloski-Davidson M, et al. T cell transfer model of chronic colitis: concepts, considerations, and tricks of the trade. *Am J Physiol Gastrointest Liver Physiol*, 2009; 296:G135-46. doi:10.1152/ajpgi.90462.2008

82. Kühn R, Löhler J, Rennick D, Rajewsky K, Müller W. Interleukin-10-deficient mice develop chronic enterocolitis. *Cell*, 1993; 75:263–274. doi:10.1016/0092-8674(93)80068-p

83. Baydi Z, Limami Y, Khalki L, Zaid N, Naya A, Mtairag EM, et al. An Update of Research Animal Models of Inflammatory Bowel Disease. *ScientificWorldJournal*, 2021; 2021:7479540. doi:10.1155/2021/7479540

84. Chassaing B, Aitken JD, Malleshappa M, Vijay-Kumar M. Dextran sulfate sodium (DSS)-induced colitis in mice. *Curr Protoc Immunol*, 2014; 104:15.25.1-15.25.14. doi:10.1002/0471142735.im1525s104

85. Wiese JJ, Manna S, Kühl AA, Fascì A, Elezkurtaj S, Sonnenberg E, et al. Myenteric Plexus Immune Cell Infiltrations and Neurotransmitter Expression in Crohn's Disease and Ulcerative Colitis. *J Crohns Colitis*, 2024; 18:121–133. doi:10.1093/ecco-jcc/jjad122

86. Margolis KG, Stevanovic K, Karamooz N, Li ZS, Ahuja A, D'Autréaux F, et al. Enteric neuronal density contributes to the severity of intestinal inflammation. *Gastroenterology*, 2011; 141:588-98, 598.e1-2. doi:10.1053/j.gastro.2011.04.047

87. Rutter M, Saunders B, Wilkinson K, Rumbles S, Schofield G, Kamm M, et al. Severity of inflammation is a risk factor for colorectal neoplasia in ulcerative colitis. *Gastroenterology*, 2004; 126:451–459. doi:10.1053/j.gastro.2003.11.010

88. Sung H, Ferlay J, Siegel RL, Laversanne M, Soerjomataram I, Jemal A, et al. Global Cancer Statistics 2020: GLOBOCAN Estimates of Incidence and Mortality Worldwide for 36 Cancers in 185 Countries. *CA: A Cancer Journal for Clinicians*, 2021; 71:209–249. doi:10.3322/caac.21660

89. Rawla P, Sunkara T, Barsouk A. Epidemiology of colorectal cancer: incidence, mortality, survival, and risk factors. *Gastroenterology Review*, 2019; 14:89–103. doi:10.5114/pg.2018.81072

90. Rhodes JM, Campbell BJ. Inflammation and colorectal cancer: IBD-associated and sporadic cancer compared. *Trends Mol Med*, 2002; 8:10–16. doi:10.1016/s1471-4914(01)02194-3

91. Uchino M, Ikeuchi H, Noguchi T, Okabayashi K, Futami K, Tanaka S, et al. Histological differentiation between sporadic and colitis-associated intestinal cancer in a nationwide study: A propensity-score-matched analysis. *J Gastroenterol Hepatol*, 2024; 39:893–901. doi:10.1111/jgh.16496

92. Hossain MS, Karuniawati H, Jairoun AA, Urbi Z, Ooi DJ, John A, et al. Colorectal Cancer: A Review of Carcinogenesis, Global Epidemiology, Current Challenges, Risk Factors, Preventive and Treatment Strategies. *Cancers (Basel)*, 2022; 14. doi:10.3390/cancers14071732

93. Sobin LH, Gospodarowicz MK, Wittekind C, eds. TNM classification of malignant tumours. Chichester: *Wiley-Blackwell*, 2009: 310 p.

94. Sahai E, Astsaturov I, Cukierman E, DeNardo DG, Egeblad M, Evans RM, et al. A framework for advancing our understanding of cancer-associated fibroblasts. *Nature Reviews Cancer*, 2020; 20:174–186. doi:10.1038/s41568-019-0238-1

95. Ye L, Zhang T, Kang Z, Guo G, Sun Y, Lin K, et al. Tumor-Infiltrating Immune Cells Act as a Marker for Prognosis in Colorectal Cancer. *Front Immunol*, 2019; 10:2368. doi:10.3389/fimmu.2019.02368

96. Kitakaze M, Uemura M, Hara T, Chijimatsu R, Motooka D, Hirai T, et al. Cancer-specific tissue-resident memory T-cells express ZNF683 in colorectal cancer. *Br J Cancer*, 2023; 128:1828–1837. doi:10.1038/s41416-023-02202-4

97. Duchalais E, Guilluy C, Nedellec S, Touvron M, Bessard A, Touchefeu Y, et al. Colorectal Cancer Cells Adhere to and Migrate Along the Neurons of the Enteric Nervous System. *Cell Mol Gastroenterol Hepatol*, 2018; 5:31–49. doi:10.1016/j.jcmgh.2017.10.002

98. Liebig C, Ayala G, Wilks J, Verstovsek G, Liu H, Agarwal N, et al. Perineural invasion is an independent predictor of outcome in colorectal cancer. *JCO*, 2009; 27:5131–5137. doi:10.1200/JCO.2009.22.4949

99. Albo D, Akay CL, Marshall CL, Wilks JA, Verstovsek G, Liu H, et al. Neurogenesis in colorectal cancer is a marker of aggressive tumor behavior and poor outcomes. *Cancer*, 2011; 117:4834–4845. doi:10.1002/cncr.26117

100. Liebl F, Demir IE, Rosenberg R, Boldis A, Yildiz E, Kujundzic K, et al. The severity of neural invasion is associated with shortened survival in colon cancer. *Clin Cancer Res*, 2013; 19:50–61. doi:10.1158/1078-0432.CCR-12-2392

101. Zhou RW, Harpaz N, Itzkowitz SH, Parsons RE. Molecular mechanisms in colitis-associated colorectal cancer. *Oncogenesis*, 2023; 12:48. doi:10.1038/s41389-023-00492-0

102. Schmitt M, Greten FR. The inflammatory pathogenesis of colorectal cancer. *Nature Reviews Immunology*, 2021; 21:653–667. doi:10.1038/s41577-021-00534-x

103. Galon J, Bruni D. Approaches to treat immune hot, altered and cold tumours with combination immunotherapies. *Nat Rev Drug Discov*, 2019; 18:197–218. doi:10.1038/s41573-018-0007-y

104. Pagès F, Mlecnik B, Marliot F, Bindea G, Ou F-S, Bifulco C, et al. International validation of the consensus Immunoscore for the classification of colon cancer: a prognostic and accuracy study. *Lancet*, 2018; 391:2128–2139. doi:10.1016/S0140-6736(18)30789-X

105. Wang L, Geng H, Liu Y, Liu L, Chen Y, Wu F, et al. Hot and cold tumors: Immunological features and the therapeutic strategies. *MedComm*, 2023; 4:e343. doi:10.1002/mco2.343

106. Liu J-L, Yang M, Bai J-G, Liu Z, Wang X-S. "Cold" colorectal cancer faces a bottleneck in immunotherapy. *World Journal of Gastrointestinal Oncology*, 2023; 15:240–250. doi:10.4251/wjgo.v15.i2.240

107. McCart AE, Vickaryous NK, Silver A. Apc mice: models, modifiers and mutants. *Pathol Res Pract*, 2008; 204:479–490. doi:10.1016/j.prp.2008.03.004

108. Krieg C, Weber LM, Fosso B, Marzano M, Hardiman G, Olcina MM, et al. Complement downregulation promotes an inflammatory signature that renders colorectal cancer susceptible to immunotherapy. *J Immunother Cancer*, 2022; 10. doi:10.1136/jitc-2022-004717

109. Rowan AJ, Lamlum H, Ilyas M, Wheeler J, Straub J, Papadopoulou A, et al. APC mutations in sporadic colorectal tumors: A mutational "hotspot" and interdependence of the "two hits". *Proc Natl Acad Sci U S A*, 2000; 97:3352–3357. doi:10.1073/pnas.97.7.3352

110. Zigmond E, Halpern Z, Elinav E, Brazowski E, Jung S, Varol C. Utilization of Murine Colonoscopy for Orthotopic Implantation of Colorectal Cancer. *PLoS One*, 2011; 6:e28858. doi:10.1371/journal.pone.0028858

111. Corbett TH, Griswold DP, Roberts BJ, Peckham JC, Schabel FM. Tumor induction relationships in development of transplantable cancers of the colon in mice

for chemotherapy assays, with a note on carcinogen structure. *Cancer Res*, 1975; 35:2434–2439.

112. Jackstadt R, van Hooff SR, Leach JD, Cortes-Lavaud X, Lohuis JO, Ridgway RA, et al. Epithelial NOTCH Signaling Rewires the Tumor Microenvironment of Colorectal Cancer to Drive Poor-Prognosis Subtypes and Metastasis. *Cancer Cell*, 2019; 36:319-336.e7. doi:10.1016/j.ccell.2019.08.003

113. Efremova M, Rieder D, Klepsch V, Charoentong P, Finotello F, Hackl H, et al. Targeting immune checkpoints potentiates immunoediting and changes the dynamics of tumor evolution. *Nat Commun*, 2018; 9:32. doi:10.1038/s41467-017-02424-0

114. Kienzl M, Maitz K, Sarsembayeva A, Valadez-Cosmes P, Gruden E, Ristic D, et al. Comparative Study of the Immune Microenvironment in Heterotopic Tumor Models. *Cancers (Basel)*, 2024; 16. doi:10.3390/cancers16020295

115. Beach C, MacLean D, Majorova D, Melemenidis S, Nambiar DK, Kim RK, et al. Improving radiotherapy in immunosuppressive microenvironments by targeting complement receptor C5aR1. *J Clin Invest*, 2023; 133. doi:10.1172/JCI168277

116. Parang B, Barrett CW, Williams CS. AOM/DSS Model of Colitis-Associated Cancer. *Methods Mol Biol*, 2016; 1422:297–307. doi:10.1007/978-1-4939-3603-8_26

117. Li J, Chen D, Shen M. Tumor Microenvironment Shapes Colorectal Cancer Progression, Metastasis, and Treatment Responses. *Front Med (Lausanne)*, 2022; 9. doi:10.3389/fmed.2022.869010

118. AlMusawi S, Ahmed M, Nateri AS. Understanding cell-cell communication and signaling in the colorectal cancer microenvironment. *Clin Transl Med*, 2021; 11:e308. doi:10.1002/ctm2.308

119. Labernadie A, Kato T, Brugués A, Serra-Picamal X, Derzsi S, Arwert E, et al. A mechanically active heterotypic E-cadherin/N-cadherin adhesion enables fibroblasts to drive cancer cell invasion. *Nat Cell Biol*, 2017; 19:224–237. doi:10.1038/ncb3478

120. Omatsu M, Nakanishi Y, Iwane K, Aoyama N, Duran A, Muta Y, et al. THBS1-producing tumor-infiltrating monocyte-like cells contribute to immunosuppression and metastasis in colorectal cancer. *Nat Commun*, 2023; 14. doi:10.1038/s41467-023-41095-y

121. Wang H, Tian T, Zhang J. Tumor-Associated Macrophages (TAMs) in Colorectal Cancer (CRC): From Mechanism to Therapy and Prognosis. *Int J Mol Sci*, 2021; 22. doi:10.3390/ijms22168470

122. Qi J, Sun H, Zhang Y, Wang Z, Xun Z, Li Z, et al. Single-cell and spatial analysis reveal interaction of FAP+ fibroblasts and SPP1+ macrophages in colorectal cancer. *Nat Commun*, 2022; 13:1742. doi:10.1038/s41467-022-29366-6

123. Schonkeren SL, Thijssen MS, Vaes N, Boesmans W, Melotte V. The Emerging Role of Nerves and Glia in Colorectal Cancer. *Cancers (Basel)*, 2021; 13. doi:10.3390/cancers13010152

124. Wang H, Huo R, He K, Cheng L, Zhang S, Yu M, et al. Perineural invasion in colorectal cancer: mechanisms of action and clinical relevance. *Cell Oncol (Dordr)*, 2024; 47:1–17. doi:10.1007/s13402-023-00857-y

125. Liebig C, Ayala G, Wilks JA, Berger DH, Albo D. Perineural invasion in cancer: a review of the literature. *Cancer*, 2009; 115:3379–3391. doi:10.1002/cncr.24396

126. Nguyen TM, Ngoc DT, Choi J-H, Lee C-H. Unveiling the Neural Environment in Cancer: Exploring the Role of Neural Circuit Players and Potential Therapeutic Strategies. *Cells*, 2023; 12. doi:10.3390/cells12151996

127. Valès S, Bacola G, Biraud M, Touvron M, Bessard A, Geraldo F, et al. Tumor cells hijack enteric glia to activate colon cancer stem cells and stimulate tumorigenesis. *EBioMedicine*, 2019; 49:172–188. doi:10.1016/j.ebiom.2019.09.045

128. Linan-Rico A, Ochoa-Cortes F, Schneider R, Christofi FL. Mini-review: Enteric glial cell reactions to inflammation and potential therapeutic implications for GI diseases, motility disorders, and abdominal pain. *Neurosci Lett*, 2023; 812:137395. doi:10.1016/j.neulet.2023.137395

129. Schneider R, Leven P, Glowka T, Kuzmanov I, Lysson M, Schneiker B, et al. A novel P2X2-dependent purinergic mechanism of enteric gliosis in intestinal inflammation. *EMBO Mol Med*, 2021; 13:e12724. doi:10.15252/emmm.202012724

130. Progatzky F, Shapiro M, Chng SH, Garcia-Cassani B, Classon CH, Sevgi S, et al. Regulation of intestinal immunity and tissue repair by enteric glia. *Nature*, 2021; 599:125–130. doi:10.1038/s41586-021-04006-z

131. Ibiza S, García-Cassani B, Ribeiro H, Carvalho T, Almeida L, Marques R, et al. Glial-cell-derived neuroregulators control type 3 innate lymphoid cells and gut defence. *Nature*, 2016; 535:440–443. doi:10.1038/nature18644

132. Brown IA, McClain JL, Watson RE, Patel BA, Gulbransen BD. Enteric glia mediate neuron death in colitis through purinergic pathways that require connexin-43 and nitric oxide. *Cell Mol Gastroenterol Hepatol*, 2016; 2:77–91. doi:10.1016/j.jcmgh.2015.08.007

133. Turco F, Sarnelli G, Cirillo C, Palumbo I, Giorgi F de, D'Alessandro A, et al. Enteroglial-derived S100B protein integrates bacteria-induced Toll-like receptor signalling in human enteric glial cells. *Gut*, 2014; 63:105–115. doi:10.1136/gutjnl-2012-302090

134. Liñán-Rico A, Turco F, Ochoa-Cortes F, Harzman A, Needleman BJ, Arsenescu R, et al. Molecular Signaling and Dysfunction of the Human Reactive Enteric Glial Cell Phenotype: Implications for GI Infection, IBD, POI, Neurological, Motility, and GI Disorders. *Inflamm Bowel Dis*, 2016; 22:1812–1834. doi:10.1097/MIB.0000000000000854

135. Rosenbaum C, Schick MA, Wollborn J, Heider A, Scholz C-J, Cecil A, et al. Activation of Myenteric Glia during Acute Inflammation In Vitro and In Vivo. *PLoS One*, 2016; 11:e0151335. doi:10.1371/journal.pone.0151335

136. Boyen GB von, Steinkamp M, Reinshagen M, Schäfer K-H, Adler G, Kirsch J. Nerve growth factor secretion in cultured enteric glia cells is modulated by proinflammatory cytokines. *J Neuroendocrinol*, 2006; 18:820–825. doi:10.1111/j.1365-2826.2006.01478.x

137. Dinarello CA. Overview of the IL-1 family in innate inflammation and acquired immunity. *Immunol Rev*, 2018; 281:8–27. doi:10.1111/imr.12621

138. Stakenborg M, Abdurahiman S, Simone V de, Goverse G, Stakenborg N, van Baarle L, et al. Enteric glial cells favor accumulation of anti-inflammatory macrophages during the resolution of muscularis inflammation. *Mucosal Immunol*, 2022; 15:1296–1308. doi:10.1038/s41385-022-00563-2

139. Morales-Soto W, Gonzales J, Jackson WF, Gulbransen BD. Enteric glia promote visceral hypersensitivity during inflammation through intercellular signaling with gut nociceptors. *Sci Signal*, 2023; 16:eadg1668. doi:10.1126/scisignal.adg1668

140. Dora D, Ferenczi S, Stavely R, Toth VE, Varga ZV, Kovacs T, et al. Evidence of a Myenteric Plexus Barrier and Its Macrophage-Dependent Degradation During Murine Colitis: Implications in Enteric Neuroinflammation. *Cell Mol Gastroenterol Hepatol*, 2021; 12:1617–1641. doi:10.1016/j.jcmgh.2021.07.003

141. Mallesh S, Schneider R, Schneiker B, Lysson M, Efferz P, Lin E, et al. Sympathetic Denervation Alters the Inflammatory Response of Resident Muscularis Macrophages upon Surgical Trauma and Ameliorates Postoperative Ileus in Mice. *Int J Mol Sci*, 2021; 22. doi:10.3390/ijms22136872

142. Gabanyi I, Muller PA, Feighery L, Oliveira TY, Costa-Pinto FA, Mucida D. Neuro-immune Interactions Drive Tissue Programming in Intestinal Macrophages. *Cell*, 2016; 164:378–391. doi:10.1016/j.cell.2015.12.023

143. Matheis F, Muller PA, Graves CL, Gabanyi I, Kerner ZJ, Costa-Borges D, et al. Adrenergic Signaling in Muscularis Macrophages Limits Infection-Induced Neuronal Loss. *Cell*, 2020; 180:64-78.e16. doi:10.1016/j.cell.2019.12.002

144. Straub RH, Wiest R, Strauch UG, Härle P, Schölmerich J. The role of the sympathetic nervous system in intestinal inflammation. *Gut*, 2006; 55:1640–1649. doi:10.1136/gut.2006.091322

145. Sharma D, Farrar JD. Adrenergic regulation of immune cell function and inflammation. *Semin Immunopathol*, 2020; 42:709–717. doi:10.1007/s00281-020-00829-6

146. Geyer R, Moussa M, Mandoiu I, Srivastava PK, Nevin J. Sympathetic nervous system-mediated β-adrenergic signaling maintains the pool of mature natural killer cells. *The Journal of Immunology*, 2022; 208:169.10-169.10. doi:10.4049/jimmunol.208.Supp.169.10

147. Hove AS ten, Mallesh S, Zafeiropoulou K, Kleer JW de, van Hamersveld PH, Welting O, et al. Sympathetic activity regulates epithelial proliferation and wound

healing via adrenergic receptor α2A. *Sci Rep*, 2023; 13:17990. doi:10.1038/s41598-023-45160-w

148. Freire BM, Melo FM de, Basso AS. Adrenergic signaling regulation of macrophage function: do we understand it yet? *Immunother Adv*, 2022; 2:ltac010. doi:10.1093/immadv/ltac010

149. Pongratz G, Straub RH. The sympathetic nervous response in inflammation. *Arthritis Res Ther*, 2014; 16:504. doi:10.1186/s13075-014-0504-2

150. Nasser Y, Ho W, Sharkey KA. Distribution of adrenergic receptors in the enteric nervous system of the guinea pig, mouse, and rat. *J Comp Neurol*, 2006; 495:529–553. doi:10.1002/cne.20898

151. Gulbransen BD, Bains JS, Sharkey KA. Enteric glia are targets of the sympathetic innervation of the myenteric plexus in the guinea pig distal colon. *J Neurosci*, 2010; 30:6801–6809. doi:10.1523/JNEUROSCI.0603-10.2010

152. Yuan R, Bhattacharya N, Kenkel JA, Shen J, DiMaio MA, Bagchi S, et al. Enteric Glia Play a Critical Role in Promoting the Development of Colorectal Cancer. *Frontiers in Oncology*, 2020; 10:595892. doi:10.3389/fonc.2020.595892

153. Thomasi B, Gulbransen B. Mini-review: Intercellular communication between enteric glia and neurons. *Neurosci Lett*, 2023; 806:137263. doi:10.1016/j.neulet.2023.137263

154. Prochera A, Rao M. Mini-Review: Enteric glial regulation of the gastrointestinal epithelium. *Neurosci Lett*, 2023; 805:137215. doi:10.1016/j.neulet.2023.137215

155. Bohórquez DV, Samsa LA, Roholt A, Medicetty S, Chandra R, Liddle RA. An enteroendocrine cell-enteric glia connection revealed by 3D electron microscopy. *PLoS One*, 2014; 9:e89881. doi:10.1371/journal.pone.0089881

156. Zhang B, Guo X, Huang L, Zhang Y, Li Z, Su D, et al. Tumour-associated macrophages and Schwann cells promote perineural invasion via paracrine loop in pancreatic ductal adenocarcinoma. *Br J Cancer*, 2024; 130:542–554. doi:10.1038/s41416-023-02539-w

157. Zhou Y, Li J, Han B, Zhong R, Zhong H. Schwann cells promote lung cancer proliferation by promoting the M2 polarization of macrophages. *Cellular Immunology*, 2020; 357:104211. doi:10.1016/j.cellimm.2020.104211

158. Zhang Y, Zhao Y, Li Q, Wang Y. Macrophages, as a Promising Strategy to Targeted Treatment for Colorectal Cancer Metastasis in Tumor Immune Microenvironment. *Front Immunol*, 2021; 12:685978. doi:10.3389/fimmu.2021.685978

159. Hou S, Zhao Y, Chen J, Lin Y, Qi X. Tumor-associated macrophages in colorectal cancer metastasis: molecular insights and translational perspectives. *J Transl Med*, 2024; 22:62. doi:10.1186/s12967-024-04856-x

160. Xie Z, Zheng G, Niu L, Du K, Li R, Dan H, et al. SPP1+ macrophages in colorectal cancer: Markers of malignancy and promising therapeutic targets. *Genes & Diseases*, 2024:101340. doi:10.1016/j.gendis.2024.101340

161. Zhang L, Li Z, Skrzypczynska KM, Fang Q, Zhang W, O'Brien SA, et al. Single-Cell Analyses Inform Mechanisms of Myeloid-Targeted Therapies in Colon Cancer. *Cell*, 2020; 181:442-459.e29. doi:10.1016/j.cell.2020.03.048

162. Schneider L, Schneider R, Hamza E, Wehner S. Extracellular matrix substrates differentially influence enteric glial cell homeostasis and immune reactivity. *Front. Immunol.*, 2024; 15. doi:10.3389/fimmu.2024.1401751

163. Schneider R, Leven P, Mallesh S, Breßer M, Schneider L, Mazzotta E, et al. IL-1-dependent enteric gliosis guides intestinal inflammation and dysmotility and modulates macrophage function. *Commun Biol*, 2022; 5:811. doi:10.1038/s42003-022-03772-4

164. van Baarle L, Simone V de, Schneider L, Santhosh S, Abdurahiman S, Biscu F, et al. IL-1R signaling drives enteric glia-macrophage interactions in colorectal cancer. *Nat Commun*, 2024; 15:6079. doi:10.1038/s41467-024-50438-2

# 3. Publications

## 3.1 Publication 1: Schneider L, *et al.* 2024 - Extracellular matrix substrates differentially influence enteric glial cell homeostasis and immune reactivity

frontiers | Frontiers in Immunology

TYPE Original Research
PUBLISHED 25 July 2024
DOI 10.3389/fimmu.2024.1401751



OPEN ACCESS

EDITED BY
Kevin P. Mollen,
University of Pittsburgh, United States

REVIEWED BY
Chhinder Sodhi,
Johns Hopkins University, United States
Rhian Stavely,
Massachusetts General Hospital and Harvard Medical School, United States

*CORRESPONDENCE
Sven Wehner
sven.wehner@ukbonn.de

RECEIVED 15 March 2024
ACCEPTED 02 July 2024
PUBLISHED 25 July 2024

CITATION
Schneider L, Schneider R, Hamza E and Wehner S (2024) Extracellular matrix substrates differentially influence enteric glial cell homeostasis and immune reactivity. *Front. Immunol.* 15:1401751. doi: 10.3389/fimmu.2024.1401751



# Extracellular matrix substrates differentially influence enteric glial cell homeostasis and immune reactivity

Linda Schneider, Reiner Schneider, Ebrahim Hamza and Sven Wehner*

Department of Surgery, Medical Faculty, University Hospital Bonn, Bonn, Germany

**Introduction:** Enteric glial cells are important players in the control of motility, intestinal barrier integrity and inflammation. During inflammation, they switch into a reactive phenotype enabling them to release inflammatory mediators, thereby shaping the inflammatory environment. While a plethora of well-established *in vivo* models exist, cell culture models necessary to decipher the mechanistic pathways of enteric glial reactivity are less well standardized. In particular, the composition of extracellular matrices (ECM) can massively affect the experimental outcome. Considering the growing number of studies involving primary enteric glial cells, a better understanding of their homeostatic and inflammatory *in vitro* culture conditions is needed.

**Methods:** We examined the impact of different ECMs on enteric glial culture purity, network morphology and immune responsiveness. Therefore, we used immunofluorescence and brightfield microscopy, as well as 3' bulk mRNA sequencing. Additionally, we compared cultured cells with *in vivo* enteric glial transcriptomes isolated from $Sox10^{iCreERT2}Rpl22^{HA/+}$ mice.

**Results:** We identified Matrigel and laminin as superior over other coatings, including poly-L-ornithine, different lysines, collagens, and fibronectin, gaining the highest enteric glial purity and most extended glial networks expressing connexin-43 hemichannels allowing intercellular communication. Transcriptional analysis revealed strong similarities between enteric glia on Matrigel and laminin with enrichment of gene sets supporting neuronal differentiation, while cells on poly-L-ornithine showed enrichment related to cell proliferation. Comparing cultured and *in vivo* enteric glial transcriptomes revealed a 50% overlap independent of the used coating substrates. Inflammatory activation of enteric glia by IL-1β treatment showed distinct coating-dependent gene expression signatures, with an enrichment of genes related to myeloid and epithelial cell differentiation on Matrigel and laminin coatings, while poly-L-ornithine induced more gene sets related to lymphocyte differentiation.

**Discussion:** Together, changes in morphology, differentiation and immune activation of primary enteric glial cells proved a strong effect of the ECM. We

identified Matrigel and laminin as pre-eminent substrates for murine enteric glial cultures. These new insights will help to standardize and improve enteric glial culture quality and reproducibility between *in vitro* studies in the future, allowing a better comparison of their functional role in enteric neuroinflammation.

KEYWORDS

enteric glia, intestinal immune response, extracellular matrix, neuroinflammation, Matrigel, laminin

# Introduction

Enteric glia are a well-integrated cell type of the enteric nervous system (ENS), and they are closely intertangled with enteric neurons and resident macrophages within the bowel wall. Recent studies have shown that enteric glia are major contributors to intestinal inflammation (1). Driven by mediators, actively or passively released during inflammation, trauma or even stress, enteric glia switch into a so-called reactive phenotype, allowing them to actively participate in the inflammation and control the intestinal immune environment. The molecules able to induce glial reactivity include extracellular ATP (2), IFNγ (3), endothelin-B (4), LPS (5, 6) and interleukin-1 (IL-1). The latter is one of the most-studied inducers of enteric glial reactivity in acute (7–9) and chronic inflammation (10–12). At the cellular level, resident macrophages (7, 11, 13), as well as infiltrating monocyte-derived macrophages (7, 9), have been shown to communicate with enteric glia during gut inflammation.

Besides a plethora of *in vivo* models, including glial-specific reporter and knockout mice, *in vitro* experiments were part of most enteric glia-related studies and have contributed largely to our current understanding of reactive glial biology, their intercellular communication and enteric glia-to-neuron signaling under physiological conditions (14). Meanwhile, most studies use primary enteric glial cultures instead of the few available enteric glial cell lines, such as CRL-2690 (15) and ClK (16). However, primary cultures have certain challenges and are far away from being used in a standardized manner. One of these challenges is the glial cell isolation from intestinal tissue. Most enteric glia are well orchestrated in ganglia and as extraganglionic fibers. Due to their well-integrated phenotype, the main problem is that excessive enzymatic tissue digestion, used to achieve single-cell suspension for *in vitro* studies, also severely disrupts their stellate projections and the extracellular matrix (ECM) of enteric glia and finally leads to cell death. Therefore, researchers developed methods to culture incompletely digested ganglia or so-called neurospheres, leaving the ganglionic glia mostly intact. Both allow the outgrowth and proliferation of enteric glia from the ganglia or neurospheres (17). The second underestimated factor in enteric glial cultures is the contamination by non-glial cell types, which can also grow out of the cultured structures. Depending on the culture conditions, these cells might grow faster and better than glia or at least "contaminate" the glia cultures to a certain degree.

A major factor influencing primary cell quality but also cellular behavior is the choice of the appropriate ECM compounds, as shown for enteric neural-crest-derived cells (18) (giving birth to enteric neurons and glia) and CNS cells (19). In the ENS, the ECM not only favors adhesion and growth of glia and neurons but also affects their cellular functions. For example, enteric neuronal crest cell migration along the developmental gut is strongly controlled by the ECM (18). Furthermore, fibronectin and laminin (20, 21), with the latter particularly expressed by fibroblast and smooth muscle cells in the bowel wall, prevented neuronal differentiation and favored GFAP$^+$ enteric glial cell differentiation in ENS cultures. Laminin (21) as well as collagen type IV and fibronectin, among others, were shown to be part of the basement membrane of enteric ganglia, but are not expressed insight the cells (20). A comparative study using various ECM coatings, including laminin, collagens, poly-lysine and heparan sulfate, found different effects on neuronal or glial differentiation (22). Additionally, macrophages, which lay in close spatial proximity to enteric glia in the intestine and can interact and communicate with them (7, 9, 13), have been shown to also be significantly affected by the ECM composition (23, 24). We hypothesized that the ECM also might influence the reactive behavior of enteric glia, one of their most important functions in intestinal diseases.

In this study, we tested the impact of various ECM compounds on the growth, network capacity, and neuronal differentiation, as well as their impact on the immune reactivity of IL-1β-stimulated reactive enteric glia. We discovered striking differences in cell numbers, intercellular networking and differentiation capacities, and differences in the transcriptional response of IL-1β-stimulated reactive enteric glia.

# Materials and methods

## Animals

8- to 16 weeks-old mice of the following lines were used in the study: C57BL/6J (JAX:000664), GFAP$^{Cre}$Ai14$^{fl/fl}$ (derived by crossing B6.Cg-Tg(Gfap-cre)73.12Mvs/J (JAX:012886) and

B6;129S6-Gt(ROSA)26Sor$^{tm14(CAG-tdTomato)Hze}$/J (JAX:007908)) or Sox10$^{iCreERT2}$Rpl22$^{HA/+}$ (B6-Tg(Sox10-icre/ERT2)388Wdr/J (Sox10$^{iCreERT2}$; kindly provided by Dr. Vassilis Pachnis (The Francis Crick Institute, London, UK) (25)) and B6N.129-Rpl22$^{tm1.1Psam}$/J (JAX:011029)). C57BL6 and GFAP$^{Cre}$Ai14$^{fl/fl}$ mice were used for primary enteric glial cell isolation, and Sox10$^{iCreERT2}$Rpl22$^{HA/+}$ was used for glial-specific mRNA isolation from intestinal tissue via the *RiboTag* approach. Sox10$^{iCreERT2}$Rpl22$^{HA/+}$ were injected intraperitoneally with 100 µl Tamoxifen (MP Biomedicals, 1 mg in 100 µL sterile corn oil) on three consecutive days and rested for at least one week before organ harvesting. All experiments were carried out under German federal law of North Rhine-Westphalia (AZ 81-02.04.2021.A424).

## Neurosphere-derived enteric glial cell cultures

Primary enteric glial cells were isolated from small intestine *muscularis externa* as described previously (2). Briefly, small intestines of 8-16 weeks old mice were harvested, flushed with cold Krebs-Henseleit buffer (126 mM NaCl; 2.5 mM KCl: 25 mM NaHCO3; 1.2 mM NaH2PO4; 1.2 mM MgCl2; 2.5 mM CaCl2, 100 IU/mL Penicillin, 100 IU/mL Streptomycin and 2.5 µg/mL Amphotericin), cut into segments and kept in oxygenated Krebs-Henseleit buffer on ice. *Muscularis externa* was peeled and collected for digestion. Tissues were digested for 15 min in DMEM containing protease Type 1 (0.25 mg/mL, Sigma-Aldrich) and collagenase A (1 mg/mL, Sigma-Aldrich) at 37°C and 130 rpm. DMEM containing 10% FBS (Sigma-Adrich) was used to stop the enzymatic reaction, and cells were pelleted at 300xg for 5 min. Cell pellets were resuspended in proliferation medium (neurobasal medium with 100 IU/Penicillin, 100 µg/mL Streptomycin, 2.5 µg/mL Amphotericin (all ThermoFisher Scientific), FGF and EGF (both 20 ng/mL, Immunotools)) and cultured on uncoated plates for seven days at 37°C and 5% CO2, applying fresh growth factors every other day. Neurospheres were collected after one week of proliferation and dissociated with trypsin (0.25%, ThermoFisher Scientific) for 5 min at 37°C prior to seeding on coated cover glasses in 24-well plates for differentiation (coating procedures described separately). Neurospheres were kept in differentiation medium (neurobasal medium with 100 IU/Penicillin, 100 µg/mL Streptomycin, 2.5 µg/mL Amphotericin, B27, N2 (all Thermo Scientific) and EGF (2 ng/mL, Immunotools)) for three days for morphological analysis, or five days for further analyses. For IL-1β stimulation, cells were treated with or without IL-1β (10 ng/mL, Immunotools) for 24 hours on day five of differentiation. Supernatants were collected, and cells were lysed with RLT buffer (Qiagen) to isolate mRNA. RNA samples were extracted using the RNeasy Mini Kit (Qiagen) according to the manufacturer's instructions.

## Coating substrates

Working solutions for coating substrates were prepared as recommended by the manufacturer, as stated in Table 1. Cover glasses in 24-well cell culture plates were incubated with 475 µl/well of coating substrates at 37°C overnight and washed according to the respective manufacturer's instructions before cell seeding (Table 1).

## Immunohistochemistry

Primary cells were fixed in 4% paraformaldehyde/PBS for 15 minutes and washed thrice with PBS. Next, cells were blocked with blocking buffer (PBS containing 5% donkey serum and 0.25% Triton X-100) for 1h at RT and incubated with primary antibodies diluted in PBS + blocking buffer (1:1) as mentioned in Table 2 at 4°C overnight. After three PBS washing steps, secondary antibodies (Table 2) were applied for 2 h at RT. Nuclei were counterstained with Hoechst, and cover glasses were mounted with Shandon$^{TM}$ Immu-Mount$^{TM}$ (Epredia) and imaged using Nikon Eclipse TE2000-E or Nikon Eclipse Ti2 fluorescent microscopes.

## Brightfield analysis for area measurement

For Brightfield analysis, cells were fixed in 4% paraformaldehyde/PBS for 15 minutes and washed thrice with PBS. Brightfield imaging was performed using a Nikon Eclipse Ti2 microscope and the Nikon DS-Qi2 camera. For each coating and experiment, three wells were imaged, acquiring large images of 5x5 images at 100x magnification, achieving an overview of the cover glass. Area measurements were done with Fiji software, as described previously (28).

## Enzyme-linked immunosorbent assay

Release of IL-6 and CCL2 was measured in enteric glial cell culture supernatants treated with or without IL-1β for 24h. Supernatants were collected, centrifuged at 500 x g for 5 min, transferred to new tubes, and stored at -20°C before being processed for the IL-6 or CCL2 ELISA. ELISA kits were purchased from Thermo Fisher Scientific and used according to the manufacturer's instructions.

## Isolation of *in vivo* enteric glial-specific RNA from *muscularis externa*

Enteric glia-specific mRNA from the naive *muscularis externa* of Sox10$^{iCreERT2}$Rpl22$^{HA/+}$ mice was performed as described previously (29). Briefly, small intestines were harvested and *muscularis externa* was mechanically separated from the mucosal layer. *Muscularis* tissue was lysed in two rounds in a Qiagen Powerlyzer24 (2600 rpm, 30 s, 5 min intermediate incubation on ice). Supernatants were incubated with 100 µl HA–coupled A/G beads (Cat.#HY-K0201 MedChemExpress Company) at 4°C and 7 rpm overnight. Magnetic separation was performed for 1 minute, and ribosomes containing mRNA were eluted from beads. RNA was isolated using the Qiagen RNeasy micro kit.

TABLE 1 Coating substrates and preparation details.

| Coating substrate | Company | Working concentration | | | Medium | Washing steps | Drying |
|---|---|---|---|---|---|---|---|
| | | lower | standard | higher | | | |
| Matrigel | Corning | 20 µg/ml (= 25 µg/cm²) | 100 µg/ml (= 25 µg/cm²) | 250 µg/ml (= 25 µg/cm²) | serum-free medium | no wash | no |
| Laminin | R&D Systems | 4 µg/ml (= 5 µg/cm²) | 20 µg/ml (= 5 µg/cm²) | 50 µg/ml (= 5 µg/cm²) | serum-free medium | no wash | no |
| Poly-L-ornithine | Sigma | 1.6 µg/ml (= 2 µg/cm²) | 8 µg/ml (= 2 µg/cm²) | 20 µg/ml (= 2 µg/cm²) | ddH2O | 3x ddH2O | no |
| Poly-L-lysine | Thermo Fisher Scientific | – | 8 µg/ml (= 2 µg/cm²) | – | ddH2O | 3x ddH2O | no |
| Poly-D-lysine | ScienCell | – | 32 µg/ml (= 8 µg/cm²) | – | PBS | 3x ddH2O | yes |
| Collagen I | Thermo Fisher Scientific | – | 20 µg/ml (= 5 µg/cm²) | – | 20 mM acetic acid | 3x PBS | no |
| Collagen IV | Corning | – | 20 µg/ml (= 5 µg/cm²) | – | 0.05M HCl | 3x PBS | no |
| Fibronectin | Sigma | – | 20 µg/ml (= 5 µg/cm²) | – | PBS | no wash | yes |

TABLE 2 Antibodies and used dilutions.

| Primary Antibodies | Company | Dilution |
|---|---|---|
| chicken anti-GFAP | Biolegend | 1:1000 |
| goat anti-SOX10 | custom-made (aliquot kindly provided by Prof. Michael Wegener, University of Erlangen (26)) | 1:3000 |
| mouse anti-αSMA | Dianova | 1:800 – 1:1000 |
| human anti-ANNA1 | kindly provided by the Mayo Clinic (USA) | 1:10000 |
| rabbit anti-Connexin 43 | custom-made (aliquot kindly provided by Prof. Christian Steinhäuser (27)) | 1:500 |
| **Secondary Antibodies** | **Company** | **Dilution** |
| donkey anti-chicken CF633 | Sigma Aldrich | 1:800 |
| donkey anti-goat Cy3 | Dianova | 1:800 |
| donkey anti-mouse AF488 | Dianova | 1:800 |
| donkey anti-human DyLight488 | Invitrogen | 1:800 |
| donkey anti-rabbit AF647 | Southern Biotech | 1:800 |

## 3' bulk mRNA sequencing

RNA sequencing was performed by the Genomics Core Facility of the University Hospital Bonn. For the preparation of libraries, QuantSeq 3' mRNA-Seq Library Prep Kit (Lexogen) according to the manufacturer's instructions. Libraries were sequenced on the NovaSeq6000 with a sequencing depth of 10M raw reads. RNA-Seq data were analyzed by PartekFlow[1] software (USA) using the Lexogen pipeline *12112017*. The pipeline consisted of two adapter trimming and a base-trimming step with subsequent quality controls (QC). Reads were aligned with star2.5.3, followed by a post-alignment QC and quantification to an annotation model. Normalized counts were subjected to a noise reduction filter (excluding features where maximum ≤ 15) followed by principal component and DESeq2 analysis. Sequencing files are deposited in the Gene Expression Omnibus (GEO) database under the GEO accession code GSE271114. Visualization was done with PartekFlow software and GraphPad Prism 10.

## Software

The software tools used for this study include PartekFlow[1], including DESeq2, PCA, and heatmaps. Venn diagrams were done in PartekFlow or using the bioinformatics web tool[2]. Microscopic images were taken with Nikon NIS-Elements version AR 5.42.04 software and analyzed using ImageJ. Graphs were prepared with GraphPad Prism 10. Graphs and images were combined into figures using Affinity Designer version 2.4.0.

## Statistical analysis

Statistical analyses were performed with Prism 10.0 (GraphPad) using one-way ANOVA or two-way ANOVA with Tukey's or

1 https://www.partek.com/partek-flow/#features.

2 https://bioinformatics.psb.ugent.be/webtools/Venn/.

Šídák's multiple comparison tests, as stated in the figure legends. In all figures, p-values are indicated as * =p<0.05, ** =p<0.01, *** =p<0.001 and **** =p<0.0001 when compared to poly-L-ornithine as reference or to naive controls as indicated. All plots are mean ± SEM of the indicated numbers of replicates. The PartekFlow software was used to analyze RNAseq data. Herein, statistical analyses were performed using Fisher's exact test which provided *p*-values with multiple testing corrections (FDR). The significance level for differentially expressed genes was set to FDR<0.05 and indicated in the figure legends were applicable.

# Results

## Matrigel and laminin advance primary enteric glial cell yield and network formation

A rising number of studies utilize primary enteric glial cell cultures to unravel their role in intestinal homeostasis and disease. However, the question of whether coating substrates used for cell adhesion can alter enteric glial biology is poorly understood. In the commonly used method of neurosphere-derived enteric glial cell cultures isolated from the murine small intestine *muscularis externa*, we analyzed their morphological properties on eight coating substrates, namely poly-L-ornithine, Matrigel, laminin, poly-D-lysine, poly-L-lysine, collagen type I, collagen type IV, and fibronectin (Figure 1A). First, we studied culture purity by isolating enteric glia from $GFAP^{Cre}Ai14^{fl/fl}$ reporter mice, expressing tdTomato in all $GFAP^{+}$ cells. Among the eight tested coating substrates, we found the highest enteric glia purity in laminin coating, with 72% enteric glia, closely followed by Matrigel with 67% (Figures 1B, B'). As a reference, we used poly-L-ornithine, a coating substrate widely used in CNS and ENS *in vitro* approaches (7, 30, 31). Accordingly, comparing laminin and Matrigel to poly-L-ornithine (51% purity), we saw significantly higher glia enrichment with these two coatings, while poly-D-lysine, poly-L-lysine, collagen I and IV, as well as fibronectin did not differ much from poly-L-ornithine with culture purities ranging from 50% to 60% (Figures 1B, B').

As enteric glia were isolated from myenteric plexus-derived neurospheres, cultures are likely to contain other stromal cells, e.g. smooth muscle cells or neurons. Indeed, a co-staining of smooth muscle actin (αSMA) and GFAP revealed αSMA expression in some $GFAP^{-}$ cells with a fibroblast-like morphology (Figure 1C). With Matrigel and laminin presenting the best glial yield, we validated whether the cultured cells also expressed another prominent glial cell marker, SOX10, keeping poly-L-ornithine as a reference. We found co-expression of GFAP and SOX10 with an overlap of ~95% in all three coating conditions (mean percentage per coating substrate: poly-L-ornithine = 94.52%, Matrigel = 96.79%, laminin = 95.22%; Figures 1D, D'). Next, we examined how different coating concentrations, affect EGC cultures. Therefore, we repeated the initially performed experiments, which were done with concentrations either recommended by the manufacturer or commonly used in the literature, and added a 5-fold lower and a 2.5-fold higher concentration for poly-L-ornithine, Matrigel, and laminin (Table 1). While no major differences could be observed between the different poly-L-ornithine concentrations, Matrigel showed the lowest EGC percentage and numbers with the highest concentration, while the lowest Matrigel concentration resulted in the highest glia enrichment, even exceeding the recommended concentration although this trend was not significant. For laminin, the standard concentration was significantly better compared to the others regarding EGC percentage and numbers (Supplementary Figures S1A, A'). We therefore conclude that ECM protein concentrations can be optimized to improve cell enrichment but the manufacturers' recommended and commonly used concentrations already are within the optimal range. Therefore, we used the recommended concentrations for our further analyses.

Since neurospheres can give rise to enteric glia but also to enteric neurons, we further examined the expression of a specific nuclear neuronal marker, namely ANNA1, as well as synapsins (SYN1/2/3), which label axon terminals. In all three coating conditions, $ANNA1^{+}$ cells were detected, but almost exclusively within the neurospheres but not in the outgrowing cells. SYN1/2/3 was very rarely detected in both, the neurospheres and the outgrown cells, indicating that immature but also differentiated neurons, the latter being able to form synapses were almost absent under all coating conditions (Figure 1E).

Microscopical images showed that enteric glia grow out from the neurospheres and form networks, while also individual cells, with no connection to the outgrown network exist. As enteric glia also build functional networks *in vivo*, we were interested if any coating condition might be superior in enabling glial network formation. Therefore, we quantified the enteric glial network area around neurospheres in both brightfield and immunofluorescent images of EGCs on different coating substrates (Supplementary Figure S1B). Again, Matrigel and laminin were superior, with a mean glial network area of 0.37 $mm^2$ and 0.41 $mm^2$ around neurospheres in brightfield images, respectively, which was around 20-fold larger than for poly-L-ornithine coating with 0.02 $mm^2$ (Figures 2A, A'). Other coating substrates differed slightly from each other but were significantly lower than Matrigel or laminin (poly-D-lysine: 0.01 $mm^2$, poly-L-lysine: 0.13 $mm^2$, collagen I: 0.1 $mm^2$, collagen IV: 0.05 $mm^2$, fibronectin 0.05 $mm^2$; Figure 2A, A'). In order to ensure that it is indeed enteric glia forming these networks, the areas were again measured in $tdTomato^{+}$ cell cultures from $GFAP^{Cre}Ai14^{fl/fl}$ reporter mice (Supplementary Figures S1C, C'). Similar to the brightfield analysis, Matrigel and lamin surpassed the other coatings also in $tdTomato^{+}$ EGC networks. Comparing the area formation of EGCs on different concentrations of Matrigel, laminin, and poly-L-ornithine, we found similar trends as for EGC percentage and numbers. In detail, no major changes in EGC network area were detected between different poly-L-ornithine concentrations, while Matrigel displayed decreased EGC areas with increasing

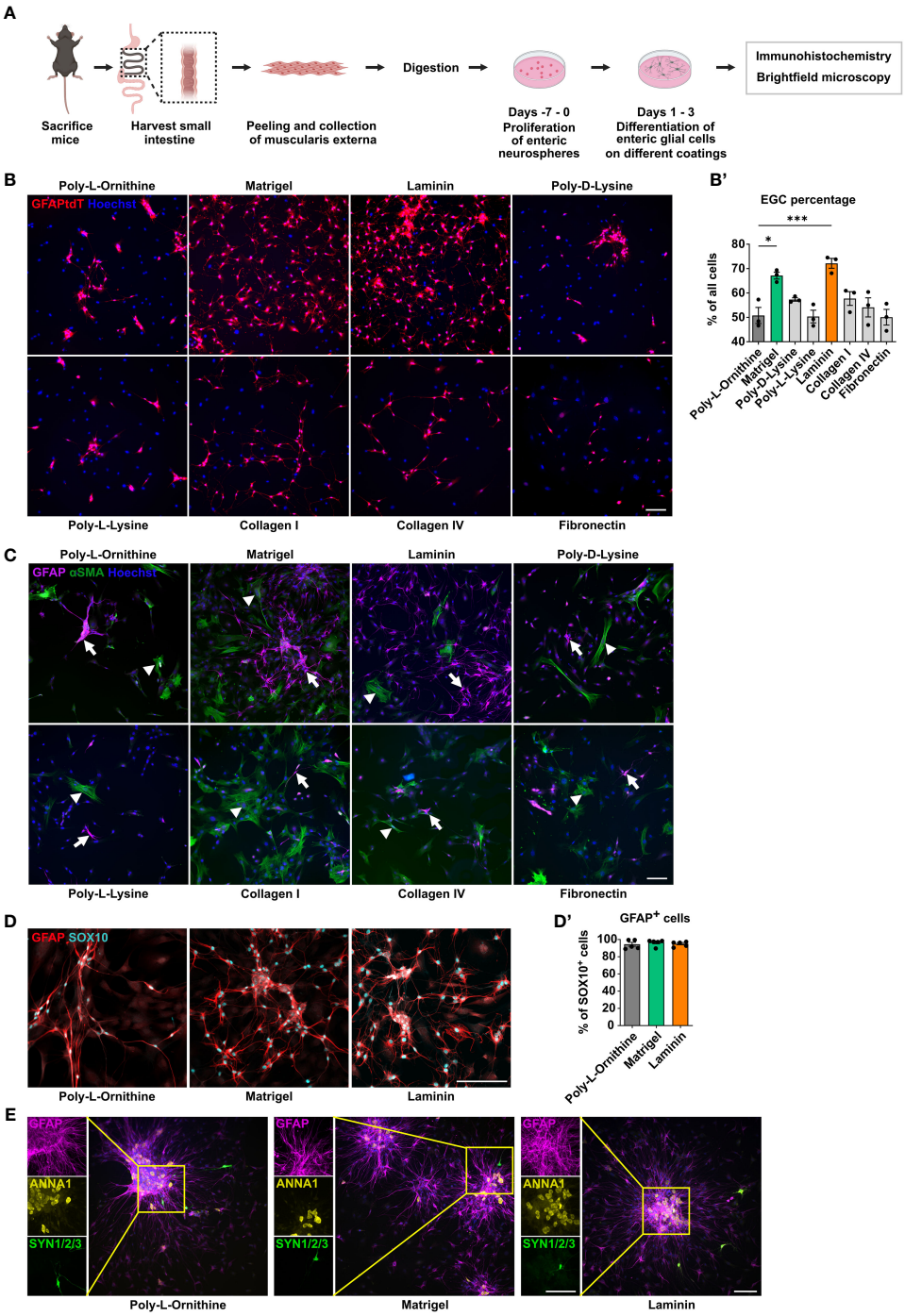


FIGURE 1
Matrigel and laminin advance primary enteric glial cell yield. **(A)** Schematic representation of the enteric glia culture model. **(B)** Enteric glia were isolated from GFAP$^{Cre}$Ai14$^{fl/fl}$ mice and differentiated on the indicated coating substrates. Representative immunofluorescence images of tdTomato$^{+}$ enteric glia and nuclei (Hoechst) on indicated coatings (scale bar 100 µm). (**B'**) Percentage of tdTomato$^{+}$ enteric glia of all cells (Hoechst) were determined, and data shown as mean ± SEM; significance to poly-L-ornithine (used as a reference) *p < 0.05 and ***p < 0.001 (one-way ANOVA with Tukey's multiple comparisons test). Data points are from three technical replicates, representative for n = 2 independent experiments. **(C-E)** Enteric glia were isolated from C57BL6 mice and differentiated on the indicated coating substrates (scale bar 100 µm). **(C)** Representative immunofluorescence images of GFAP, αSMA, and nuclei (Hoechst) in enteric glia cultures on the indicated coatings. Arrows show GFAP$^{+}$ glial cells; arrowheads show αSMA$^{+}$ smooth muscle cells. **(D)** Representative immunofluorescence images of GFAP and SOX10 in enteric glia cultures on the indicated coatings. (**D'**) Percentage of GFAP$^{+}$ cells among all SOX10$^{+}$ cells in enteric glial cell cultures. Data show one experiment with 5 technical replicates representative for n = 3 biological replicates. Mean percentage per coating substrate: poly-L-ornithine = 94.52%, Matrigel = 96.79%, laminin = 95.22%. **(E)** Representative immunofluorescence images and corresponding close-up images showing GFAP (magenta), ANNA1 (yellow), and Synapsin 1/2/3 (green) in EGC cultures on indicated coatings.

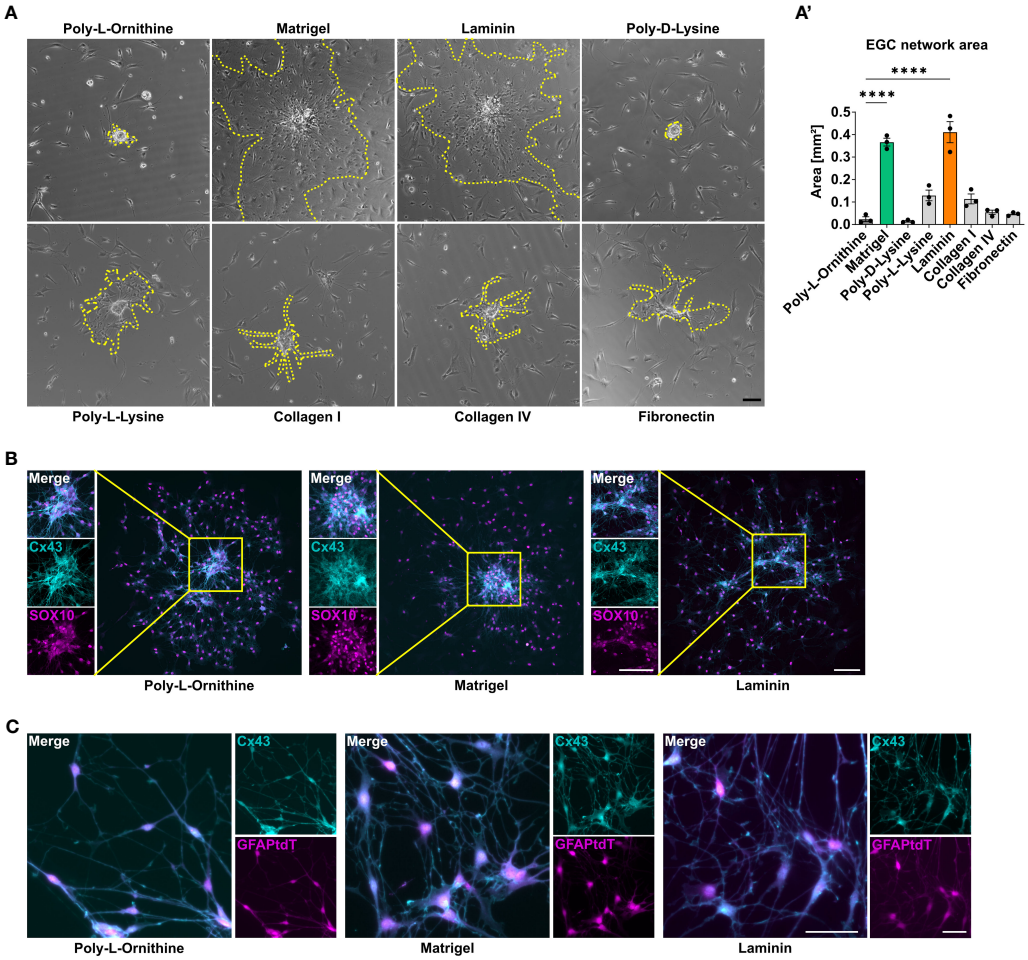


FIGURE 2
Matrigel and laminin advance primary enteric glial cell network formation. **(A, B)** Enteric glia were isolated from C57BL6 mice and differentiated on different coating substrates. Scale bar 100 µm. **(A)** Representative brightfield images of enteric glia network areas on the indicated coatings. The yellow dotted lines mark the outgrowing glial network arising from one neurosphere. (**A'**) Quantification of enteric glia network area in immunofluorescence images at day three of differentiation on different coating substrates. Data are shown as mean ± SEM and significance to poly-L-ornithine is displayed as ****p < 0.0001 (one-way ANOVA with Tukey's multiple comparisons test). The data show an experiment with three technical replicates. Five neurosphere network areas were measured for each replicate. Data representative for n = 3 independent experiments. **(B)** Representative immunofluorescence images of connexin (Cx) 43 and SOX10 in enteric glia cultures on the indicated coatings showing Cx43 and SOX10 co-staining and corresponding close-up images of outgrowing sphere regions (scale bar 100 µm). **(C)** Enteric glia were isolated from $GFAP^{Cre}Ai14^{fl/fl}$ mice and differentiated on the indicated coating substrates. Representative immunofluorescence images of $tdTomato^{+}$ glia and Cx43 in enteric glia connections (scale bar 50 µm).

concentrations. Again, the lowest Matrigel concentration showed a slightly higher potency than the recommended one, but this difference was not significant. For laminin, the standard concentration was surpassing both other concentrations (Supplementary Figure S1D).

As connexin-43 (Cx43) hemichannels have been shown to be required for intercellular signal transduction and communication in glial networks *in vivo* (32), we studied the formation of Cx43. Cx43 expression was detected in enteric glia in all coating conditions, both in outgrowing network forming areas and spheres, suggesting that all studied coatings allow functional glial network formation *in vitro* (Figures 2B, C).

Together, Matrigel and laminin yielded the highest purity and network formation capacity among the tested ECM substrates and therefore, we performed all following experiments with the standard concentrations of these both coatings in comparison to poly-L-ornithine as a reference.

## Enteric glia on Matrigel and laminin coating display similar transcriptional profiles but differ from poly-L-ornithine

Since the influence of ECM constituents reaches beyond cell morphology, culture purity and cellular network formation, we next analyzed the transcriptomic differences of enteric glia cultured on Matrigel, laminin or poly-L-ornithine. Principal component analysis revealed a separation of enteric glial cultured on poly-L-ornithine from those cultured on Matrigel or laminin, which were very similar (Figure 3A). Looking at the number of differentially

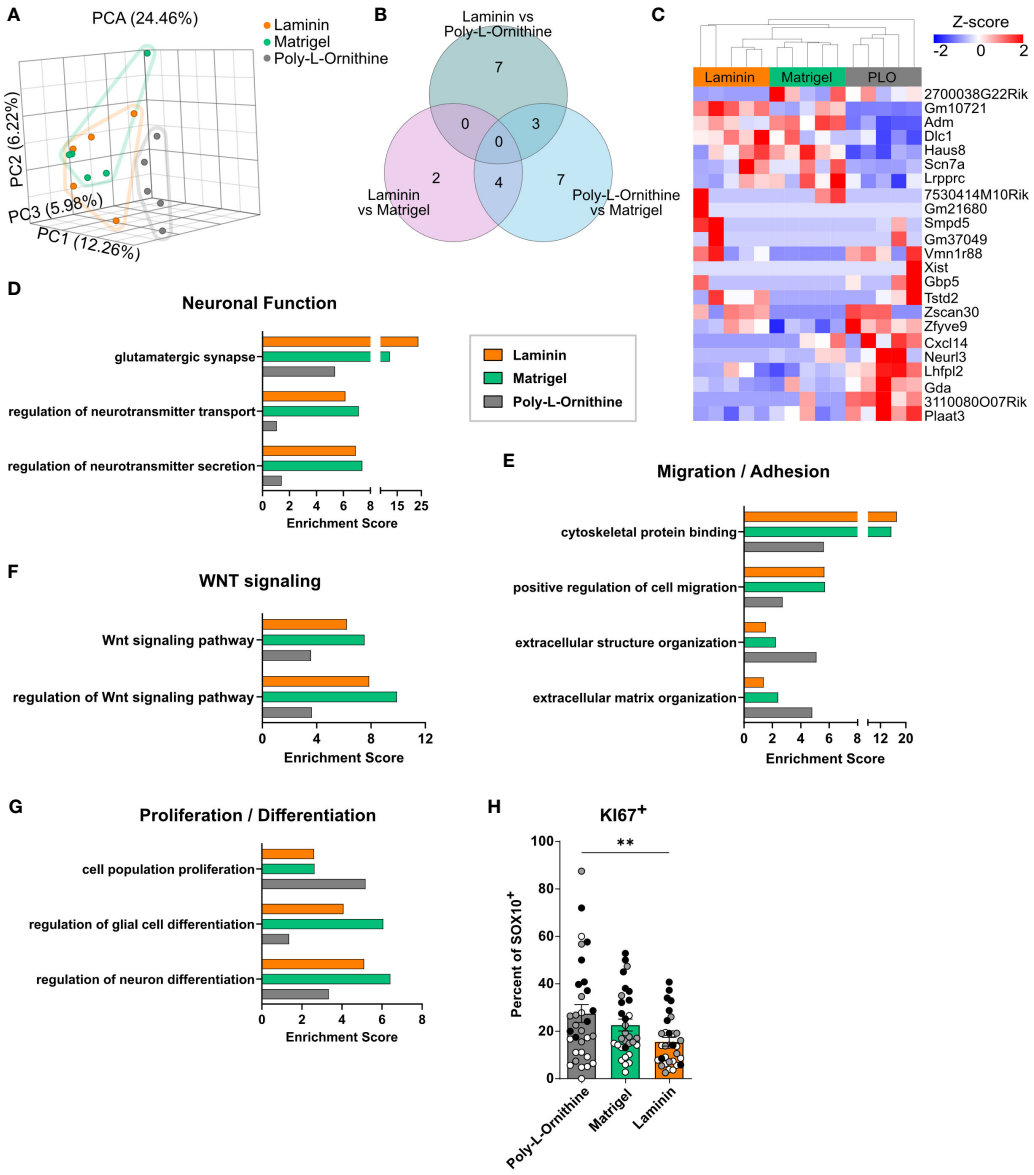


FIGURE 3
Enteric glia on Matrigel and laminin coating display similar transcriptional profiles but differ from poly-L-ornithine. **(A-G)** Enteric glia were isolated from C57BL6 mice, differentiated on indicated coatings, and processed for bulk 3' mRNA sequencing (n = 5 biological replicates). **(A)** Principal component analysis (PCA) of enteric glial cell cultures on different coatings. Each dot represents one biological replicate. **(B, C)** Venn diagram **(B)** and heatmap **(C)** showing differentially expressed genes of enteric glia on different coating substrates (FDR < 0.05). PLO = poly-L-ornithine. **(D-G)** Gene set enrichment analysis for genes highly expressed (maximum counts > 15) by enteric glia under naive conditions on poly-L-ornithine (grey), Matrigel (green) and laminin (orange) coating. Selected gene sets are displayed and related to neuronal function **(D)**, migration/adhesion **(E)**, WNT signaling **(F)** and proliferation/differentiation **(G)**. **(H)** Enteric glia were isolated from C57BL6 mice and differentiated on indicated coatings. Percentage of KI67$^+$ cells of SOX10$^+$ glia were determined in EGC cultures. Data are shown as mean ± SEM and significance is displayed as **p < 0.01 (one-way ANOVA with Tukey's multiple comparisons test). The data show 10-12 spheres per coating and per biological replicate (n = 3). Dots are colored by biological replicate.

expressed genes (DEG), we found laminin and Matrigel showing the lowest amount of DEG (6 genes), while poly-L-ornithine differed from Matrigel or laminin by 14 and 10 genes, respectively (Figure 3B). Hierarchical clustering of these DEGs confirmed increased expression of genes related to homeostasis (*Adm* (33)), cytoskeletal organization and migration (*Dlc1*, *Haus8*, *Lrpprc*) as well as signal transduction (*Scn7a* (34)) in enteric glia on Matrigel and laminin compared to poly-L-ornithine. Interestingly, recent single-cell RNAseq studies found a strong expression of *Scn7a* in enteric glia and a subset of stromal cells but not in enteric neurons[3]. Genes with higher expression in enteric glia on poly-L-ornithine were related to membrane damage (*Plaat3*) and

inflammatory pathways (*Gbp5* (35), *Zfyve9*, *Neurl3*). The latter genes were described as more expressed in enteric glia than enteric neurons[3]. Although typical glial markers like *Sox10*, *Gfap*, *Plp1* or *S100b* were not differentially expressed between the three different coating conditions, DEGs related to homeostasis, signal transduction, and inflammation supported our hypothesis of a difference between Matrigel and laminin versus poly-L-ornithine cultured glia (Figure 3C).

To further address the transcriptional pathways activated in enteric glia by different coating substrates, we performed a gene set enrichment analysis of highly expressed genes (maximum counts > 15) for each coating. Here, we found gene sets related to neuronal functions, such as "glutamatergic synapse", "regulation of neurotransmitter transport", and "regulation of neurotransmitter secretion" enriched in Matrigel and laminin (Figure 3D). As we could only rarely detected neurons in our glial cultures, these enrichments indicate a neurosupportive function of enteric glia and not differentiation of the glia towards a neuronal phenotype. Moreover, gene sets related to "cytoskeletal protein binding" and "positive regulation of cell migration" showed 2-fold enrichment in Matrigel and laminin compared to poly-L-ornithine, suggesting higher regulation of genes related to adhesion and cell motility (Figure 3E). On the other hand, enteric glia on poly-L-ornithine showed stronger enrichment of the GO terms "extracellular structure organization" and "extracellular matrix organization", hinting at an enhanced reaction of enteric glia to their "artificial" environment. Interestingly, gene sets for "Wnt signaling pathway" and "regulation of Wnt signaling pathway" displayed more pronounced enrichment scores in Matrigel- and laminin-treated enteric glia, suggesting functional differences of these cells regarding Wnt-induced neural differentiation processes (36) and Wnt-regulated epithelial homeostasis, a well-known feature of enteric glia (37) (Figure 3F). Importantly, gene sets for "regulation of glial cell differentiation" and "regulation of neuron differentiation" were enriched in Matrigel- and laminin-treated glia, while poly-L-ornithine-treated glia exhibited enrichment for the gene set "cell population proliferation" (Figure 3G). To further analyze the aspect of proliferation, we quantified the amount of $KI67^+$ cells in EGC cultures on different coatings. Indeed, the percentage of $KI67^+$ cells among the $SOX10^+$ enteric glia was significantly higher in poly-L-ornithine compared to laminin cultures, with a similar trend, although not significant, compared to Matrigel (Figure 3H, Supplementary S2A, B). Together, this suggests a rather proliferative state of cells on poly-L-ornithine and a more differentiated enteric glia phenotype on Matrigel and laminin coatings.

In conclusion, transcriptomes of enteric glia on different coating substrates revealed differential expression of genes related to homeostasis, migration, adhesion, Wnt signaling and neuronal cell differentiation, identifying Matrigel and laminin as substrates, potentially promoting glial cell differentiation and homeostatic functionality *in vitro*.

3 www.gutcellatlas.org.

## Enteric glial *in vitro* and *in vivo* depict distinct transcriptomic differences

As cell culture models should mimic *in vivo* states, our next goal was to compare (*in vitro*) enteric glia on different coating substrates with their native (*in vivo*) counterparts. To this end, we used $Sox10^{iCreERT2}Rpl22^{HA/+}$ (*RiboTag*) mice, which enable glial-cell specific mRNA isolation directly from tissues (29) (Supplementary Figure S3A). Principal component analysis of RNAseq data showed clear differences between the *in vivo* and *in vitro* cultured glia (Supplementary Figure S3B). PC1-related genes were responsible for the vast difference (28.18%) between all samples. However, disregarding quantitative differences among the top 1000 genes expressed in each condition, we found about 60% overlap between *in vitro* and *in vivo* samples, not differing between the tested coatings (poly-L-ornithine: 60.1%, Matrigel: 60.5%, laminin 60.4%). Overall, 569 of 1000 genes overlapped between all *in vitro* and *in vivo* conditions, hinting at the conservation of ~57% of genes *in vitro*. Interestingly, 369 genes were only expressed in the *RiboTag* group, and 336 genes were exclusively expressed within all *in vitro* conditions (Supplementary Figure S3C), highlighting also substantial differences between *in vivo* and *in vitro* enteric glia. To further address these differences, we evaluated the expression of marker genes uniquely expressed by enteric glia (derived from (38)). Although a few *in vitro* samples displayed high expression of single genes (*Aldh1a1*, *Clu*) comparable to the expression in *RiboTag* samples, the vast majority of genes, including *Gfap*, *S100b*, *Sox10,* and *Plp1*, showed a much stronger expression within the *in vivo* enteric glia, with no obvious differences between coating substrates (Supplementary Figure S3D). Together, these data suggest the existence of both a conserved genetic profile that is independent of the cellular environment and environmentally dependent genes whose expression differs between cultured and *in vivo* glia. Nevertheless, it should be noted that the transcriptional patterns detected *in vitro* are not uniquely representing enteric glia responses as other contaminating cell types are also included in these cultures. Our comparison with the *Ribotag* approach underlines the need for suitable *in vivo* model systems to study enteric glia biology.

## ECM substrates differentially affect reactive enteric glia transcriptomes after IL-1β activation

As enteric glia are of rising interest in inflammatory diseases, we next addressed the effect of coating substrates on enteric glial immune reactivity. Enteric glia were cultured on Matrigel, laminin or poly-L-ornithine and treated with interleukin-1β (IL-1β), a cytokine well-known to induce an immune-reactive state of enteric glia *in vivo* and *in vitro* (Figure 4A). *Il1r1* expression in enteric glia was comparable between all coatings under naive conditions and increased by IL-1β treatment in all coatings to the same extent (Supplementary Figure S4A). Protein concentration measurements of IL-6 and CCL2 in culture supernatants determined the reactivity of IL-1β-triggered enteric glia. We found significant and comparable increases of IL-6 and CCL2

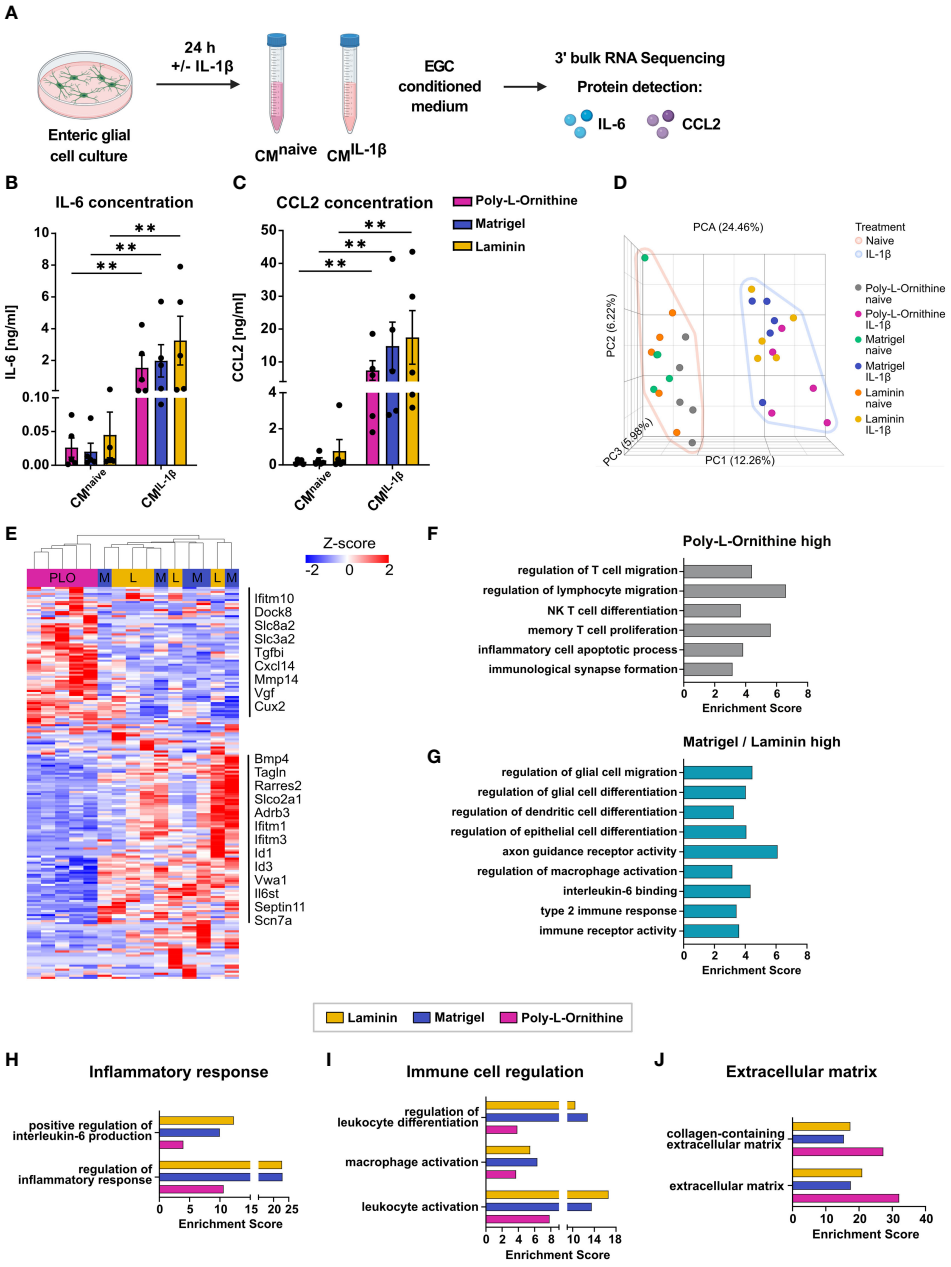


FIGURE 4
ECM substrates differentially affect reactive enteric glia transcriptomes after IL-1β activation. **(A-J)** Enteric glial cell cultures on poly-L-ornithine, Matrigel or laminin coating were treated with or without IL-1β (10 ng/ml) for 24h. Medium was collected for supernatant protein detection, and cells were processed for bulk 3' mRNA sequencing. **(A)** Schematic representation of enteric glia IL-1β stimulation. **(B, C)** Protein concentrations of IL-6 **(B)** and CCL2 **(C)** in enteric glia supernatants after stimulation with or without IL-1β on poly-L-ornithine (magenta), Matrigel (blue) or laminin (yellow) coating substrates. Data shown as mean ± SEM; significance to naive displayed as **p < 0.01 (two-way ANOVA with Šídák's multiple comparisons test). Each dot represents one biological replicate (n = 5). **(D)** Principal component analysis (PCA) of naive and IL-1β-treated primary enteric glia cultures on different coating substrates. Each dot represents one biological replicate (n = 5). **(E)** Heatmap of differentially expressed genes between IL-1β-treated enteric glial cultures. Displayed genes are differentially expressed between coatings (FDR < 0.05). Selected gene names are marked. PLO = Poly-L-ornithine, M = Matrigel, and L = laminin. **(F)** Gene set enrichment analysis of genes upregulated in IL-1β-treated enteric glia on poly-L-ornithine coating compared to IL-1β-treated enteric glia on Matrigel or laminin coatings (FDR < 0.05). **(G)** Gene set enrichment analysis of genes upregulated in IL-1β-treated enteric glia on Matrigel or laminin coatings compared to IL-1β-treated enteric glia on poly-L-ornithine coating (FDR < 0.05). **(H-J)** Gene set enrichment analysis of genes upregulated in IL-1β-treated vs. naive enteric glia for each coating (FDR < 0.05). Displayed gene sets are related to inflammatory response **(H)**, immune cell regulation **(I)**, and extracellular matrix **(J)**.

protein levels in IL-1β-treated enteric glia compared to naive glia for all coatings (Figures 4B, C), suggesting that although coating substrates affect enteric glia under naive conditions, their innate immune response regarding IL-6 and CCL2 protein secretion is unaffected by the ECM *in vitro*. This aligns with the overall transcriptional profile, as the principal component analysis of naive and IL-1β-treated enteric glia on different coatings revealed distinct clustering of all naive and all IL-1β-treated samples, with no

major differences between different coatings (Figure 4D). However, comparing only IL-1β-treated samples, differences between coating substrates became more evident, with poly-L-ornithine again differing from Matrigel and laminin (Supplementary Figure S4B).

We found 173 DEGs in IL-1β-triggered enteric glia with no overlap between all three coating substrates. Generally, gene expression was comparable between Matrigel and laminin but differed from poly-L-ornithine (Figure 4E, Supplementary S4C). Among all DEGs, a subset was upregulated in poly-L-ornithine but not in Matrigel or laminin, which included genes involved in immune cell recruitment and activation (*Ifitm10*, *Dock8*, *Cxcl14*), regulation of homeostatic calcium levels (*Slc8a2*, *Slc3a2*) and cell-collagen interactions (*Tgfbi*, *Mmp17*). Another subset was upregulated in Matrigel and laminin but not in poly-L-ornithine with genes related to glial immune functions and gliogenesis (*Bmp4*, *Tagln*, *Tmem176a*), signal transduction (*Slco2a1*, *Adrb3*, *Il6st*) or interferon-I signaling (*Ifitm1*, *Ifitm3*) (Figure 4E). To further resolve potential pathways related to this differential expression pattern, we performed gene set enrichment analysis for genes upregulated in enteric glia on poly-L-ornithine but not on Matrigel and laminin, as well as the other way around (Figures 4F,G). Interestingly, pathways enriched in enteric glia on poly-L-ornithine coating were related to T cell immunity and inflammatory processes (Figure 4F), while enteric glia on Matrigel or laminin showed enrichment for pathways in context to glial, epithelial and dendritic cell differentiation, as well as regulation of macrophage activation (Figure 4G). This suggests a potential functionally diverse immune state of enteric glia dependent on the coating substrate.

To further study the effect of the IL-1β stimulus between the different coatings, we compared IL-1β-treated enteric glia to their respective naive control. Although IL-1β-activation resulted in similar numbers of up- and downregulated genes in all coatings (Matrigel: 349 up, 355 down; laminin: 340 up, 292 down; poly-L-ornithine: 341 up, 353 down), their functional implications differed. To this end, we found stronger enrichment of gene sets related to "regulation of inflammatory response" in enteric glia cultured on Matrigel and laminin than on poly-L-ornithine (Figures 4H). Interestingly, although no obvious differences were observed for IL-6 protein levels of enteric glial cultures (Figure 4B), the gene set "positive regulation of interleukin-6 production" showed stronger enrichment in laminin and Matrigel, compared to poly-L-ornithine coatings (Figure 4H). Confirming a potentially more pronounced involvement of enteric glia on Matrigel and laminin in immune regulation, gene sets related to immune cell activation and differentiation also displayed higher enrichment scores and expression levels (Figure 4I, Supplementary S4D). Notably, gene sets associated with ECM biology showed higher enrichment scores in enteric glia on poly-L-ornithine compared to Matrigel and laminin, as observed under naive conditions (Figure 4J).

Subsumed, IL-1β-triggered immune activation of enteric glial cells resulted in the secretion of proinflammatory mediators and the enrichment of immune regulating pathways in glia on all coating substrates. The transcriptional analysis of enteric glia on Matrigel and laminin compared to poly-L-ornithine coating showed distinct differences regarding their ability in glia-immune cell communication with glia on Matrigel and laminin affecting rather myeloid cells and glial maturation, while poly-L-ornithine affected their ability to act on lymphocyte immunity. Most gene sets related to immune responses were enriched in enteric glia on Matrigel and laminin, suggesting a stronger transcriptional response towards the IL-1β-stimulus with these coating substrates.

Taken together, our study revealed an impact of ECM substrates on both homeostatic and immune-reactive enteric glia *in vitro*. Given the superior action of Matrigel and laminin coatings on glial cell numbers, purity, networking formation, and leukocyte-related immune activity, both conditions are favored over others. Therefore, they should become standard in future studies, allowing researchers to standardize and better compare *in vitro* studies related to enteric glial biology.

# Discussion

Over the last few years, primary enteric glial cultures helped to identify novel interaction pathways of enteric glia with other intestinal cell types, including intestinal epithelial (39) and immune cells, such as macrophages (7). Various *in vivo* studies revealed an immunoactive role of enteric glia in intestinal diseases, and *in vitro* studies added further mechanistic insight into enteric glia-immune cell interactions (7, 9, 11, 13, 40). However, the influence of the non-cellular environment, particularly constituents of the ECM, on enteric glia immune responses needs to be better understood. As the intestinal ECM exhibits a complex architecture and is composed of various constituents, such as different collagens and laminins (41), it has a major impact on cellular functions, including differentiation and migration. While the effects of different ECM constituents on cellular and molecular responses of enteric glia are difficult to study *in vivo* and are mostly limited to immunohistochemical analyses, *in vitro* studies allow proper analyses under homeostasis and inflammatory stimuli.

## Impact of ECM substrates on enteric glia differentiation

Herein, we used primary neurosphere-derived enteric glial cells, which were first allowed to proliferate under floating culture conditions in non-coated plates. Afterwards, cells were allowed to attach to and differentiate on eight different ECM substrates. The coating substrates were chosen based on natural components of the ECM *in vivo* and/or widely used substrates in central or peripheral nervous system cultures and, notably, have been used before in primary enteric glial cultures: poly-L-ornithine (42), Matrigel (43), laminin (44), poly-D-lysine (45), poly-L-lysine (44, 46), collagen I (47), collagen IV (22), and fibronectin (44, 48) although only two ECM components are indeed highly abundant in the intestine, with collagen being most strongly expressed in submucosal and mucosal regions (49) and laminin in the *muscularis externa* (44). Except for Matrigel, all coating substrates are composed of only one type of matrix protein, while Matrigel is a mixture of ECM constituents, namely laminin (60%), collagen IV (30%), and entactin (8%) (43). Our data show that laminin and Matrigel coatings resulted in higher purity and percentage of enteric glia than all other conditions.

The differentiation process of primary enteric glia usually takes several days in murine neurosphere-derived cultures. At differentiation day three, GFAP$^+$ glial cells mostly do not express β3-tubulin, a neuronal marker (44) expressed during prolonged culture periods (more than seven days). The same study showed that after 21-24 days, enteric glial cell cultures even display stronger expression of β3-tubulin and induction of synaptic genes, i.e. PSD95, as well as a strong drop in GFAP and SOX10 marker expression. Notably, *in vivo*, enteric glia have the ability to trans-differentiate into neurons (25, 50); possibly, the same mechanisms can also be induced by certain *in vitro* conditions over time. In addition, evidence of glial cell de-differentiation was shown for Schwann cells *in vitro* (51) and increased expression of progenitor markers was found in enteric neural crest-derived cells after co-culture with enteric mesenchymal cells (52). In line, a single-cell study confirmed EGCs as neuronal progenitors *in vitro* (53). Together, these data suggest multi-functional properties of EGCs with the ability to adapt dependent on their *in vitro* environment. In our study, we first determined the percentage and, thereby, purity of glial cells in cultures seeded on different coating substrates, and among all substrates, Matrigel and laminin delivered the highest percentages of glial cell numbers. However, glial cultures are never 100% pure, and it is well established that enteric neurospheres can give rise to enteric neurons and enteric glia during differentiation (17, 44). Interestingly, cocultures of enteric glia and fibroblasts with laminin coating have been shown to support glial differentiation while inhibiting neurogenesis (44). By immunostaining for ANNA1, a pan-neuronal marker not expressed by enteric glia, and synapsin 1/2/3, we confirmed that the outgrowing and network-forming cells are indeed glia, not neurons. A few ANNA1$^+$ neurons remain within the core of the differentiating neurosphere, but synapsin-expressing neurons are very rare at this state. A similar observation was previously defined as "neurocore" and was described for CNS neurospheres with detectable neurons only in the sphere's core at day three of differentiation (54), proving that the aggregation of young neurons initiates this structure. The same mechanism could apply to our ENS cultures. Of note, different enteric glia subsets with differential marker expression have been described *in vivo* (53, 55). Quantifying SOX10 and GFAP signals, we did not observe enteric glial subsets in our *in vitro* cultures. In general, the number of primary cells and culture purity are important aspects of *in vitro* studies. Others have described procedures resulting in a surprisingly high percentage of more than 95% when cells were isolated from mucosal and submucosal regions but not proliferated as neurospheres but as single-cell suspensions (56). However, although these cells express GFAP, they did not form prototypically long extensions but built islets of unconnected cells rather than an interconnected glia network. As the differentiation state of primary cells is equally relevant as their purity, primary enteric glia cultures should also be analyzed for the differentiation features of network formation. The area size of these networks surrounding the neurospheres can be used as an indication of cell differentiation (28). While neurosphere differentiation areas were biggest with Matrigel and laminin coatings, poly-L-ornithine and other coatings displayed only small regions of differentiating cells. In line, transcriptional analysis of enteric glia on Matrigel and laminin revealed enrichment of gene sets related to neuronal cell differentiation and Wnt signaling, both needed for epithelium maintenance and integrity (37). Poly-L-ornithine-treated glia displayed increased numbers of KI67$^+$ cells, enrichment of GO terms related to cellular proliferation, and ECM structure and organization. As this suggests a potentially stronger reaction to the ECM environment, one could speculate about a higher need for EGCs on poly-L-ornithine in remodeling or even new production of a suitable ECM environment. Therefore, we propose a direct effect of Matrigel and laminin on enteric glia, promoting differentiation, which resulted in enteric glial network formation on day three of differentiation. On the other hand, poly-L-ornithine, as well as poly-D-lysine, poly-L-lysine, collagen I, collagen IV, and fibronectin displayed comparatively slower differentiation as shown by sphere outgrowth and for poly-L-ornithine, also transcriptionally. Notably, we cannot exclude an effect of the reduced glial cell number and purity in poly-L-ornithine compared to Matrigel and laminin on the transcriptional analysis. However, coating substrates with less differentiation capacity in our study have been widely used at later differentiation stages in other studies, hinting at a slower but not generally compromised differentiation of enteric glia cultured on these substrates. Besides the outgrowth and the morphological observation of network formation, the expression of Cx43 is a prerequisite for enteric glial differentiation and intercellular communication. Cx43 hemichannels are also needed for the promotion of hypersensitivity during inflammation (10, 32) as well as control of neuronal death by glial-released nitric oxide and ATP (57). As we found a clear expression of Cx43, independent of the tested ECM coatings, we conclude that enteric neurosphere-derived glia growing on ECM substrates are, per se, able to form functional networks, with network areas being coating-specific.

Of note, the efficacy of some ECM substrates, such as Matrigel and laminin, was dependent on their concentration, while concentration-dependent differences were weaker in poly-L-ornithine. Generally, the manufacturer´s recommended concentrations yielded preferable results, compared with 2.5-fold higher and 5-fold lower concentrations not significantly improving experimental outcomes. For Matrigel, however, the lower concentration resulted in a non-significant slight enrichment in EGC percentage, numbers and area, suggesting that Matrigel could be used more cost-efficiently with higher dilutions. Still, optimal concentrations in terms of price-performance ratio would need further evaluation. As Matrigel's primary components are laminin (60%) and collagen IV (30%) (58), it is not unexpected that Matrigel is also a superior coating material, but this has so far never been shown. This finding is of particular interest for coculture experiments as it confirms that enteric glia differentiate well on Matrigel and can, therefore, be used in direct 3D coculture systems with epithelial organoid cultures, which are typically grown in Matrigel. As epithelial organoid cultures have been just stimulated with glial culture supernatants instead of applying direct cocultures (37, 59, 60), this would be a major advantage in studies interested in the direct intercellular communication between primary enteric glia and enterocytes.

## Comparison of *in vitro* and *in vivo* enteric glia

Another important finding of this study is the difference between enteric glia in culture and enteric glia *in vivo*. Using

$Sox10^{iCreERT2}Rpl22^{HA/+}$ mice, we generated *in vivo* transcriptomes of enteric glia from naive mice and compared these to the ones from primary enteric glial cultures on different ECMs. Among the top 1000 expressed genes, more than 50% overlapped between all samples, while more than 30% were solely expressed *in vivo* or in all *in vitro* conditions. No discernible difference was detected between coating substrates, which is likely due to the strong influence of the glial cell origin (*in vivo* versus *in vitro*) and the accompanying difference. We interpret the strong transcriptional difference due to multiple reasons. One of them is that the *Ribotag* approach delivers glial-specific transcriptomes, while the *in vitro* glial cultures contain further cell types. Another one is the microenvironmental differences between the *in vivo* and *in vitro* settings. Cell types, like neurons, with which glial cells usually interact and gain tissue-specific functionality *in vivo* and the complex extracellular matrix composition are missing in the *in vitro* cultures. However, it remains an open question whether cultured glial cells would become more closely related to *in vivo* glia after being cultured for longer periods and/or in the presence of other cells, typically surrounding them in the gut wall. At least some evidence exists for cocultures of enteric glia, for example, with fibroblasts, that promote glial differentiation (44) and with neurons, where both cell types support each other in cellular maturation (61). Accordingly, we hypothesize that cocultures of enteric glia with enteric neurons, fibroblasts, smooth muscle cells, or resident macrophages might trigger a more *in vivo*-like glial phenotype. Using enteric cell cultures from, e.g. $Sox10^{iCreERT2}Rpl22^{HA/+}$ mice would be an elegant tool to study glial-specific reactions within these cocultures.

## ECM substrates impact enteric glial immune reactivity

In the last years, enteric glia have been shown to exert immune-modulatory functions. Triggered by immune mediators like IFN-γ (3), IL-1β (8, 9), noradrenalin (40) or ATP (2), they switch into a "reactive" phenotype during inflammation, releasing immunomodulatory factors like cytokines and chemokines. Some of them have been identified to play a particular role in the pathogenesis of postoperative *muscularis externa* inflammation and colitis (i.e. IL-6 (2, 7, 38, 40), CCL2 (9) and CSF-1 (9, 13)), while others play a particular role in worm infection (i.e. CXCL10 (3)). Besides some of these well-known immune factors, extracellular basement membrane molecules, like laminin or ECM modeling enzymes, have been shown to be an important environmental cue in intestinal immune cell differentiation (23), transmigration (62) and immune tolerance (63). While the ECM composition evidently affects enteric glial biology, we wondered if it also changes their immune response. We stimulated enteric glia cultures on poly-L-ornithine, laminin and Matrigel with IL-1β, a well-established inflammatory mediator inducing enteric glial reactivity *in vitro* and *in vivo* (7, 9). All cultures responded with a strong IL-6 and CCL2 release with a non-significant trend of increased expression of both factors in the laminin-coated group. However, on the transcriptional level, we discovered that poly-L-ornithine-treated cells clustered differently from Matrigel and laminin-treated ones, which clustered together. Interestingly, within the GO terms derived from IL-1β-induced DEGs, glia cultured on laminin and Matrigel showed enrichment in gene clusters regulating glial migration, but also myeloid differentiation, macrophage activation and type 2 immune response. These GO terms are in line with recent literature describing the close proximity of glial cells with intestinal resident and monocyte-derived macrophages (7, 11). Herein, glial cells were not only shown to contribute to macrophage migration and their accumulation around myenteric ganglia (7, 11), but also to shape their differentiation during inflammation (9). Within the poly-L-ornithine IL-1β-stimulated cultures, we found an enrichment of genes related to lymphocyte migration, differentiation and proliferation. While the interaction of lymphocytes and enteric glia is so far less well understood, some studies indicate that T-cells interact with enteric glia, controlling Crohn's disease-associated myenteric plexitis in humans (64) and T-cell activation by antigen presentation (65). Furthermore, innate lymphoid cell type 3 (ILC3) aggregates were infiltrated by enteric glial projections, which can control ILC3's IL-22 production in a MyD88-dependent manner (66). Future studies must prove the potential impact of ECM composition on glial cell action regarding different immune cell populations. However, given that the gene expression signatures suggest a more pronounced immune response and effect of glia on leukocytes, particularly macrophages, with laminin and Matrigel coatings, these coatings might be preferable for studies addressing enteric glia-macrophage interactions.

## Overall impact

Subsumed, our findings revealed distinct differences in ECM substrates used for enteric glia cultures. Matrigel and laminin coatings delivered the highest enteric glia purity and the widest cellular network outgrowth. Transcriptional analysis of enteric glia on poly-L-ornithine displayed a decelerated differentiation, while Matrigel and laminin coatings promoted glial support in neuronal differentiation and gene signatures related to cell adhesion and migration. A significant amount of genes was expressed in both *in vivo* and *in vitro* enteric glia, but their expression levels also differed strongly in terms of EGC genes. Notably, the transcriptional *in vivo* and *in vitro* comparison comes with some shortcomings due to the cell culture purity but also the simplicity of the microenvironment *in vitro* compared to the *in vivo* condition. Furthermore, the IL-1β-induced immune reactivity of enteric glia differed between coating substrates and revealed that enteric glia on Matrigel and laminin coatings were transcriptionally more active regarding glial biology and myeloid immune cells, while poly-L-ornithine coating promoted pathways related to T cell immunity. Overall, Matrigel and laminin displayed strong similarities and surpassed poly-L-ornithine, as well as poly-D-lysine, poly-L-lysine, collagen I, collagen IV, and fibronectin in all investigated aspects. Our findings support the use of these superior ECM substrates to allow a better comparison of future studies related to enteric glial biology in homeostasis and neuroinflammation.

## Data availability statement

Sequencing data generated for this study are deposited in the Gene Expression Omnibus (GEO) database under the GEO accession code GSE271114, found here: https://www.ncbi.nlm.nih.gov/geo/query/acc.cgi?acc=GSE271114.

## Ethics statement

The animal study was approved by the state agency for nature, environment and consumer protection (LANUV, AZ 81-02.04.2021.A242). The study was conducted in accordance with the local legislation and institutional requirements.

## Author contributions

LS: Conceptualization, Data curation, Investigation, Methodology, Software, Visualization, Writing – original draft, Writing – review & editing, Formal analysis, Project administration, Validation. RS: Conceptualization, Project administration, Supervision, Writing – review & editing, Methodology. EH: Data curation, Writing – review & editing. SW: Conceptualization, Funding acquisition, Project administration, Resources, Supervision, Writing – original draft, Writing – review & editing, Methodology.

## Funding

The author(s) declare financial support was received for the research, authorship, and/or publication of this article. SW, LS and EH were supported by the DFG-funded ImmunoSensation2 cluster of excellence EXC2151-190873048. SW and RS received funding from BONFOR.

## Acknowledgments

We acknowledge all members of the group for the fruitful scientific discussions. We would like to thank Bianca Schneiker and Patrik Efferz for technical assistance. Furthermore, we acknowledge the Next Generation Sequencing core facility of the Medical Faculty, University of Bonn. We thank Prof. Christian Steinhäuser for providing the Cx43 antibody, Prof. Michael Wegener for the SOX10 antibody and the Mayo Clinic for the ANNA1 antibody. We thank Dr. Vassilis Pachnis for sharing the Sox10$^{iCreERT2}$ mice with us. BioRender was used for creating graphical images.

## Conflict of interest

The authors declare that the research was conducted in the absence of any commercial or financial relationships that could be construed as a potential conflict of interest.

## Publisher's note

All claims expressed in this article are solely those of the authors and do not necessarily represent those of their affiliated organizations, or those of the publisher, the editors and the reviewers. Any product that may be evaluated in this article, or claim that may be made by its manufacturer, is not guaranteed or endorsed by the publisher.

## Supplementary material

The Supplementary Material for this article can be found online at: https://www.frontiersin.org/articles/10.3389/fimmu.2024.1401751/full#supplementary-material

## References

1. Progatzky F, Pachnis V. The role of enteric glia in intestinal immunity. *Curr Opin Immunol.* (2022) 77:102183. doi: 10.1016/j.coi.2022.102183

2. Schneider R, Leven P, Glowka T, Kuzmanov I, Lysson M, Schneiker B, et al. A novel P2X2-dependent purinergic mechanism of enteric gliosis in intestinal inflammation. *EMBO Mol Med.* (2021) 13:e12724. doi: 10.15252/emmm.202012724

3. Progatzky F, Shapiro M, Chng SH, Garcia-Cassani B, Classon CH, Sevgi S, et al. Regulation of intestinal immunity and tissue repair by enteric glia. *Nature.* (2021) 599:125–30. doi: 10.1038/s41586-021-04006-z

4. Mazzotta E, Grants I, Villalobos-Hernandez E, Chaudhuri S, McClain JL, Seguella L, et al. BQ788 reveals glial ETB receptor modulation of neuronal cholinergic and nitrergic pathways to inhibit intestinal motility: Linked to postoperative ileus. *Br J Pharmacol.* (2023) 180:2550–76. doi: 10.1111/bph.16145

5. Liñán-Rico A, Turco F, Ochoa-Cortes F, Harzman A, Needleman BJ, Arsenescu R, et al. Molecular signaling and dysfunction of the human reactive enteric glial cell phenotype: implications for GI infection, IBD, POI, neurological, motility, and GI disorders. *Inflammation Bowel Dis.* (2016) 22:1812–34. doi: 10.1097/MIB.0000000000000854

6. Rosenbaum C, Schick MA, Wollborn J, Heider A, Scholz C-J, Cecil A, et al. Activation of myenteric glia during acute inflammation *in vitro* and in vivo. *PloS One.* (2016) 11:e0151335. doi: 10.1371/journal.pone.0151335

7. Schneider R, Leven P, Mallesh S, Breßer M, Schneider L, Mazzotta E, et al. IL-1-dependent enteric gliosis guides intestinal inflammation and dysmotility and modulates macrophage function. *Commun Biol.* (2022) 5:811. doi: 10.1038/s42003-022-03772-4

8. Stoffels B, Hupa KJ, Snoek SA, van Bree S, Stein K, Schwandt T, et al. Postoperative ileus involves interleukin-1 receptor signaling in enteric glia. *Gastroenterology.* (2014) 146:176–87.e1. doi: 10.1053/j.gastro.2013.09.030

9. Stakenborg M, Abdurahiman S, de Simone V, Goverse G, Stakenborg N, van Baarle L, et al. Enteric glial cells favor accumulation of anti-inflammatory macrophages during the resolution of muscularis inflammation. *Mucosal Immunol.* (2022) 15:1296–308. doi: 10.1038/s41385-022-00563-2

10. Morales-Soto W, Gonzales J, Jackson WF, Gulbransen BD. Enteric glia promote visceral hypersensitivity during inflammation through intercellular signaling with gut nociceptors. *Sci Signal.* (2023) 16:eadg1668. doi: 10.1126/scisignal.adg1668

11. Dora D, Ferenczi S, Stavely R, Toth VE, Varga ZV, Kovacs T, et al. Evidence of a myenteric plexus barrier and its macrophage-dependent degradation during murine colitis: implications in enteric neuroinflammation. *Cell Mol Gastroenterol Hepatol.* (2021) 12:1617–41. doi: 10.1016/j.jcmgh.2021.07.003

12. Gonzalez Acera M, Bubeck M, Mascia F, Diemand L, Sturm G, Kühl AA, et al. Dynamic, transient, and robust increase in the innervation of the inflamed mucosa in inflammatory bowel diseases. *Cells.* (2021) 10. doi: 10.3390/cells10092253

13. Grubišić V, McClain JL, Fried DE, Grants I, Rajasekhar P, Csizmadia E, et al. Enteric glia modulate macrophage phenotype and visceral sensitivity following inflammation. *Cell Rep.* (2020) 32:108100. doi: 10.1016/j.celrep.2020.108100

14. Boesmans W, Hao MM, Fung C, Li Z, van den Haute C, Tack J, et al. Structurally defined signaling in neuro-glia units in the enteric nervous system. *Glia*. (2019) 67:1167–78. doi: 10.1002/glia.23596

15. Rühl A, Trotter J, Stremmel W. Isolation of enteric glia and establishment of transformed enteroglial cell lines from the myenteric plexus of adult rat. *Neurogastroenterol Motil*. (2001) 13:95–106. doi: 10.1046/j.1365-2982.2001.00246.x

16. Zanoletti L, Valdata A, Nehlsen K, Faris P, Casali C, Cacciatore R, et al. Cytological, molecular, cytogenetic, and physiological characterization of a novel immortalized human enteric glial cell line. *Front Cell Neurosci*. (2023) 17:1170309. doi: 10.3389/fncel.2023.1170309

17. Chen J-C, Yang W, Tseng L-Y, Chang H-L. Enteric neurospheres retain the capacity to assemble neural networks with motile and metamorphic gliocytes and ganglia. *Stem Cell Res Ther*. (2023) 14:290. doi: 10.1186/s13287-023-03517-y

18. Mueller JL, Stavely R, Guyer RA, Soos Á, Bhave S, Han C, et al. Agrin inhibition in enteric neural stem cells enhances their migration following colonic transplantation. *Stem Cells Transl Med*. (2024) 13:490–504. doi: 10.1093/stcltm/szae013

19. Rauti R, Renous N, Maoz BM. Mimicking the brain extracellular matrix in vitro A review of current methodologies and challenges. *Israel J Chem*. (2020) 60:1141–51. doi: 10.1002/ijch.201900052

20. Bannerman PG, Mirsky R, Jessen KR, Timpl R, Duance VC. Light microscopic immunolocalization of laminin, type IV collagen, nidogen, heparan sulphate proteoglycan and fibronectin in the enteric nervous system of rat and Guinea pig. *J Neurocytol*. (1986) 15:733–43. doi: 10.1007/BF01625191

21. Nakazawa N, Miyahara K, Okawada M, Yamataka A, Suzuki R, Akazawa C, et al. Laminin-1 promotes enteric nervous system development in mouse embryo. *Pediatr Surg Int*. (2013) 29:1205–8. doi: 10.1007/s00383-013-3388-3

22. Raghavan S, Gilmont RR, Bitar KN. Neuroglial differentiation of adult enteric neuronal progenitor cells as a function of extracellular matrix composition. *Biomaterials*. (2013) 34:6649–58. doi: 10.1016/j.biomaterials.2013.05.023

23. Li L, Song J, Chuquisana O, Hannocks M-J, Loismann S, Vogl T, et al. Endothelial basement membrane laminins as an environmental cue in monocyte differentiation to macrophages. *Front Immunol*. (2020) 11:584229. doi: 10.3389/fimmu.2020.584229

24. Jha A, Moore E. Laminin-derived peptide, IKVAV, modulates macrophage phenotype through integrin mediation. *Matrix Biol Plus*. (2024) 22:100143. doi: 10.1016/j.mbplus.2024.100143

25. Laranjeira C, Sandgren K, Kessaris N, Richardson W, Potocnik A, Vanden Berghe P, et al. Glial cells in the mouse enteric nervous system can undergo neurogenesis in response to injury. *J Clin Invest*. (2011) 121:3412–24. doi: 10.1172/JCI58200

26. Wüst HM, Wegener A, Fröb F, Hartwig AC, Wegwitz F, Kari V, et al. Egr2-guided histone H2B monoubiquitination is required for peripheral nervous system myelination. *Nucleic Acids Res*. (2020) 48:8959–76. doi: 10.1093/nar/gkaa606

27. Khan D, Dupper A, Deshpande T, de Graan PN, Steinhäuser C, Bedner P. Experimental febrile seizures impair interastrocytic gap junction coupling in juvenile mice. *J Neurosci Res*. (2016) 94:804–13. doi: 10.1002/jnr.23726

28. Mucci S, Rodriguez-Varela MS, Isaja L, Ferriol-Laffouillere SL, Sevlever GE, Scassa ME, et al. Protocol for morphometric analysis of neurons derived from human pluripotent stem cells. *STAR Protoc*. (2022) 3:101487. doi: 10.1016/j.xpro.2022.101487

29. Leven P, Schneider R, Siemens KD, Jackson WS, Wehner S. Application of a RiboTag-based approach to generate and analyze mRNA from enteric neural cells. *Neurogastroenterol Motil*. (2022) 34:e14309. doi: 10.1111/nmo.14309

30. Tanti GK, Srivastava R, Kalluri SR, Nowak C, Hemmer B. Isolation, culture and functional characterization of glia and endothelial cells from adult pig brain. *Front Cell Neurosci*. (2019) 13:333. doi: 10.3389/fncel.2019.00333

31. Hu H, Ding Y, Mu W, Li Y, Wang Y, Jiang W, et al. DRG-derived neural progenitors differentiate into functional enteric neurons following transplantation in the postnatal colon. *Cell Transplant*. (2019) 28:157–69. doi: 10.1177/0963689718811061

32. McClain J, Grubišić V, Fried D, Gomez-Suarez RA, Leinninger GM, Sévigny J, et al. Ca2+ responses in enteric glia are mediated by connexin-43 hemichannels and modulate colonic transit in mice. *Gastroenterology*. (2014) 146:497–507.e1. doi: 10.1053/j.gastro.2013.10.061

33. Martínez-Herrero S, Martínez A. Adrenomedullin: not just another gastrointestinal peptide. *Biomolecules*. (2022) 12. doi: 10.3390/biom12020156

34. Dolivo D, Rodrigues A, Sun L, Li Y, Hou C, Galiano R, et al. The Nax (SCN7A) channel: an atypical regulator of tissue homeostasis and disease. *Cell Mol Life Sci*. (2021) 78:5469–88. doi: 10.1007/s00018-021-03854-2

35. Li Y, Lin X, Wang W, Wang W, Cheng S, Huang Y, et al. The proinflammatory role of guanylate-binding protein 5 in inflammatory bowel diseases. *Front Microbiol*. (2022) 13:926915. doi: 10.3389/fmicb.2022.926915

36. Scharr M, Hirt B, Neckel PH. Spatial gene expression profile of Wnt-signaling components in the murine enteric nervous system. *Front Immunol*. (2024) 15:1302488. doi: 10.3389/fimmu.2024.1302488

37. Baghdadi MB, Ayyaz A, Coquenlorge S, Chu B, Kumar S, Streutker C, et al. Enteric glial cell heterogeneity regulates intestinal stem cell niches. *Cell Stem Cell*. (2022) 29:86–100.e6. doi: 10.1016/j.stem.2021.10.004

38. van Baarle L, de Simone V, Schneider L, Santhosh S, Abdurahiman S, Biscu F, et al. IL-1R signaling drives enteric glia-macrophage interactions in colorectal cancer. (2023). doi: 10.1101/2023.06.01.543246

39. Prochera A, Rao M. Mini-Review: Enteric glial regulation of the gastrointestinal epithelium. *Neurosci Lett*. (2023) 805:137215. doi: 10.1016/j.neulet.2023.137215

40. Leven P, Schneider R, Schneider L, Mallesh S, Vanden Berghe P, Sasse P, et al. β-adrenergic signaling triggers enteric glial reactivity and acute enteric gliosis during surgery. *J Neuroinflamm*. (2023) 20:255. doi: 10.1186/s12974-023-02937-0

41. Pompili S, Latella G, Gaudio E, Sferra R, Vetuschi A. The charming world of the extracellular matrix: A dynamic and protective network of the intestinal wall. *Front Med (Lausanne)*. (2021) 8:610189. doi: 10.3389/fmed.2021.610189

42. Yuan H, Hu H, Chen R, Mu W, Wang L, Li Y, et al. Premigratory neural crest stem cells generate enteric neurons populating the mouse colon and regulating peristalsis in tissue-engineered intestine. *Stem Cells Transl Med*. (2021) 10:922–38. doi: 10.1002/sctm.20-0469

43. Zhang Y, Hu W. Mouse enteric neuronal cell culture. *Methods Mol Biol*. (2013) 1078:55–63. doi: 10.1007/978-1-62703-640-5_6

44. Veríssimo CP, Da Carvalho JS, da Silva FJ, Campanati L, Moura-Neto V, Coelho-Aguiar Jd. Laminin and environmental cues act in the inhibition of the neuronal differentiation of enteric glia in *vitro*. *Front Neurosci*. (2019) 13:914. doi: 10.3389/fnins.2019.00914

45. Smith TH, Ngwainmbi J, Grider JR, Dewey WL, Akbarali HI. An in-vitro preparation of isolated enteric neurons and glia from the myenteric plexus of the adult mouse. *J Vis Exp*. (2013) 78:e50688. doi: 10.3791/50688

46. Melissa T, Bradley WA, Mariant CL, Alex HR, van Landeghem L. Enteric glial cells of the two plexi of the enteric nervous system exhibit phenotypic and functional inter- and intra-heterogeneity. (2022). doi: 10.1101/2022.06.28.497986

47. Bergsteinsdottir K, Hashimoto Y, Brennan A, Mirsky R, Jessen KR. The effect of three dimensional collagen type I preparation on the structural organization of Guinea pig enteric ganglia in culture. *Exp Cell Res*. (1993) 209:64–75. doi: 10.1006/excr.1993.1286

48. Laddach A, Chng SH, Lasrado R, Progatzky F, Shapiro M, Erickson A, et al. A branching model of lineage differentiation underpinning the neurogenic potential of enteric glia. *Nat Commun*. (2023) 14:5904. doi: 10.1038/s41467-023-41492-3

49. Baidoo N, Sanger GJ, Belai A. Histochemical and biochemical analysis of collagen content in formalin-fixed, paraffin embedded colonic samples. *MethodsX*. (2023) 11:102416. doi: 10.1016/j.mex.2023.102416

50. Sunardi M, Cirillo C. Mini-review: "Enteric glia functions in nervous tissue repair: Therapeutic target or tool?". *Neurosci Lett*. (2023) 812:137360. doi: 10.1016/j.neulet.2023.137360

51. Stavely R, Hotta R, Picard N, Rahman AA, Pan W, Bhave S, et al. Schwann cells in the subcutaneous adipose tissue have neurogenic potential and can be used for regenerative therapies. *Sci Transl Med*. (2022) 14:eabl8753. doi: 10.1126/scitranslmed.abl8753

52. Stavely R, Bhave S, Ho WL, Ahmed M, Pan W, Rahman AA, et al. Enteric mesenchymal cells support the growth of postnatal enteric neural stem cells. *Stem Cells*. (2021) 39:1236–52. doi: 10.1002/stem.3388

53. Guyer RA, Stavely R, Robertson K, Bhave S, Mueller JL, Picard NM, et al. Single-cell multiome sequencing clarifies enteric glial diversity and identifies an intraganglionic population poised for neurogenesis. *Cell Rep*. (2023) 42:112194. doi: 10.1016/j.celrep.2023.112194

54. Lee J-H, Shaker MR, Lee E, Lee B, Sun W. NeuroCore formation during differentiation of neurospheres of mouse embryonic neural stem cells. *Stem Cell Res*. (2020) 43:101691. doi: 10.1016/j.scr.2019.101691

55. Rao M, Rastelli D, Dong L, Chiu S, Setlik W, Gershon MD, et al. Enteric glia regulate gastrointestinal motility but are not required for maintenance of the epithelium in mice. *Gastroenterology*. (2017) 153:1068–1081.e7. doi: 10.1053/j.gastro.2017.07.002

56. Wang Z, Ocadiz-Ruiz R, Sundaresan S, Ding L, Hayes M, Sahoo N, et al. Isolation of enteric glial cells from the submucosa and lamina propria of the adult mouse. *J Vis Exp*. (2018) 138:57629. doi: 10.3791/57629

57. Brown IA, McClain JL, Watson RE, Patel BA, Gulbransen BD. Enteric glia mediate neuron death in colitis through purinergic pathways that require connexin-43 and nitric oxide. *Cell Mol Gastroenterol Hepatol*. (2016) 2:77–91. doi: 10.1016/j.jcmgh.2015.08.007

58. Aisenbrey EA, Murphy WL. Synthetic alternatives to matrigel. *Nat Rev Mater*. (2020) 5:539–51. doi: 10.1038/s41578-020-0199-8

59. Baghdadi MB, Kim T-H. Analysis of mouse intestinal organoid culture with conditioned media isolated from mucosal enteric glial cells. *STAR Protoc*. (2022) 3:101351. doi: 10.1016/j.xpro.2022.101351

60. Meir M, Kannapin F, Diefenbacher M, Ghoreishi Y, Kollmann C, Flemming S, et al. Intestinal epithelial barrier maturation by enteric glial cells is GDNF-dependent. *Int J Mol Sci*. (2021) 22. doi: 10.3390/ijms22041887

61. Gomes P, Chevalier J, Boesmans W, Roosen L, van den Abbeel V, Neunlist M, et al. ATP-dependent paracrine communication between enteric neurons and glia in a primary cell culture derived from embryonic mice. *Neurogastroenterol Motil*. (2009) 21:870–e62. doi: 10.1111/j.1365-2982.2009.01302.x

62. Nighot M, Ganapathy AS, Saha K, Suchanec E, Castillo EF, Gregory A, et al. Matrix metalloproteinase MMP-12 promotes macrophage transmigration across intestinal epithelial tight junctions and increases severity of experimental colitis. *J Crohns Colitis*. (2021) 15:1751–65. doi: 10.1093/ecco-jcc/jjab064

63. Au KM, Wilson JE, Ting JP-Y, Wang AZ. An injectable subcutaneous colon-specific immune niche for the treatment of ulcerative colitis. *Nat BioMed Eng*. (2023) 36:203–20. doi: 10.1038/s41551-023-01136-9

64. Pabois J, Durand T, Le Berre C, Filippone RT, Noël T, Durieu E, et al. Role of ICAM-1 in the Adhesion of T cells to Enteric Glia: Perspectives in the Formation of Plexitis in Crohn's disease. *Cell Mol Gastroenterol Hepatol*. (2024) 18:133–53. doi: 10.1016/j.jcmgh.2024.02.016

65. Chow AK, Grubišić V, Gulbransen BD. Enteric glia regulate lymphocyte activation via autophagy-mediated MHC-II expression. *Cell Mol Gastroenterol Hepatol*. (2021) 12:1215–37. doi: 10.1016/j.jcmgh.2021.06.008

66. Ibiza S, García-Cassani B, Ribeiro H, Carvalho T, Almeida L, Marques R, et al. Glial-cell-derived neuroregulators control type 3 innate lymphoid cells and gut defence. *Nature*. (2016) 535:440–3. doi: 10.1038/nature18644

## 3.2 Publication 2: Leven P and Schneider R, *et al.* 2023 – β-adrenergic signaling triggers enteric glial reactivity and acute enteric gliosis during surgery

Leven *et al. Journal of Neuroinflammation* (2023) 20:255
https://doi.org/10.1186/s12974-023-02937-0

Journal of Neuroinflammation

RESEARCH Open Access

# β-adrenergic signaling triggers enteric glial reactivity and acute enteric gliosis during surgery

Patrick Leven[1†], Reiner Schneider[1*†], Linda Schneider[1], Shilpashree Mallesh[1], Pieter Vanden Berghe[2], Philipp Sasse[3], Jörg C. Kalff[1] and Sven Wehner[1*]

**Abstract**

**Background** Enteric glia contribute to the pathophysiology of various intestinal immune-driven diseases, such as postoperative ileus (POI), a motility disorder and common complication after abdominal surgery. Enteric gliosis of the intestinal *muscularis externa* (*ME*) has been identified as part of POI development. However, the glia-restricted responses and activation mechanisms are poorly understood. The sympathetic nervous system becomes rapidly activated by abdominal surgery. It modulates intestinal immunity, innervates all intestinal layers, and directly interfaces with enteric glia. We hypothesized that sympathetic innervation controls enteric glia reactivity in response to surgical trauma.

**Methods** *Sox10*$^{iCreERT2}$/*Rpl22*$^{HA/+}$ mice were subjected to a mouse model of laparotomy or intestinal manipulation to induce POI. Histological, protein, and transcriptomic analyses were performed to analyze glia-specific responses. Interactions between the sympathetic nervous system and enteric glia were studied in mice chemically depleted of TH$^{+}$ sympathetic neurons and glial-restricted *Sox10*$^{iCreERT2}$/*JellyOP*$^{fl/+}$/*Rpl22*$^{HA/+}$ mice, allowing optogenetic stimulation of β-adrenergic downstream signaling and glial-specific transcriptome analyses. A laparotomy model was used to study the effect of sympathetic signaling on enteric glia in the absence of intestinal manipulation. Mechanistic studies included adrenergic receptor expression profiling in vivo and in vitro and adrenergic agonism treatments of primary enteric glial cell cultures to elucidate the role of sympathetic signaling in acute enteric gliosis and POI.

**Results** With ~ 4000 differentially expressed genes, the most substantial enteric glia response occurs early after intestinal manipulation. During POI, enteric glia switch into a reactive state and continuously shape their microenvironment by releasing inflammatory and migratory factors. Sympathetic denervation reduced the inflammatory response of enteric glia in the early postoperative phase. Optogenetic and pharmacological stimulation of β-adrenergic downstream signaling triggered enteric glial reactivity. Finally, distinct adrenergic agonists revealed β-1/2 adrenoceptors as the molecular targets of sympathetic–driven enteric glial reactivity.

**Conclusions** Enteric glia act as early responders during post-traumatic intestinal injury and inflammation. Intact sympathetic innervation and active β-adrenergic receptor signaling in enteric glia is a trigger of the immediate glial

†Patrick Leven and Reiner Schneider are contributed equally to the work.

*Correspondence:
Reiner Schneider
Reiner.Schneider@ukbonn.de
Sven Wehner
Sven.Wehner@ukbonn.de
Full list of author information is available at the end of the article

postoperative inflammatory response. With immune-activating cues originating from the sympathetic nervous system as early as the initial surgical incision, adrenergic signaling in enteric glia presents a promising target for preventing POI development.

**Keywords** Enteric glia, *RiboTag*, Gut inflammation, Postoperative ileus, Sympathetic nervous system, Neuroimmunology, Adrenergic Signaling

## Background

The enteric nervous system (ENS), consisting of enteric neurons and enteric glia, is a branch of the autonomous nervous system that governs various functions throughout the alimentary tract, such as gastric motility, fluid homeostasis, and blood flow [1]. Enteric glia are diverse neuroglia, displaying several subtypes based on morphology and location in intestinal structures [1]. Most enteric glia also show a unique co-expression pattern of SRY-Box transcription factor 10 (SOX10) together with either the glial markers S100B or glial fibrillary acidic protein (GFAP) [2], or proteolipid protein 1 (PLP1) [2, 3].

At first, enteric glia were mainly considered solely as neuron-supporting cell populations of the ENS, providing nutrition and protection for enteric neurons [1]. More recent studies provided new insights into enteric glia involvement in gastrointestinal (GI) homeostasis [1] and discovered their vital role in chronic [4] and acute [5] gut inflammation. Enteric glia switch to a reactive state during gut inflammation, altering their morphology, expression pattern, and functional character [1]. So far, broader enteric glial reactivity in POI has only been analyzed in vivo in the full tissue context, also described as a POI-related "enteric gliosis", but cell-intrinsic molecular responses of enteric glia and their primary activating mechanism were still missing. We termed the reactive inflammatory tissue state of the muscularis externa tissue "enteric gliosis" [5] as it shares molecular expression patterns with tissue gliosis in the central nervous system (CNS). Notably, this CNS gliosis is defined by the reactivity of glial cells, such as microglia, oligodendrocytes, and most importantly, astrocytes [6], the counterpart to enteric glia, which become activated during neuroinflammation in chronic disease states [7, 8] and after neurological traumata [9].

Part of the enteric gliosis state are reactive enteric glia, which modulate their microenvironment by secreting cytokines and chemokines like interleukin (IL)-6, C–C motif chemokine ligand (CCL)-2 [5, 10], and C–X–C motif chemokine ligand (CXCL)-10 [11], pro-inflammatory molecules, such as nitric oxide [12], and molecules that elicit an anti-inflammatory response, including glial cell-derived neurotrophic factor (GDNF) [13] and S-Nitrosoglutathione [14].

Although a comprehensive picture of reactive enteric glia in intestinal inflammation is still missing, recent studies provide evidence about stimuli being able to induce gliosis in the gut. These include lipopolysaccharide (LPS) [15], cytokines such as interleukin (IL)-1β [10], tumor necrosis factor (TNF)α [16], and interferon-gamma (IFNγ) [17], as well as purines, e.g., ADP [4] or ATP [5]. The latter is released by both intrinsic and extrinsic enteric neurons innervating the gut and is co-released with norepinephrine (NE) from sympathetic neurons. NE is the principal neurotransmitter of the sympathetic nervous system (SNS) [18], known to interact with enteric glia through adrenergic receptors [19]. More recently, several publications highlighted the involvement of the SNS in inflammation-based infectious [20] and non-infectious bowel diseases [21] and its ambivalent effect on the inflammatory milieu, depending on the disease stage, neurotransmitter concentration, and receptor binding [22].

We recently showed that the SNS affects the postoperative inflammatory immune cell milieu in postoperative ileus (POI) and functionally impacts the disease progression [23]. POI is a frequent transient GI-motility disorder and complication of abdominal surgery. Patients with POI suffer from nausea, abdominal distension pain, reduced oral food tolerance, delayed recovery, and finally, an extended hospitalization phase with a high medico-economic burden on our health care systems [24]. A prominent response to abdominal surgery is a dysbalance of the sympathetic and parasympathetic inputs of the intestine towards sympathetic overactivation. Notably, this sympathetic overactivity is already induced by the skin incision [25], and the subsequent surgical manipulation of the intestine (or other visceral organs) enhances this overactivity. Hallmarks of enteric gliosis have been identified as part of POI (5, 10, 26) and are discussed to be of potential value for therapeutic interventions in POI and other intestinal inflammation-driven diseases [26]. As SNS-released mediators directly act on enteric glia [19, 27], we hypothesized that adrenergic signaling might be an early trigger of acute postoperative enteric glial reactivity in the onset phase of POI.

To test this hypothesis, we used *Sox10*$^{iCreERT2}$/*Rpl22*$^{HA/+}$ mice to extract cell-specific mRNA from hemagglutinin-labeled ribosomes of enteric glia [28, 29]

within three phases of POI: the immediate initiation phase, the manifestation, and the resolution phase. We found striking evidence of strong enteric glial reactivity in the immediate postoperative phase. Furthermore, we discovered that laparotomy, the first step of abdominal surgery, which does not include manipulation of any other visceral organs, is sufficient to trigger enteric glial activation in the intestine. Sympathetic denervation studies, live calcium imaging in ex vivo ganglia, enteric glia-restricted optogenetic activation of β-adrenergic downstream signaling in *Sox10$^{iCreERT2}$/JellyOP$^{fl/+}$/Rpl22$^{HA/+}$* mice, and stimulation of primary EGC cultures gave insight into the distinct β-adrenergic signaling pathways triggering enteric glial reactivity in POI.

## Materials and methods

### Materials

#### *Animals*

*Sox10$^{iCreERT2}$* (*B6-Tg(Sox10-icre/ERT2)388Wdr/J*) mice were crossbred with *Rpl22$^{HA/+}$* (*B6N.129-Rpl22tm1.1Psam/J*)/tdTomato (*B6;129S6-Gt(ROSA)26Sortm14(CAG-tdTomato)Hze*) mice. Additionally, *Sox10$^{iCreERT2}$/RiboTag/tdTomato* were crossbred with *JellyOP* mice (*CD1-Gt(ROSA)26Sor$^{em1(CAG-JellyOp-eGFP)}$*; Additional file 1: Method S2, S3) [30] for optogenetic activation experiments. Animals were housed under SPF conditions in the central housing facility or our laboratory (Immunpathophysiology, University Hospital Bonn, Bonn, Germany). Male mice (10–12 weeks) were used in the intestinal manipulation and laparotomy experiments, and mice of both sexes (10–20 weeks) were used for optogenetic activation experiments and pharmacological modification with reserpine and tyramine carried out under German federal law (Az.: 81-02.04.2016 A367 and 81-02-04-02018.A221, 84–02.04.2017.A114).

Inducible Cre was activated by intraperitoneal injections of 100 µl Tamoxifen [MP Biomedicals, Irvine, CA, USA] dissolved in 10% ethanol and 90% sterile corn oil (final concentration 10 mg/ml) for three consecutive days. Experiments were performed one week after the last injection.

Calcium imaging studies were conducted on female *Wnt1-Cre; R26R-GCaMP3* mice as approved by the Animal Ethics Committee of the University of Leuven (Belgium) in the laboratory of Pieter Vanden Berghe.

#### *In vivo optogenetic activation of adrenergic signaling in enteric glia*

*Sox10$^{iCreERT2}$/RiboTag/tdTomato*|*JellyOP* animals and *JellyOP*-negative littermate controls received pain medication (Tramadol [Grünenthal, Aachen, NRW, DE]; i.p.) 15 min before surgery. During surgery, animals were anesthetized with Isoflurane and kept on a heating pad to stabilize body temperature. After abdominal shaving, the abdominal cavity was opened (2 cm incision) along the *linea alba* and held open by clamps while the small bowel was gently lifted and placed on gauze. The *JellyOP* construct was activated with supramaximal blue light (470 nm, > 0.5 mW/mm$^2$) at a distance of 10 cm for 15 min with regular moisturization with saline. Activation of the *JellyOP* construct triggers a $G_s$ signaling cascade downstream from 1D4, that resembles activation by β-adrenergic stimulation. The intestine was gently replaced, and the opened cavity was sutured. Animals were replaced in their cages and slowly woke from the narcosis under heating lamps during the following 30 min. Animals received further pain medication orally (Tramadol [Aliud Pharma, Laichingen, BW, DE]) via their water supply.

#### *Post-operative ileus (POI) model*

Animals received pain medication (Tramadol [Grünenthal, Aachen, NRW, DE]; i.p.) 15 min before surgery. During surgery, animals were anesthetized with Isoflurane and kept on a heating pad to stabilize body temperature. After abdominal shaving, the abdominal cavity was opened (2 cm incision) along the *linea alba* and held open by clamps, while the small bowel was gently lifted and placed on gauze (Fig. 1A). The small bowel was mechanically manipulated by light pressure with moist cotton swaps in a rolling motion towards the *Caecum* (2x). The intestine was gently replaced, and the opened cavity was sutured. Additionally, we performed a modified laparotomy model in which no manipulation was performed. Animals were replaced in their cages and slowly woke from the narcosis under a red light during the following 30 min. Animals received further pain medication orally (Tramadol [Aliud Pharma, Laichingen, BW, DE]) via their water supply.

#### *Gastrointestinal transit*

Animals received 100 µl of FITC-dextran [Sigma Aldrich, St. Louis, MO, USA] via gavage and rested for 90 min without additional food or water. Subsequently, animals were sacrificed, intestines eventrated, and separated into segments (stomach 1; small bowel 2–11, ~ 3 cm each; caecum 12; colon 13–15, ~ 2 cm each). Segments were flushed with Krebs–Henseleit buffer (Additional file 1: Table S1), and eluates were analyzed for FITC fluorescence. The geometric center was calculated to generate GI-transit time for naïve, Lap 24 h, IM 24 h, and IM 72 h animals.

#### *Sympathetic denervation*

*Sox10$^{iCreERT2}$/Rpl22$^{HA/+}$mice* were injected with 250 µl 6-Hydroxydopamine (6-OHDA; 80 mg/kg body weight in saline [Sigma Aldrich, St. Louis, MO, USA]) for three consecutive days as described before [23]. Animals rested for fourteen days after the final injection before subsequent experiments were performed.

#### *Pharmaceutical adrenergic modulation (reserpine and tyramine)*

*Sox10$^{iCreERT2}$/Rpl22$^{HA/+}$*mice were injected s.c. with 100 µl reserpine (20 mg/kg body weight in saline [#83,580, Sigma Aldrich, St. Louis, MO, USA]) adapted from [31] and kept for 24 h. Animals subsequently underwent laparotomy as described above (with and without prior administration of reserpine) and were sacrificed 3 h later.

*Sox10$^{iCreERT2}$/Rpl22$^{HA/+}$* mice were injected i.p. with 100 µl tyramine (100 mg/kg body weight in saline [#W421501, Sigma Aldrich, St. Louis, MO, USA]) adapted from [32] or 100 µl saline and sacrificed 3 h later.

#### *Primary murine enteric glial cell (EGC) cultures*

Primary EGC cultures were generated from small bowel *muscularis externa (ME)* of 8–12-week-old *Sox10$^{iCreERT2}$/Rpl22$^{HA/+}$/Ai14$^{fl/fl}$* mice. Briefly, the intestine was eventrated, flushed with oxygenated Krebs–Henseleit buffer (cell culture; Additional file 1: Table S1), dissected into 3–5 cm long segments, and transferred to ice-cold, oxygenated Krebs–Henseleit buffer. *ME* tissue was mechanically separated from the mucosal layer, centrifuged (300 g, 5 min), and digested in dissociation buffer (Additional file 1: Table S1) in a water bath (15 min, 37 °C, 150 rpm). The enzymatic reaction was stopped by the addition of 5 ml DMEM + 10% FBS [Sigma Aldrich, St. Louis, MO, USA], centrifugation (300 g, 5 min), and resuspension in proliferation media (Additional file 1: Table S1). Cells were kept in proliferation media for 7 days (37 °C, 5% $CO_2$) before dissociation with trypsin (0.25%, 5 min, 37 °C) [Thermo Fisher Scientific, Waltham, MA, USA] and seeding on Poly-L-Ornithine [Sigma Aldrich, St. Louis, MO, USA] coated 6-well plates at 50% confluence in differentiation media (Additional file 1: Table S1). Cells were differentiated for seven days before treatment with norepinephrine (NE; 10 µM, 100 µM), adrenergic receptor (AR) agonists (β-AR/isoprenaline (1 µM, 10 µM); α2a-AR/guanfacine (10 µM); β3-AR/CL-316243 (10 µM) [all Tocris Bioscience, Bristol, UK]), or forskolin [#HY-15371, MedChemExpress, Monmouth Junction, NJ, USA] in PBS for 3 h or 24 h. Cell culture constituted mainly of enteric glia (> 85%) and small amounts of fibroblasts (< 10%), described in more detail in [5]. Conditioned media was used for ELISA analysis, and cells were processed for RNA analysis.

#### *In vitro optogenetic activation of adrenergic signaling in enteric glial cell cultures*

*JellyOP$^{fl/+}$* animals were used to isolate primary enteric glial cells as described above. Cells were transfected with 1 µl ($1.69 \times 10^8$ VG/ml) of an rAAV2/1-hGFAP-NLS-Cre virus construct ("AAV-GFAP-Cre"; Additional file 1: Method S4) to activate the JellyOP construct and subsequently differentiated for seven days. Differentiated cells were subjected to four consecutive 1 min pulses of blue light (470 nm, 32 µW/mm$^2$) in a custom-built illuminator for cell culture plates. Media from illuminated and dark-kept cells was used for ELISA.

#### *Calcium imaging*

Female *Wnt1-Cre;R26R-GCaMP3* mice were killed by cervical dislocation, as approved by the Animal Ethics Committee of the University of Leuven (Belgium). These mice express the fluorescent $Ca^{2+}$ indicator GCaMP3 in all enteric neurons and glia [33, 34].

The ileum was carefully removed, opened along the mesenteric border, and pinned flat in a sylgard-lined dissection dish in cold $O_2/CO_2$ (95%/5%) suffused Krebs buffer (120.9 mM NaCl; 5.9 mM KCl; 1.2 mM $MgCl_2$;

(See figure on next page.)

**Fig. 1** Enteric glia react to mechanical stimuli and transition into an acute gliosis state. **A** Schematic description of the surgical procedure (intestinal manipulation, IM) with follow-up *RiboTag* approach in *Sox10$^{iCreERT2}$/Rpl22$^{HA/+}$* enteric glia and immunohistological image of HA (green) and SOX10 (magenta) co-expression in *ME*. Scale bar (100 µm). The *RiboTag* procedure was performed 3 h, 24 h, or 72 h after surgery. **B** Confocal images of SOX10 (magenta) and Ki67 (green) expression in whole mounts of small bowel *ME* at different time points. Scale bar (100 µm). **C** Histological analysis (mean ± SEM) of SOX10$^+$ and SOX10$^+$ Ki67$^+$ cells per field of view (n = 6–14 animals per time point; mean counts of 5 images per n ± SEM; two-way ANOVA, to naive *** < 0.01, between IM24/IM72h ### < 0.01). **D** Principal component analysis (PCA) of a bulk RNA-Seq of *Sox10$^{iCreERT2}$/Rpl22$^{HA/+}$ RiboTag* mRNA at different time points. **E** Volcano plot for actively transcribed genes at IM3h in *Sox10$^{iCreERT2}$/Rpl22$^{HA/+}$*enteric glia with significantly differentially transcribed genes (p-value < 0.05, > ± twofold) marked in red (upregulated) and blue (downregulated) and annotation of notable genes. **F** Venn diagrams of the top 50 induced genes at IM3h, IM24h, and IM72h separated into clusters. **G** Analysis of enriched GO-terms in mRNA from *Sox10$^{iCreERT2}$/Rpl22$^{HA/+}$*enteric glia for POI hallmarks related to migration and inflammatory response. **H** RNA-Seq heat maps for naïve and IM3h samples of *Sox10$^{iCreERT2}$/Rpl22$^{HA/+}$RiboTag* mRNA and total RNA "acute enteric gliosis" induction and an indication of genes related to key POI hallmarks. (n = 3–4 animals per time point)

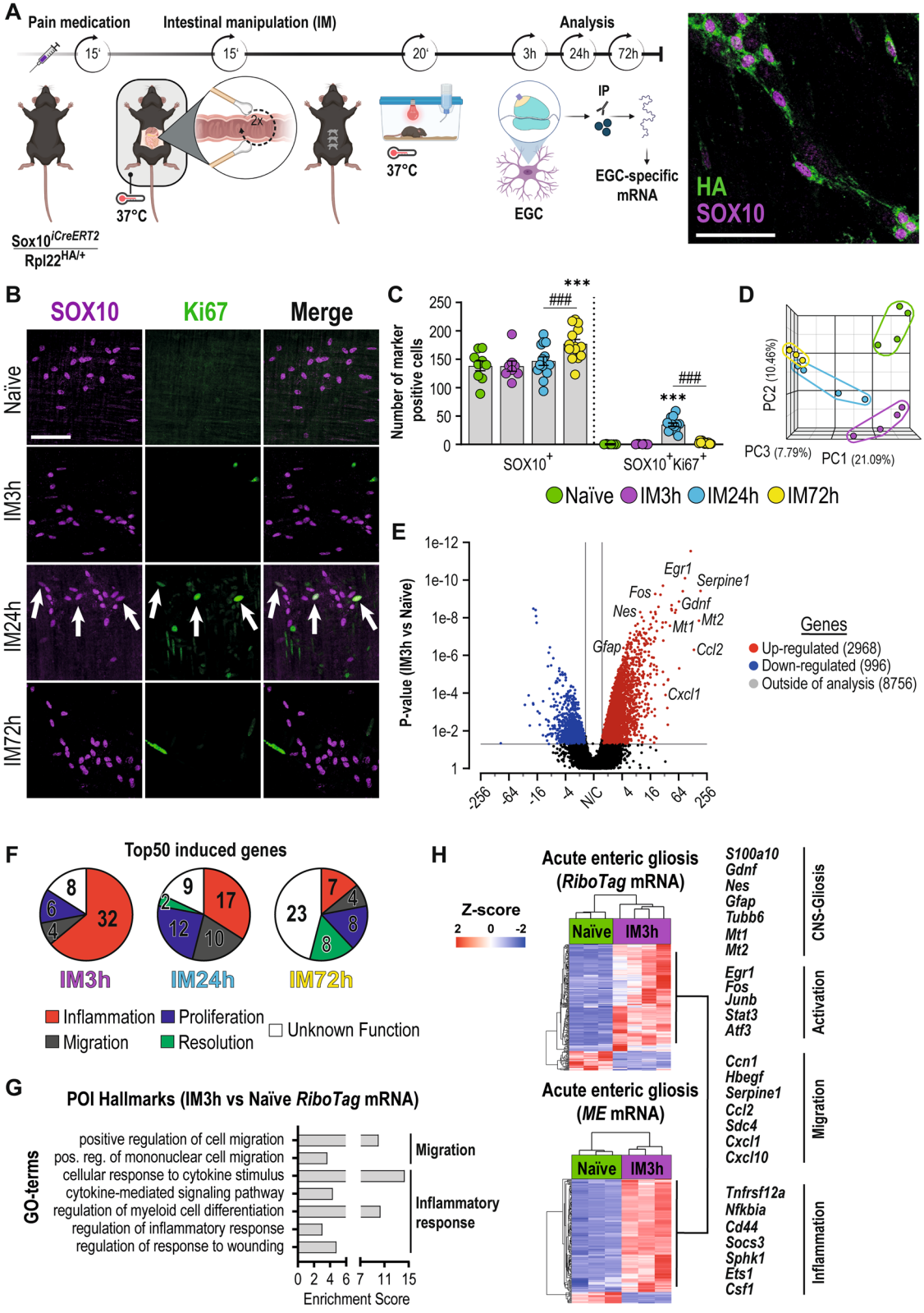


**Fig. 1** (See legend on previous page.)

1.2 mM $NaH_2PO_4$; 14.4 mM $NaHCO_3$; mM 11.5 Glucose; 2.5 mM $CaCl_2$). The mucosa, submucosa, and circular muscle were removed by microdissection to expose the myenteric plexus. These preparations were stabilized over an inox ring using a matched o-ring [35], which was mounted in a cover glass bottom chamber on the microscope stage. 3D recordings of the GCaMP3 were made on an inverted spinning disk confocal microscope (Nikon Ti—Andor Revolution—Yokogawa CSU-X1 Spinning Disk [Andor, Belfast, UK]) with a Nikon 20×lens (NA 0.8), excitation 488 nm and detection 525/50 nm. A Piezo Z Stage controller (PI) was used to record fast 3D stacks at 2 Hz. Tissues were constantly supplied with oxygenated Krebs buffer via a gravity-fed perfusion system that allowed instantaneous switching between control and high $K^+$, Substance P ($10^{-5}$ M, to identify the glia network, [36]) or isoprenaline ($10^{-5}$ M) containing Krebs buffer. The tissues were constantly perfused by $O_2/CO_2$ (95%/5%) suffused Krebs buffer containing 2 µM nifedipine to prevent most of the muscle contractions.

#### *Analysis of calcium imaging*

All calcium image analysis was performed with custom-written routines (available via [37]) in Igor Pro [Wavemetrics, Lake Oswego, OR, USA]. Image registration was performed in Fiji using the descriptor-based registration algorithm developed by Preibish et al. [38]. Registered images were further analyzed in Igor 8, and regions of interest were drawn to extract temporal information. Peak amplitude calculation was performed using custom-written procedures as previously described [37, 39]. The average $Ca^{2+}$ signal intensity was calculated, normalized to the initial GCaMP3 signal, and reported as $F/F_0$.

#### *Immunohistochemistry*

Immunohistochemistry was performed on terminal ileum parts. Briefly, the ileum was placed in Sylgard gel-covered Petri dishes and opened along the mesentery. After fixation with 4% PFA for 20 min, mucosal-free *ME* whole mounts were prepared through mechanical separation of both layers. Next, whole mounts were permeabilized (1% Triton X-100/PBS; RT, 20 min) and blocked with (5% donkey serum, 0.25% Triton X-100/PBS; RT, 1 h) before antibody incubation (primary: 4 °C, overnight; secondary: 1.5 h, RT; Additional file 1: Table S2).

#### *Microscopy imaging*

Widefield images used for quantitative analysis of proliferation, numbers of SOX10 positive cells, and MPO infiltration were obtained on a Nikon Eclipse TE2000-E with a magnification of 20×and a field of view of 397 µm×317 µm or a Nikon Eclipse T*i*2 with a magnification of 20×and a field of view of 769 µm×769 µm. Representative images are confocal slices obtained with a Leica SP8 AOTF confocal microscope using a 40×objective.

#### *Hanker-Yates histology*

Hanker-Yates staining was performed on the terminal ileum. Briefly, the ileum was pinned to Sylgard gel-covered Petri dishes and opened along the mesentery. After fixation with pure ethanol for 10 min, mucosal-free *ME* whole mounts were prepared by mechanically separating both layers. Before mounting, whole mounts were subjected to Hanker-Yates myeloperoxidase staining solution (RT, 10 min).

#### *Western Blot*

A BCA protein assay kit [Thermo Fisher Scientific, Waltham, MA, USA] was used to assess protein lysate concentrations. SDS-PAGE was performed with 100 µg of protein. The primary and secondary antibodies (Additional file 1: Table S2) were incubated overnight at 4 °C and 1 h at RT, respectively.

#### *ELISA*

Conditioned media from EGC cultures treated with NE or agonists for the indicated time points was collected, centrifuged (5000*g*, 5 min), and snap-frozen in liquid nitrogen. According to the manufacturer's instruction manual, media was analyzed for IL-6 release with an ELISA kit [R&D Systems, Abingdon, GB].

#### *RiboTag approach*

*RiboTag* immunoprecipitation was performed according to a previously established protocol (Additional file 1: Method S1, [28]). Briefly, the muscle layer of the whole small bowel tissue was mechanically separated from the mucosal layer and placed in RNA*later* [Thermo Fisher Scientific, Waltham, MA, USA]. Muscle tissue was lysed on a Precellys homogenizer [Bertin Instruments, Montigny-le-Bretonneux, FR] (3×5000 rpm, 45 s; 5 min intermediate incubation on ice) in pre-cooled homogenization buffer (Additional file 1: Table S1), centrifuged (10 min, 10,000*g*, 4 °C), and supernatants saved. "Input" controls were generated from 50 µl cleared lysate. Samples were incubated with anti-HA antibody (5 µl; 1 mg/ml; Additional file 1: Table S2; 4 h, 4 °C, 7 rpm). Lysate/Antibody conjugates were added to 200 µl of washed A/G dynabeads [Thermo Fisher Scientific, Waltham, MA, USA] and incubated (overnight, 4 °C, 7 rpm). Beads were washed thrice with high salt buffer (Additional file 1: Table S1). Ribosomes containing specific mRNA were eluted from beads, and RNA was extracted with a Qiagen micro kit.

#### *cDNA Synthesis and quantitative PCR Analysis*

Purified RNA (10 µg) was transcribed with the Applied Biosystems™ High-Capacity cDNA Reverse Transcription Kit [Applied Biosystems, Foster City, CA, USA] according to the manufacturer's instruction manual. cDNA (1:10 diluted) was added to SYBR™ Green PCR Master Mix [Applied Biosystems, Foster City, CA, USA] and analyzed by qPCR [Applied Biosystems, Foster City, CA, USA] (Additional file 1: Table S3).

#### *RNA-Seq analysis*

Libraries were prepared with QuantSeq 3′ mRNA-Seq Library Prep Kit [Lexogen, Greenland, NH, USA] and sequenced (single-end 50 bp, 10 M reads) on an Illumina Hiseq 2500. "Partek Flow" software was used to analyze RNA-Seq data (Lexogen pipeline 12,112,017), and Ensemble transcripts release 99 for mm10 mouse alignment. The pipeline consisted of two adapter trimming and a base-trimming step with subsequent quality controls (QC). Reads were aligned with star2.5.3, followed by a post-alignment QC, and quantification to an annotation model. Normalized counts were subjected to principal component and gene set analysis. Pipeline information can be found within our uploaded sequencing files (*GSE198889*).

#### *Statistical analysis*

Statistical analysis was performed with Prism 9.0 [GraphPad, San Diego, CA, USA] using Student's t-test, multiple unpaired t-test, one-way, or two-way ANOVA as indicated in the figure legends. Significance to controls is resembled by *, while significance to other samples is indicated by #. All plots are mean ± SEM. Animals for experiments were age- and sex-matched and randomly assigned to the experimental groups.

## Results

### Intestinal inflammation induces enteric gliosis during post-operative ileus development

In a previous study, we re-defined the inflammatory state of the post-operative *ME*, containing reactive enteric glia, based on a publication-based gene selection associated with the term "gliosis" in the CNS [5] and termed this condition "enteric gliosis". As the underlying gene selection only defined the overall transcriptional inflammatory responses of the enteric glial-containing tissue but did not reflect individual cell-type-specific changes of enteric glia, we aimed to precisely determine their reactivity and better understand their role during acute inflammation. Therefore, we assessed the transcriptional changes of enteric glia by a *RiboTag* approach. The *RiboTag,* in conjunction with a *Sox10*$^{iCreERT2}$ system (Fig. 1A, [28]), enabled the isolation of actively transcribed mRNA from enteric glia-specific HA-tagged ribosomes and subsequent RNA-Seq analysis with glial mRNA (Additional file 2: Fig. S1A). Enteric glia reactivity was induced through a standardized model of intestinal inflammation resulting in post-operative ileus (POI). A proper tissue response was confirmed by our previously defined enteric gliosis gene panel [5]. POI progresses in three stages, and the selection of representative time points 3 h, 24 h, and 72 h after intestinal manipulation (IM) enabled us to define the molecular responses within the early/immediate phase (IM3h), inflammatory/manifestation phase (IM24h), and recovery/resolution phase (IM72h). IM (Fig. 1A) triggered acute gut inflammation in the *muscularis externa* (*ME*) (Additional file 2: Fig. S1B), with a decrease in gastrointestinal motility (Additional file 2: Fig. S1C) and an induction of a substantial influx of infiltrating leukocytes (Additional file 2: Fig. S1D) peaking at IM24h, confirming that *Sox10*$^{iCreERT2}$ *RiboTag* mice develop POI. The existence of enteric gliosis was shown by increased protein expression of GFAP and vimentin (VIM) during POI progression (Additional file 2: Fig. S1E). Notably, the number of Sox10$^{+}$Ki67$^{+}$ enteric glia in the *ME* increased at IM24h (35 ± 3 vs. 0.17 ± 0.15 cells/ field of view) but not at IM3h (0.5 ± 0.18 cells/ field of view). SOX10$^{+}$ Ki67$^{+}$ enteric glia numbers dropped to baseline levels at IM72h (3 ± 0.6 cells/ field of view) (Fig. 1B, C), indicating the presence of a timely-limited trigger of glial cell proliferation in the acute phase of inflammation. Supportively, total numbers of SOX10$^{+}$ enteric glia increased at IM72h compared to naïve and IM24h time points (Fig. 1C), showing that molecular features of proliferation indeed resulted in increased EGC numbers in the recovery phase. These changes coincided with POI hallmarks and an overall strong transcriptional response related to inflammation in the *ME* (Additional file 2: Fig. S1B).

Principal component analysis of *RiboTag* samples revealed a clear separation of gene expression patterns at investigated POI time points (Fig. 1D). Volcano plots comparing naïve with IM samples showed the most substantial enteric glial activation at IM3h with 2968 genes up- and 996 genes down-regulated (Fig. 1E), compared to IM24h (101 up- and 1703 down-regulated genes) and IM72h (42 up- and 2218 down-regulated genes) (Additional file 2: Fig. S1F, G). Validation of the top 50 induced genes at all disease time points with gene databanks (*GeneCards* and *Mouse Genome Informatics*) revealed a change of enteric glia toward an inflammation-related cell type (Fig. 1F). Enteric glia displayed a strong expression of inflammatory genes (32 of the top 50; e.g., metallothioneins *Mt1* and *Mt2*, *Tnfrsf12a*, *Nfkbia*, *Sphk1*) in the initial phase that declined during POI progression and was replaced by a strong expression of migratory

(10 of the top 50; e.g., *Ccl2*, *Ccl6*, *Ccl9*) and proliferation-associated genes (12 of the top 50; e.g., *Mcm3*, *Chaf1a*) at IM24h. A so far undefined resolution phenotype arose at IM72h (8 resolution genes of the top 50), showing the induction of olfactory receptors (e.g., *Olfr373*, *Olfr95*, *Olfr1254*), implicated in gut inflammation [40] (Fig. 1F). Notably, the number of actively transcribed genes pulled down with the *RiboTag* approach was also the highest during disease onset at IM3h (12,720 genes) compared to IM24h (8129 genes) and IM72h (3599 genes) (Additional file 2: Fig. S1H). The high transcriptional activity at IM3h aligns with the early enteric glial reactivity. GO analyses showed the enrichment of genes associated with multiple immunological aspects and POI hallmarks, including migration regulation, cytokine signaling, and myeloid cell differentiation (Fig. 1G). To define inflammation-induced enteric glial activation on a transcriptional level, we generated the novel gene ontology (GO) term "acute enteric gliosis" (Additional file 1: Table S4). Therein, we validated the expression of published gliosis genes, previously defined by our group [5], in the *RiboTag* data set and added highly induced genes at IM3h (> tenfold vs. naïve; e.g., *Serpine1, Mt2, Gdnf*) together with genes that were only detected in samples at the IM3h time point (naïve 0 counts; IM3h > 5 counts per sample; e.g., *Fosl, Ucn2, Areg*). Notably, around half of the published gliosis genes are also expressed by enteric glia during POI (Additional file 1: Fig. S1I, Additional file 2: Table S4). Application of this novel GO term showed strong induction of gliosis genes in enteric glia 3 h after manipulation with a steep decline at IM24h and IM72h (Additional file 2: Fig. S1J). To test the applicability of the "acute enteric gliosis" GO term as an indicator of acute enteric gliosis in the full *ME* tissue, we analyzed an RNA-Seq data set generated of total *ME* from POI mice. The resulting heat map mirrored the prominent induction of gliosis genes from our *RiboTag* analysis at IM3h (Additional file 2: Fig. S1K), with most of the upregulated gliosis genes induced exclusively in the early disease phase (IM3h, 94 genes), some overlapping genes at IM3h and IM24h (49 genes; Additional file 2: Fig. S1L) and only one induced gene overlapping between IM3h and IM72h. Highly induced genes at IM3h included known astrogliosis genes (*Gfap*, *Nes, Mt1, Mt2, Gdnf*), early response genes (*Egr1*, *Fos*), migration factors (*Ccl2*, *Cxcl1, Cxcl10, Serpine1*), and inflammatory factors (*Nfkbia, Socs3, Sphk1, Cd44*) (Fig. 1H). Notably, almost no acute enteric gliosis gene panel genes were upregulated in the *ME* at later postoperative time points, supporting its usefulness as an acute enteric gliosis marker panel.

These data provide evidence of the strong plasticity of enteric glia during acute intestinal inflammation, wherein an acute immune-reactive phenotype is a very early event. At the disease peak, 24 h after surgery, enteric glial reactivity switched towards a phenotype supporting migration and proliferation, which further declined towards a resolution type at IM72h.

#### Sympathetic signaling triggers acute enteric glia gliosis

The rapid transition of enteric glia into an inflammatory phenotype raised the question of which mechanisms might trigger this immediate enteric glial activation. A previous study from our group showed that extracellular ATP levels quickly rose after abdominal surgery, thereby triggering an enteric glial immune activation during POI [5]. As ATP is co-stored with norepinephrine (NE) in synaptic vesicles of sympathetic nerves and intestinal sympathetic activity is known to become immediately over-activated during surgery, we hypothesized that sympathetic pathways might contribute to the acute enteric gliosis phenotype. We performed a comparative GO-term analysis and found enriched expression of genes associated with “beta-2-adrenergic receptor binding” and “adrenergic signaling pathway” (Fig. 2A). Interestingly, the enrichment scores were comparable with GO terms linked to IL-1 signaling and ATP-guided expression changes, albeit drastically lower than general ATP binding, both pathways known to activate enteric glia upon surgery [5, 41]. Heat maps of differentially expressed genes related to G-protein-coupled receptor

(See figure on next page.)

**Fig. 2** Acute enteric gliosis is modulated by sympathetic innervation. **A** Analysis of enriched GO-terms in mRNA from *Sox10*$^{iCreERT2}$/*Rpl22*$^{HA/+}$enteric glia 3 h after IM for POI hallmarks related to gliosis triggering pathways. **B** Heat map for the GO-term "GPCR signaling" in naïve and IM3h samples of mRNA from *Sox10*$^{iCreERT2}$/*Rpl22*$^{HA/+}$ enteric glia and with selected genes highlighted. **C** Schematic description of chemical sympathetic denervation of C57BL6 mice with three consecutive intraperitoneal 6-OHDA injections (days 1–3). After 14 days, mice underwent IM. *ME* was isolated three hours later (IM3h) for qPCR and RNA sequencing. **D** Confocal images of immunohistological stainings of TUBB3 (magenta) and TH (green) expression in whole mounts of control (saline) and 6-OHDA treated (sympathectomized/STX) small bowel *ME* 17 days after injection. (n = 6 animals per condition). Scale bar (100 µm). **E** qPCR analysis showing fold changes of mRNA levels (mean ± SEM) from IM3h/Saline and IM3h/STX mice for enteric gliosis-related genes ($2^{-\Delta\Delta CT}$, *18S*, IM3h + saline; n = 6 animals per condition; Student’s t-test, * < 0.05, ** < 0.01). **F** Analysis of enriched POI hallmark GO-terms in IM3h/Saline total RNA and comparatively reduced in IM3h/STX samples related to inflammatory response and migration. **G** RNA-Seq heat map of our “acute enteric gliosis” GO-term for naïve and IM3h samples treated with saline or 6-OHDA (STX), and an indication of STX-affected genes (black line)

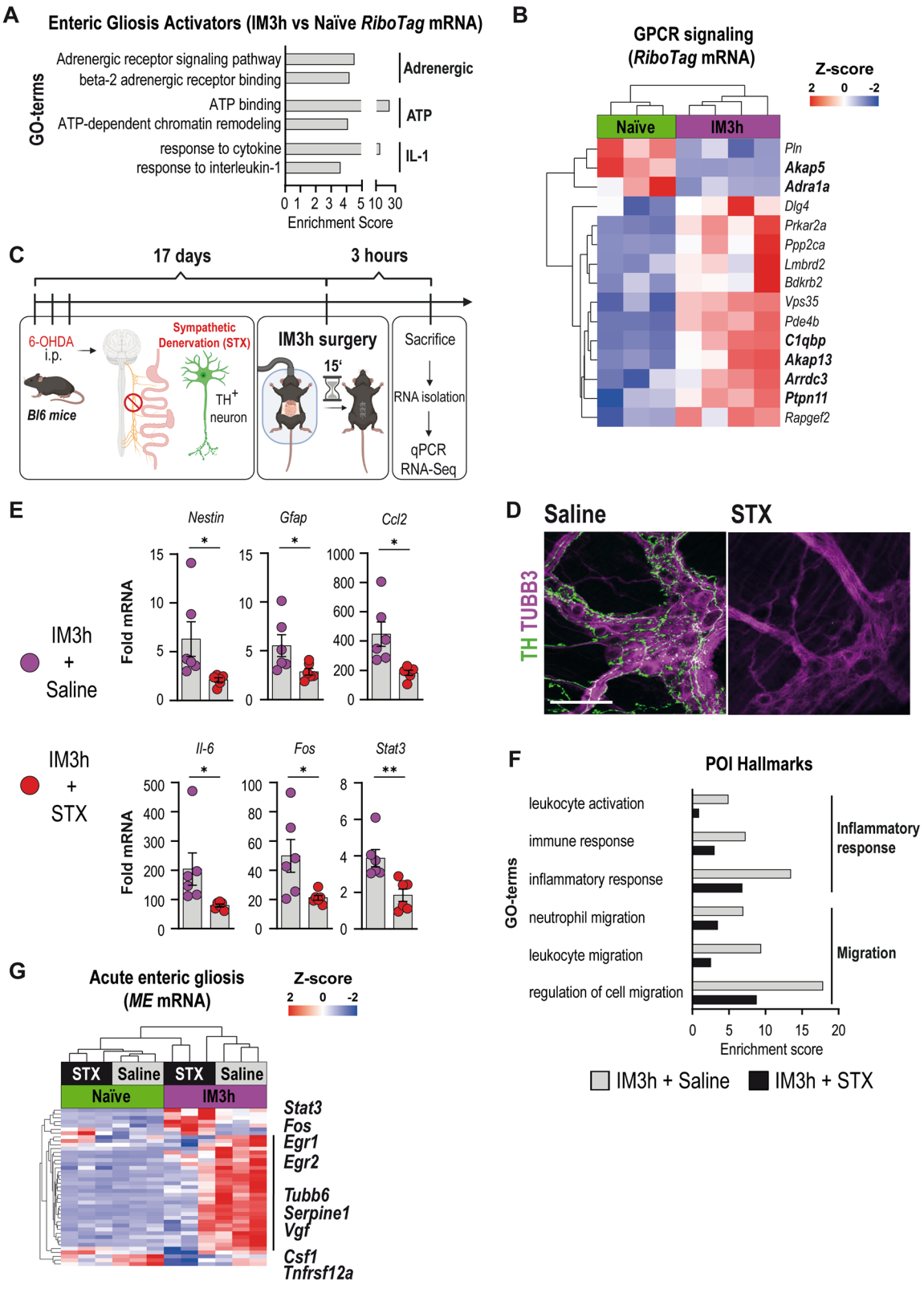


**Fig. 2** (See legend on previous page.)

(GPCR) signaling showed a clear pattern between naïve and IM3h enteric glia in our *RiboTag* mice (Fig. 2B). Activation of enhanced adrenergic signaling was confirmed in *ME* tissue samples, depicting a similar gene expression pattern for adrenergic signaling activity (Additional file 2: Fig. S2A).

Since acute gliosis triggered changes in genes related to adrenergic signaling, we theorized that ablation of the intestinal sympathetic innervation affects acute enteric gliosis. To test this hypothesis, we chemically ablated sympathetic neurons (sympathectomy/STX). Denervation was facilitated by the established model of i.p. injection of 6-Hydroxydopamine (6-OHDA), starting 17 days before surgery (Fig. 2C), resulting in a complete depletion of $TH^+$ neurons within the *ME* of C57BL6 wildtype mice (Fig. 2D). A proof-of-concept analysis by qPCR of *ME* RNA samples from IM3h animals showed a significant reduction of gliosis markers (*Nestin, Gfap*), early response genes (*Stat3, Fosb*), and pro-inflammatory mediators (*Il-6, Ccl2*) in denervated animals (Fig. 2E). Next, we re-analyzed an RNA-Seq data set published by our group [23] for a more comprehensive study of early inflammation. GO term analysis on genes related to POI hallmarks revealed a decrease in genes associated with migration (e.g., leukocytes and neutrophils) and inflammation (e.g., immune and inflammatory response and leukocyte activation) after STX (Fig. 2F). Additionally, we also detected substantial alterations in gene clusters related to changes in the ENS, previously shown to be upregulated at IM3h in our *RiboTag* mice (Additional file 2: Fig. S2B), suggesting a direct effect of denervation on enteric glial reactivity and communication during gut inflammation (Additional file 2: Fig. S2C).

Consequently, we used the "acute enteric gliosis" GO term to investigate the transcriptional status of enteric glia and affected tissue after STX. While only a minority of genes were altered between naïve mice with and without 6-OHDA treatment, strong differences were observed in the majority of enteric gliosis genes at IM3h following STX, highlighting SNS involvement in the development of acute post-operative enteric gliosis (Fig. 2G).

These data suggest that increased sympathetic inputs, known to start simultaneously with surgery, immediately trigger enteric glial reactivity and modulate inflammatory and migratory gene expression.

#### Sympathetic innervation triggers enteric glial reactivity already in the absence of intestinal manipulation

Earlier work showed that inflammation within the small intestinal *ME* already occurs upon abdominal incision without surgical manipulation of the visceral organs. As intestinal sympathetic over-activation is known to start with the abdominal incision [42], we speculated that sympathetic projections of $TH^+$ neurons, innervating the *ME,* might also signal to enteric glia by an immediate release of NE after the abdominal incision, thereby directly activating enteric glia. Confocal microscopy revealed close proximity of $TH^+$ nerve fibers with $MAP^+$ neurons and $GFAP^+$ enteric glia in myenteric ganglia (Fig. 3A), anatomically supporting the idea of a direct SNS to enteric glia communication. To test this hypothesis, we subjected *Sox10$^{iCreERT2}$ RiboTag* mice to a laparotomy without eventration or manipulation of the intestine (Fig. 3B). FOS expression, an early cellular activation marker, and a representative enteric gliosis gene was not detected in $SOX10^+$ enteric glia in naïve mice. At the same time, laparotomy elicited FOS immunoreactivity in myenteric ganglia, including $SOX10^+$ expressing enteric glia (arrows, Fig. 3C). Notably, intestinal manipulation aggravated FOS immunoreactivity in the *ME*, particularly in enteric glia (marked by arrows, Additional file 2: Fig. S3A). These data show that an enteric glial activation already occurs immediately after the surgical incision without surgical manipulation of the intestine, while the latter is a potent enhancer of enteric glial reactivity. To confirm that a laparotomy is sufficient to trigger acute enteric gliosis genes, we performed a laparotomy in *Sox10$^{iCreERT2}$ RiboTag* mice. We detected the induction of representative acute enteric gliosis genes (i.e., *Il6*, *Ccl2,* and *Stat3*) compared to naïve animals (Fig. 3D). Consequently, we used 6-OHDA in *RiboTag* mice to test whether sympathetic innervation triggers the laparotomy-induced enteric gliosis genes. Analogous to our wildtype mice, 6-OHDA depleted the $TH^+$ neuronal processes in *RiboTag* mice and left the glial network intact (Fig. 3E). In line with our hypothesis, *Il6*, *Ccl2*, and *Stat3* gene expression levels were reduced in enteric glia in STX mice compared to saline-treated controls (Fig. 3F). Notably, cellular and functional POI hallmarks also occur in laparotomized mice, although to a lesser extent, with a distinct increase in infiltrating $myeloperoxidase^+$ cells (Additional file 2: Fig. S3B) and reduced gastrointestinal motility compared to naïve mice (Additional file 2: Fig. S3C).

Overall, these data uncovered that the SNS contributes to the induction of genes involved in acute enteric glial reactivity already after the initial abdominal incision, which is further aggravated by mechanical manipulation of the intestine.

#### NE triggers acute enteric gliosis and activates enteric glia via β-adrenergic receptors

As ablation of $TH^+$ neurons led to a reduced acute enteric gliosis, we next assessed whether NE, the principal postganglionic sympathetic neurotransmitter, induces

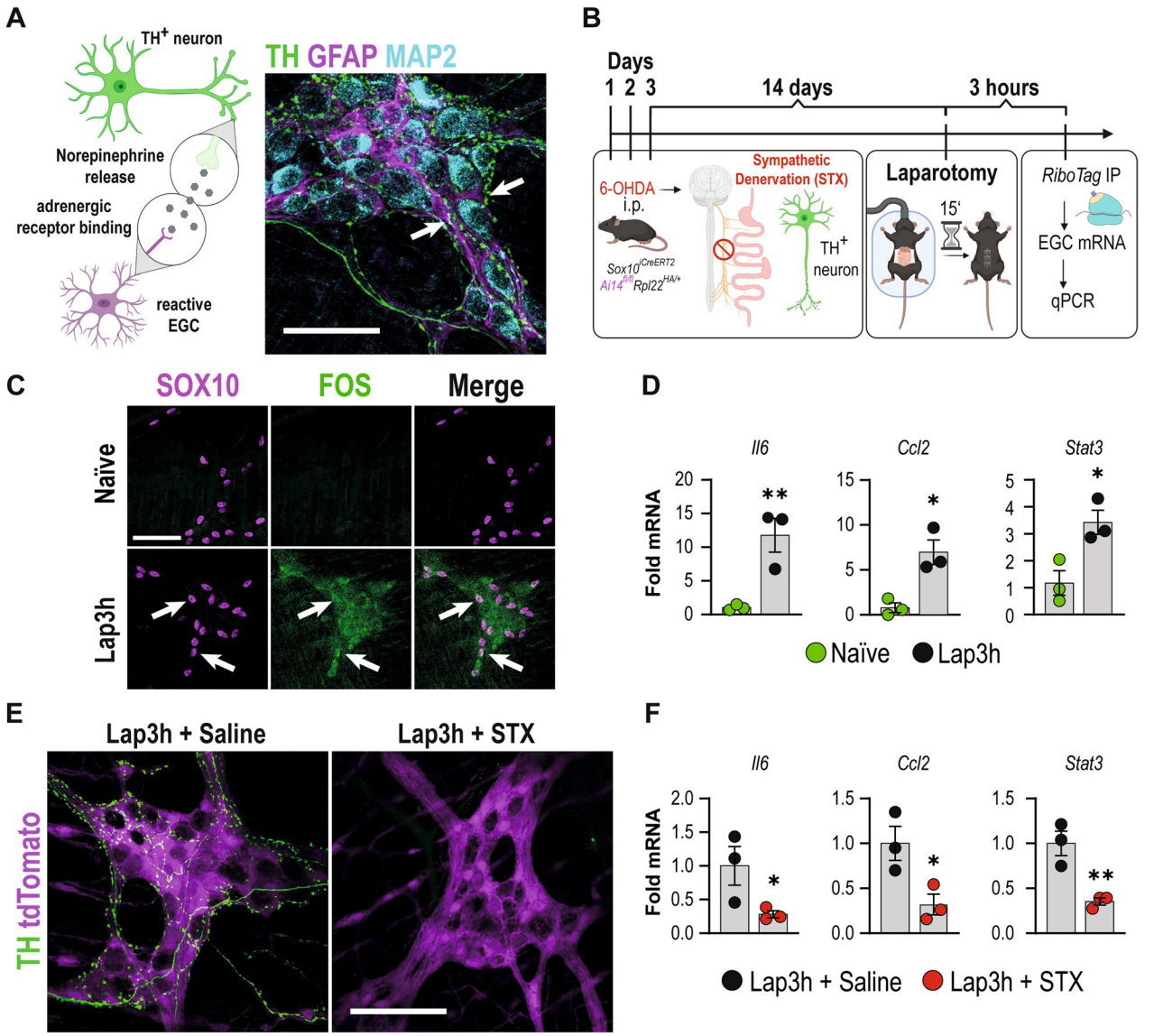


**Fig. 3** Enteric glia react before overt inflammation by receiving cues from the sympathetic nervous system. **A** Illustration of our hypothesis of TH$^+$ neuron released NE triggering enteric glial activation and confocal images of immunohistological staining of sympathetic nerve fibers (TH, green), enteric neurons (MAP2; light blue), and enteric glia (GFAP, magenta). Arrows indicate TH$^+$ fibers innervating the *ME*. Scale bar (50 µm). **B** Schematic description of chemical sympathetic denervation of *Sox10*$^{iCreERT2}$/*Rpl22*$^{HA/+}$ mice with three consecutive intraperitoneal 6-OHDA injections (days 1–3). After 14 days, the mice underwent Lap. *ME* was isolated three hours later (Lap3h), processed according to the RiboTag approach, and analyzed by qPCR. **C** Confocal images of immunohistological stainings of SOX10 (magenta) and FOS (green) expression in whole mounts of naïve and Lap3h small bowel *ME*. (n = 3 animals per condition). Arrows indicate FOS$^+$ SOX10$^+$ enteric glia. Scale bar (100 µm). **D** qPCR analysis showing fold changes of mRNA levels (mean ± SEM) of *Sox10*$^{iCreERT2}$/*Rpl22*$^{HA/+}$ *RiboTag* mRNA from naïve and Lap3h mice for cytokines (*Ccl2, Il6*) and an early response marker (Stat3) ($2^{-\Delta\Delta CT}$, *18S/Tubb4*, Naïve; n = 3 animals per condition; Student's t-test, * < 0.05, ** < 0.01). **(E)** Confocal images of immunohistological stainings of TH (green) and endogenous SOX10-tdTomato (magenta) expression in whole mounts of Lap3h + Saline and Lap3h + STX small bowel *ME*. (n = 3 animals per condition). Scale bar (100 µm). **F** qPCR analysis showing fold changes of mRNA levels (mean ± SEM) of *Sox10*$^{iCreERT2}$/*Rpl22*$^{HA/+}$ *RiboTag* mRNA from Lap3h + Saline and Lap3h + STX mice for cytokines (*Ccl2, Il6*), and an early response marker (Stat3) ($2^{-\Delta\Delta CT}$, *Tubb4/Actb/PGK/GAPDH*, Naïve; n = 3 animals per condition; Student's t-test, * < 0.05, ** < 0.01)

enteric glial reactivity. Therefore, we treated primary murine EGC cultures from small bowel *ME* specimens (Fig. 4A) with NE, which caused an almost threefold increase in IL-6 protein release after 3 h (Fig. 4B) that further increased in a dose-dependent manner 24 h after NE treatment (Additional file 2: Fig. S4B). In addition, NE also triggered *Gfap*, *Nestin*, *Stat3*, *Fos*, and *Ccl2* gene expression 3 h post-treatment (Additional file 2: Fig.

S4C). Notably, the induction of these reactive glia marker genes was transient and disappeared after 24 h (Additional file 2: Fig. S4C), resembling the immediate in vivo enteric glial activation pattern seen in laparotomized and intestinally manipulated mice.

Since NE signals through various adrenergic receptors, we next aimed to characterize their expression profile in primary EGCs to elucidate possible receptors involved in acute enteric gliosis induction. RNA samples of naïve *Sox10*$^{iCreERT2}$ *RiboTag* mice and cultured primary EGCs revealed α2a adrenergic receptor (AR) and the three β-ARs β3 > β1 > β2 as the highest expressed on primary EGCs in vitro and in vivo (Fig. 4C). However, immunocytochemistry of α2a-AR showed no expression in primary EGCs, while it was strongly expressed in non-glial cells in vitro in primary EGC cultures (Additional file 2: Fig. S4D). We next stimulated the three β-ARs and the α2a-AR (as an anticipated negative control) with selective adrenergic agonists in cultured primary EGCs. We analyzed IL-6 and CCL2 release by ELISA and other representative enteric gliosis genes by qPCR. The pan-β-AR agonist isoprenaline elicited IL-6 and CCL2 protein release to the same extent as NE, while neither the α2a-AR-specific agonist (guanfacine) nor the β3-AR-specific agonist (CL-316243) triggered any release (Fig. 4D). Accordingly, isoprenaline and NE significantly induced *Ccl2, Il6, Nestin,* and *Fos* gene expression (Fig. 4E). By immunohistochemistry of *ME* whole-mounts and intestinal cross-sections, we detected β1-AR in GFAP$^+$ ganglia (Fig. 4F**,** Additional file 2: Fig. S4E) and verified the signal with an IgG control (Additional file 2: Fig. S4F). Furthermore, we wanted to investigate the activation of adrenergic signaling cascades upon treatment with isoprenaline. We performed SDS-PAGE and western blotting in combination with an antibody specifically binding to the consensus phosphorylation sequence (RRXS*/T*) of all targets of the activated/phosphorylated form of cAMP-dependent protein kinase A (Fig. 4G), a primary signaling molecule for the adrenergic pathway. Here, we observed a significant increase in the amount of phosphorylated targets after treatment of primary EGCs with 10 µM isoprenaline for 1 h (Fig. 4G), comparable to the activation induced by our positive control treatment forskolin (10 µM).

Since the pan-β-AR agonist isoprenaline, but not the β3-AR-specific agonist, induced a molecular enteric gliosis signature and activated downstream kinases in primary EGCs, we deduced that NE released by the SNS after the onset of surgery activates β1- or β2-AR signaling in enteric glia.

### Ex vivo and optogenetic activation of adrenergic downstream signaling triggers enteric glial reactivity

To better understand the in vivo activation of enteric glia by beta-adrenergic signaling in living tissue and in vivo, we utilized several additional models. We first assessed glial responses in an ex vivo approach wherein we used ileal tissue from *Wnt1-Cre;R26R-GCaMP3* mice to test whether isoprenaline (10 µM) would elicit a glial $Ca^{2+}$ response in the myenteric ganglia. Using a local perfusion system, isoprenaline was applied directly onto the ganglion (Fig. 5A; Additional file 3A and B). Additionally, using the same multi-barrel perfusion tip, Substance P (10 µM) was used to identify the glia cell network [36], and high $K^+$ to identify the neurons (Additional file 2: Fig. S5A). Fourteen ganglia were imaged in separate preparations, and although the responses were variable between recordings and mice, some clear glial cell network activation was seen in a fraction of the recordings (4/14). In contrast, in others (4/14), at least one enteric glial cell in the field of view (FOV) responded (Fig. 5B). In the six other recordings, isoprenaline induced a small contraction, and no cellular (neither neuronal nor glial) $Ca^{2+}$ response could be detected. The relative amplitude

(See figure on next page.)

**Fig. 4** NE triggers acute primary enteric gliosis and glial reactivity via β-adrenergic receptors. **A** Schematic of primary EGC cultures from *Sox10*$^{iCreERT2}$*/Rpl22*$^{HA/+}$*/Ai14*$^{fl/fl}$ mice. **B** ELISA analysis for IL-6 (mean ± SEM) from conditioned medium of cultured EGCs after stimulation with vehicle (PBS) or NE (3 h; 10 µM, 100 µM) (n = 8 distinct cell culture wells per condition; multiple unpaired t-tests, comparison to vehicle, *** < 0.001). **C** qPCR analysis (mean ± SEM) of *Sox10*$^{iCreERT2}$*/Rpl22*$^{HA/+}$ *RiboTag* mRNA and RNA from cultured primary EGCs for different adrenergic receptors ($2^{-\Delta\Delta CT}$, *Tubb4/Actb/PGK/GAPDH*, n = 5 distinct cell culture wells per condition). **D** ELISA analysis for IL-6 and CCL2 (mean ± SEM) from conditioned medium of cultured primary EGCs after stimulation (3 h) with vehicle (PBS), adrenergic agonists (against: α2a, β3, pan-β (isoprenaline)), and NE (all 10 µM); CCL2: n = 6 distinct cell culture wells per condition; IL-6: n = 9–21 distinct cell culture wells per condition; multiple unpaired t-tests, comparison to vehicle, *** < 0.001). **E** qPCR analysis (mean ± SEM) of cultured primary EGCs for acute gliosis genes after vehicle (PBS), isoprenaline (100 µM), or NE (100 µM) treatment ($2^{-\Delta\Delta CT}$, *18S*, Naïve; n = 4–7 distinct cell culture wells per condition; multiple unpaired t-tests, comparison to vehicle, * < 0.05). **F** Immunohistochemistry of cryo-embedded intestinal specimens stained for GFAP$^+$ enteric glia (magenta) and ADRβ1 (green) in the *ME*; Hoechst was used to detect cell nuclei (white). Arrows indicate double-positive cells. Scale bar (50 µm). **G** Western blot and corresponding densitometry (mean ± SEM) of lysates of primary EGC cultures treated with vehicle, isoprenaline (10 µM), or forskolin (10 µM) stained for phosphorylated cAMP-dependent protein kinase (pPKA) (multiple bands) and β-actin (~ 42 kDa) as loading control (n = 4 cultures from 4 different animals treated with the compounds or vehicle; representative blot shows three technical replicates of one biological repeat per condition); multiple unpaired t-tests, comparison to vehicle, ** < 0.01)

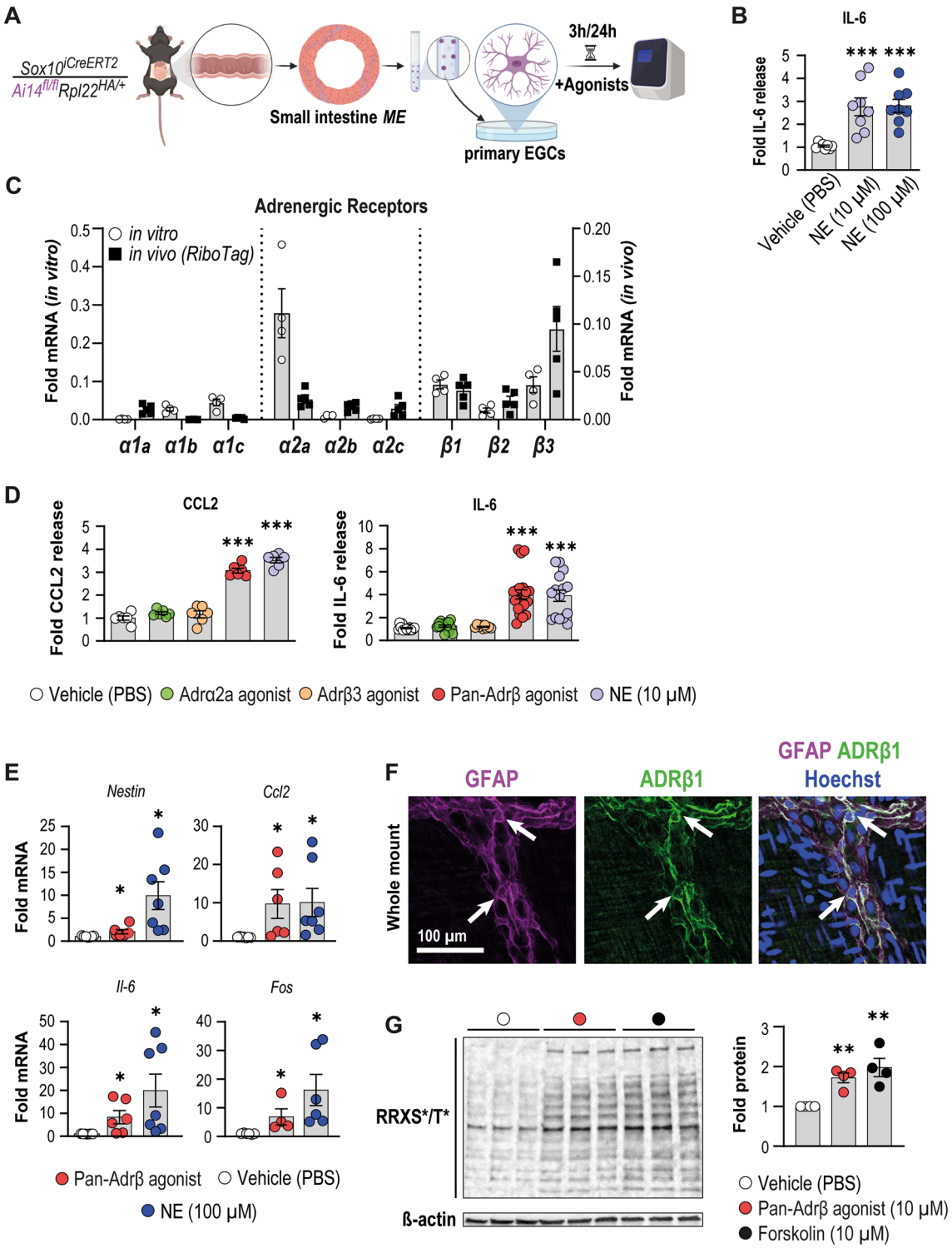


**Fig. 4** (See legend on previous page.)

of those glial cells that were responding to isoprenaline showed a small delay in reaction time with half the amplitude (47 ± 6%) of Substance P used to identify them as glial cells (n = 45 cells; Additional file 2: Fig. S5B). Therefore, we assume that β-AR-stimulated enteric glia acquire a reactive state and can react with distinct $Ca^{2+}$ responses.

Furthermore, we attempted to expand on our denervation experiments by pharmacological manipulation of adrenergic signaling. Therefore, we injected reserpine, a long-lasting inhibitor of monoamines and subjected these mice, as well as mice without reserpine injection, to our laparotomy model (Additional file 2: Fig. S5D). Since sympathetic denervation led to reduced gliosis, we expected the injection of reserpine to mimic this effect, but could not detect significant changes between the laparotomy groups with and without reserpine (Additional file 2: Fig. S5E). We next tested if a chemical increase in NE release induces a POI-like phenotype. Therefore, we applied tyramine, an indirect sympathomimetic compound facilitating catecholamine release [31] (Additional file 2: Fig. S5F). However, no significant changes were observed between the tyramine and control group with the chosen administration scheme (Additional file 2: Fig. S5G).

Finally, we addressed the question if β-adrenergic signaling can indeed directly trigger enteric glial reactivity by utilization of an optogenetic tool, the Jellyfish-Opsin (*JellyOP)*-construct, which enables selective optogenetic activation of the adrenergic $G_s$ signaling by blue light stimulation [43]. For cell-type specific expression of JellyOP and GFP after Cre-mediated excision of a floxed stop cassette, a new mouse line (*JellyOP-GFP*$^{fl/+}$) was generated by CRISPR/Cas9 mediated gene-editing of the Rosa26 locus (30). Starting with an in vitro approach, primary EGCs from *JellyOP-GFP*$^{fl/+}$ mice were transfected with an AAV-GFAP-Cre during their seven days of maturation (Fig. 5C) to generate EGFP-expressing *JellyOP* EGCs. These *JellyOP* EGCs were blue light stimulated and analyzed 24 h later for GFAP and GFP expression as well as IL-6 and CCL2 expression by ELISA. Confocal microscopy revealed a strong GFP expression in GFAP$^+$ enteric glia, indicating successful viral transfection and Cre-activity (Fig. 5D) in primary EGCs. In line with the previous isoprenaline treatment, we detected a significant increase in IL-6 and CCL2 release after blue light stimulation (Fig. 5E), proving that optogenetic activation of adrenergic ($G_s$) downstream signaling in EGCs causes an inflammatory glial phenotype.

Next, we performed an in vivo study with the *JellyOP* system by generating a specific mouse line that utilizes our *Sox10*$^{iCreERT2}$ *RiboTag* approach in conjunction with the *JellyOP-GFP*$^{fl/+}$ mice. The resulting glial *JellyOP RiboTag* mice enable the direct optogenetic activation of enteric glial-restricted adrenergic downstream signaling and assessment of their transcriptome. Immunohistochemistry confirmed the successful expression of the *JellyOP*-GFP construct exclusively in enteric glia of the small intestinal *ME* (Additional file 2:: Fig. S6A). To validate an immediate glial response upon the beginning of surgery, our glial *JellyOP* mice and *JellyOP*-negative litter mates were laparotomized, the small bowel was carefully eventrated, and the jejunum and ileum were illuminated with blue light (Fig. 5F). Immunohistochemistry revealed a strong FOS expression already 1 h after blue light stimulation (Fig. 5G) in glial *JellyOP*-positive animals, while reactivity was almost absent in mice lacking the *JellyOP*.

Interestingly, smooth muscle cell nuclei, identified by their longitudinal shape (Fig. 5G, asteriks) and SOX10-negative ganglionic cells, likely enteric neurons (Fig. 5G, arrowheads), also stained positive for FOS, indicating that these cells become activated due to the glial-specific activation of $G_s$ signaling. Similar FOS histology results were obtained 3 h after stimulation (Additional file 2: Fig. S6B) showing even more cells activated, which is comparable to IM3h whole mount specimens of *JellyOP RiboTag* mice (Additional file 2: Fig. S6C). Strikingly, when we compared blue light-treated glial *JellyOP*-positive and *JellyOP*-negative *RiboTag* mice by qPCR analysis, a strong upregulation of several gliosis panel genes, e.g., *Il6, Fos, Stat3, Gfap,* and *Nestin*, were detected (Fig. 5H). Of note, *Ccl2* expression was only detectable in 2 of 3 glial *JellyOP*-negative *RiboTag* mice, but it was highly expressed in *JellyOP*-positive litter mates (data not shown). To

(See figure on next page.)

**Fig. 5** Ex vivo and optogenetic activation of adrenergic downstream signaling triggers enteric glial reactivity. **A** Image frames taken during the acute exposure to isoprenaline (left panel, 10 µM) or Substance P (right panel, 10 µM) in *Wnt1-Cre; R26R-GCaMP3*$^{fl/fl}$ mice. **B** Pie plot depicting the response types observed in the 14 ganglia (n = 4 mice). **C** Schematic of the primary culture preparation, viral transfection, and in vitro activation process of *JellyOP*$^{fl/+}$ mice with blue light. **D** Confocal images of the *JellyOP-GFP* construct in tdTomato-Sox10$^+$ cells seven days after transfection with the AAV-GFAP-Cre. Arrows indicate GFP$^+$/GFAP$^+$ glia. Scale bar (100 µm). **E** ELISA analysis for IL-6 and CCL2 (mean ± SEM) from conditioned medium of cultured primary EGCs from *JellyOP*$^{fl/+}$ mice transfected with an AAV-GFAP-Cre after stimulation with blue light or without stimulation (n = 24–42 separately transfected wells from two distinct isolations; Student's t-test, *** < 0.001). **F** Schematic of the in vivo activation process of *Sox10*$^{iCreERT2}$*/Rpl22*$^{HA/+}$*/Ai14*$^{fl/+}$*/JellyOP*$^{fl/+}$ mice. **G** Confocal images of IHC for FOS (green) and SOX10 (magenta) in whole mounts of *Sox10*$^{iCreERT2}$*/Rpl22*$^{HA/+}$*/Ai14*$^{fl/+}$*/JellyOP*$^{fl/+}$ or *Sox10*$^{iCreERT2}$*/Rpl22*$^{HA/+}$*/Ai14*$^{fl/+}$*/JellyOP*$^{+/+}$ *mice* 1 h after stimulation with blue light. Arrows indicate FOS-positive SOX10 glia. Scale bar (100 µm). **H** qPCR analysis of mRNA (mean ± SEM) from *Sox10*$^{iCreERT2}$*/Rpl22*$^{HA/+}$*/Ai14*$^{fl/+}$*/JellyOP*$^{fl/+l}$ mice or *Sox10*$^{iCreERT2}$*/Rpl22*$^{HA/+}$*/Ai14*$^{fl/+}$*/JellyOP*$^{+/+}$ *mice* 3 h after optogenetic activation and laparotomy for gliosis hallmark genes ($2^{-\Delta\Delta CT}$, *18S*, *JellyOP*-negative animals, n = 3–7 animals per genotype; Student's t-test, *** < 0.001, * < 0.05)

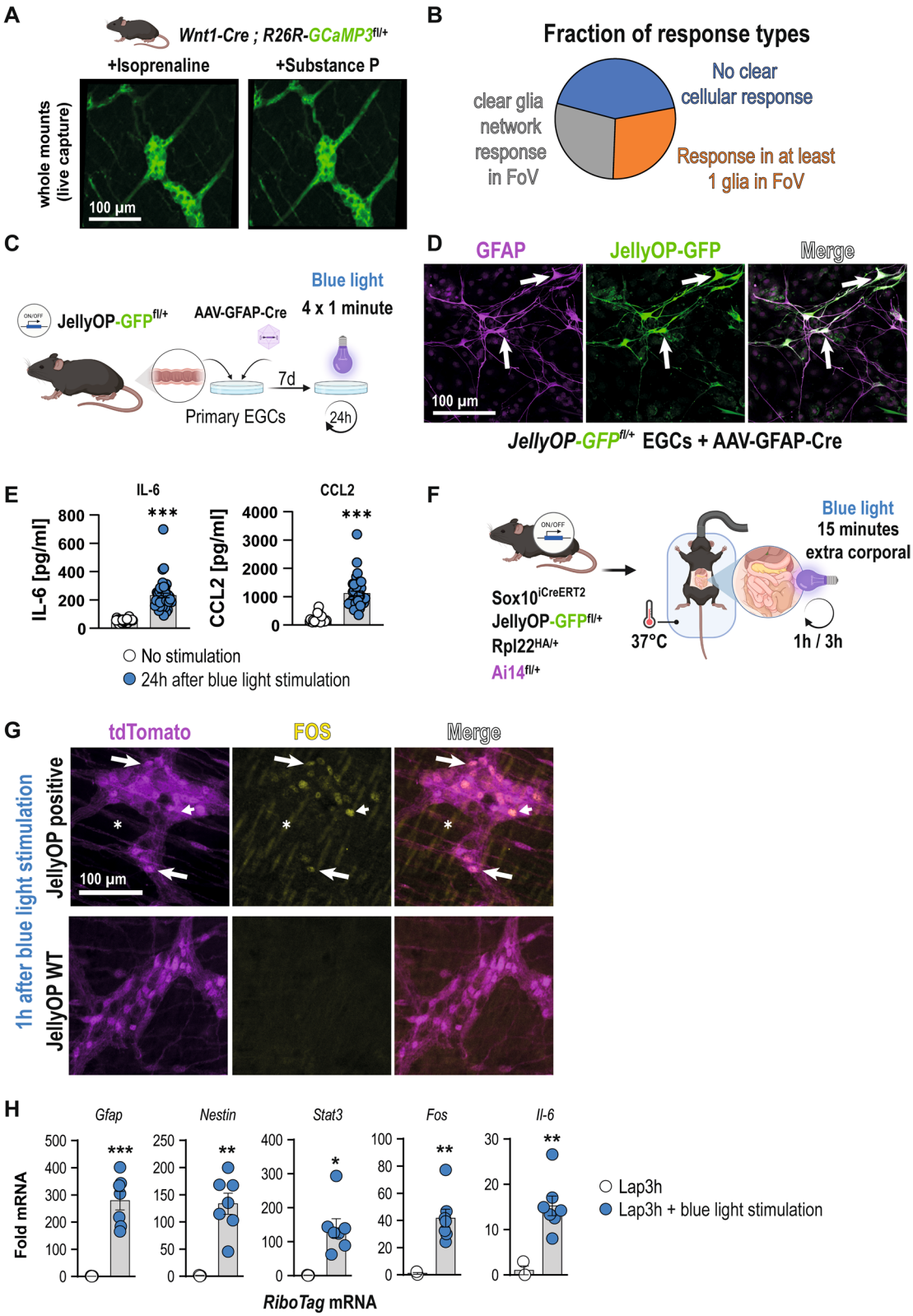


**Fig. 5** (See legend on previous page.)

ensure that JellyOP RiboTag mice with a mixed CD1/BL6 background develop a classical POI, we performed IM and analyzed general disease hallmarks. IM evoked a distinct increase in leukocyte infiltration in JellyOP RiboTag mice (Additional file 2: Fig. S6D, SE) and a reduction of gastrointestinal motility (Additional file 2: Fig. S6H) 24 h after surgery compared to naïve littermates. These changes were similar to those observed in mice on a pure BL6 background. Moreover, to validate the gliosis state, we analyzed glial cell proliferation and detected a comparable increase in Ki67 + /SOX10 + cells 24 h after IM (Additional file 2: Fig. S6F, G) as seen before in BL6 mice (Fig. 1B; [5]), solidifying the use of this strain even without backcrossing to a pure BL6 background.

In conclusion, our data show that abdominal surgery immediately induces a transient reactive enteric glia phenotype in the small intestine *ME*. Surgery-induced SNS activity, confirmed by optogenetically induced $G_S$ and chemically induced β-adrenergic stimulation of enteric glia, can trigger this phenotype directly via β1/2-AR signaling immediately after the initial surgical incision. Selective antagonism of these receptors might be a potential future target to modulate enteric glial reactivity and their functional consequences in immune-driven intestinal disorders.

## Discussion

Enteric glia are an immuno-active cell type involved in intestinal homeostasis that act on the level of local tissue inflammation. They communicate with neurons and immune cells [44] and are discussed as potential targets in treating or preventing immune-driven intestinal disorders [45]. In our previous studies, we have shown that enteric glia trigger a tissue-related inflammatory state, termed "enteric gliosis", triggered amongst others by immune-mediators IL-1 [41] and ATP [5], finally resulting in postoperative *ME* inflammation and POI. However, the individual molecular mechanism in this disease-specific acute enteric gliosis state and the cellular response of enteric glia remained elusive. Herein, we now selectively analyzed enteric glia-specific transcriptional responses by the *RiboTag* approach [46], a tool to isolate actively transcribed mRNA selectively from a target cell population in the tissue of interest [28]. This technique delivered longitudinal transcriptional data of enteric glia in all relevant POI stages, thereby depicting a compelling transition of enteric glial reactivity within different phases of POI. This transition is structured in three stages: an early transcriptional switch of enteric glia into an inflammatory type, a stage defined by an active release of chemotactic factors (migratory), and an increase in proliferation markers (proliferation), and ultimately a state of tissue regeneration and inflammatory resolution (resolution) (Fig. 6A), which are remarkably similar to the classical POI disease development [25]. Notably, gene expression patterns do not significantly overlap between these phases.

Our Ribotag approach generated a list of 243 early induced and actively transcribed genes that we compiled into a novel GO term, "acute enteric gliosis". We hypothesize that reactive enteric glia are a crucial starting point for the subsequent inflammatory changes in cellular and molecular composition in the *ME* environment [47], thereby resembling a critical time point for potential intervention strategies involving enteric glia. Some of the genes immediately induced in enteric glia by IM confirmed our previous studies, e.g., induction of IL-1 and purinergic target genes [5, 41]. In these studies, we showed that ATP via the P2X2 receptor leads to enteric gliosis and cytokine release [5], and IL-1 signaling evokes enteric glial reactivity that leads to *ME* macrophage recruitment [41]. However, our new findings demonstrate that early enteric glial activation emerges as a multifactorial process requiring a variety of stimuli. Furthermore, other factors that are also well-known markers for glial reactivity in the CNS, including *Ccl2* [48], *Cxcl1* [48, 49], *Mt2* [50], *Nes* [9, 49], and *Il6* [48], can now be directly attributed to enteric glial reactivity in the acutely inflamed small bowel *ME*. Notably, some of these molecules, e.g., CCL2 [51], IL-6 [52], and CXCL1 [53], have already been analyzed for their molecular or immune-modulatory function in POI. Another important chemokine-induced in enteric glia during POI is CXCL10, which was recently implicated during acute infection [11] and is also known in context with CNS gliosis [49]. Moreover, metallothioneins *Mt1* and *Mt2*, essential regulators of oxidative stress in reactive astrocytes of MS patients [54], were highly induced during early inflammation. In addition to the prominently expressed chemotactic factors and immune mediators, we detected others that are novel in this context. For instance, genes of the EGF-family, such as *betacellulin* (*Btc*), previously indicated in ileal growth and homeostasis [55] during health, and *amphiregulin* (*Areg*), implicated in intestinal homeostasis during colitis [56], was induced (*Btc*) or even de novo expressed (*Areg*) upon trauma. Regarding gliosis, we detected an upregulation of *Ier5l* and *Ifrd1*, two genes of the "immediate-early gene" group that regulate cell growth and immune function [57] and include other factors., e.g., *Fos*, *Egr1/2*, *Nr4a1/2*, *Jun*, *Atf3,* and *Fosl*, all strongly induced upon IM. Nevertheless, most (thirty-six) of the top 50 induced genes have inflammatory and chemotactic functions supporting the central role of enteric glia as modulators and initiators of acute inflammatory responses in the gut [1, 44].

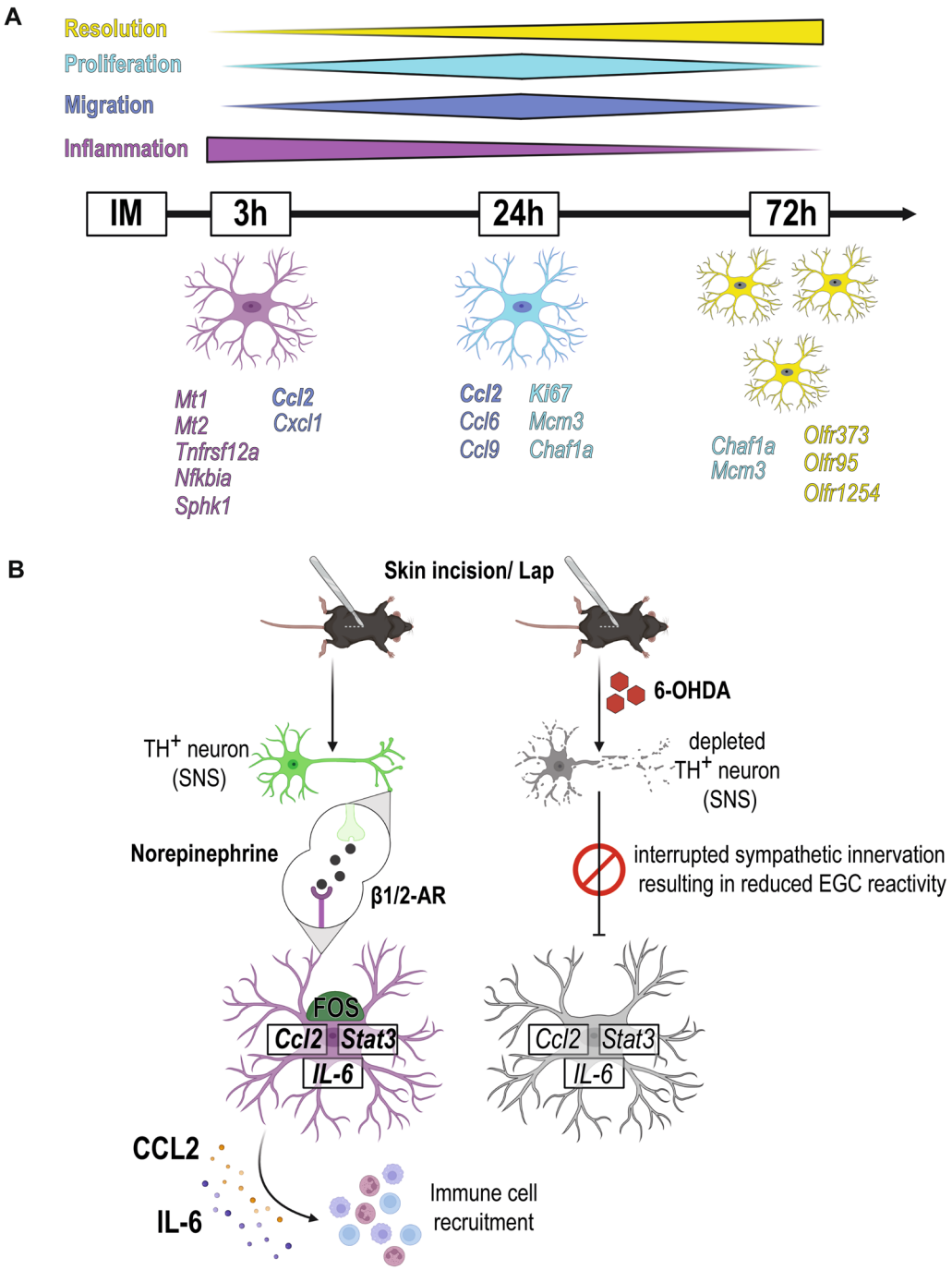


**Fig. 6** β-adrenergic signaling in enteric glia triggers enteric glial reactivity and modulates intestinal inflammation in POI. **A** Graphical abstract of the longitudinal analysis of enteric glia after intestinal manipulation (IM) showing a distinct separation into three stages defined by specific hallmarks. Initial reaction (IM3h, magenta) includes an immediate inflammatory reaction and the shaping of the intestinal environment in concert with the initiation of cell migration (blue). This migratory phenotype manifests further 24 h after IM and is accompanied by elevated proliferation (light blue). Finally, inflammatory reactions of enteric glia continuously taper off and are gradually replaced by resolution-related genes (yellow) that initiate a return to the regular intestinal environment. **B** Graphical abstract of SNS activation of enteric glia. Skin incision and laparotomy (in the absence of IM) lead to immediate activation of the SNS, which triggers enteric glial reactivity in the small bowel *ME*. Sympathetic nerve endings in the *ME* release NE, which binds to adrenergic receptors β1 or β2 on myenteric enteric glia. Enteric glia subsequently become reactive (FOS, *Stat3*) and induce upregulation and release of inflammatory mediators (CCL2, IL-6) that in turn modulate immune cells. Chemical disruption of the sympathetic innervation reduces the reactive enteric glia phenotype and the postsurgical inflammatory response

The transcriptional profiling suggests the enormous plasticity of enteric glia in acute inflammation. The high enteric glial plasticity was recently analyzed and discussed by Guyer et al., substantiating the enteric glia potential to manage multiple gut functions [58]. Within the progression of POI, the enteric glia phenotype switches from the initial inflammatory phenotype over a proliferation state towards a so far undefined phenotype. In the proliferation state, we detected a substantial increase in $Ki67^+/SOX10^+$ enteric glia and attributed this cell cycle activation to the POI-related enteric gliosis phenotype. Our countings of the total number of $SOX10^+$ enteric glia could verify the increase in cell numbers 72 h after surgery. Interestingly, recent publications also discuss additional functions of Ki67, such as its role in cell cycle arrest and/or cell synchronization [59, 60]. These functions may play a role in the phenotypic switch of enteric glia during intestinal inflammation in POI.

In the late phase, enteric glia express several olfactory receptors (e.g., *Olfr373* and *Olfr95*) recently shown as "resolution genes" of intestinal inflammation [40, 61] and discussed as potential therapeutic targets to control inflammation and healing [62]. Other OLFRs like OLFR544 [61] or OLFR78 [40] also control gut inflammation, and some were shown to detect and signal to short-chain fatty acids, e.g., butyrate and propionate, produced by luminal bacteria, which act on multiple levels to control intestinal health and disease [63].

Overall, the first part of our study delivers new molecular insight into enteric glial plasticity during intestinal inflammation. While glial reactivity is highly tissue, trigger and disease state dependent, resulting in a different outcome for the cells and their surrounding environment, these distinct molecular signatures will be a valuable starting point for other research. Certainly, enteric glial reactivity varies with treatment conditions in different disease models, including inflammatory bowel diseases [15, 64] or colorectal cancer [65].

Any abdominal surgery starts with the incision of the skin and the abdominal wall before any surgical manipulation of the visceral organs occurs. More than two decades ago, Kalff et al. found that the initial steps of a laparotomy already triggered *ME* inflammation [42]. Accordingly, sympathetic reflexes and activation of the SNS are known to occur early in surgery. The SNS connects to a variety of cells, including enteric ganglia [27] and intestinal macrophages, wherein they exert β2-AR-mediated immune-modulatory function in infectious [20] and immune-driven diseases [21]. Furthermore, sympathetic neurotransmitters, such as NE, regulate motility [66] and control immune cell migration during inflammatory events. As our findings revealed a particular role of enteric glial reactivity within the immediate postoperative phase, when the SNS becomes activated by surgery, and the principal sympathetic neurotransmitter NE is known to modulate the postoperative immune response in POI [23], we were wondering if sympathetic pathways might trigger the early activation of enteric glia.

Indeed, enteric glia responded to the initial bowel wall incision before the actual surgical manipulation of the intestine began. Enteric glia released cytokines such as *Il6* and *Ccl2*, and ablation of SNS nerve fibers ameliorated the acute postsurgical enteric gliosis by reducing cytokine production and early response gene transcription. This diminished glial reactivity was accompanied by a decrease in several POI hallmarks, such as migration and inflammatory response (Fig. 6B).

Further evidence about functional alterations of glial cells to adrenergic stimulation comes from observations in the CNS [67]. The findings of Tong et al. supported the immunomodulatory role of sympathetic inputs, as 6-OHDA-mediated ablations of sympathetic nerves resulted in diminished activation of spinal cord glia [68]. Another study showed that the blockage of β-AR prior to cytotoxic insults to the spinal cord reduced reactive gliosis [69]. SNS neurotransmitters can elicit pro- or anti-inflammatory cytokine release depending on the tissue environment, concentration, and AR binding [70]. In the CNS, for example, NE reduced astrocyte swelling after spinal cord injury [71] and elicited neuroprotective effects in $H_2O_2$-treated neuron/glia co-cultures [72]. In contrast, preconditioning with NE before ischemic injury exacerbated reactive gliosis [73], and β-2AR agonist treatment increased IL-6 expression after TNFα-induced inflammation in vivo and in vitro [74]. Another pathway triggered by adrenergic activation, partially glimpsed in our experiments, might be the modulation of calcium signaling, which was recently observed in vitro in HEK cells [75] and in vivo in cardiac myocytes [76]. Moreover, adrenergic agonists evoked calcium changes in cultured astrocytes and astrocyte networks in hippocampal slices [77], further prompting future research into this interaction in the gut.

Interestingly, SNS action during inflammation can have opposing effects. While chemical denervation showed beneficial effects during acute inflammation in POI [23] it had adverse effects in chronic intestinal inflammation [78, 79] and mice suffering from physical stress together with colitis [80]. Supporting the beneficial effect of the SNS in chronic inflammation, a recent study by Schiller et al. showed that repeated optogenetic stimulation of $TH^+$ fibers attenuated symptoms of DSS colitis by reducing immune cell abundance [81]. In IBD patients, the use of β-blockers is associated with an increased relapse risk [82]. Based on the spontaneous increase in glial calcium signaling upon β-adrenergic stimulation, the immediate

induction of reactive glia marker genes after blue light activation of a downstream $G_s$ cascade that mimics β-adrenergic pathways [43] in our *JellyOP* experiments, and the observation that a chemical sympathetic denervation improves symptoms of POI [23], we believe that sympathetic actions in acute inflammatory conditions are rather detrimental. To this end, we expected a more profound insight from our in vivo experiments with reserpine and tyramine application. However, the tested conditions, adapted from previous publications that used these drugs in vivo [31, 32], failed to show changes in POI symptoms and transcriptional glial reactivity compared to the control groups. The lack of strong pharmacological in vivo studies for both compounds, particularly in gastrointestinal physiology and immunology, thus warrants a need for further studies. These should include in-depth pharmacological analyses, comparisons of different administration routes, use of different drug concentrations, time points, and durations before a clear statement about the mode of action of reserpine and tyramine in sympathetic in vivo modulation within the intestine can be claimed.

Our study emphasizes that adrenergic signaling is complex and exerts distinct roles in different cell types, organs, and diseases to control cellular reactivity during inflammation. This knowledge might also be of clinical relevance, e.g., in the application of adrenergic blockers in patients suffering or expected to suffer from acute or chronic intestinal inflammatory diseases. Depending on the nature of the underlying disease, adrenergic blockers can evoke beneficial or detrimental health effects.

As chemical denervation ameliorated postoperative glial reactivity and reduced acute enteric gliosis, we propose SNS-based neurotransmitter release acting on enteric glia as the mechanism of their early activation, a state aggravated by the manipulation of the intestine and additional signaling cascades such as ATP and IL1 signaling. Imura et al. provided supporting evidence of an adrenergic signaling-induced reactive astrocyte phenotype upon stimulation with isoprenaline [83] accompanied by an increased β-AR expression in reactive astrocytes in vivo. Our findings suggest β1- or β2-AR as the relevant receptors to propagate SNS-stimulated inflammatory changes in enteric glia, as the pan-β-AR agonist isoprenaline, but not β3-AR agonism evoked a cytokine release. Applying β2-AR agonist salbutamol also ameliorated DSS-induced ulcerative colitis [84]. Interestingly, antagonists against β-ARs reduced both cardiac inflammation (metoprolol) [85] and ulcerative colitis (propranolol) [86]. Further studies utilizing additional β-AR-specific agonists (e.g., isoprenaline or salbutamol), antagonists (e.g., metoprolol and propranolol), or glial-specific AR-knockouts can help to decipher inflammation-driven diseases involving glial activation as part of their pathophysiology.

It should be noted that adrenergic signaling-induced enteric glial reactivity might not, per se, be a purely detrimental factor in inflammation. Enteric glia appear to be highly plastic during inflammation. While initial NE interaction aggravates the acute enteric glial reactivity, prolonged NE exposure, as it occurs during prolonged or chronic inflammation, might drive enteric glia to a beneficial phenotype and partially explain the positive influence of the SNS during those stages [78, 79, 84]. Moreover, the inflammatory environment changes during the disease course, altering the cellular and molecular composition and thus might also affect the responses to adrenergic signaling. For instance, in the presence of TNFα, NE binding to β-ARs inhibited further TNFα and downstream IL-6 secretion, while adrenergic signaling in the absence of TNFα directly stimulated IL-6 secretion [70]. Moreover, AR receptor expression is modulated during inflammation, previously shown for astrocytes [83], and in the intestine controlled by sympathetic inputs [23]. As inflammation can be accompanied by a later loss [70], the absence of feedback loops might also explain the differences in adrenergic immune-related responses between acute and chronic inflammation. Notably, differences in the adrenergic reactions might also occur within different locations of the same organ. While chronic intestinal disease models focus on the mucosal layer, the acute postoperative response to surgery is mainly limited to the *ME* [87], which comprises a different cellular composition and more distant localization to the luminal contents of the gut.

Overall, our study delivers an unknown longitudinal insight into enteric glial molecular responses and reactivity during different phases of an acute inflammation-driven intestinal disorder. We introduced sympathetic adrenergic signaling as a priming factor of enteric glial reactivity and a potential therapeutic target. These data are of important future value, as they not only present an interventional target to control inflammation but will also help to understand similarities and differences in enteric glial reactivity in other inflammation-driven diseases, such as IBD and gastrointestinal cancer development.

**Abbreviations**

| | |
|---|---|
| EGC | Enteric glial cell |
| POI | Postoperative ileus |
| ENS | Enteric nervous system |
| CNS | Central nervous system |
| SNS | Sympathetic nervous system |
| GI | Gastro-intestinal |
| LPS | Lipopolysacharrid |

| | |
|---|---|
| Lap | Laparotomy |
| STX | Sympathetectomy (chemical) |
| NE | Norepinephrine |
| ME | Muscularis externa |
| AR | Adrenergic receptor |
| GO | Gene ontology |
| IM | Intestinal manipulation |
| 6-OHDA | 6-Hydroxydopamine |
| GFAP | Glial fibrilliary acidic protein |
| SOX10 | SRY-Box transcription factor 10 |
| IL-6 | Interleukin-6 |
| IL-1β | Interleukin-1β |
| CCL2 | C–C motif chemokine ligand 2 |
| TNFα | Tumor necrosis factor α |
| IFNγ | Interferone γ |
| GDNF | Glial-cell derived neurotrophic factor |
| PLP1 | Proteolipid protein 1 |

## Supplementary Information

The online version contains supplementary material available at https://doi.org/10.1186/s12974-023-02937-0.

**Additional file 1: Method S1.** RiboTag approach in the muscularis externa. **Method S2.** Construction of the *JellyOP* targeting vector for the mouse Rosa26 locus. **Method S3.** *JellyOP* animal creation. **Method S4.** Recombinant adeno-associated virus (rAAV) preparation. **Table S1.** Buffer and media. **Table S2.** Antibodies. **Table S3.** PCR primer. **Table S4.** Acute enteric gliosis GO-term.

**Additional file 2: Figure S1.** Characterization of POI in *Sox10*$^{iCreERT2}$/*Rpl22*$^{HA/+}$ mice. **Figure S2.** Sympathetic signaling is involved in enteric glia functions. **Figure S3.** Laparotomy affects molecular functions. **Figure S4.** Effect of NE and tissue expression of ADRβ1. **Figure S5.** Ex vivo β-adrenergic stimulation elicits enteric glia calcium signaling. **Figure S6.** JellyOP mice with a mixed genetic background develop regular POI.

**Additional file 3: Video SA.** Isoprenaline. **Video SB.** Substance P.

**Acknowledgements**

We thank Mariola Lysson, Bianca Schneiker, Patrik Efferz, Frank Holst and Jana Müller for their excellent technical support and animal handling. Moreover, we thank the Bioinformatics Core, the Next Generation Sequencing Core, and the Microscopy Core Facility of the University Hospital Bonn for providing help, services, and devices funded, among others, by the German research council (DFG, German Research Foundation) – Project number 388159768. We would like to thank the Gene-Editing Core Facility of the Medical Faculty at the University of Bonn for the generation of the Gt(ROSA)26Sor$^{em1(CAG-JellyOp-eGFP)}$ mouse line and Vanessa Dusend, Daniela Malan, Wanchana Jangsangthong for generation of targeting constructs and characterization of the JellyOP-GPF fl/+ mouse line. We furthermore thank the Viral Core Facility of the Medical Faculty at the University of Bonn for the production of the rAAV2/1-hGFAP-NLS-Cre. Graphical visualizations were created with *BioRender* software. Furthermore, we would like to express our gratitude to Professor Vassilis Pachnis for kindly providing the Sox10$^{iCreERT2}$ mouse line, Prof. Sasse and Prof. Pfeifer for sharing adrenergic agonists with us, and Prof. Wegner for providing us with a goat Sox10 antibody. Finally, we would like to thank Professor Walker S. Jackson and Dr. Eileen C. Haring for their valuable input on the manuscript.

**Author contributions**

PL, RS, LS, SM and PVB performed research; PL, RS, and SW designed the study and analyzed the data; PL, RS, LS, PVB, PS, JCK, and SW wrote the manuscript. All authors reviewed the manuscript.

**Funding**

Open Access funding enabled and organized by Projekt DEAL. This publication was financed by a grant from the German research council (DFG) to SW (WE4204/3-1) and, BonnNI to SW (Q-611.0754), Bonfor to RS (O-112.0066) and the ImmunoSensation$^2$ Cluster of Excellence (EXC 2151–390873048). PS received support from DFG (SA 1785/7-1, SA 1785/9-1). P. Vanden Berghe receives support from FWO G021.15, G012223N and I000123N (in support of the Cell & tissue Imaging Core (CIC)-Flanders BioImaging). The Andor Revolution Spinning Disk System was obtained via Hercules Grant AKUL/09/50 to P. Vanden Berghe.

**Availability of data and materials**

The datasets used and analyzed during the current study have been submitted to the GEO database under the accession number *GSE198889* with the following token: cdupiqaotjsnvgf.

## Declarations

**Ethical approval and consent to participate**

Mouse work was conducted under the ethical approval for animal experiments number: Az.81–02.04.2016.A367 and Az.1–02.04.2018.A221. Since no patient data were included in this study, consent to participate is not applicable.

**Consent for publication**

Not applicable.

**Competing interests**

SW and JCK receive royalties from Wolter Kluwer for his contribution to the postoperative ileus section of the *UpToDate* library. All other authors declare no competing interests.

**Author details**

[1]Department of Surgery, University Hospital Bonn, Venusberg-Campus 1, 53127 Bonn, Germany. [2]Laboratory for Enteric NeuroScience (LENS), Translational Research Center for Gastrointestinal Disorders (TARGID), University of Leuven, Louvain, Belgium. [3]Institute of Physiology I, Medical Faculty, University of Bonn, Bonn, Germany.

Received: 27 May 2022 Accepted: 27 October 2023
Published online: 08 November 2023

**References**

1. Seguella L, Gulbransen BD. Enteric glial biology, intercellular signalling and roles in gastrointestinal disease. Nat Rev Gastroenterol Hepatol. 2021. https://doi.org/10.1038/s41575-021-00423-7.
2. Boesmans W, Lasrado R, Vanden Berghe P, Pachnis V. Heterogeneity and phenotypic plasticity of glial cells in the mammalian enteric nervous system. Glia. 2015;63:229–41. https://doi.org/10.1002/glia.22746.
3. Rao M, Nelms BD, Dong L, Salinas-Rios V, Rutlin M, Gershon MD, Corfas G. Enteric glia express proteolipid protein 1 and are a transcriptionally unique population of glia in the mammalian nervous system. Glia. 2015;63:2040–57. https://doi.org/10.1002/glia.22876.
4. Brown IAM, McClain JL, Watson RE, Patel BA, Gulbransen BD. Enteric glia mediate neuron death in colitis through purinergic pathways that require connexin-43 and nitric oxide. Cell Mol Gastroenterol Hepatol. 2016;2:77–91. https://doi.org/10.1016/j.jcmgh.2015.08.007.
5. Schneider R, Leven P, Glowka T, Kuzmanov I, Lysson M, Schneiker B, et al. A novel P2X2-dependent purinergic mechanism of enteric gliosis in intestinal inflammation. EMBO Mol Med. 2021;13: e12724. https://doi.org/10.15252/emmm.202012724.
6. Burda JE, Sofroniew MV. Reactive gliosis and the multicellular response to CNS damage and disease. Neuron. 2014;81:229–48. https://doi.org/10.1016/j.neuron.2013.12.034.
7. das Neves SP, Sousa JC, Sousa N, Cerqueira JJ, Marques F. Altered astrocytic function in experimental neuroinflammation and multiple sclerosis. Glia. 2021;69:1341–68. https://doi.org/10.1002/glia.23940.
8. Liddelow SA, Guttenplan KA, Clarke LE, Bennett FC, Bohlen CJ, Schirmer L, et al. Neurotoxic reactive astrocytes are induced by activated microglia. Nature. 2017;541:481–7. https://doi.org/10.1038/nature21029.
9. Hara M, Kobayakawa K, Ohkawa Y, Kumamaru H, Yokota K, Saito T, et al. Interaction of reactive astrocytes with type I collagen induces astrocytic scar formation through the integrin-N-cadherin pathway after spinal cord injury. Nat Med. 2017;23:818–28. https://doi.org/10.1038/nm.4354.

10. Stoffels B, Hupa KJ, Snoek SA, van Bree S, Stein K, Schwandt T, et al. Postoperative ileus involves interleukin-1 receptor signaling in enteric glia. Gastroenterology. 2014;146:176-87.e1. https://doi.org/10.1053/j.gastro.2013.09.030.
11. Progatzky F, Shapiro M, Chng SH, Garcia-Cassani B, Classon CH, Sevgi S, et al. Regulation of intestinal immunity and tissue repair by enteric glia. Nature. 2021;599:125–30. https://doi.org/10.1038/s41586-021-04006-z.
12. Turco F, Sarnelli G, Cirillo C, Palumbo I, de Giorgi F, D'Alessandro A, et al. Enteroglial-derived S100B protein integrates bacteria-induced Toll-like receptor signalling in human enteric glial cells. Gut. 2014;63:105–15. https://doi.org/10.1136/gutjnl-2012-302090.
13. Meir M, Kannapin F, Diefenbacher M, Ghoreishi Y, Kollmann C, Flemming S, et al. Intestinal epithelial barrier maturation by enteric glial cells is GDNF-dependent. Int J Mol Sci. 2021. https://doi.org/10.3390/ijms22041887.
14. Cheadle GA, Costantini TW, Lopez N, Bansal V, Eliceiri BP, Coimbra R. Enteric glia cells attenuate cytomix-induced intestinal epithelial barrier breakdown. PLoS ONE. 2013;8: e69042. https://doi.org/10.1371/journal.pone.0069042.
15. Liñán-Rico A, Turco F, Ochoa-Cortes F, Harzman A, Needleman BJ, Arsenescu R, et al. Molecular signaling and dysfunction of the human reactive enteric glial cell phenotype: implications for GI infection, IBD, POI, neurological, motility, and GI disorders. Inflamm Bowel Dis. 2016;22:1812–34. https://doi.org/10.1097/MIB.0000000000000854.
16. von Boyen GBT, Steinkamp M, Reinshagen M, Schäfer K-H, Adler G, Kirsch J. Nerve growth factor secretion in cultured enteric glia cells is modulated by proinflammatory cytokines. J Neuroendocrinol. 2006;18:820–5. https://doi.org/10.1111/j.1365-2826.2006.01478.x.
17. Cirillo C, Sarnelli G, Turco F, Mango A, Grosso M, Aprea G, et al. Proinflammatory stimuli activates human-derived enteroglial cells and induces autocrine nitric oxide production. Neurogastroenterol Motil. 2011;23:e372–82. https://doi.org/10.1111/j.1365-2982.2011.01748.x.
18. Duan H, Cai X, Luan Y, Yang S, Yang J, Dong H, et al. Regulation of the autonomic nervous system on intestine. Front Physiol. 2021. https://doi.org/10.3389/fphys.2021.700129.
19. Nasser Y, Ho W, Sharkey KA. Distribution of adrenergic receptors in the enteric nervous system of the guinea pig, mouse, and rat. J Comp Neurol. 2006;495:529–53. https://doi.org/10.1002/cne.20898.
20. Matheis F, Muller PA, Graves CL, Gabanyi I, Kerner ZJ, Costa-Borges D, et al. Adrenergic signaling in muscularis macrophages limits infection-induced neuronal loss. Cell. 2020;180:64-78.e16. https://doi.org/10.1016/j.cell.2019.12.002.
21. Gabanyi I, Muller PA, Feighery L, Oliveira TY, Costa-Pinto FA, Mucida D. Neuro-immune interactions drive tissue programming in intestinal macrophages. Cell. 2016;164:378–91. https://doi.org/10.1016/j.cell.2015.12.023.
22. Brinkman DJ, ten Hove AS, Vervoordeldonk MJ, Luyer MD, de Jonge WJ. Neuroimmune interactions in the gut and their significance for intestinal immunity. Cells. 2019. https://doi.org/10.3390/cells8070670.
23. Mallesh S, Schneider R, Schneiker B, Lysson M, Efferz P, Lin E, et al. Sympathetic denervation alters the inflammatory response of resident muscularis macrophages upon surgical trauma and ameliorates postoperative ileus in mice. IJMS. 2021;22:6872. https://doi.org/10.3390/ijms22136872.
24. Augestad KM, Delaney CP. Postoperative ileus: impact of pharmacological treatment, laparoscopic surgery and enhanced recovery pathways. World J Gastroenterol. 2010;16:2067–74. https://doi.org/10.3748/wjg.v16.i17.2067.
25. Boeckxstaens GE, de Jonge WJ. Neuroimmune mechanisms in postoperative ileus. Gut. 2009;58:1300–11. https://doi.org/10.1136/gut.2008.169250.
26. Mazzotta E, Villalobos-Hernandez EC, Fiorda-Diaz J, Harzman A, Christofi FL. Postoperative ileus and postoperative gastrointestinal tract dysfunction: pathogenic mechanisms and novel treatment strategies beyond colorectal enhanced recovery after surgery protocols. Front Pharmacol. 2020;11: 583422. https://doi.org/10.3389/fphar.2020.583422.
27. Gulbransen BD, Bains JS, Sharkey KA. Enteric glia are targets of the sympathetic innervation of the myenteric plexus in the guinea pig distal colon. J Neurosci. 2010;30:6801–9. https://doi.org/10.1523/JNEUROSCI.0603-10.2010.
28. Leven P, Schneider R, Siemens KD, Jackson WS, Wehner S. Application of a RiboTag-based approach to generate and analyze mRNA from enteric neural cells. Neurogastroenterol Motil. 2021. https://doi.org/10.1111/nmo.14309.
29. Delvalle NM, Dharshika C, Morales-Soto W, Fried DE, Gaudette L, Gulbransen BD. Communication between enteric neurons, glia, and nociceptors underlies the effects of tachykinins on neuroinflammation. Cell Mol Gastroenterol Hepatol. 2018;6:321–44. https://doi.org/10.1016/j.jcmgh.2018.05.009.
30. van Chu T, Weber T, Graf R, Sommermann T, Petsch K, Sack U, et al. Efficient generation of Rosa26 knock-in mice using CRISPR/Cas9 in C57BL/6 zygotes. BMC Biotechnol. 2016;16:4. https://doi.org/10.1186/s12896-016-0234-4.
31. Poll BG, Xu J, Jun S, Sanchez J, Zaidman NA, He X, et al. Acetate, a short-chain fatty acid, acutely lowers heart rate and cardiac contractility along with blood pressure. J Pharmacol Exp Ther. 2021;377:39–50. https://doi.org/10.1124/jpet.120.000187.
32. Olfe J, Domanska G, Schuett C, Kiank C. Different stress-related phenotypes of BALB/c mice from in-house or vendor: alterations of the sympathetic and HPA axis responsiveness. BMC Physiol. 2010;10:2. https://doi.org/10.1186/1472-6793-10-2.
33. Danielian PS, Muccino D, Rowitch DH, Michael SK, McMahon AP. Modification of gene activity in mouse embryos in utero by a tamoxifen-inducible form of Cre recombinase. Curr Biol. 1998;8:1323–6. https://doi.org/10.1016/s0960-9822(07)00562-3.
34. Zariwala HA, Borghuis BG, Hoogland TM, Madisen L, Tian L, de Zeeuw CI, et al. A Cre-dependent GCaMP3 reporter mouse for neuronal imaging in vivo. J Neurosci. 2012;32:3131–41. https://doi.org/10.1523/JNEUROSCI.4469-11.2012.
35. Vanden Berghe P, Kenyon JL, Smith TK. Mitochondrial Ca2+ uptake regulates the excitability of myenteric neurons. J Neurosci. 2002;22:6962–71. https://doi.org/10.1523/JNEUROSCI.22-16-06962.2002.
36. Boesmans W, Hao MM, Fung C, Li Z, van den Haute C, Tack J, et al. Structurally defined signaling in neuro-glia units in the enteric nervous system. Glia. 2019;67:1167–78. https://doi.org/10.1002/glia.23596.
37. Li Z, Hao MM, van den Haute C, Baekelandt V, Boesmans W, Vanden BP. Regional complexity in enteric neuron wiring reflects diversity of motility patterns in the mouse large intestine. Elife. 2019. https://doi.org/10.7554/eLife.42914.
38. Preibisch S, Saalfeld S, Schindelin J, Tomancak P. Software for bead-based registration of selective plane illumination microscopy data. Nat Methods. 2010;7:418–9. https://doi.org/10.1038/nmeth0610-418.
39. Boesmans W, Martens MA, Weltens N, Hao MM, Tack J, Cirillo C, Vanden BP. Imaging neuron-glia interactions in the enteric nervous system. Front Cell Neurosci. 2013;7:183. https://doi.org/10.3389/fncel.2013.00183.
40. Kotlo K, Anbazhagan AN, Priyamvada S, Jayawardena D, Kumar A, Chen Y, et al. The olfactory G protein-coupled receptor (Olfr-78/OR51E2) modulates the intestinal response to colitis. Am J Physiol Cell Physiol. 2020;318:C502–13. https://doi.org/10.1152/ajpcell.00454.2019.
41. Schneider R, Leven P, Mallesh S, Breßer M, Schneider L, Mazzotta E, et al. IL-1-dependent enteric gliosis guides intestinal inflammation and dysmotility and modulates macrophage function. Commun Biol. 2022;5:811. https://doi.org/10.1038/s42003-022-03772-4.
42. Kalff JC, Türler A, Schwarz NT, Schraut WH, Lee KKW, Tweardy DJ, et al. Intra-abdominal activation of a local inflammatory response within the human muscularis externa during laparotomy. Ann Surg. 2003;237:301–15. https://doi.org/10.1097/01.SLA.0000055742.79045.7E.
43. Makowka P, Bruegmann T, Dusend V, Malan D, Beiert T, Hesse M, et al. Optogenetic stimulation of Gs-signaling in the heart with high spatiotemporal precision. Nat Commun. 2019;10:1281. https://doi.org/10.1038/s41467-019-09322-7.
44. Progatzky F, Pachnis V. The role of enteric glia in intestinal immunity. Curr Opin Immunol. 2022;77: 102183. https://doi.org/10.1016/j.coi.2022.102183.
45. Gulbransen BD, Christofi FL. Are we close to targeting enteric glia in gastrointestinal diseases and motility disorders? Gastroenterology. 2018;155:245–51. https://doi.org/10.1053/j.gastro.2018.06.050.
46. Sanz E, Bean JC, Carey DP, Quintana A, McKnight GS. RiboTag: ribosomal tagging strategy to analyze cell-type-specific mRNA expression in vivo. Curr Protoc Neurosci. 2019;88: e77. https://doi.org/10.1002/cpns.77.
47. Wehner S, Vilz TO, Stoffels B, Kalff JC. Immune mediators of postoperative ileus. Langenbecks Arch Surg. 2012;397:591–601. https://doi.org/10.1007/s00423-012-0915-y.

48. Nieves MD, Furmanski O, Doughty ML. Sensorimotor dysfunction in a mild mouse model of cortical contusion injury without significant neuronal loss is associated with increases in inflammatory proteins with innate but not adaptive immune functions. J Neurosci Res. 2021;99:1533–49. https://doi.org/10.1002/jnr.24766.
49. Zamanian JL, Xu L, Foo LC, Nouri N, Zhou L, Giffard RG, Barres BA. Genomic analysis of reactive astrogliosis. J Neurosci. 2012;32:6391–410. https://doi.org/10.1523/JNEUROSCI.6221-11.2012.
50. Mathys H, Davila-Velderrain J, Peng Z, Gao F, Mohammadi S, Young JZ, et al. Single-cell transcriptomic analysis of Alzheimer's disease. Nature. 2019;570:332–7. https://doi.org/10.1038/s41586-019-1195-2.
51. Farro G, Stakenborg M, Gomez-Pinilla PJ, Labeeuw E, Goverse G, Di Giovangiulio M, et al. CCR2-dependent monocyte-derived macrophages resolve inflammation and restore gut motility in postoperative ileus. Gut. 2017;66:2098–109. https://doi.org/10.1136/gutjnl-2016-313144.
52. Wehner S, Schwarz NT, Hundsdoerfer R, Hierholzer C, Tweardy DJ, Billiar TR, et al. Induction of IL-6 within the rodent intestinal muscularis after intestinal surgical stress. Surgery. 2005;137:436–46. https://doi.org/10.1016/j.surg.2004.11.003.
53. Docsa T, Bhattarai D, Sipos A, Wade CE, Cox CS, Uray K. CXCL1 is upregulated during the development of ileus resulting in decreased intestinal contractile activity. Neurogastroenterol Motil. 2020;32: e13757. https://doi.org/10.1111/nmo.13757.
54. Penkowa M, Espejo C, Ortega-Aznar A, Hidalgo J, Montalban X, Martínez Cáceres EM. Metallothionein expression in the central nervous system of multiple sclerosis patients. Cell Mol Life Sci. 2003;60:1258–66. https://doi.org/10.1007/s00018-003-3021-z.
55. Howarth GS, Bastian SEP, Dunbar AJ, Goddard C. Betacellulin promotes growth of the gastrointestinal organs and effects a diuresis in normal rats. Growth Factors. 2003;21:79–86. https://doi.org/10.1080/08977190310001605779.
56. Chen F, Yang W, Huang X, Cao AT, Bilotta AJ, Xiao Y, et al. Neutrophils promote amphiregulin production in intestinal epithelial cells through TGF-β and contribute to intestinal homeostasis. J Immunol. 2018;201:2492–501. https://doi.org/10.4049/jimmunol.1800003.
57. Bahrami S, Drabløs F. Gene regulation in the immediate-early response process. Adv Biol Regul. 2016;62:37–49. https://doi.org/10.1016/j.jbior.2016.05.001.
58. Guyer RA, Stavely R, Robertson K, Bhave S, Mueller JL, Picard NM, et al. Single-cell multiome sequencing clarifies enteric glial diversity and identifies an intraganglionic population poised for neurogenesis. Cell Rep. 2023;42:112194. https://doi.org/10.1016/j.celrep.2023.112194.
59. Miller I, Min M, Yang C, Tian C, Gookin S, Carter D, Spencer SL. Ki67 is a graded rather than a binary marker of proliferation versus quiescence. Cell Rep. 2018;24:1105-1112.e5. https://doi.org/10.1016/j.celrep.2018.06.110.
60. Sun X, Kaufman PD. Ki-67: more than a proliferation marker. Chromosoma. 2018;127:175–86. https://doi.org/10.1007/s00412-018-0659-8.
61. Wu C, Jeong M-Y, Kim JY, Lee G, Kim J-S, Cheong YE, et al. Activation of ectopic olfactory receptor 544 induces GLP-1 secretion and regulates gut inflammation. Gut Microbes. 2021;13:1987782. https://doi.org/10.1080/19490976.2021.1987782.
62. Lee S-J, Depoortere I, Hatt H. Therapeutic potential of ectopic olfactory and taste receptors. Nat Rev Drug Discov. 2019;18:116–38. https://doi.org/10.1038/s41573-018-0002-3.
63. van der Beek CM, Dejong CHC, Troost FJ, Masclee AAM, Lenaerts K. Role of short-chain fatty acids in colonic inflammation, carcinogenesis, and mucosal protection and healing. Nutr Rev. 2017;75:286–305. https://doi.org/10.1093/nutrit/nuw067.
64. Biskou O, Meira de-Faria F, Walter SM, Winberg ME, Haapaniemi S, Myrelid P, et al. Increased numbers of enteric glial cells in the Peyer's patches and enhanced intestinal permeability by glial cell mediators in patients with ileal Crohn's disease. Cells. 2022;11:335. https://doi.org/10.3390/cells11030335.
65. Schonkeren SL, Thijssen MS, Vaes N, Boesmans W, Melotte V. The emerging role of nerves and glia in colorectal cancer. Cancers (Basel). 2021. https://doi.org/10.3390/cancers13010152.
66. Lomax AE, Sharkey KA, Furness JB. The participation of the sympathetic innervation of the gastrointestinal tract in disease states. Neurogastroenterol Motil. 2010;22:7–18. https://doi.org/10.1111/j.1365-2982.2009.01381.x.
67. Madrigal JL. Noradrenaline, Astroglia, and Neuroinflammation. In: Vardjan N, Zorec R, editors. Noradrenergic signaling and astroglia. London: Academic Press; 2017. p. 273–87. https://doi.org/10.1016/B978-0-12-805088-0.00014-1.
68. Tong F, He Q, Du W-J, Yang H, Du D, Pu S, Han Q. Sympathetic nerve mediated spinal glia activation underlies itch in a cutaneous T-cell lymphoma model. Neurosci Bull. 2021. https://doi.org/10.1007/s12264-021-00805-6.
69. Sutin J, Griffith R. Beta-adrenergic receptor blockade suppresses glial scar formation. Exp Neurol. 1993;120:214–22. https://doi.org/10.1006/exnr.1993.1056.
70. Straub RH, Wiest R, Strauch UG, Härle P, Schölmerich J. The role of the sympathetic nervous system in intestinal inflammation. Gut. 2006;55:1640–9. https://doi.org/10.1136/gut.2006.091322.
71. Vardjan N, Horvat A, Anderson JE, Yu D, Croom D, Zeng X, et al. Adrenergic activation attenuates astrocyte swelling induced by hypotonicity and neurotrauma. Glia. 2016;64:1034–49. https://doi.org/10.1002/glia.22981.
72. Yoshioka Y, Negoro R, Kadoi H, Motegi T, Shibagaki F, Yamamuro A, et al. Noradrenaline protects neurons against H2 O2 -induced death by increasing the supply of glutathione from astrocytes via β3 -adrenoceptor stimulation. J Neurosci Res. 2021;99:621–37. https://doi.org/10.1002/jnr.24733.
73. Danková M, Domoráková I, Fagová Z, Stebnický M, Kunová A, Mechírová E. Bradykinin and noradrenaline preconditioning influences level of antioxidant enzymes SOD, CuZn-SOD, Mn-SOD and catalase in the white matter of spinal cord in rabbits after ischemia/reperfusion. Eur J Histochem. 2019. https://doi.org/10.4081/ejh.2019.3045.
74. Laureys G, Gerlo S, Spooren A, Demol F, de Keyser J, Aerts JL. $\beta_2$-adrenergic agonists modulate TNF-α induced astrocytic inflammatory gene expression and brain inflammatory cell populations. J Neuroinflammation. 2014;11:21. https://doi.org/10.1186/1742-2094-11-21.
75. Galaz-Montoya M, Wright SJ, Rodriguez GJ, Lichtarge O, Wensel TG. β2-Adrenergic receptor activation mobilizes intracellular calcium via a non-canonical cAMP-independent signaling pathway. J Biol Chem. 2017;292:9967–74. https://doi.org/10.1074/jbc.M117.787119.
76. Maxwell JT, Domeier TL, Blatter LA. β-adrenergic stimulation increases the intra-SR Ca termination threshold for spontaneous Ca waves in cardiac myocytes. Channels (Austin). 2013;7:206–10. https://doi.org/10.4161/chan.24173.
77. Duffy S. Adrenergic calcium signaling in astrocyte networks within the hippocampal slice. J Neurosci. 1995. https://doi.org/10.1523/JNEUROSCI.15-08-05535.1995.
78. Willemze RA, Welting O, van Hamersveld P, Verseijden C, Nijhuis LE, Hilbers FW, et al. Loss of intestinal sympathetic innervation elicits an innate immune driven colitis. Mol Med. 2019. https://doi.org/10.1186/s10020-018-0068-8.
79. Willemze RA, Welting O, van Hamersveld HP, Meijer SL, Folgering JHA, Darwinkel H, et al. Neuronal control of experimental colitis occurs via sympathetic intestinal innervation. Neurogastroenterol Motil. 2018. https://doi.org/10.1111/nmo.13163.
80. Schneider KM, Blank N, Alvarez Y, Thum K, Lundgren P, Litichevskiy L, et al. The enteric nervous system relays psychological stress to intestinal inflammation. Cell. 2023;186:2823-2838.e20. https://doi.org/10.1016/j.cell.2023.05.001.
81. Schiller M, Azulay-Debby H, Boshnak N, Elyahu Y, Korin B, Ben-Shaanan TL, et al. Optogenetic activation of local colonic sympathetic innervations attenuates colitis by limiting immune cell extravasation. Immunity. 2021;54:1022-1036.e8. https://doi.org/10.1016/j.immuni.2021.04.007.
82. Willemze RA, Bakker T, Pippias M, Ponsioen CY, de Jonge WJ. β-Blocker use is associated with a higher relapse risk of inflammatory bowel disease: a Dutch retrospective case-control study. Eur J Gastroenterol Hepatol. 2018;30:161–6. https://doi.org/10.1097/MEG.0000000000001016.
83. Imura T, Shimohama S, Sato M, Nishikawa H, Madono K, Akaike A, Kimura J. Differential expression of small heat shock proteins in reactive astrocytes after focal ischemia: possible role of β-adrenergic receptor. J Neurosci. 1999;19:9768–79. https://doi.org/10.1523/JNEUROSCI.19-22-09768.1999.
84. Deng L, Guo H, Wang S, Liu X, Lin Y, Zhang R, Tan W. The attenuation of chronic ulcerative colitis by (R)-salbutamol in repeated DSS-induced mice. Oxid Med Cell Longev. 2022;2022:9318721. https://doi.org/10.1155/2022/9318721.

85. Clemente-Moragón A, Gómez M, Villena-Gutiérrez R, Lalama DV, García-Prieto J, Martínez F, et al. Metoprolol exerts a non-class effect against ischaemia-reperfusion injury by abrogating exacerbated inflammation. Eur Heart J. 2020;41:4425–40. https://doi.org/10.1093/eurheartj/ehaa733.
86. Ramadan N, El-Menshawy S, Amal Elsayed S, Shireen Sami MO. Protective effects of propranolol and carvedilol on experimentallyinduced ulcerative colitis in male albino rat. Eur J Mol Clin Med. 2021. https://doi.org/10.13140/RG.2.2.22062.38724.
87. Snoek SA, Dhawan S, van Bree SH, Cailotto C, van Diest SA, Duarte JM, et al. Mast cells trigger epithelial barrier dysfunction, bacterial translocation and postoperative ileus in a mouse model. Neurogastroenterol Motil. 2012;24:172-e91. https://doi.org/10.1111/j.1365-2982.2011.01820.x.

## Publisher's Note

## 3.3 Publication 3: Schneider R, *et al.* 2022 – IL-1-dependent enteric gliosis guides intestinal inflammation and dysmotility and modulates macrophage function

communications biology

ARTICLE

https://doi.org/10.1038/s42003-022-03772-4 OPEN

# IL-1-dependent enteric gliosis guides intestinal inflammation and dysmotility and modulates macrophage function

Reiner Schneider[1], Patrick Leven[1], Shilpashree Mallesh[1], Mona Breßer[1], Linda Schneider[1], Elvio Mazzotta[2], Paola Fadda[2], Tim Glowka[1], Tim O. Vilz[1], Philipp Lingohr[1], Jörg C. Kalff[1], Fievos L. Christofi[2,3] & Sven Wehner[1,3]✉

*Muscularis Externa* Macrophages (*ME*-Macs) and enteric glial cells (EGCs) are closely associated cell types in the bowel wall, and important interactions are thought to occur between them during intestinal inflammation. They are involved in developing postoperative ileus (POI), an acute, surgery-induced inflammatory disorder triggered by IL-1 receptor type I (IL1R1)-signaling. In this study, we demonstrate that IL1R1-signaling in murine and human EGCs induces a reactive state, named enteric gliosis, characterized by a strong induction of distinct chemokines, cytokines, and the colony-stimulating factors 1 and 3. Ribosomal tagging revealed enteric gliosis as an early part of POI pathogenesis, and mice with an EGC-restricted IL1R1-deficiency failed to develop postoperative enteric gliosis, showed diminished immune cell infiltration, and were protected from POI. Furthermore, the IL1R1-deficiency in EGCs altered the surgery-induced glial activation state and reduced phagocytosis in macrophages, as well as their migration and accumulation around enteric ganglia. In patients, bowel surgery also induced IL-1-signaling, key molecules of enteric gliosis, and macrophage activation. Together, our data show that IL1R1-signaling triggers enteric gliosis, which results in *ME*-Mac activation and the development of POI. Intervention in this pathway might be a useful prophylactic strategy in preventing such motility disorders and gut inflammation.

[1] Department of Surgery, University Hospital Bonn, Bonn, Germany. [2] Department of Anesthesiology, Wexner Medical Center, The Ohio State University, Columbus, OH, USA. [3] These authors contributed equally: Fievos L. Christofi, Sven Wehner. ✉email: Sven.Wehner@ukbonn.de

Abdominal surgery induces an acute intestinal inflammation within the *muscularis externa* (*ME*)[1], resulting in functional motility disturbances, clinically known as postoperative ileus (POI). POI occurs in up to 27% of patients undergoing abdominal surgery[2] and is associated with prolonged hospitalizations, increased morbidity, and a high medico-economic burden[3]. As a result, patients suffer from nausea, vomiting, increased inflammatory response, and a higher risk of anastomotic leakage after colorectal surgery[4].

Studies of the past decades demonstrated that resident muscularis macrophages (*ME*-Macs)[5] as well as enteric glial cells (EGCs)[6] are key players and early responders in the postoperative *ME* inflammation[5,7,8]. In addition, both cell types lie in close anatomical association with enteric neurons, and there is growing evidence of communication between these cell types in health and gastrointestinal diseases in the context of inflammation[9–11].

EGCs express markers including S100β, glial-fibrillary acid protein (GFAP), proteolipid-protein-1 (PLP-1), or Sox10, commonly used as glial biomarkers to identify these cells throughout the intestine[11]. EGCs are present along the entire gastrointestinal tract, are known to modulate motility[12], and contribute to neuroinflammation in the gut[13]. Notably, some studies showed that EGCs maintain gut homeostasis[14] and that deletion of EGCs driven by the GFAP-promoter led to a massive inflammatory reaction in the GI tract[15,16], indicating a crucial immune-regulatory role of EGCs in the gut. However, these findings were challenged by a recent study showing that a proteolipid-protein-1 (PLP-1) driven depletion of EGC did not affect barrier maintenance nor sensitize mice to intestinal inflammation[12]. Despite controversial findings, EGCs are still discussed as promising interventional targets in several GI diseases, including POI[13,17]. EGC presence in the mucosa[18] and the *ME*[19] requires, in turn, the presence of intestinal microbiota. Furthermore, EGCs release immune mediators like interleukin-6 (IL-6) after stimulation with innate immune stimuli, including bacterial lipopolysaccharides[13], and host-derived factors like interleukin-1 (IL-1)[11]. Our group recently demonstrated that EGCs acquire a reactive phenotype after extracellular ATP treatment[20]. That study was the first to define the molecular identity of a reactive EGC phenotype, which we named "enteric gliosis". The general term *gliosis* is a well-established part of posttraumatic injury in the CNS[21] that involves intercellular communication between classical CNS immune cells, e.g., microglia, and neural cell types, including neurons and astrocytes. Based on similar functions and transcriptional profiles[22–25], *ME*-Macs and EGCs are often compared to microglia and astrocytes, respectively, and the bidirectional communication of the latter is a well-defined mechanism determining the functional fate of both cell types during inflammation[26].

In the intestine, there is growing evidence for an interaction of *ME*-Macs and cells of the enteric nervous system. Cell-to-cell communication between enteric neurons and *ME*-Macs has been shown to involve the release of colony-stimulating factor 1 (CSF1) and bone morphogenetic protein 2, respectively, and this interaction is thought to fine-tune intestinal motility[27]. Interactions between EGCs and *ME*-Macs were also recently described, showing that EGCs are a more potent source of CSF1. EGCs modulate visceral sensitivity through mechanisms that require interleukin-1β (IL-1β) and connexin-43 hemichannels (Cx43) to release CSF1, to activate *ME*-Macs[28]. While this study was the first to provide evidence on EGC–*ME*-Macs interactions in chronic intestinal inflammation, proof for this interaction in acute inflammation, occurring during POI, remains elusive. It is also unknown whether there is a link between EGC–*ME*-Macs interactions and abnormal motility in an acute inflammatory motility disorder such as POI.

We previously demonstrated that IL-1 is an essential cytokine in POI development, and pharmacological IL-1-antagonism with the drug anakinra or a global genetic IL1R1 depletion was shown to protect mice from POI[6]. Furthermore, we elucidated the role of the two ligands, IL-1 and IL-1β, in POI with a particular focus on IL-1β[29]. EGCs express IL1R1, and IL-1 stimulation results in the release of IL-6 and CCL2, which are known to play a role in POI[30–32]. Recently, IL-1-signaling in EGCs was also suspected of exerting pro-tumorigenic functions[33]. However, these studies demonstrated IL-1-induced cytokine release by EGCs only by carrying out in vitro experiments. Moreover, an EGC-specific approach, i.e., by cell-specific depletion of IL1R1 in EGCs, has not been used so far. Therefore, solid evidence of the cell-specific role of IL-1-signaling and focused analyses of EGC reactivity in vivo are still missing.

Herein, we aimed to fill this gap using two transgenic mouse models. First, the transgenic *RiboTag* mouse model allows a comprehensive in vivo "snapshot" of actively transcribed mRNA in EGCs[34]. Secondly, we generated a mouse with a targeted depletion of IL1R1 in glial-fibrillary acid (GFAP) expressing cells, one exclusive marker of EGCs. Additionally, we investigated if and how IL-1-signaling in EGCs affects *ME*-Mac responses by a series of transcriptional and functional analyses. Finally, we aimed to confirm our findings from our mouse study in human bowel specimens taken during a duodenopancreatectomy and in primary human EGC cultures isolated from GI surgical specimens. Together, our results show that IL-1 induces stimulus-specific enteric gliosis in EGCs that affects *ME*-Mac function and accounts for POI development in mice. Furthermore, findings in mice are translatable to humans since we discovered that the same molecular pathways are activated in the *ME* of the human postoperative bowel.

## Results

**IL-1 induces a specific type of gliosis in enteric glial cells.** Recently, we showed that surgical trauma and intestinal manipulation induce a reactive enteric glial cell (EGC) phenotype, also referred to as "enteric gliosis", coinciding with the release of various cytokines and chemokines[20]. We hypothesized that IL-1 triggers reactive gliosis, so we stimulated primary murine EGC cultures (Fig. S1a) with IL-1β and confirmed gliosis induction by validating known biomarkers that serve as hallmarks of a gliotic phenotype. IL-1β induced IL-6 release (Fig. S1b), proliferation (Fig. S1c), and changes in morphology (Fig. S1d) in EGCs. To generate a more comprehensive molecular signature profile of the IL-1 triggered alterations in gene expression in EGCs, we performed a bulk-RNA-Seq analysis. A principal component analysis (PCA) indicated a clear separation between IL-1β and vehicle-treated EGCs (Fig. 1a). Upon IL-1β treatment, 496 genes were up, and 826 were down-regulated (Fig. 1b, $p < 0.05$; fold-change 1.5). Among the 20 most highly induced genes, we found inflammatory mediators like *IL-6*, chemokines (*Cxcl2*, *Cxcl5*, *Ccl2*, *Ccl5*), and colony-stimulating factors (*Csf1*, *Csf3*) (Fig. 1b). In addition, heat map analyses of genes sorted for induced inflammatory mediators confirmed these inductions (Fig. S1e). Next, we specified the reactive EGC state by gene ontology (GO) analysis, which revealed a gene enrichment within the terms "glial activation", "IL-1-signaling", "migration", and "inflammatory response" (Fig. 1c). Concurring heat maps confirmed a clear pattern in IL-1-activated EGCs (Fig. 1d + e), underlining their reactive state. Furthermore, by implementing our previously established "enteric gliosis" gene panel identified by ATP stimulation[20], we found a unique gene expression induced by IL-1β in EGCs, vastly different from our previously published ATP-induced gene panel (Fig. S1f). Comparison of our data set to published data investigating various stimuli for EGC activation, i.e.,

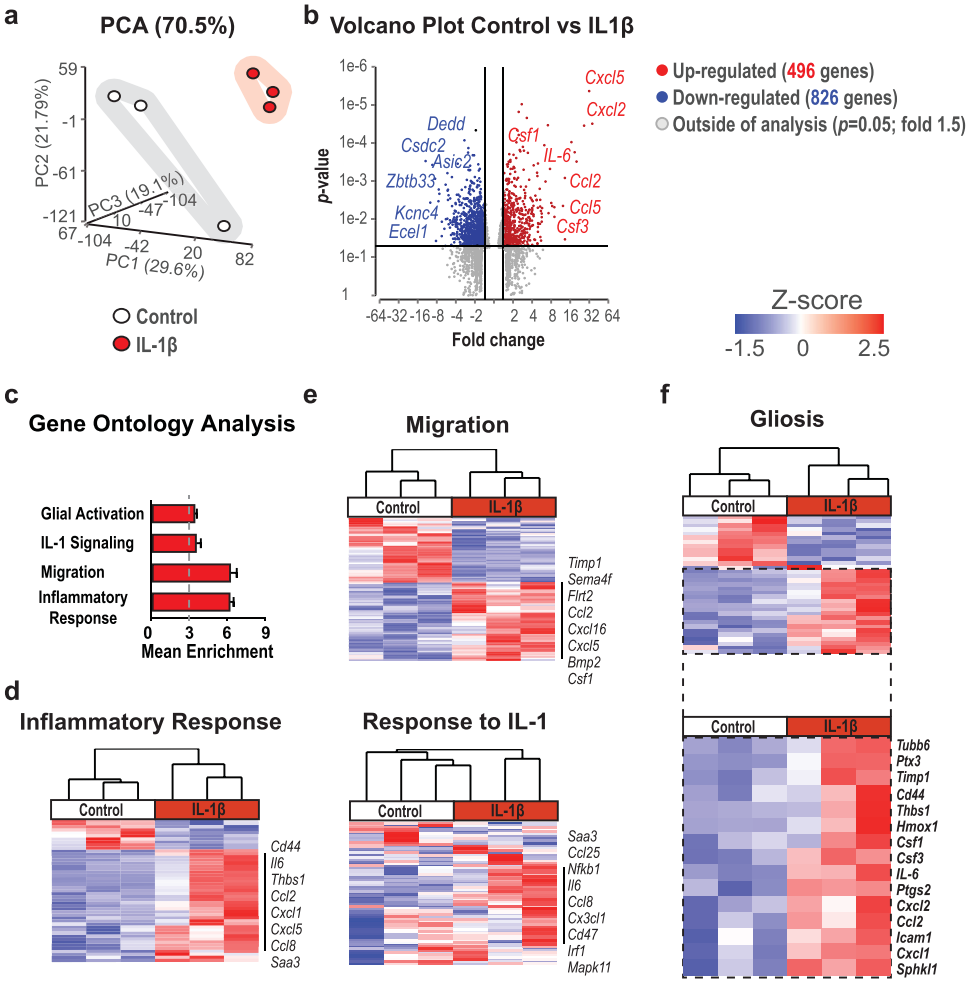


**Fig. 1 IL-1 induces a specific reactive phenotype in EGCs.** EGCs were treated with IL-1β (10 ng/ml) or vehicle (control) for 24 h and processed for bulk-RNA-Seq. **a** PCA plot shows a clear separation between both groups. **b** Volcano plot showing all significantly regulated genes. **c** Gene ontology (GO) analysis of IL1β-treated EGCs showing enrichment of genes connected to the indicated GO terms. **d**, **e** Heat maps of differentially expressed genes involved in "inflammatory response", "migration", and "response to IL-1" between IL-1β- and vehicle-treated EGCs. **f** Heat map of genes involved in "gliosis" highlighting the induced gene panel. Statistics were done with Fisher's exact test, $n = 3$ per group.

infection[35] or DNBS colitis[36], also revealed a distinct pattern for the IL-1β induced enteric gliosis phenotype with an inevitable overlap in key genes (Fig. S1g and Table S5). This analysis indicates that gliosis and EGC reactivity greatly depends on the inducing immune stimulus. IL-1-treated EGCs showed a prominent elevation of chemokine and cytokine levels involved in gliotic processes. Moreover, two new essential factors were identified in reactive glia in POI, *Csf1* and *Csf3* (Fig. 1f), with Csf1 recently implicated in EGC responses in a murine colitis model and human Crohn's Disease[28].

We conclude that IL-1 induces a specific transcriptome activation signature in EGCs, resulting in a distinct form of EGC gliosis leading to dysmotility and POI, with possible functions in inflammatory processes in the gut.

**IL-1-induced enteric gliosis resembles the EGC reactivity profile after surgical trauma**. In order to prove that the before-mentioned most prominent markers of the IL-1β-induced gliosis (see Fig. 1) are indeed selectively expressed by EGCs and not by other cell types present at low levels in EGC primary cell cultures, we used a Cre-recombinase-driven approach to analyze the expression of actively transcribed key gliosis genes. This approach is based on Cre-mediated (*Sox10*$^{CreERT2}$) tagging of the ribosomal Rpl22 protein with a hemagglutinin (HA) tag and subsequent immunoprecipitation of the ribosomes, including actively transcribed mRNA (Fig. 2a and ref. [34]). Immunofluorescence microscopy confirmed selective expression of the HA tag in SOX10$^+$ EGCs in cell cultures in vitro and, importantly, in vivo within *ME* whole mounts (Fig. 2b). Furthermore, after IL-1β treatment, key signature genes of gliosis (*GFAP*, *Nestin*) together with cytokines (*IL-6*, *TNFα*), chemokines (*Ccl2*, *Ccl5*, *Cxcl2*, *Cxcl5*), and growth factors (*Csf1*, *Csf3*) were selectively expressed and induced in EGCs (Figs. 2c and S2a).

As previous work implicated an immune-modulating role of EGCs in the postoperative inflammation of the *ME* resulting in POI[6,20], we next subjected *Sox10*$^{CreERT2+}$*xRpl22*$^{HA/+}$ mice to intestinal surgical manipulation (IM) to investigate the reactive state of EGCs in vivo (Figs. 2d and S2b). As expected, 24 h after IM, these mice exhibited a strong postoperative infiltration of blood-derived leukocytes within the *ME* (Fig. S2c) and impaired GI-transit time (Fig. S2d), confirming regular induction of POI. Since we expected an early activation of EGCs after surgery, we then analyzed another group of the *Sox10*$^{CreERT2+}$*xRpl22*$^{HA/+}$ mice at an early postoperative time point (IM3h). Bulk-RNA-Seq analyses of HA-precipitated EGC-specific mRNA revealed significant gene enrichment within the terms "*IL-1-signaling*", "*migration*", and "*inflammation*" (Fig. 2e). Heat maps for these GO-terms confirmed the activation pattern for an inflammatory

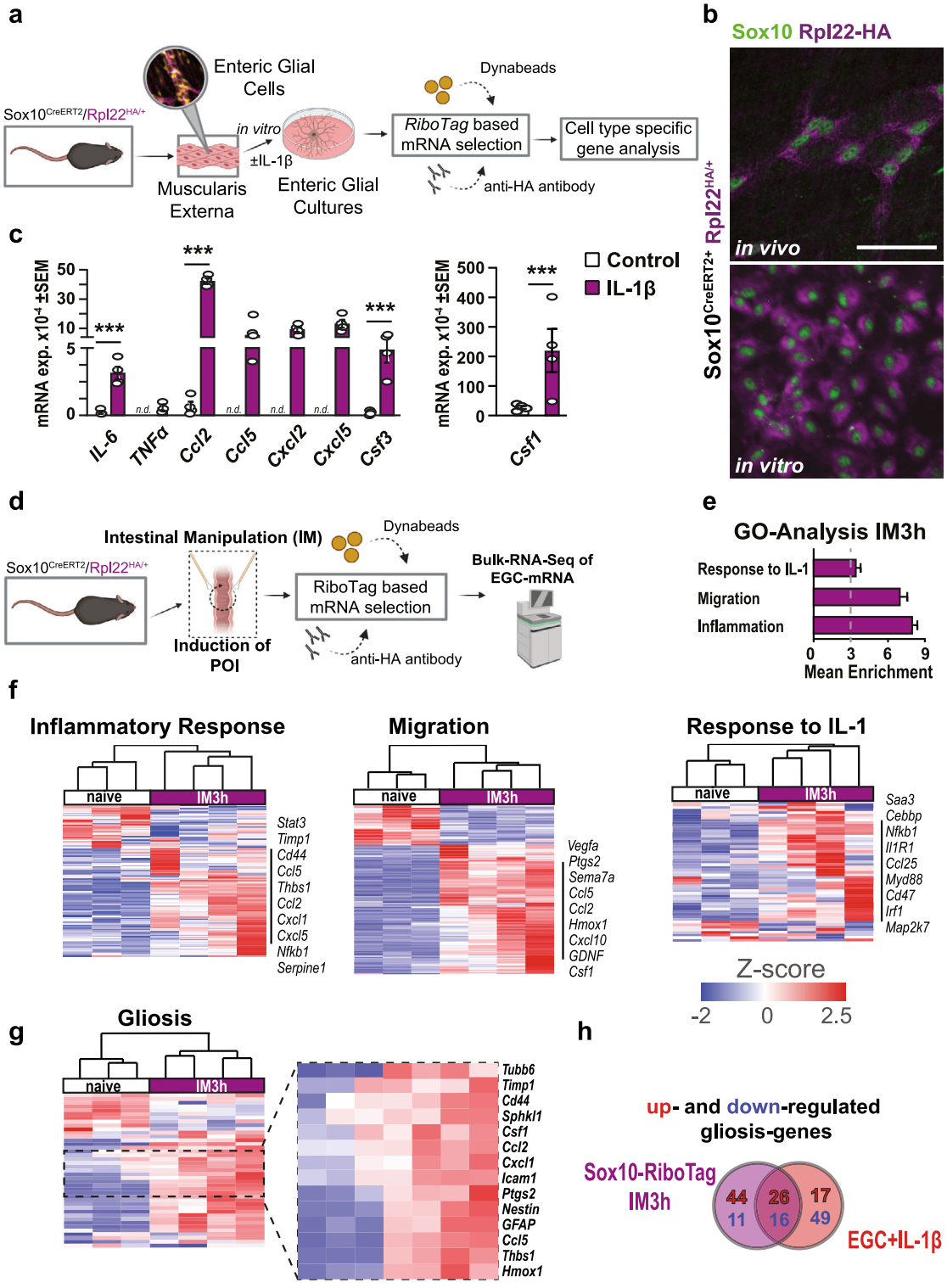


**Fig. 2 IL-1-induced enteric gliosis resembles the EGC reactivity profile after surgical trauma. a** Schematic overview of the *RiboTag* method applied in primary EGCs treated with IL-1β (10 ng/ml) or vehicle (control) for 3 h and processed for qPCR. $n = 4$ per group. **b** Representative immunofluorescence microscopy for EGCs (SOX10$^+$, green) and the *RiboTag* (HA$^+$, violet) in vivo (small intestine *ME*) and in vitro (EGC cultures) from *Sox10*$^{CreERT2+}$-*Rpl22*$^{HA/+}$ mice. Scale bar 50 µm. **c** qPCR analysis for gliosis-associated genes in primary EGCs treated with IL-1β. Bars showing mean gene expression compared to 18S. $n = 4$. **d** Schematic overview of the *RiboTag* method applied in the POI animal model. *Sox10*$^{CreERT2+}$-*Rpl22*$^{HA/+}$ mice underwent intestinal manipulation to induce POI, and EGC-specific mRNA was immunoprecipitated and used for bulk-RNA-Seq. $n = 3$–4 per group. **e** GO analysis of enriched genes at IM3h. **f** Heat maps of genes involved in "inflammatory response", "response to IL-1", and "migration". **g** Heat map of genes involved in "gliosis" highlighting the induced gene panel. **h** Venn-diagram of differentially expressed gliosis genes in IL-1β-treated EGCs and *Sox10*$^{CreERT2+}$-*Rpl22*$^{HA/+}$ mice at IM3h. Statistics were done with Student's *t*-test. ***<0.001, * were compared to untreated EGC cultures.

response, as well as genes involved in migration and IL-1 responsiveness (Fig. 2f). Applying our enteric gliosis gene panel, we discovered an overlap of multiple IL-1-induced and IM-induced genes in EGCs. A heat map visualized the shared, induced genes, including inflammatory mediators (e.g., *Ccl2*, *Ccl5*, *Cxcl1*), structural proteins (e.g., *GFAP*, *Nestin, Tubb6*), activation markers (e.g., *Cd44*, *Icam1*, *Hmox1*), and growth factors (*Csf1*, *Csf3*) (Fig. 2g). A Venn-diagram showed the exact transcriptional overlap in gliosis genes between IL-1β-stimulated EGCs and the reactive EGC phenotype induced by surgical trauma (Fig. 2h and Table S6). More than 20% of the up-and downregulated gliosis genes overlapped, revealing IL-1 as a substantial part of surgery-induced EGC reactivity in vivo.

**EGC-restricted IL1R1 deficiency prevents postoperative macrophage activation and protects mice from POI**. Given that IL-1 induces EGC reactivity in POI, we next analyzed the functional significance of IL-1-triggered EGC gliosis on POI development. We subjected mice with an EGC-restricted IL1R1-deficiency ($GFAP^{cre}xIL1R1^{fl/fl}$, Fig. S3a) and IL1R1 competent control mice ($GFAP^{WT}xIL1R1^{fl/fl}$) to IM (Fig. 3a). To validate IL1R1-deficiency, we analyzed $GFAP^{Cre+}xAi14^{fl/fl}$ mice by immunohistochemistry for SOX10 and tdtomato expression, which confirmed a 95% overlay between the glial marker and the transgenic signal, thereby validating *Gfap* as a suitable Cre-promotor for a reliable IL1R1-deficiency in EGCs (Fig. S3b). Next, we performed bulk-RNA-Seq analysis on IM3h *ME* of conditional KO mice and wild-type littermates. The PCA plot revealed a clear separation between both groups (Fig. 3b), with 287 upregulated and 437 downregulated genes in $GFAP^{cre}xIL1R1^{fl/fl}$ mice (Fig. S3c). Genes listed under the GO-terms "glial activation", "IL-1-signaling", "migration", and "inflammatory response" were enriched and more expressed in IL1R1 competent mice (Fig. 3c). A heat map of all differentially expressed genes ($p < 0.05$) revealed the downregulation of distinct gliosis genes in $GFAP^{cre}xIL1R1^{fl/fl}$ mice at IM3h, e.g., chemokines (*Ccl2*, *Cxcl1*, *Cxcl2*, *Ccl7*) and structural proteins (*GFAP*, *Cx43*, *Tubb6*) (Fig. 3d). To validate if these transcriptional alterations also affect the postoperative inflammation and the clinical outcome of POI (i.e., slow GI transit), we quantified the postoperative GI-transit and leukocyte infiltration 24 and 72 h after IM. Impressively, $GFAP^{cre+}xIL1R1^{fl/fl}$ mice were almost entirely protected from postoperative motility disturbances 24 h after IM (Fig. 3e), and leukocyte infiltration was severely reduced by more than 50% for myeloperoxidase$^+$ and 45% for CD45$^+$ leukocytes compared to $GFAP^{WT}xIL1R1^{fl/fl}$ mice (Figs. 3f and S3d). Gastrointestinal motility did not differ between genetically modified mouse strains (Fig. 3e) and C57BL6 wild-type mice upon surgery. Flow cytometry analyses confirmed reduced leukocyte infiltration by diminished numbers of F4/80$^+$ monocyte-derived macrophages, Ly6C$^+$ monocytes, activated (CD68$^+$) *ME*-Macs, and Ly6G$^+$ neutrophils in $GFAP^{cre+}xIL1R1^{fl/fl}$ mice (Figs. 3g and S3d). Notably, confocal microscopy confirmed decreased numbers of MHCII$^+$ leukocytes around ENS ganglia in the postoperative *ME* of $GFAP^{cre+}xIL1R1^{fl/fl}$ mice (Fig. 3h), an effect probably based on the diminished expression of chemokines by EGCs. Indeed, a *NanoString* inflammatory panel revealed a severely diminished gene expression of inflammatory mediators (e.g., *Ccl2*, *Cxcl2*, *Cxcl5*), cytokines (e.g., *IL-6*), and a macrophage activation marker (*Arg1*) in the postoperative *ME* of $GFAP^{cre+}xIL1R1^{fl/fl}$ mice (Fig. 3i). In line, the postoperative increase of immune cell activation markers (*CD68*, *Mip-1a*, *Csf1*, *Csf3*), as well as gliosis markers (*IL-6*, *Ccl2*, *Nestin*, and *GFAP* was abrogated in $GFAP^{cre+}xIL1R1^{fl/fl}$ mice (Figs. 3j and S3e). Notably, similar results were observed in $GFAP^{cre}xMyd88^{fl/fl}$ mice, with an EGC-restricted Myd88-deficiency, an essential adaptor molecule in the IL1R1 pathway. $GFAP^{cre+}xMyd88^{fl/fl}$ mice showed comparable downregulated gene expression patterns as $GFAP^{cre+}xIL1R1^{fl/fl}$ mice and were protected from POI (Fig. S3f + g).

Based on these data, we conclude that an IL-1-mediated macrophage-glial interaction might be critical in POI development.

**Intestinal organotypic cultures demonstrate IL-1-dependent involvement in ME-Mac-EGC interactions**. Previously, we and others have shown that resident *ME*-Macs also play a critical role in POI. The close anatomical relation between EGCs and resident *ME*-Macs and the multiple immune mediators released by EGCs that can activate macrophages indicate that these cells communicate with each other, and EGCs might influence *ME*-Mac activation. However, upon surgical manipulation, inflammation attracts monocyte-derived macrophages that can hardly be distinguished from resident *ME*-Macs. In order to focus exclusively on the latter's response, we established an in vitro intestinal organotypic culture (IOC) model that closely reflects the resident in vivo cell composition and structures without being compromised by infiltrating immune cells. An aseptic separation procedure of the mouse jejunum *ME* was used to simulate the mechanical activation after surgical trauma. Separated *ME* specimens were either directly used as controls or cultivated for 3 h, reflecting the IM3h time point of the in vivo model (Fig. 4a). Notably, the separation procedure produced a stronger immune response in the *ME* than the gentle in vivo IM, which was indicated by the increased gene expression of gliosis genes in IOCs than in vivo manipulated ME after 3 h (Fig. S4a). Immunofluorescence microscopy for the activation marker FOSb as well as SOX10 and β-3-tubulin (TUBB3) showed intact and activated FOSb$^+$ EGCs after 3 h incubation but no activation in control *ME* (Fig. S4b). Strong *Fosb* induction was confirmed by qPCR (Fig. S4c). Interestingly, after the 3 h incubation period, we counted significantly more activated CD68$^+$ *ME*-Macs around enteric ganglia (Figs. 4b + c and S4d). Moreover, 3D reconstruction identified the near localization of CD68$^+$ *ME*-Macs around enteric ganglia (Fig. S4e). In line with our in vivo POI mouse data, qPCR measurements of established markers for gliosis (*Nestin*, *GFAP*), intestinal inflammation (*IL-6*, *IL-1β*, *Ccl2*), and immune cell activation (*Mip-1a*, *CD68, Csf1*, *Csf3*), showed significant induction in the 3 h cultured IOCs (Fig. 4d). We transferred this model also to IOCs generated from $GFAP^{cre+}xIL1R1^{fl/fl}$ and their Cre-negative littermates. The former showed a weaker induction of gliosis, intestinal inflammation, and immune cell activation genes (Fig. 4e), indicating that the absence of EGC-specific IL-1-signaling reduces the trauma-induced *ME*-Mac activation.

**The impact of EGC-derived factors on macrophage function**. To further elucidate the interactions of EGCs and *ME*-Macs, we treated primary EGCs with IL-1β or vehicle and transferred the conditioned media (CM) to IL1R1-deficient bone-marrow-derived macrophage (BMDM) cultures (Fig. 5a). The primary EGC cultures consist of at least 80% glia and low amounts of neurons (Fig. S5a) and fibroblasts, verified by ICC[20] and RNA-Seq analysis for relevant cell type markers (Fig. S5b). To verify the IL-1-induced gliosis and routinely perform quality control of the CMs, we measured protein levels of prominent inflammatory markers, IL-6 and CCL2 (Fig. S5c). Moreover, to confirm that only the EGCs in our primary cultures react to the IL-1-activation by releasing inflammatory mediators, we generated primary EGCs from $GFAP^{Cre+}xIL1R1^{fl/fl}$ and $GFAP^{WT}xIL1R1^{fl/fl}$ mice. $GFAP^{Cre+}$ EGC cultures showed lower expression of inflammatory mediators on protein (Fig. S5d) and mRNA (Fig. S5e) levels,

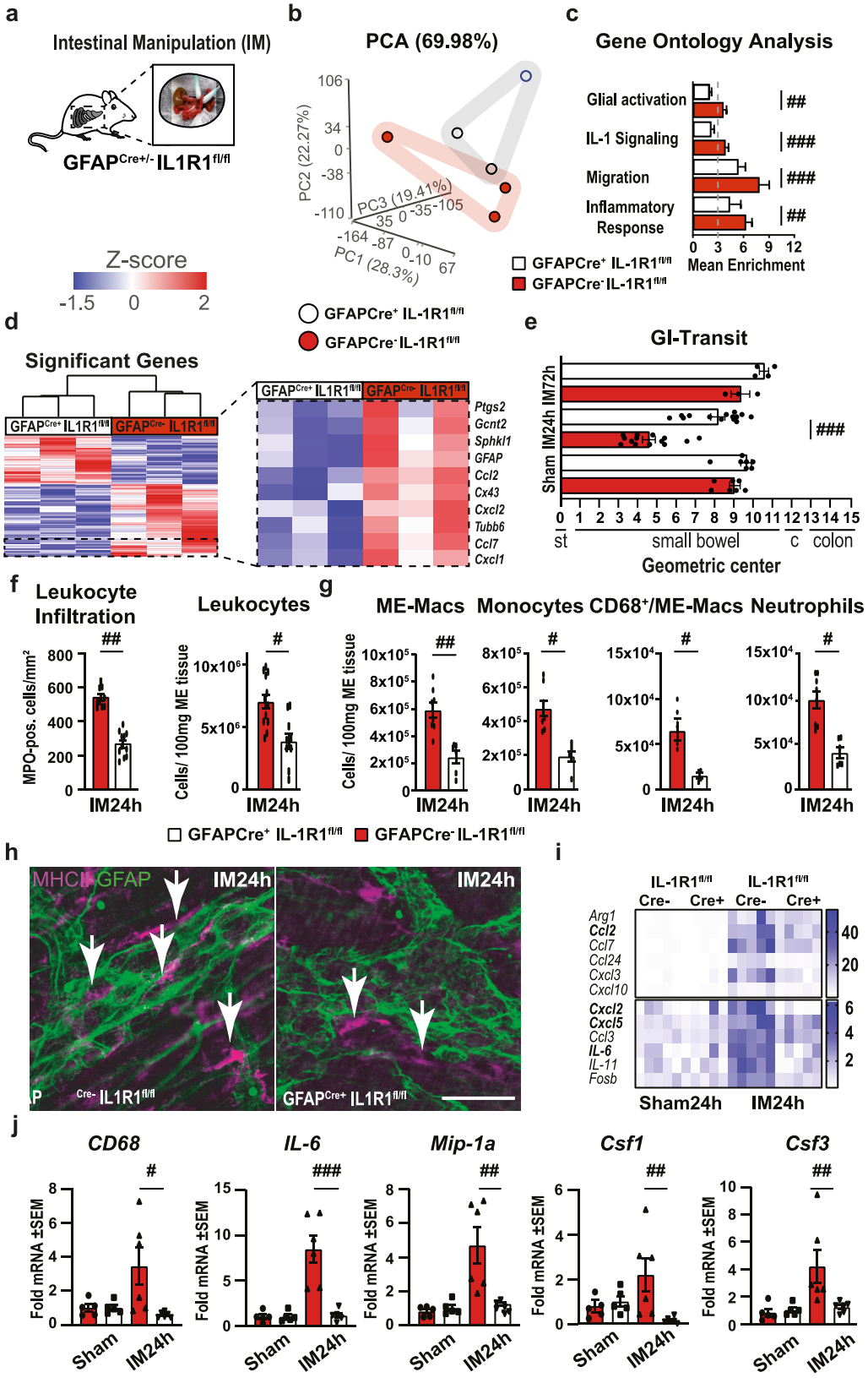


proving that these factors are released by EGCs into the CM after IL-1 treatment ($CM^{IL\text{-}1}$).

After 3 h treatment with the EGC-conditioned media, BMDMs were analyzed by bulk-RNA-Seq. The resulting PCA demonstrated a clear separation of the groups (Fig. 5b). Notably, we already observed altered functionality between naïve BMDMs and those treated with CM of vehicle-treated EGCs ($CM^{Veh}$). This effect was even more pronounced in BMDMs treated with the $CM^{IL\text{-}1}$ (Fig. S5f), resulting in 762 up- and 1656 downregulated genes (Fig. 5c). Within the list of differentially expressed genes, classical M1 (*Il1b*, *Tlr4*, *Sphk1*) and M2 (*Arg1*, *Socs3*, *Tgfb1*) markers showed that IL-1-triggered EGC factors affect the

**Fig. 3 EGC-restricted IL1R1 deficiency prevents postoperative macrophage activation and protects mice from POI. a–d** $GFAP^{Cre+}$-$IL1R1^{fl/fl}$ and $GFAP^{Cre-}$-$IL1R1^{fl/fl}$ mice underwent intestinal manipulation (IM) to induce POI. After 3 h, RNA of the ME was processed for bulk-RNA-Seq. $n = 3$ per group. **b** PCA plot of $Cre^+$ and $Cre^-$ groups. **c** GO enrichment analysis at IM3h comparing $Cre^+$ and $Cre^-$ animals, normalized to respective sham mice. **d** Heat map of differentially expressed genes highlighting induced gliosis genes. **e–j** $GFAP^{Cre+}$-$IL1R1^{fl/fl}$ and $GFAP^{Cre-}$-$IL1R1^{fl/fl}$ mice were analyzed at IM24h. **e** GI-transit analysis in IM72, IM24h, and sham24h groups of $Cre^+$ and $Cre^-$ mice. $n = 7$ (Sham); 14 (IM24h); 3–4 (IM72h). **f** Leukocyte infiltration quantification by MPO histology and FACS in IM24h groups of $Cre^+$ and $Cre^-$ mice. $n = 10$ per group. **g** FACS analysis for *ME*-Macs ($CD45^+$, $F4/80^+$), monocytes ($CD45^+$, $Ly6C^-$, $Ly6G^+$), activated ME-Macs ($CD68^+$, $F4/80^+$), and neutrophils ($CD45^+$, $Ly6C^+$, $Ly6G^-$) in IM24h groups of $Cre^+$ and $Cre^-$ mice. $n = 5$ per group. **h** Representative immunofluorescence microscopy of *ME* whole mounts showing EGCs ($GFAP^+$, green) and ME-Macs ($MHCII^+$, violet) in IM24h groups of $Cre^+$ and $Cre^-$ mice. Scale bar 50 µm. **i, j** Gene expression analysis by inflammatory *NanoString* panel (**i**) and by qPCR (**j**) for genes related to inflammation (*IL-6*) and immune cell activation (*CD68, Mip-1a, Csf1, Csf3*) at IM24h in $Cre^+$ and $Cre^-$ mice, normalized to corresponding sham groups. $n = 5$ per group. Statistics were done with Student's *t*-test and Fisher's exact test. # < 0.05, ## < 0.01, ###<0.001, # were compared to $Cre^-$ littermates.

macrophage polarization status. GO analysis and heat maps displayed substantial changes in gene clusters for "migration", "phagocytosis", and "inflammatory response" (Fig. 5d + e). Consequently, we analyzed EGC-CM-treated BMDMs for migration and phagocytosis, with the FCS treatment as a positive control. In wound-healing and transwell assays, we observed increased migration of BMDMs treated with $CM^{IL\text{-}1}$ compared to control and $CM^{Veh}$ (Figs. 5f + g and S5g). Phagocytosis, measured by FITC-dextran uptake after 2 h, was also increased (Fig. 5h). Overall, our data indicate that EGCs already affect macrophage function and polarization under resting conditions; however, macrophage activation and functionality are far more altered by factors released from IL-1β-stimulated EGCs.

**Enteric gliosis and IL-1-signaling are involved in acute intestinal inflammation after abdominal surgery**. Finally, we validated the existence of IL-1-dependent enteric gliosis in humans. Histology on intraoperatively taken jejunal specimens from patients undergoing open abdominal surgery for pancreatic head resection confirmed the close association of $CD68^+$ *ME*-Macs and $GFAP^+$ EGCs in the *ME* (Fig. 6a) and a strong IL1R1 expression in EGCs (Fig. S6a + b). Notably, this oncological surgery allowed the collection of tumor-free bowel samples at an early and a late time point during surgery (Fig. 6b). By validating the enteric gliosis status in the patient samples, we discovered the induction of inflammatory mediators (*IL-1α, IL-1β, IL-6*, *CCL2*, *CXCL2*), immune cell activators (*CSF1*, *CSF3*, *MIP-1a*), and EGC gliosis markers *(GFAP*, *NESTIN)* (Figs. 6c and S6c), previously identified in our mouse studies. To expand our understanding of ongoing mechanisms in the tissue after surgery, we performed bulk-RNA-Seq on early and late intraoperatively taken jejunal *ME* specimens and found more than 400-differentially regulated genes (Fig. 6d + e). In line with our murine data sets, gene clusters associated with "glial activation", "IL-1-signaling", "migration", and "inflammatory response" were enriched in intestinal samples from late surgery time points (Fig. 6f), correlating with corresponding heat maps (Fig. S6d). Moreover, heat map visualization of significantly regulated genes ($p < 0.05$) revealed the upregulation of distinct gliosis genes, e.g., chemokines (*CCL2*, *CXCL2*), structural proteins (*TUBB6*), and activation markers (*HMOX1*, *SOCS3*, *ICAM1*) during surgery (Fig. 6g), indicating the manifestation of enteric gliosis during surgery. To validate the effect of IL-1 on surgical samples, we prepared human jejunal IOCs from late collected patient material and incubated them with the IL1R1-antagonist anakinra for 24 h, previously used in vivo in the POI model[6]. Anakinra-treated human IOCs showed lower expression of CCL2 and IL-6 (Fig. S6e), indicating a dampened inflammatory activation response. We finally tested if primary human EGC cultures also become reactive upon IL-1β-stimulation (Fig. 6h). We detected induction of inflammatory mediators such as *IL-6*, *TNFα*, *CCL2*, *CXCL2*, and *IL-8* on mRNA level (Fig. 6i) as well as IL-6, and CCL2 on protein level (Fig. S6f) after IL-1β treatment, underlining that the gliosis phenotype is conserved across species.

Together, our data demonstrate that enteric gliosis is also induced in patients and that IL-1 induces EGC reactivity and production of various mediators that can modulate *ME*-Mac activation and functionality, thereby guiding postoperative intestinal inflammation and POI.

Overall, our investigation demonstrates that IL-1 induces a reactive phenotype in mouse EGCs. This distinct enteric gliosis state is part of the postoperative immune cascade in the *ME* in both mice and humans, and an EGC-restricted IL1R1 deficiency ameliorates POI in mice. Furthermore, mediators released by reactive EGCs alter the phenotype and function of resident *ME*-Macs towards an activated macrophage type with stronger migratory and phagocytic capabilities.

## Discussion

Over the last 2 decades or so, the role of glial cells evolved from "giving structural support" to "issuing orders", especially after trauma and under inflammatory conditions, with a multitude of examples in the central[21] and enteric nervous system[11]. The present study advances our understanding of the molecular mechanisms in EGCs in an inflamed gut, and it provides an assessment of the communication between EGCs and macrophages during acute intestinal inflammation in POI. In particular, we demonstrate that EGCs acquired a reactive phenotype after surgical trauma and defined this reactive state as enteric gliosis. A key discovery is that IL1R1-signaling is a critical driver of EGC reactivity in this process. Furthermore, we found that reactive EGCs communicate with intestinal *ME*-Macs, whose cellular functions become altered towards an activated phenotype, characterized by increased migratory and phagocytic activity. Selective disruption of IL1R1-signaling in EGCs prevented reactive gliosis and protected mice from postoperative *ME* inflammation, motility disturbances, and POI.

Previously, we revealed that a pan-IL1R1 deficiency protected mice from postoperative bowel wall inflammation[6]. Our study added IL-1 signaling to a list of key factors in immune-mediated motility disorders that are used as an indicator for a successful therapy like the cytokine IL-6[30], which is also induced by IL-1[6,29], or TNFα, which is essential in the later stages of POI[37]. In POI development, various inflammatory mediators, like danger-associated molecular patterns (DAMPs: e.g., ATP[20] and IL-1α[29]) and pathogen-associated molecular patterns (PAMPs: e.g., dsRNA[7], and LPS[38]), play an essential role and contribute to the disease progression[39]. However, our recent work highlighted that IL1R1 is expressed on EGCs, and discovered that IL-1-signaling in EGCs might be a key component in intestinal inflammation and motility impairment after abdominal surgery[6].

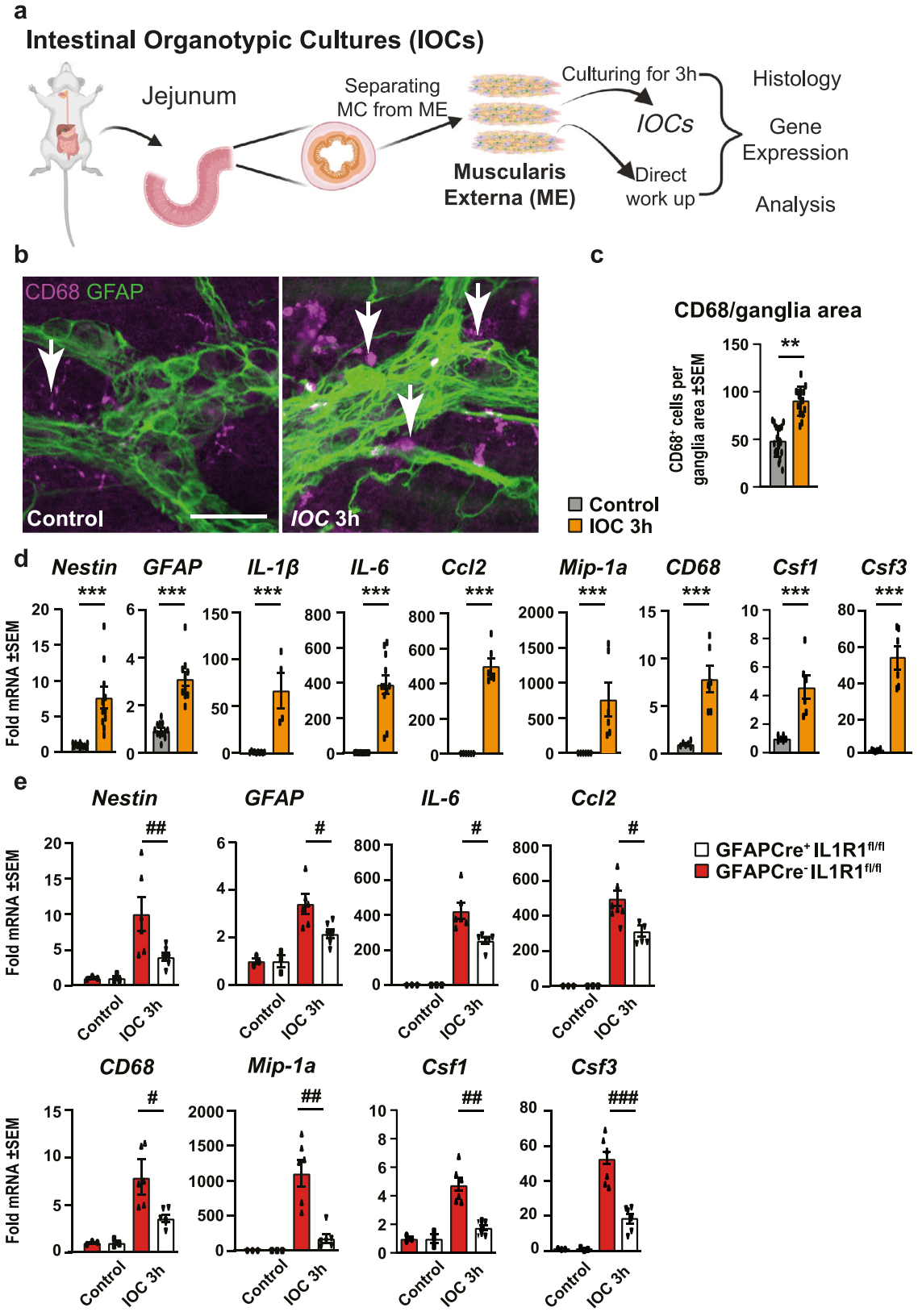


Herein, we now proved the importance of glial IL1R1-signaling with several transgenic mouse models that allowed us to precisely analyze and modify EGC reactivity in vivo and in vitro. One of these models is the *Sox10*$^{CreERT2+}$*xRpl22*$^{HA/+}$ (*RiboTag*) mouse, suitable for generating an in vivo "snapshot" of actively transcribed RNA selectively in EGCs[34,36]. Analysis of *RiboTag* mice confirmed that IL1R1-signaling is part of post-operative EGC reactivity. Around 2/3 of upregulated genes overlap between IL-1β-stimulated EGCs in vitro and the reactive EGC phenotype induced by IM in vivo. We conclude that an IL-1-induced EGC reactivity is a major trigger of surgery-induced enteric gliosis.

**Fig. 4 Intestinal organotypic cultures demonstrate IL-1-dependent involvement in ME-Mac-EGC interactions. a** Experimental workflow scheme. Intestinal organotypic cultures (IOC) from *muscularis externa* (*ME*) were prepared from C57BL/6 wild-type mouse jejunum by surgical dissection of the *lamina propria* and mucosa tissue, a procedure that mimics the surgical trauma in vivo. This model allows the analysis of resident cell types in the absence of any infiltrating blood-derived immune cells. IOCs were either directly processed or incubated for 3 h, corresponding to the IM3h time point in the POI mouse model. $n = 6$ per group. **b**, **c** Histological visualization (**b**) and quantification (**c**) of activated macrophages ($CD68^+$, violet) surrounding enteric ganglia (GFAP+, green). $n = 5$ mice per group; quantifying ganglia in 3–4 IOCs per mouse. Scale bar 50 µm. **d** Gene expression analysis in IOCs by qPCR for genes involved in "enteric gliosis" (*Nestin, GFAP*), *inflammation* (*IL-1β, IL-6, Ccl2*), and *immune cell activation* (*Mip-1a, CD68, Csf1, Csf3*). **e** IOCs were prepared from $GFAP^{Cre+}$-$IL1R1^{fl/fl}$ and $GFAP^{Cre-}$-$IL1R1^{fl/fl}$ mice according to the same experimental workflow shown in **a** and either directly processed or incubated for 3 h. Gene expression analysis by qPCR for genes involved in "enteric gliosis", "inflammation", and "immune cell activation". $n = 3$–8 per group. Statistics were done with Student's *t*-test. */#<0.05, **/##<0.01, ***/###<0.001, All * compared to control IOCs, all # compared to $Cre^-$ littermates.

Further evidence for stimulus-selective reactivity in EGCs comes from the comparison of IL-1β- and ATP-stimulated EGCs. We recently showed that ATP induces enteric gliosis[20]. Compared to ATP, IL-1β caused a stronger induction of several chemokines, suggesting a specific role in reactive processes upon surgery. These findings imply that the term "reactive glia", commonly used to describe a general glial activation, does not represent a hardwired phenotype as it depends on the specific stimulus. However, some genes were upregulated in ATP-and IL-1β-stimulated EGCs, including *IL-6*, *Cxcl1*, and *Cxcl2*, prominently induced in astrogliosis[40], and *Hmox1*, a marker for neurodegeneration[41] and reactive glial cells[42]. These genes might be part of an overarching response found in multiple reactive EGC phenotypes, pointing to a core gliosis signature across various organs and stimuli. Future comparisons of enteric gliosis signatures from other glial cell populations as well as other diseases might help to specify both the core gliosis signature and the stimulus- and disease-specific responses of reactive glial cells. Usage of published data sets from activated EGCs under inflammatory conditions (infection[35] and colitis[36]) showed that IL-1 induced gliosis shares induced genes and shows individual molecular responses. However, the available data were collected with different approaches, mouse models, intestinal parts, and transcriptional analysis methods, providing only a rough initial idea of core genes and conditions leading to specific gliosis expression patterns. More comprehensive comparisons with multiple conditions are required and expected to be published in the future to allow reliable conclusions on core and conditions-specific gliosis signatures.

Given that IL-1-signaling induced the expression of a variety of immune mediators, which might preferably act on immune cells located in anatomical proximity, we focused on the interactions of EGCs and *ME*-Macs. These *ME*-Macs have previously been shown to be crucial in the postoperative immune response in POI[5,37,43]. An ex vivo IOC model allowed us to explicitly focus on the EGCs and ME-Macs interaction. In manipulated IOCs, we found an upregulation of several molecules depending on glial IL1R1-signaling known to act on macrophages and affect their function. Among these genes, we found unspecific macrophage activation markers (*Mip1* and *CD68*) and members of the *Csf1* family (*Csf1* and *Csf3*), which exert distinct functions on macrophage differentiation.

Furthermore, CSF1 was described as an essential factor in maintaining *ME*-Macs[44]. Although enteric neurons were first identified as a CSF1 source in the intestine[27], a recent study by the Gulbransen group showed that EGCs produce more *Csf1* than enteric neurons in a colitis model[28]. They also showed that IL-1 triggers CSF1 release from EGC cultures in vitro *and* increases MHCII and CD68 expression in BMDM cultures. Our IOC model and in vivo data add to this hypothesis, showing that EGCs indeed produce CSF1 and activate *ME*-Macs in their native environment. Notably, the IOCs' initial immune response was stronger than the in vivo manipulated ME response at 3 h after mechanical separation or surgical manipulation. We interpret this difference as a consequence of an increased release of additional factors due to the stronger mechanical forces applied to the IOCs during their preparation than the more gentle in vivo ME manipulation. These mediators might trigger additional immune responses independent of IL-1 release.

Consequently, IL1R1 depletion or antagonism does not dampen the cytokine production and EGC activation in the IOC model to the same extent as in the more gentle in vivo surgical manipulation approach. Here, it should be noted that the IOC does not fully reflect POI as it is missing important characteristics of POI development. First peripheral innervation of the SNS and PNS, known to modulate the ME immune response to surgery, is missing. Secondly, and more critical for the later inflammatory phase IOCs do not become infiltrated by blood-derived leukocytes, which extravasate into the *ME* after surgical manipulation. For these reasons, IOCs do not represent an ex vivo POI model but a suitable model for studying local tissue responses to mechanical or surgical trauma without systemic stimuli. Research using *ME* IOCs might be a tool to investigate how the tissue can immunologically respond in vitro to what might affect molecular and functional measurements, e.g., in pharmacological and physiological studies, respectively.

Another interesting molecule expressed by EGCs in an IL-1-dependent manner is *Csf3*. Compared to other members of the *Csf* family, *Csf3* is less well studied, and to date, it has been linked to neutrophil migration and activation[45,46]. As we also observed a prominent induction of the neutrophil chemokines *Cxcl2* and *Cxcl5* and a significant reduction of infiltrating neutrophils in $GFAP^{Cre}$x$IL1R1^{fl/fl}$ mice after surgery, EGCs might indeed affect the recruitment and maybe even the function of these cells. As neutrophils are not present at the beginning of intestinal surgery and instead infiltrate at later stages, an interaction of reactive EGCs with these infiltrating immune cell populations is likely and warrants future investigation. Importantly, recent studies showed that *Csf3* is able to alter macrophage polarization in vitro[47] and induce the expression of regulatory macrophage markers in DSS-colitis[48]. In breast cancer, *Csf3*-signaling also caused immunosuppressive behavior in macrophages[49], making *Csf3*, next to *Csf1*, one of the most promising EGC-released factors that impact the state and function of *ME*-Macs and/or infiltrating monocyte-derived macrophages.

EGC-selective IL1R1-deficiency completely abolished the expression of all the mediators directly acting on macrophages (i.e., Csf1, Csf3, Cxcl1, Cxcl2, Il6, Ccl2, and Mip1α), we expected that this would also alter macrophage transcriptomes and function. The capacity of EGCs to induce inflammatory responses in macrophages was indeed confirmed by RNA-Seq analysis showing changes in the inflammatory response and the expression of M1 and M2 markers. In addition to the general induction of immune responses, genes shaping essential macrophage functions

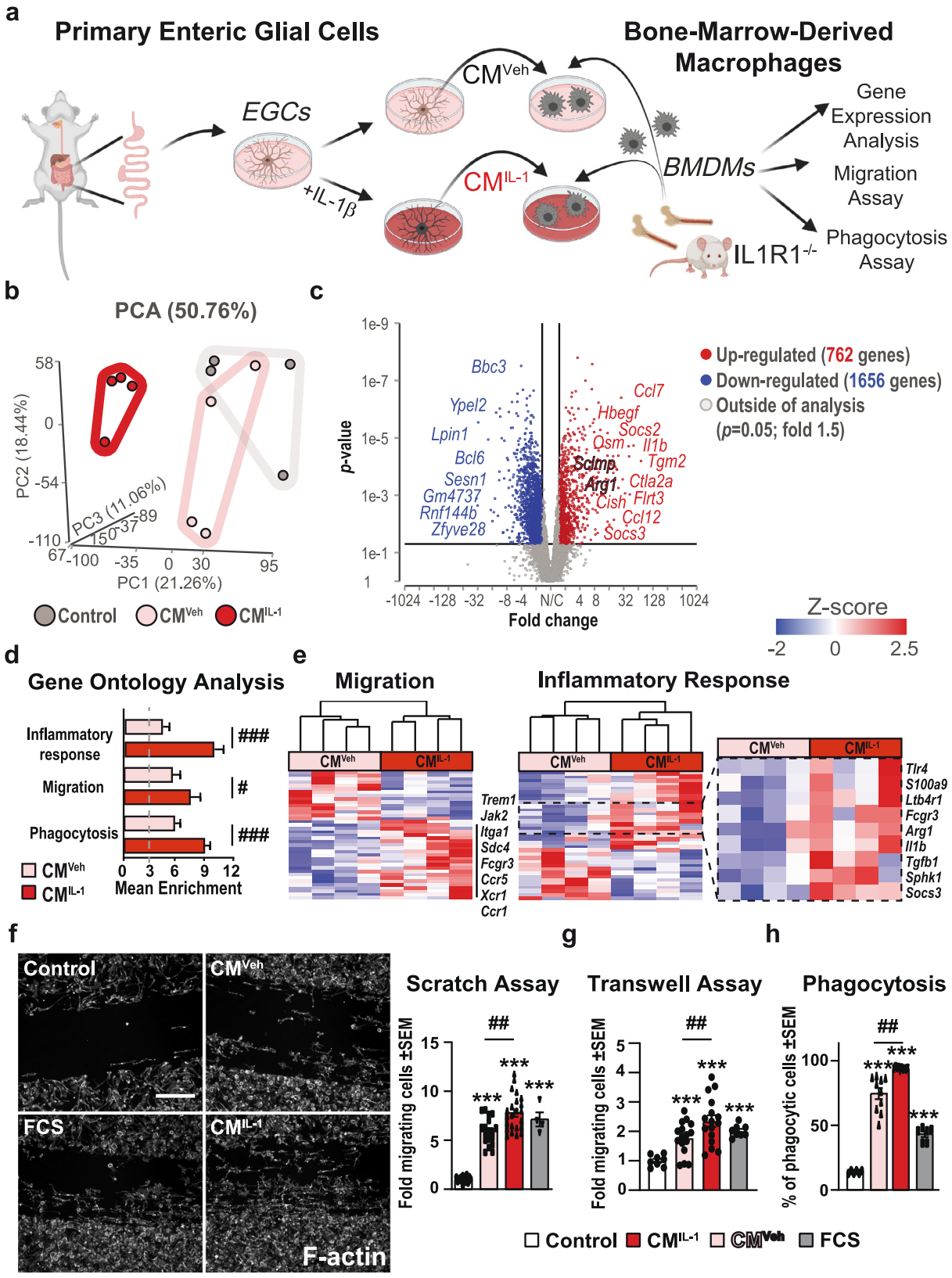


like migration and phagocytosis were also transcriptionally altered in response to reactive EGC-released factors. The accumulation of CD68$^{+}$ *ME*-Macs around enteric ganglia and their morphological changes towards a round-shaped cell type showed that *ME*-Mac migration and activation are increased upon exposure to EGC-derived mediators. Similar to microglia in the CNS, the attraction of *ME*-Macs to the vicinity of enteric ganglia might be part of a protective mechanism involving either rapid clearance of neuronal debris or neuroprotective features against excessive inflammatory responses to restore intestinal function. Increased resident macrophage accumulation at sites of neuronal damage is also observed in models of spinal cord[50] and brain

**Fig. 5 The impact of EGC-derived factors on macrophage function. a** Schematic overview showing the generation of primary EGCs and production of $CM^{IL\text{-}1}$ (EGCs treated with IL-1β (10 ng/ml) for 24 h) and $CM^{Veh}$ before transferring CM to Bone-marrow-derived macrophages (BMDMs). BMDMs were isolated from $IL1R1^{-/-}$ mice to exclude any side effects of IL1β-residues in the collected $CM^{IL\text{-}1}$. After BMDM maturation, cells were treated with $CM^{IL\text{-}1}$, $CM^{Veh}$, or were left untreated for 3 h (RNA-Seq) and 24 h (functional assays). **b** Bulk-RNA-Seq analyses of BMDMs after 3 h incubation showed a separation between the three treatment groups in a PCA plot. $n = 4$ per group. **c** Volcano plot from bulk-RNA-Seq analyses of BMDMs after 3 h treatment with $CM^{IL\text{-}1}$ or $CM^{Veh}$ highlighting the top 20 regulated genes (Fold 2, *p*-value 0.05). **d**, **e** GO enrichment analysis in BMDMs after $CM^{IL\text{-}1}$ and $CM^{Veh}$ stimulation and heat maps of genes involved in "migration" and "inflammatory response" highlighting induced genes related to macrophage function. **f–h** BMDMs were processed 24 h after CM incubation in **f** scratch ($n = 4$ independent BMDM cultures; multiple technical replicates per culture; Control (20 readings); $CM^{Veh}$ (20 readings); $CM^{IL\text{-}1}$ (20 readings); FCS (4 readings). **g** transwell ($n = 3$ independent BMDM cultures; multiple technical replicates per culture; Control (8 readings); $CM^{Veh}$ (16 readings); $CM^{IL\text{-}1}$ (16 readings); FCS (8 readings), and **h** phagocytosis ($n = 3$ independent BMDM cultures; multiple technical replicates per culture; Control (6 readings); $CM^{Veh}$ (10 readings); $CM^{IL\text{-}1}$ (10 readings); FCS (6 readings) assays. Scale bar 100 µm. Statistics were done with Student's *t*-test and Fisher's exact test. */#<0.05, **/##<0.01, ***/###<0.001, All * compared to control BMDMs, all # compared to $CM^{Veh}$-treated BMDMs.

injury[51,52], wherein microglia, the CNS counterparts of *ME*-Macs, accumulate in the damaged areas. Support for increased clearance of dying cells or debris comes from our observation that IL-1-triggered EGCs stimulate phagocytosis in macrophages. As ENS homeostasis is well-ordered by apoptosis and neurogenesis[53], an enhanced elimination of damaged neurons or their protection from excessive inflammation by phagocytosis of cell debris might be a conserved mechanism. Indeed, a neuroprotective role of *ME*-Macs during homeostasis[22] and infection has recently been shown[54]. When enteric gliosis is a key element of this neuroprotective response, a logical argumentation would be that its blockage might have detrimental effects. However, as we observed a clear improvement of POI and a reduction of postoperative inflammation by inhibiting IL1R1-mediated enteric gliosis, we suppose that neuroprotective mechanisms might play a minor role during acute postoperative inflammation and that compensatory pathways are activated to maintain this function. Another possibility is that *ME*-Mac migration to ganglia might be fundamentally a protective homeostatic mechanism, although a stronger reactive glial cell phenotype with more surgical trauma may cause an exaggerated response and activation of macrophages to act instead in a detrimental way to exacerbate the inflammatory response. Our previous work[5] and other investigators[31] have provided evidence that activated macrophages are essential contributors to the development of POI. We propose that glial IL1R1 knockout may protect mice from POI by causing a milder macrophage induction in these mice. However, a causative link between glia-to-macrophages-to neurons has not yet been established in our study for the glial IL1R1 knockout model and the resolution of the GI-transit phenotype in the POI model in $GFAP^{Cre}xIL1R1^{fl/fl}$ animals does not necessarily depend on a milder macrophage induction and glial-to-macrophage signaling. An alternative hypothesis to be tested is that IL1-induced EGCs directly influence enteric neurons that control peristalsis to cause POI and that a glial IL1R1 knockout prevents it. Recent studies show that EGCs can interact with enteric neurons, triggering cell death[55,56], neuronal dysregulation[57], and homeostasis functions[58]. These interesting questions need to be addressed in future studies. Notably, different subtypes of *ME*-Macs with different innate responsiveness have recently been described by us[7], and previous single-cell-RNA-Seq studies revealed four distinct clusters of *ME*-Macs[22]. Unfortunately, the individual subpopulation-specific cellular functions and interactions are largely unknown, and future studies have to investigate whether EGCs preferably interact with one of these distinct subtypes.

As already stated above, besides interacting with resident *ME*-Macs, EGCs might also act on infiltrating monocytes, which are non-exclusively attracted by EGC-released CCL2. CCL2 is a major chemoattractant for monocyte-derived leukocytes in POI[32,59]. Although three groups independently demonstrated that these cells do not affect POI 24 h after surgery, they are involved in the late-phase resolution, and CCR2-deficient mice (i.e., the receptor target for CCL2) recover more slowly from POI than wild-type animals[31,32,59]. This observation might point towards a potential beneficial role of EGC-derived CCL2 in POI resolution. However, in our view, this seems unlikely as we already observed a clear improvement of POI after 24 h and normalization of GI-transit after 72 h in $GFAP^{Cre+}$-$IL1R1^{fl/fl}$ mice. Hence, it is evident that there is no delay in POI at later stages.

The human data included in our study showed evidence that IL-1-signaling and enteric gliosis also occur during GI-tract surgery. Although the time between sampling of the early and late intraoperative specimen was less than 3 h, the earliest time point in our mouse studies, we observed a strong induction of cytokines and chemokines comparable to murine IL-1-triggered enteric gliosis. Notably, IL-1β was also strongly induced, and human EGCs had a strong transcriptional response, indicating a preserved mechanism of enteric gliosis in rodents and humans. Moreover, the GO analyses underlined the induction of common glial activation and immune-activating pathways. The data is translatable from mice to humans, and we conclude that the blockade of IL-1-triggered enteric gliosis might therefore prevent the development of POI in surgical patients. Previous preclinical data from our group already demonstrated that an antibody-mediated depletion of IL-1α or IL-1β or pharmacological inhibition of IL1R1 by Anakinra effectively prevented POI in mice[6]. Our findings in human IOCs, isolated from surgical patients, showing reduced IL-6 and CCL2 upon ex vivo stimulation in the presence of Anakinra, confirm our theory about an immediate EGC immune-responsiveness to IL-1 signaling. These findings emphasize our view that the initial inflammatory activation of the EGC/*ME*-Mac axis is crucial for POI development, and interaction with IL-1-signaling might be rather useful for prevention than treatment of existing POI. In line, multiple trials with Anakinra show anti-inflammatory effects in inflammation-associated intestinal diseases, such as mucositis (NCT03233776) and colorectal cancer (NCT02090101). Anakinra or other pharmacological interventions targeting IL1-signaling in EGCs could potentially serve as a prophylactic treatment in POI in surgical patients to add to the benefits of ERAS (enhanced recovery after surgery) protocols[60].

In conclusion, our study provides insights into the molecular mechanism of postoperative IL-1-triggered enteric gliosis and its consequence on the communication between EGCs and *ME*-Macs. Inhibition of this gliotic state ameliorated postoperative inflammation and protected mice from POI. Moreover, we confirmed the induction of enteric gliosis and activation of IL-1-signaling in surgical patients, supporting the idea of an intervention in the IL-1 pathway as a promising and clinically suitable strategy to prevent inflammation-induced motility disorders.

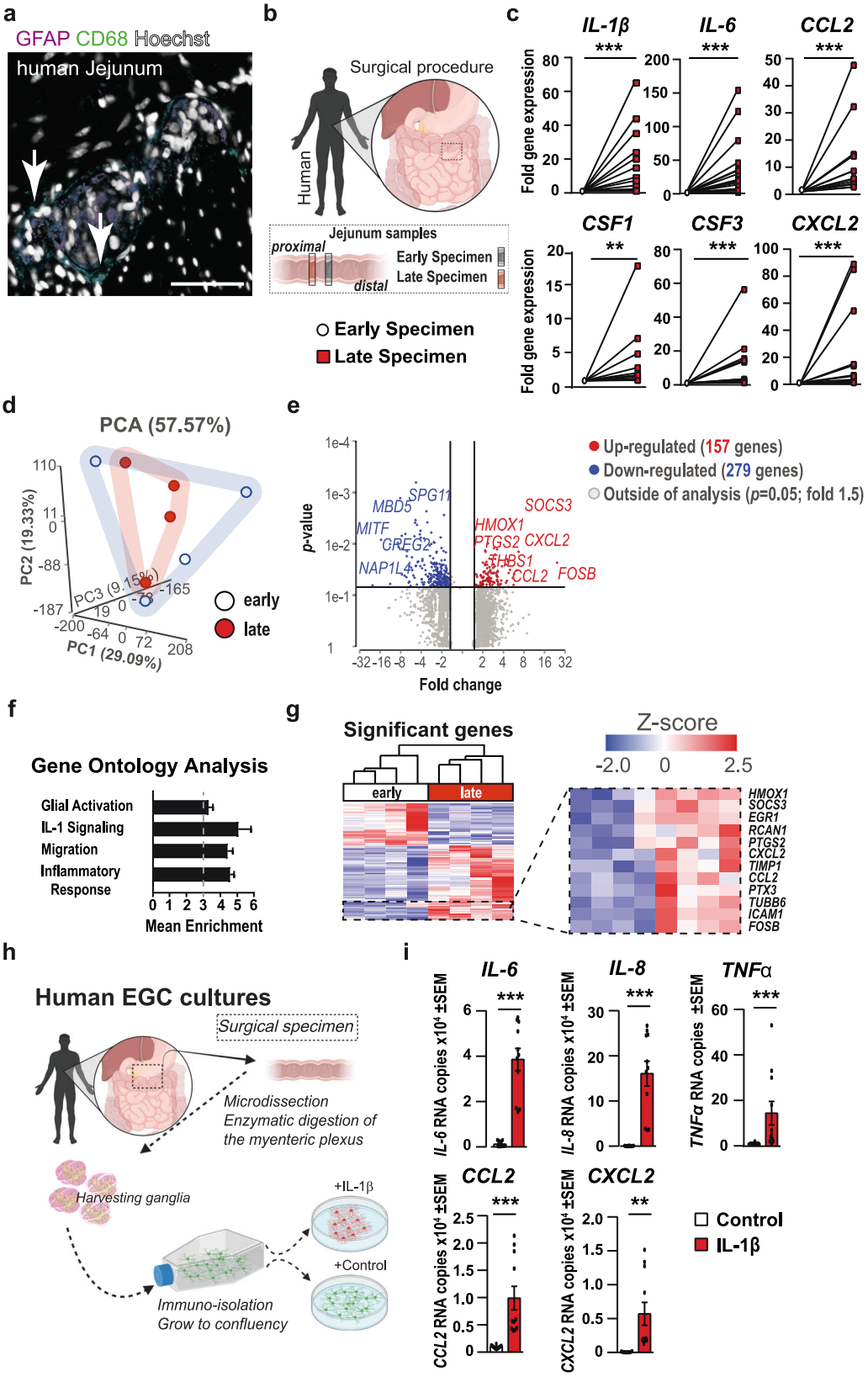


## Methods

**Animals**. Experiments were performed using 8–12-week-old Sox10-$^{CreERT2}$xRpl22$^{HA/+}$ or GFAP$^{cre}$xIL1R1$^{fl/fl}$ mice kept in a pathogen-free animal facility with standard rodent food and tap water ad libitum. Appropriate authorities of North-Rhine-Westphalia, Germany (81-02.04.2016.A367) approved experiments.

The POI mouse model was induced by intestinal manipulation as described previously[6]. Animals were sacrificed 3 and 24 h after manipulation.

**Murine enteric glia cell cultures**. Primary enteric glial cell (EGC) cultures were obtained by sacrificing C57BL/6 or GFAP$^{cre+}$ Ai14$^{fl/fl}$ mice, 8–16 weeks of age, extracting the small intestine, and cleansing it with 20 ml of oxygenated Krebs-

**Fig. 6 Enteric gliosis and IL-1-signaling are involved in acute intestinal inflammation after abdominal surgery. a** Immunohistochemistry for macrophages ($CD68^+$, green) and EGCs ($GFAP^+$, violet) in jejunal cross-sections. Hoechst (white) was used as counterstain. White arrows indicate ganglia-associated macrophages. Scale bar 50 µm. **b** Schematic overview showing the patient specimen collection of jejunal *ME* at an early and late time point during pancreatic head resection. **c** qPCR analysis of jejunal *ME* specimens for inflammation- and macrophage function-associated genes. $n = 10$–15; IL1β (14), IL-6 (15), CCL2 (13), CSF1 (10), CSF3 (11), CXCL2 (13). **d**–**g** Bulk-RNA-Seq analysis of jejunal *ME* specimens, including a PCA plot (**d**) and a Volcano plot visualizing differentially expressed genes (**e**) between late and early specimens ($p = 0.05$, fold: 1.5). $n = 4$. **f** GO term analysis of all differentially expressed genes between early and late specimens showed enrichment in gene clusters related to "glial activation", "IL-1-signaling", "migration", and "inflammatory response". **g** Heat map of significantly regulated genes highlighting gliosis-related genes. **h** Schematic overview of the generation and treatment of primary human EGCs from patient specimens. **i** *NanoString* analysis of primary human EGCs treated with IL1β or vehicle for 24 h. $n = 10$. Data are shown as mean RNA counts. Statistics were done with Student's *t*-test and Fisher's exact test. *<0.05, **<0.01, ***<0.001, All * compared to early *ME* specimens or untreated hEGCs.

Henseleit buffer (126 mM NaCl; 2.5 mM KCl: 25 mM NaHCO3; 1.2 mM NaH2PO4; 1.2 mM MgCl2; 2.5 mM CaCl2, 100 IU/ml Pen, 100 IU/ml Strep and 2.5 µg/ml Amphotericin). The small bowel was cut into 3–5 cm long segments and kept in oxygenated ice-cold Krebs-Henseleit buffer. Each segment was then drawn onto a sterile glass pipette, and the *ME* was stripped with forceps to collect muscle tissue for further digestion steps. After centrifugation (300xg for 5 min), the tissue was incubated for 15 min in 5 ml DMEM containing Protease Type1 (0.25 mg/ml, Sigma-Aldrich) and Collagenase A (1 mg/ml, Sigma-Aldrich) in a water bath at 37 °C, 150 rpm. The enzymatic digestion was stopped by adding 5 ml DMEM containing 10% FBS (Sigma-Aldrich), centrifugation for 5 min at 300xg, and re-suspended in proliferation medium (neurobasal medium with 100 IU/ Pen, 100 µg/ml Strep, 2.5 µg/ml Amphotericin (all Thermo Scientific), FGF and EGF (both 20 ng/ml, Immunotools). Cells in proliferation media were kept at 37 °C, 5% $CO_2$ for 4 days to promote the formation of enteric neurospheres. For experiments, enteric neurospheres were dissociated with trypsin (0.25%, Thermo Scientific) for 5 min at 37 °C and distributed at 50% confluency on Poly-Ornithine (Sigma-Aldrich) coated 6 well plates in differentiation medium (neurobasal medium with 100 IU/ Pen, 100 µg/ml Strep, 2.5 µg/ml Amphotericin, B27, N2 (all Thermo Scientific) and EGF (2 ng/ml, Immunotools). After 7 days in differentiation medium, mature enteric glia cells were treated with ATP (100 µM, Sigma) and IL-1 (10 ng/ml, Immunotools) and further processed for RNA isolation or their conditioned medium used for enzyme-linked immunosorbent assay (ELISA) or qPCR analysis.

**Murine bone-marrow-derived macrophage cultures**. Primary bone-marrow-derived macrophage (BMDM) cultures were obtained by sacrificing $IL1R1^{-/-}$ mice, 8–16 weeks of age, extracting the femoral bones and isolating bone-marrow stem cells with a syringe, and culturing the cells in RPMI supplemented with FCS (10%, Thermo Scientific), β-mercaptoethanol (1 mM, SIGMA) and 10 ng/ml rmCSF-1 (Immunotools). After 4 days in culture, the medium was changed to remove all dead cells, and on day 6, cells were used for all planned experiments.

For the scratch assays, BMDMs were transferred to 24-well plates and grown to 90% confluency. The "scratch" was performed with a 200 µl pipette tip, and damaged/dead cells were immediately removed by one wash step with PBS. BMDMs were treated with $CM^{Veh}$, $CM^{IL-1}$, neurobasal medium (NB) supplemented with 10% FCS, and NB without serum (control) for 24 h. After treatment, BMDMs were fixed with 4% PFA for 15 min and stained for F-Actin with Phalloidin FITC (Thermo Scientific) for 1 h, and processed with the fluorescence microscope Nikon TE2000 in the cell culture well plates.

For the transwell assays, BMDMs were placed in transwells (10,000 cells, Ibidi) and treated with $CM^{Veh}$, $CM^{IL-1}$, NB supplemented with 10% FBS, and NB without serum (control) for 3 h. Afterwards, transwells were fixed with 4% PFA for 15 min, and cells were stained for F-Actin with Phalloidin FITC (Thermo Scientific) and Hoechst for 1 h. Transwells were mounted on glass slights and processed with the fluorescence microscope Nikon TE2000.

For the phagocytosis assays, BMDMs were transferred to 24-well plates (10,000 cells/well) and treated with $CM^{Veh}$, $CM^{IL-1}$, neurobasal medium (NB) supplemented with 10% FBS and NB without serum (control) for 24 h. After removing the treatment medium, BMDMs were incubated with Dextran-Cascade Blue 10,000 MW (50 µg/ml, Thermo Scientific) for 1 h. Then washed two times with warmed PBS and collected by EDTA/Trypsin (0.05%) and processed by FACS analysis for high and low phagocytic cells.

**Human surgical specimens**. The ethics committee of the College of Medicine at the Ohio State approved the human IRB protocol[13] (Table S1).

The ethics committee of the University of Bonn, Germany, approved the collection of patient surgical specimens (*266_14*) (Table S2).

The human IRB protocol was approved by the ethics committee of the College of Medicine at The Ohio State University. Informed consent was obtained to procure viable human surgical tissue from the colon or small bowel from patients with polyps undergoing a colectomy (sigmoid colon) or patients undergoing Roux-en-Y by-pass surgery (jejunum) (Table S1). Human EGCs (hEGCs) in culture from 9 GI surgical specimens were used to study gene expression and IL1R1 immunoreactivity.

Human surgical tissue for the IOC experiments was collected from four patients undergoing pancreatectomy. Human jejunum specimens were collected in ice-cold oxygenated Krebs-Henseleit buffer during the surgical procedure and transported to the laboratory. Full-thickness jejunum specimens were incubated for 24 h with or without Anakinra (100 µg/ml) in DMEM/F12 with 10% FBS at 5%$CO_2$ and 37 °C. After 24 h, media were collected, centrifuged, and frozen in liquid nitrogen for ELISA analyses.

**Human EGC cultures**. Myenteric plexus tissue of patients was processed and cultured as described before[13,20]. Briefly, tissue collection was performed by the surgeon and immersed immediately in ice-cold oxygenated Krebs-Henseleit solution and promptly transported to the research facilities within 15 min in coordination with the Clinical Pathology Team. For isolating myenteric ganglia, tissue was pinned luminal side facing upwards under a stereoscopic microscope, and the mucosa, submucosa, and most of the circular muscle were dissected away using scissors and then flipped over to remove longitudinal muscle by dissection.

Myenteric plexus tissue was cut and enzymatically dissociated as described elsewhere (LIT) with modifications as follows: Myenteric plexus tissue was minced into 0.1–0.2 $cm^2$ pieces and dissociated in an enzyme solution (0.125 mg/ml Liberase, 0.5 µg/ml Amphotericin B) prepared in Dulbecco's modified Eagle's medium (DMEM)-F12, for 60 min at 37 °C with agitation. Ganglia were removed from the enzymatic solution by spinning down (twice), and re-suspending in a mixture of DMEM-F12, bovine serum albumin 0.1%, and DNase 50 µg/ml DNase (once). Solution containing the ganglia was transferred to a 100 mm culture dish, and isolated single ganglia free of smooth muscle or other tissue components were collected with a micropipette while visualized under a stereoscopic microscope and plated into wells of a 24-well culture plate and kept in DMEM-F12 (1:1) medium containing 10% fetal bovine serum (FBS) and a mixture of antibiotics (penicillin 100 U/ml, streptomycin 100 µg/ml, and amphotericin B 0.25 µg/ml) at 37 °C in an atmosphere of 5% $CO_2$ and 95% humidity.

After cells reach semi-confluence after 3–4 weeks (P1), hEGCs were enriched and purified by eliminating/separating fibroblasts, smooth muscle, and other cells. EGC enrichment and purification were achieved by labeling the isolated cells with magnetic microbeads linked to the anti-specific antigen, D7-Fib, and passing them through a magnetic bead separation column following the manufacturer's instructions (*Miltenyi Biotec Inc*, San Diego, CA). This purification protocol was performed twice (P2 and P3) to reach a cell enrichment of up to 10,000 fold, and 20,000 cells were plated on glass coverslips pre-coated with 20 µg/ml laminin/P-D-Lys in 50 mm bottom glass #0 culture dishes for immunostaining and imaging or 12-well plates for IL-6 or CCl2 release experiments. Cultured hEGCs were kept until confluent and harvested for additional experiments (4 to 10 days). On the day of the experiment, hEGCs were stimulated as indicated. Parallel to this, cells at each passage were split and seeded in plastic 25 $mm^2$ culture flasks and used for study in passages three to six.

**NanoString nCounter gene expression assay**. The RNA quality has been evaluated using Agilent RNA 6000 Nano Chip. NanoString nCounter technology is based on the direct detection of target molecules using color-coded molecular barcodes, providing a digital simultaneous quantification of the number of target molecules. Total (RNA 100 ng) was hybridized overnight with nCounter Reporter (20 µl) probes in hybridization buffer and excess of nCounter Capture probes (5 µl) at 65 °C for 16–20 h. The hybridization mixture containing target/probe complexes was allowed to bind to magnetic beads containing complementary sequences on the capture probe. After each target found a probe pair, excess probes were washed, followed by a sequential binding to sequences on the reporter probe. Biotinylated capture probe-bound samples were immobilized and recovered on a streptavidin-coated cartridge. The abundance of specific target molecules was then quantified using the nCounter digital analyzer. Individual fluorescent barcodes and target molecules in each sample were recorded with a CCD camera by performing a high-density scan (600 fields of view). Images were processed internally into a digital format and were normalized using the NanoString nSolver software analysis tool.

Counts were normalized for all target RNAs in all samples based on the positive control RNA to account for differences in hybridization efficiency and post-hybridization processing, including purification and immobilization of complexes. The average was normalized by background counts for each sample obtained from the average of the eight negative control counts. Subsequently, a normalization of mRNA content was performed based on internal reference housekeeping genes Gusb, TBP, NMNAT1, RBP1, STX1A, CTNNB1 using nSolver Software (NanoString Technologies, Seattle, WA).

**Immunohistochemistry**. Whole-mount specimens were mechanically prepared by dissection of the (sub)mucosa, fixed in 4% paraformaldehyde/PBS for 30 min, permeabilized with 1% Triton-X 100/PBS for 15 min, blocked with 5% donkey serum/PBS for 1 h, and incubated with primary IgGs mentioned in appendix Table S4 at 4 °C overnight. After three PBS washing steps, secondary antibodies (Dianova, anti-rat IgG-Cy2 1:800, anti-guinea pig IgG-Cy3, anti-chicken IgY-FITC, and anti-rabbit IgG-FITC or - Cy3 1:800 were incubated for 90 min (Table S4). Specimens were mounted in Epredia Shando Immu-Mount (Thermo Scientific) and imaged on a Leica confocal imaging system or a Nikon 2000TE fluorescent microscope.

Primary cells were fixed in 4% paraformaldehyde/PBS for 30 min, permeabilized with 0.25% Triton-X 100/PBS for 15 min, blocked with 5% donkey serum in PBS for 1 h, and incubated with primary IgGs mentioned in Table S4 at 4 °C overnight.

After three PBS washing steps, secondary antibodies (Dianova, anti-mouse IgG-Cy2 1:800, anti-guinea pig IgG-FITC, and anti-rabbit IgG-FITC or - Cy3 1:800 were incubated for 60 min. Specimens were mounted in Fluorogel-Tris and imaged using a Leica confocal imaging system or a Nikon TE 2000 fluorescent microscope.

**Quantitative PCR**. Total RNA was extracted from *ME* specimens at indicated time points after IM using the RNeasy Mini Kit (Qiagen, Hilden, Germany), followed by deoxyribonuclease I treatment (Ambion, Austin, TX). Complementary DNA was synthesized using the High Capacity cDNA Reverse Transcription Kit (Applied Biosystems, Darmstadt, Germany). The expression of mRNA was quantified by real-time RT-PCR with primers shown in Table S3. Quantitative polymerase chain reaction was performed with SYBR Green PCR Master Mix (Applied Biosystems, Darmstadt, Germany).

**Flow cytometry (FACS)**. FACS analysis was performed on isolated *ME* samples of the small bowel 24 h after IM in $GFAP^{Cre}xIL1R1^{fl/fl}$ animals. Isolation of *ME* was achieved by sliding small bowel segments onto a glass rod, removing the outer muscularis circumferentially with moist cotton applicators and cutting the *ME* into fine pieces. *ME* was digested with a 0.1% collagenase type II (Worthington Biochemical, Lakewood, NJ, USA) enzyme mixture, diluted in PBS, containing 0.1 mg/ml DNase I (La Roche, Germany), 2.4 mg/ml Dispase II (La Roche, Germany), 1 mg/ml BSA (Applichem), and 0.7 mg/ml trypsin inhibitor (Applichem) for 40 min in a 37 °C shaking water bath. Afterwards single-cell suspension was obtained using a 70 µm filter mesh and cells were stained for 30 min at 4 °C with the appropriate antibodies. For antibodies used in this study see Table S4. Flow cytometry analyses were performed on *FACSCantoI*(BD Biosciences) using *FACSDiva* software and data were analyzed with the latest *FlowJo* software (Tree Star, Ashland, OR, USA).

**Enzyme-linked immunosorbent assay (ELISA)**. Release of IL-6 and CCL2 was measured in *ME* RIPA lysates isolated from small intestine segments at the indicated time points after IM. Release of IL-6 in EGC cultures incubated with various treatments was measured at the indicated time points. All ELISAs were purchased from (Thermo Scientific) and used according to the manufacturer's instructions. Values were normalized to tissue weights or untreated EGCs. Briefly, for animal tissue, the isolated *ME* (~50 mg) was lysed with 1xRIPA buffer for 30 min, centrifuged for 30 min at maximum speed and the protein concentration was determined with a BCA kit (Thermo Scientific). 100 µg of total protein was used to measure the release of IL-6 or CCL2 in duplicates. For EGCs, cells were treated with the indicated substances for 24 h, the supernatant was collected, centrifuged at 5000 rcf for 5 min, and snap-frozen in liquid nitrogen before being processed for the IL-6 or CCL2 ELISA.

**In vivo gastrointestinal transit**. Gastrointestinal transit (GIT) was assessed by measuring the intestinal distribution of orally administered fluorescently labeled dextran-gavage 90 min after administration as described previously[6]. The gastrointestinal tract was divided into 15 segments (stomach to the colon). The geometric center (GC) of labeled dextran distribution was calculated as described previously. The stomach (st) correlates with a GC of 1, the small bowel correlates with a GC of 2–11, the cecum (c) correlates with a GC of 12, and the colon correlates with a GC of 13–15. GIT measurements were performed with sham and IM24h animals of $GFAP^{Cre}xIL1R1^{fl/fl}$ or $Sox10^{CreERT2}xRpl22^{HA/+}$ animals.

**$MPO^+$-cell infiltration**. Jejunal mucosa-free ME whole-mount specimens were fixed in ethanol and stained with Hanker Yates reagent (Polyscience Europe, Germany) to identify myeloperoxidase expressing cells ($MPO^+$). The mean number of $MPO^+$ cells/$mm^2$ for 5 random areas per animal was determined. $MPO^+$ measurement was performed with animals 24h after IM.

**RNA-Seq**. RNA samples were extracted using the RNeasy Mini Kit (*Qiagen*). RNA-Seq libraries were prepared using the QuantSeq 3′ mRNA-Seq Library Prep Kit (*Lexogen*) according to the manufacturer's instructions by the Genomics Core Facility of the University Hospital Bonn. The method has high strand specificity (>99.9%), and most sequences are generated from the last exon and the 3′ untranslated region. The technique generates only one fragment per transcript, and the number of reads mapped to a given gene is proportional to its expression. Fewer reads than in classical RNA-seq methods are needed to determine unambiguous gene expression levels, allowing a high level of multiplexing. Library preparation involved reverse transcription of RNA with oligodT primers, followed by removal of RNA and second-strand cDNA synthesis with random primers. The resulting fragments containing both linker fragments were PCR amplified with primers containing the Illumina adaptors and sample-specific barcodes. All libraries were sequenced (single-end 50 bp) on one lane of the Illumina Hiseq 2500. Only genes with an adjusted *p*-value below 0.05 and a minimum fold-change greater than 1.5 were considered to be differentially expressed between conditions.

**RiboTag method**. *RiboTag* IP was performed according to Leven et al.[34]. Briefly, the muscle layer of the whole small bowel tissue was mechanically separated from the mucosal layer and placed in RNA*later* (Thermo Scientific). Muscle tissue was lysed on a Precellys homogenizer [Bertin Instruments] (3 × 5000 rpm, 45 s; 5 min intermediate incubation on ice) in pre-cooled homogenization buffer (50 mM Tris/HCl, 100 mM KCl, 12 mM $MgCl_2$, 1% NP-40, 1 mg/ml Heparin, 100 µg/ml Cycloheximide, 1 mM DTT, 200 U/ml RNAsin, 1× Protease Inhibitor P8340), centrifuged (10 min, 10,000 × *g*, 4 °C), and supernatants saved. "Input" controls were generated from 50 µl cleared lysate. Supernatants were incubated with anti-HA antibody (5 µl; 1 mg/ml; Table S4; 4 h, 4 °C, 7 rpm) and conjugates added to 200 µl of equilibrated A/G dynabeads (Thermo Scientific) and incubated (overnight, 4 °C, 7 rpm). High salt buffer (50 mM Tris/HCl, 300 mM KCl, 12 mM $MgCl_2$, 1% NP-40, 100 µg/ml Cycloheximide, 0.5 mM DTT) was used to wash beads before elution of cell-specific mRNA and subsequent mRNA extraction (Qiagen RNeasy micro kit).

**Software**. The software tools used for this study include Partek Flow, available from https://www.partek.com/partek-flow/#features; Subread/Feature Counts[61], available from http://subread.sourceforge.net/; Venn-Diagram Software, available from http://bioinformatics.psb.ugent.be/webtools/Venn/; and Gene Set Enrichment Analysis, available from https://www.partek.com/partek-flow/#features.

**Statistics and reproducibility**. Statistical analysis was performed with Prism V9.01 (GraphPad, USA) using Student *t*-test or one-way ANOVA as indicated. In all figures, *p*-values are indicated as $^*p < 0.05$, $^{**}p < 0.01$ and $^{***}p < 0.001$ when compared to control or $\#p < 0.05$, $\#\#p < 0.01$ and $\#\#\#p < 0.001$ compared to indicated samples. All plots show the means of indicated expression levels ± standard error of the mean (SEM).

For all shown RNA-seq data, the Partek software was used for all analyses. Partek software performs statistical analyses by the Fisher's exact test and provides *p*-values with multiple testing corrections (FDR).

Experiments were repeated with more samples when the result was close to statistical significance, and sample sizes for animal studies were chosen following previously reported studies that have used the POI animal model; at least 6–10 independent mice per experimental setup. All animals were handled by standardized housing procedures and kept in precisely the same environmental conditions and were genotyped at 6 weeks of age and received a randomized number by which they were identified. Age- and sex-matched animals were grouped randomly and used in the POI animal model. All the control or experimental mice in each experimental set were treated with the same procedure and manipulation. By this, we avoided any group or genotype-specific effects due to the timing of experiments or handling of animals.

**Reporting summary**. Further information on research design is available in the Nature Research Reporting Summary linked to this article.

## Data availability

The data sets produced in this study are available upon reasonable request and in the following databases: RNA-Seq data from mRNA of *ME*-tissue from patients in GSE149181. The *RiboTag* data of control and IM3h mice is available under the accession number *GSE198889*, and the data of EGCs treated with IL1β, and BMDMs treated with conditioned media is available under the accession number *GSE205610*. All raw data used for the main figures were included in an excel sheet named supplementary data 1.

Received: 23 December 2021; Accepted: 26 July 2022;
Published online: 12 August 2022

## References

1. Kalff, J. et al. Surgically induced leukocytic infiltrates within the rat intestinal muscularis mediate postoperative ileus. *Gastroenterology* **117**, 378–387 (1999).
2. Wolthuis, A. M. et al. Incidence of prolonged postoperative ileus after colorectal surgery: a systematic review and meta-analysis. *Colorectal Dis.* **18**, O1–9 (2016).
3. Asgeirsson, T. et al. Postoperative ileus. it costs more than you expect. *J. Am. Coll. Surg.* **210**, 228–231 (2010).
4. Peters, E. G. et al. Relation between postoperative ileus and anastomotic leakage after colorectal resection: a post hoc analysis of a prospective randomized controlled trial. *Colorectal Dis.* **19**, 667–674 (2017).
5. Wehner, S. et al. Inhibition of macrophage function prevents intestinal inflammation and postoperative ileus in rodents. *Gut* **56**, 176–185 (2007).
6. Stoffels, B. et al. Postoperative ileus involves interleukin-1 receptor signaling in enteric glia. *Gastroenterology* **146**, 176–87.e1 (2014).
7. Enderes, J. et al. A population of radio-resistant macrophages in the deep myenteric plexus contributes to postoperative ileus via toll-like receptor 3 signaling. *Front. Immunol.* **11**, 581111 (2020).
8. Matteoli, G. et al. A distinct vagal anti-inflammatory pathway modulates intestinal muscularis resident macrophages independent of the spleen. *Gut* **63**, 938–948 (2014).
9. Yoo, B. B. & Mazmanian, S. K. The enteric network: interactions between the immune and nervous systems of the gut. *Immunity* **46**, 910–926 (2017).
10. Wang, H., Foong, J. P. P., Harris, N. L. & Bornstein, J. C. Enteric neuroimmune interactions coordinate intestinal responses in health and disease. *Mucosal Immunol.* https://doi.org/10.1038/s41385-021-00443-1 (2021).
11. Seguella, L. & Gulbransen, B. D. Enteric glial biology, intercellular signalling and roles in gastrointestinal disease. *Nat. Rev. Gastroenterol. Hepatol.* https://doi.org/10.1038/s41575-021-00423-7 (2021).
12. Rao, M. et al. Enteric glia regulate gastrointestinal motility but are not required for maintenance of the epithelium in mice. *Gastroenterology* **153**, 1068–1081.e7 (2017).
13. Liñán-Rico, A. et al. Molecular signaling and dysfunction of the human reactive enteric glial cell phenotype: implications for GI infection, IBD, POI, neurological, motility, and GI disorders. *Inflamm. Bowel Dis.* **22**, 1812–1834 (2016).
14. Rosenberg, H. J. & Rao, M. Enteric glia in homeostasis and disease: From fundamental biology to human pathology. *iScience* **24**, 102863 (2021).
15. Bush, T. G. et al. Fulminant jejuno-ileitis following ablation of enteric glia in adult transgenic mice. *Cell* **93**, 189–201 (1998).
16. Cornet, A. et al. Enterocolitis induced by autoimmune targeting of enteric glial cells. a possible mechanism in Crohn's disease? *Proc. Natl Acad. Sci. USA* **98**, 13306–13311 (2001).
17. Gulbransen, B. D. & Christofi, F. L. Are we close to targeting enteric glia in gastrointestinal diseases and motility disorders? *Gastroenterology* **155**, 245–251 (2018).
18. Kabouridis, P. S. et al. Microbiota controls the homeostasis of glial cells in the gut lamina propria. *Neuron* **85**, 289–295 (2015).
19. Vicentini, F. A. et al. Intestinal microbiota shapes gut physiology and regulates enteric neurons and glia. *Microbiome* **9**, 210 (2021).
20. Schneider, R. et al. A novel P2X2-dependent purinergic mechanism of enteric gliosis in intestinal inflammation. *EMBO Mol. Med.* **13**, e12724 (2021).
21. Burda, J. E. & Sofroniew, M. V. Reactive gliosis and the multicellular response to CNS damage and disease. *Neuron* **81**, 229–248 (2014).
22. Schepper, S. D. et al. Self-maintaining gut macrophages are essential for intestinal homeostasis. *Cell* **175**, 400–415.e13 (2018).
23. Rao, M. et al. Enteric glia express proteolipid protein 1 and are a transcriptionally unique population of glia in the mammalian nervous system. *Glia* https://doi.org/10.1002/glia.22876 (2015).
24. Rosenbaum, C. et al. Activation of myenteric glia during acute inflammation in vitro and in vivo. *PLoS ONE* **11**, e0151335 (2016).
25. Brykczynska, U. et al. Distinct transcriptional responses across tissue-resident macrophages to short-term and long-term metabolic challenge. *Cell Rep.* **30**, 1627–1643.e7 (2020).
26. Jha, M. K., Jo, M., Kim, J.-H. & Suk, K. Microglia-astrocyte crosstalk: an intimate molecular conversation. *Neuroscientist* **25**, 227–240 (2019).
27. Muller, P. A. et al. Crosstalk between muscularis macrophages and enteric neurons regulates gastrointestinal motility. *Cell* **158**, 300–313 (2014).
28. Grubišić, V. et al. Enteric glia modulate macrophage phenotype and visceral sensitivity following inflammation. *Cell Rep.* **32**, 108100 (2020).
29. Hupa, K. J. et al. AIM2 inflammasome-derived IL-1β induces postoperative ileus in mice. *Sci. Rep.* **9**, 10602 (2019).
30. Wehner, S. et al. Induction of IL-6 within the rodent intestinal muscularis after intestinal surgical stress. *Surgery* **137**, 436–446 (2005).
31. Farro, G. et al. CCR2-dependent monocyte-derived macrophages resolve inflammation and restore gut motility in postoperative ileus. *Gut* **66**, 2098–2109 (2017).
32. Stein, K. et al. Leukocyte-derived interleukin-10 aggravates postoperative ileus. *Front. Immunol.* **9**, 2599 (2018).
33. Valès, S. et al. Tumor cells hijack enteric glia to activate colon cancer stem cells and stimulate tumorigenesis. *EBioMedicine* **49**, 172–188 (2019).
34. Leven, P., Schneider, R., Siemens, K., Jackson, W., & Wehner, S. Application of a RiboTag based approach to generate and analyze mRNA from enteric neural cells. *Neurogastroenterol. Motility* https://doi.org/10.1111/nmo.14309 (2021).
35. Progatzky, F. et al. Regulation of intestinal immunity and tissue repair by enteric glia. *Nature* **599**, 125–130 (2021).
36. Delvalle, N. M. et al. Communication between enteric neurons, glia, and nociceptors underlies the effects of tachykinins on neuroinflammation. *Cell. Mol. Gastroenterol. Hepatol.* **6**, 321–344 (2018).
37. Wehner, S. & Engel, D. R. Resident macrophages in the healthy and inflamed intestinal muscularis externa. *Pflügers Arch. Eur. J. Physiol.* **469**, 541–552 (2017).
38. Lin, S.-S. et al. Alterations in the gut barrier and involvement of Toll-like receptor 4 in murine postoperative ileus. *Neurogastroenterol. Motil.* **30**, e13286 (2018).
39. Sommer, N. P., Schneider, R., Wehner, S., Kalff, J. C. & Vilz, T. O. State-of-the-art colorectal disease: postoperative ileus. *Int. J. Colorectal Dis.* https://doi.org/10.1007/s00384-021-03939-1 (2021).
40. Hyvärinen, T. et al. Co-stimulation with IL-1β and TNF-α induces an inflammatory reactive astrocyte phenotype with neurosupportive characteristics in a human pluripotent stem cell model system. *Sci. Rep.* **9**, 1–15 (2019).
41. Muñoz, A. M., Rey, P., Parga, J., Guerra, M. J. & Labandeira-Garcia, J. L. Glial overexpression of heme oxygenase-1: a histochemical marker for early stages of striatal damage. *J. Chem. Neuroanat.* **29**, 113–126 (2005).
42. Andersson, H. C. et al. Trauma-induced reactive gliosis is reduced after treatment with octanol and carbenoxolone. *Neurological Res.* **33**, 614–624 (2011).
43. Kalff, J. C., Schraut, W. H., Simmons, R. L. & Bauer, A. J. Surgical manipulation of the gut elicits an intestinal muscularis inflammatory response resulting in postsurgical ileus. *Ann. Surg.* **228**, 652–663 (1998).
44. van Wesenbeeck, L. et al. The osteopetrotic mutation toothless (tl) is a loss-of-function frameshift mutation in the rat Csf1 gene. Evidence of a crucial role for CSF-1 in osteoclastogenesis and endochondral ossification. *Proc. Natl Acad. Sci. USA* **99**, 14303–14308 (2002).
45. Bendall, L. J. & Bradstock, K. F. G-CSF: From granulopoietic stimulant to bone marrow stem cell mobilizing agent. *Cytokine Growth Factor Rev.* **25**, 355–367 (2014).
46. Pinheiro, D., Mawhin, M.-A., Prendecki, M. & Woollard, K. J. In-silico analysis of myeloid cells across the animal kingdom reveals neutrophil evolution by colony-stimulating factors. *eLife* **9**, https://doi.org/10.7554/eLife.60214 (2020).
47. Wen, Q. et al. G-CSF-induced macrophage polarization and mobilization may prevent acute graft-versus-host disease after allogeneic hematopoietic stem cell transplantation. *Bone Marrow Transplant.* **54**, 1419–1433 (2019).
48. Meshkibaf, S., Martins, A. J., Henry, G. T. & Kim, S. O. Protective role of G-CSF in dextran sulfate sodium-induced acute colitis through generating gut-homing macrophages. *Cytokine* **78**, 69–78 (2016).
49. Hollmén, M. et al. G-CSF regulates macrophage phenotype and associates with poor overall survival in human triple-negative breast cancer. *Oncoimmunology* **5**, e1115177 (2016).
50. Fu, H. et al. Depletion of microglia exacerbates injury and impairs function recovery after spinal cord injury in mice. *Cell Death Dis.* **11**, 528 (2020).
51. Lou, N. et al. Purinergic receptor P2RY12-dependent microglial closure of the injured blood-brain barrier. *Proc. Natl Acad. Sci. USA* **113**, 1074–1079 (2016).
52. Simon, D. W. et al. The far-reaching scope of neuroinflammation after traumatic brain injury. *Nat. Rev. Neurol.* **13**, 171–191 (2017).
53. Kulkarni, S. et al. Adult enteric nervous system in health is maintained by a dynamic balance between neuronal apoptosis and neurogenesis. *Proc. Natl Acad. Sci. USA* **114**, E3709–18 (2017).
54. Ahrends, T. et al. Enteric pathogens induce tissue tolerance and prevent neuronal loss from subsequent infections. *Cell* **184**, 5715–5727.e12 (2021).
55. Brown, I. A. M., McClain, J. L., Watson, R. E., Patel, B. A. & Gulbransen, B. D. Enteric glia mediate neuron death in colitis through purinergic pathways that require connexin-43 and nitric oxide. *Cell. Mol. Gastroenterol. Hepatol.* **2**, 77–91 (2016).

56. Costa, D. V. S. et al. 5-fluorouracil induces enteric neuron death and glial activation during intestinal mucositis via a S100B-RAGE-NFκB-dependent pathway. *Sci. Rep.* **9**, 665 (2019).
57. Aube, A. C. et al. Changes in enteric neurone phenotype and intestinal functions in a transgenic mouse model of enteric glia disruption. *Gut* **55**, 630–637 (2006).
58. Gulbransen, B. D. & Sharkey, K. A. Purinergic neuron-to-glia signaling in the enteric nervous system. *Gastroenterology* **136**, 1349–1358 (2009).
59. Pohl, J. M. et al. Irf4-dependent CD103(+)CD11b(+) dendritic cells and the intestinal microbiome regulate monocyte and macrophage activation and intestinal peristalsis in postoperative ileus. *Gut* **66**, 2110–2120 (2017).
60. Mazzotta, E., Villalobos-Hernandez, E. C., Fiorda-Diaz, J., Harzman, A. & Christofi, F. L. Postoperative ileus and postoperative gastrointestinal tract dysfunction: pathogenic mechanisms and novel treatment strategies beyond colorectal enhanced recovery after surgery protocols. *Front. Pharmacol.* **11**, 583422 (2020).
61. Liao, Y., Smyth, G. K. & Shi, W. FeatureCounts: an efficient general purpose program for assigning sequence reads to genomic features. *Bioinformatics* **30**, 923–930 (2014).

## Acknowledgements

The authors thank the Next Generation Sequencing Core Facility and the Institute for Genomic Statistics and Bioinformatics of the University Clinics Bonn for supporting the RNA-Seq analysis. In addition, the authors thank the Flow Cytometry Core Facility of the University Clinics Bonn for supporting all FACS experiments. We thank the technicians Patrik Efferz, Mariola Lysson, Jana Müller, and Bianca Schneiker for their support with the readouts like ELISA and qPCR and for handling the transgenic mouse lines. We thank Prof. Vachilis Pachnis for sharing the *Sox10*$^{CreERT2}$ mice with us. We thank PD Valentin Schäfer for sharing the Anakinra substance for in vitro assays. We thank Prof. Vanda A. Lennon for sharing the ANNA-1 antibody to visualize enteric neurons in our primary cell cultures. We thank Prof. Nico Schlegel and Prof. Wouter de Jonge for reading our manuscript and providing helpful suggestions for wording our results and conclusions. Graphical visualizations were created with BioRender software. We thank the following funding organizations for supporting our research: National Institutes of Health Grant (NCI Cost shared resource for COM, The Ohio State University): P30CA16058 National Institutes of Health, National Institutes of Diabetes, Digestive and Kidney Diseases (NIH, NIDDK) Grants: R01DK113943 and R01DK125809 (F.L.C.). BonnNI medical student Grant: Q-611.0754 (S.W.). ImmunoSensation2 Cluster of Excellence: EXC 2151–390873048 (S.W.). German research council (D.F.G.): WE4204/3-1 (S.W.).

## Author contributions

Conceptualization: R.S., F.L.C., and S.W. Methodology: R.S., J.C.K., F.L.C., P.L., S.M., M.B., T.G., P.h.L., T.O.V., and S.W. Investigation: R.S., P.L., M.B., S.M., L.S., E.Z., and P.F. Visualization: R.S., P.L., M.B., S.M., and P.F. Funding acquisition: J.C.K., F.L.C., and S.W. Project administration: J.C.K., F.L.C., and S.W. Patient material and clinical organization: T.G., P.h.L., T.O.V. Supervision: R.S., F.L.C., and S.W. Writing—original draft: R.S., J.C.K., F.L.C., and S.W. Writing—review & editing: R.S., J.C.K., F.L.C., P.L., S.M., T.G., P.h.L., T.O.V., L.S., M.B., and S.W.

## Funding

Open Access funding enabled and organized by Projekt DEAL.

## Competing interests

The authors declare the following competing interests: S.W. and J.C.K. receive royalties from Wolter Kluwer for contributing to the postoperative ileus section of the *UpToDate* library. All other authors declare no competing interests.

## Additional information

**Supplementary information** The online version contains supplementary material available at https://doi.org/10.1038/s42003-022-03772-4.

**Correspondence** and requests for materials should be addressed to Sven Wehner.

**Peer review information** *Communications Biology* thanks Ulrika Marklund and the other, anonymous, reviewer(s) for their contribution to the peer review of this work. Primary handling editor: Zhijuan Qiu. Peer reviewer reports are available.

**Reprints and permission information** is available at http://www.nature.com/reprints

**Publisher's note** Springer Nature remains neutral with regard to jurisdictional claims in published maps and institutional affiliations.

## 3.4 Publication 4: van Baarle L, De Simone V, Schneider L, *et al.* 2024 – IL-1R signaling drives enteric glia-macrophage interactions in colorectal cancer

nature communications

Article

https://doi.org/10.1038/s41467-024-50438-2

# IL-1R signaling drives enteric glia-macrophage interactions in colorectal cancer

Received: 16 September 2023

Accepted: 11 July 2024

Published online: 19 July 2024

Check for updates

Lies van Baarle[1,14], Veronica De Simone[1,14], Linda Schneider[2,14], Sneha Santhosh[1,3], Saeed Abdurahiman[1], Francesca Biscu[1,4], Reiner Schneider[2], Lisa Zanoletti[1,5], Renata Siqueira de Mello[1], Sara Verbandt[6], Zedong Hu[6], Michelle Stakenborg[1], Bo-Jun Ke[1], Nathalie Stakenborg[7], Raquel Salvador Laureano[8], Balbina García-Reyes[2,9], Jonas Henn[2], Marieta Toma[10], Maxime Vanmechelen[11,12], Guy Boeckxstaens[7], Frederik De Smet[11,12], Abhishek D. Garg[8], Sales Ibiza[13], Sabine Tejpar[6], Sven Wehner[2,15] ✉ & Gianluca Matteoli[1,12,15] ✉

Enteric glia have been recently recognized as key components of the colonic tumor microenvironment indicating their potential role in colorectal cancer pathogenesis. Although enteric glia modulate immune responses in other intestinal diseases, their interaction with the colorectal cancer immune cell compartment remains unclear. Through a combination of single-cell and bulk RNA-sequencing, both in murine models and patients, here we find that enteric glia acquire an immunomodulatory phenotype by bi-directional communication with tumor-infiltrating monocytes. The latter direct a reactive enteric glial cell phenotypic and functional switch via glial IL-1R signaling. In turn, tumor glia promote monocyte differentiation towards pro-tumorigenic SPP1$^{+}$ tumor-associated macrophages by IL-6 release. Enteric glia cell abundancy correlates with worse disease outcomes in preclinical models and colorectal cancer patients. Thereby, our study reveals a neuroimmune interaction between enteric glia and tumor-associated macrophages in the colorectal tumor microenvironment, providing insights into colorectal cancer pathogenesis.

Identified as the world's third most common tumor, colorectal cancer (CRC) represents one of the preeminent causes of cancer-associated deaths worldwide. Although innovative technologies have significantly impacted the diagnosis and treatment of CRC, patients with advanced disease still have a poor prognosis. In fact, while the 5-year survival rates of patients with early-stage CRC can reach up to 90%, the survival rate plummets dramatically to as low as 10% for patients diagnosed with metastatic disease[1]. Hence, a better understanding of the pathogenesis of CRC is crucial to develop advanced therapeutic strategies along with advanced patient stratification for precision medicine. CRC consists of rapidly evolving neoplasms where acquired mutations in oncogenes and tumor-suppressor genes lead to increasing complexity of the tumor microenvironment (TME), unleashing interaction of the tumor cells with the stroma and the immune system, including fibroblasts, tumor-infiltrating immune cells, and cells of the enteric nervous system[2,3]. This process contributes to the formation of a complex network of cell types within the TME, which is leading to increased tumor fitness.

In recent years, enteric glial cells (EGCs) have also been identified as a constituent of the colon carcinoma microenvironment[4,5]. EGCs, once regarded as merely supportive and accessory cells for neurons within the enteric nervous system[6], have now gained increased

A full list of affiliations appears at the end of the paper. ✉e-mail: sven.wehner@ukbonn.de; gianluca.matteoli@kuleuven.be

attention for their more complex roles in both health and disease[7]. In homeostasis, EGCs regulate intestinal reflexes and support neurotransmission via communication with enteric neurons. However, accumulating evidence highlights EGCs as crucial mediators of interactions not only among enteric neurons but also intestinal epithelium, enteroendocrine cells, and immune cells[7–10]. Of particular interest is their significant role in modulating immune responses in various intestinal diseases[11–14]. Being highly responsive to inflammatory mediators, including Adenosine triphosphate (ATP), Interleukin (IL)−1 cytokines, or Lipopolysaccharides, EGCs are rapidly activated during intestinal diseases. Upon activation during intestinal pathologies, EGCs contribute to the shaping of the inflammatory milieu through the secretion of a plethora of cytokines and chemokines[15–18]. In this regard, we recently demonstrated the profound influence EGCs exert on macrophage dynamics in the setting of acute intestinal inflammation, promoting the recruitment of monocytes and their differentiation into pro-resolving macrophages[17,19].

So far, in the context of CRC, a few studies suggested that EGCs exert a pro-tumorigenic effect during tumor development[4,5]. In a study by Yuan et al., glial cell depletion led to reduced tumor burden in a CRC mouse model[5], indicating a central role of EGCs in CRC development. A xenograft model confirmed this role, and in vitro work suggested that EGC activation by IL-1 resulted in a pro-tumorigenic EGC phenotype[4], pointing to a direct interaction of EGCs with the TME. However, the mechanisms by which EGCs interact with the different components of the colorectal cancer TME to exert their pro-tumorigenic role remain poorly understood. Especially the molecular and cellular communication pathways involved are so far insufficiently explored and display a substantial lack of in vivo evidence.

In this work, we demonstrate, using in vitro and in vivo models, that upon exposure to the colorectal TME, EGCs undergo a reactive phenotypic switch, leading to the activation of immunomodulatory processes that promote the differentiation of tumor-associated macrophages (TAMs). Tumor-infiltrating monocytes are found to influence the phenotype and function of CRC EGCs through IL-1 signaling. In turn, EGC-derived IL-6 promotes the differentiation of monocytes towards $SPP1^+$ TAMs. This IL-1R/IL-6 axis is found to be essential for the tumor-supportive functions of EGCs. Our findings uncover a critical neuroimmune interaction in the colon cancer microenvironment, potentially facilitating the development of additional therapeutic approaches to treat this devastating disease.

## Results

### EGCs shape the CRC immune compartment

Recent studies identified EGCs as an important component of the colon TME[4,5]. However, their contribution to CRC pathogenesis and their possible interaction with the tumor immune compartment remains largely unexplored. Hence, to study the immunomodulatory role of EGCs in CRC in vivo, we utilized an established murine model[20], in which MC38 colorectal cancer cells were orthotopically injected into the colonic submucosa (Fig. 1a and Supplementary Fig. 1a). This model is characterized by a strong immune cell infiltration and tumor epithelial cell proliferation (Supplementary Fig. 1b, c). After initial tamoxifen exposure, diphtheria toxin (DT) was administered via colonoscopy-guided injections into the colonic wall of $PLP1^{CreERT2}$iDTR mice on days −5 and −3 prior to the submucosal injection of MC38 tumor cells (Fig. 1b). This approach enabled the temporal and localized depletion of enteric glia during the development of colon tumors (Supplementary Fig. 1d–h). Of note, the DT-triggered glial cell death by d0 was not associated with any significant differences in immune infiltrate between vehicle-treated and DT-treated mice (Supplementary Fig. 1i). Seven days after colonic MC38 cells injection, a significant reduction of tumor size was observed in DT pre-treated mice compared to the vehicle group (Fig. 1c). Tumors treated with DT exhibited a sustained reduction in glial marker expression at day 7, with no impact on colon length (Supplementary Fig. 1j–l). Although absolute numbers of both immune and non-immune cells per milligram of tumor tissue decreased within the tumor microenvironment in the absence of glial cells, the composition of the tumor microenvironment remained unchanged, as evidenced by the consistent percentage of immune and non-immune cells. Thus, it is evident that the reduction in tumor size is not solely attributable to a decline in immune cells (Supplementary Fig. 1m, n). To address any potential non-specific DT toxicity or unspecific immune activation, we subjected C57BL/6J mice to the same injection protocol used for $PLP1^{CreERT2}$iDTR mice. Our findings revealed no difference in tumor growth or immune infiltration between DT- and saline-injected WT mice, excluding non-specific DT toxicity in this model (Supplementary Fig. 1o–q).

Interestingly, during this early phase of tumor growth, the depletion of EGCs resulted also in fewer TAMs (Fig. 1d and Supplementary Fig. 2a). Furthermore, a decrease in the numbers of monocytes and eosinophils was observed in tumors after enteric glia depletion, whereas no differences were observed for neutrophils, T and B cells (Fig. 1d and Supplementary Fig. 2b).

To further validate the effect of EGCs on the CRC immune compartment, we established a co-injection model of MC38 cells together with primary EGCs in the colonic mucosa of C57BL/6J mice (Fig. 1e). Co-injection of MC38 and EGCs resulted in increased tumor growth associated with higher numbers of TAMs, as well as $CD4^+$ T cells, $CD8^+$ T cells, and $T_{reg}$ cells compared to mice orthotopically injected with MC38 cells alone (Fig. 1f, g and Supplementary Fig. 2c). No differences were observed in the numbers of monocytes, eosinophils, neutrophils, and B cells (Fig. 1g and Supplementary Fig. 2c). Spatial tissue mapping via confocal microscopy confirmed proximity between EGCs ($GFAP^+$) and TAMs ($F4/80^+$) within orthotopic colonic tumors injected in C57BL/6J mice (Fig. 1h), further suggesting the existence of a glial-macrophage interplay within the TME.

Overall, these findings suggest that EGCs participate in shaping the CRC immune microenvironment, by expanding the TAM population.

### EGCs display an immunomodulatory phenotype in CRC

To examine the molecular mechanisms by which EGCs influence the immune CRC compartment with particular regard to the TAMs, we first investigated their transcriptional adaptations upon CRC onset. To this end, we established an in vitro tumor EGC model, able to mimic the response of enteric glia to the factors secreted by the colonic TME. Primary embryonic-derived EGCs were treated with conditioned medium (CM) of digested murine MC38 orthotopic tumors, from now onwards, defined as TME-CM EGCs (Fig. 2a). Control groups consisted of EGCs stimulated with supernatants derived from healthy colonic tissue (H-CM) and naive unstimulated EGCs. At 6 h, 12 h, and 24 h post-stimulation, bulk RNA sequencing (RNA-seq) was performed to uncover the transcriptional differences among the various EGC groups. Principal component analysis (PCA) demonstrated a significant similarity between the H-CM and unstimulated EGC samples (Fig. 2b). In contrast, TME-CM EGCs exhibited a distinct separation from both H-CM and unstimulated EGCs, suggesting a noticeable difference in their transcriptional programs. At 24 h post-stimulation, the segregation of the samples was highly driven by the upregulation of several chemokines, cytokines and typical markers for pan-reactive astrocytes (*Lnc2* and *Timp1*)[21], suggesting an activated and immunomodulatory role for EGCs within the tumor microenvironment (Supplementary Fig. 3a, b).

Next, using weighted gene correlation network analysis (WGCNA) we identified 12 gene co-expression modules. TME-CM EGCs showed a specific correlation to modules 7 and 8 and an inverse correlation to module 4 (Fig. 2c and Supplementary Data 1). Module 7 showed a functional association with several pro-tumoral processes and

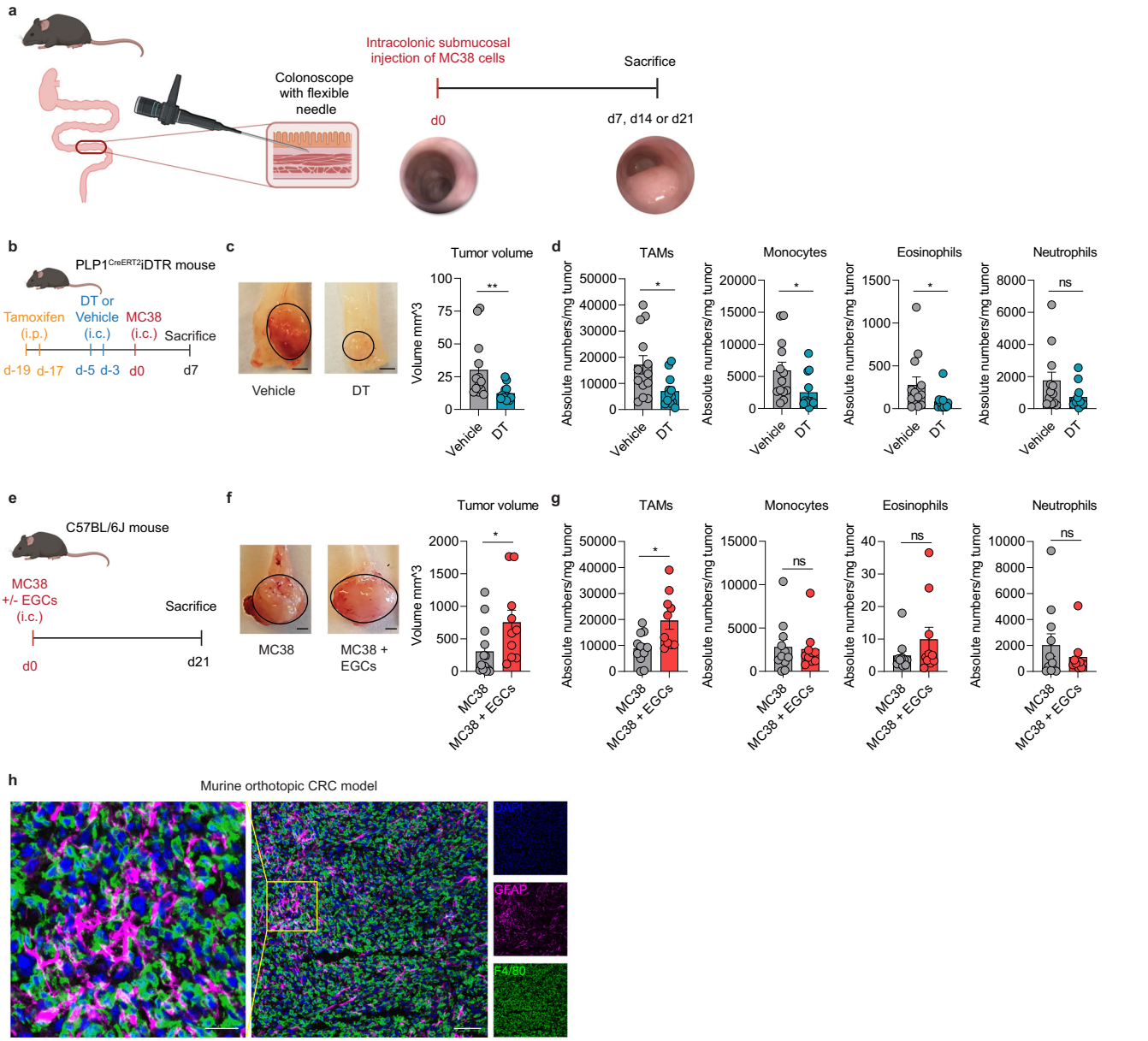


**Fig. 1 | EGCs shape the CRC immune compartment. a** Schematic representation of the murine orthotopic CRC model. Adult mice were injected endoscopically in the colonic submucosa with MC38 cells and tumors were assessed at day (d)7, d14 or d21. **b**–**d** PLP1$^{CreERT2}$iDTR mice were intraperitoneally (i.p.) injected with tamoxifen at d-19 and d-17, followed by intracolonic (i.c.) injection at d-5 and d-3 with 40 ng Diphtheria toxin (DT) or saline (Vehicle). At d0, MC38 cells were i.c. injected in both groups. Tumor growth and immune infiltration were assessed at d7. Schematic representation of EGCs depletion mouse model (**b**) with representative pictures (scale bar 2 mm) and quantitative comparison of tumor volume (**c**). Data show absolute tumor-infiltrating myeloid immune cell numbers per mg tumor tissue (**d**) ($n = 13$ Vehicle, $n = 12$ DT). **e**–**g** WT C57BL/6J mice were i.c. injected with MC38 cells with or without embryonic neurosphere-derived EGCs (1:1 ratio). Tumor growth and immune infiltration were assessed at d21. Schematic representation of EGCs co-injection mouse model (**e**) with representative pictures (scale bar 2 mm) and quantitative comparison of tumor volume (**f**). Data show absolute tumor-infiltrating myeloid immune cell numbers per mg tumor tissue (**g**) ($n = 11$ MC38, $n = 10$ MC38 + EGCs). **h** Immunostaining of orthotopic murine tumor sections showing GFAP (magenta), F4/80 (green) and DAPI (blue) (scale bar 70 μm and 25 μm) representative of 4 independent experiments. Data show mean ± SEM (**c**, **d**, **f**, **g**). Statistical analysis: unpaired two-tailed Mann-Whitney test (**c**, **d**, **f**, **g**) $^*p < 0.05$, $^{**}p < 0.005$, ns not significant. Source data and exact *p* values are provided as a Source Data file.

contained the glial reactivity markers *Lcn2* and *Timp1* (Fig. 2d and Supplementary Fig. 3c). Module 8 consisted of genes, associated with immunomodulatory functions of EGCs, such as "myeloid cell differentiation", "macrophage activation" and "myeloid leukocyte migration" (e.g., *Ccl2, Cxcl1, Cxcl10* and *Il6*). Conversely, the genes of module 4, such as *Ntsr1* and *Sparcl1*, were associated with the homeostatic functions of EGCs[22]. In line, gene set enrichment analysis of the 24 h TME-CM EGCs signature revealed impairment for functions previously ascribed to healthy EGCs, including GO terms like *"Positive regulation of stem cell differentiation", "Regulation of glial cell differentiation and gliogenesis", "Neuron projection guidance"*, and *"Positive regulation of neurogenesis"*[7,23] (Fig. 2e and Supplementary Data 2). Notably, in line with the previous in vitro findings of Valès et al., TME-CM EGCs were enriched for the GO terms *"Positive regulation of prostaglandin biosynthetic process"*, and *"Interleukin 1 receptor activity"*, supporting the possible paracrine effect of IL-1/$PGE_2$ signaling[4]. Lastly, gene set enrichment analysis predicted a direct interaction of CRC EGCs with TAMs, reflected by functional enrichment for the GO terms *"Macrophage differentiation"* and *"Positive regulation of macrophage activation* and *migration"* (Fig. 2e).

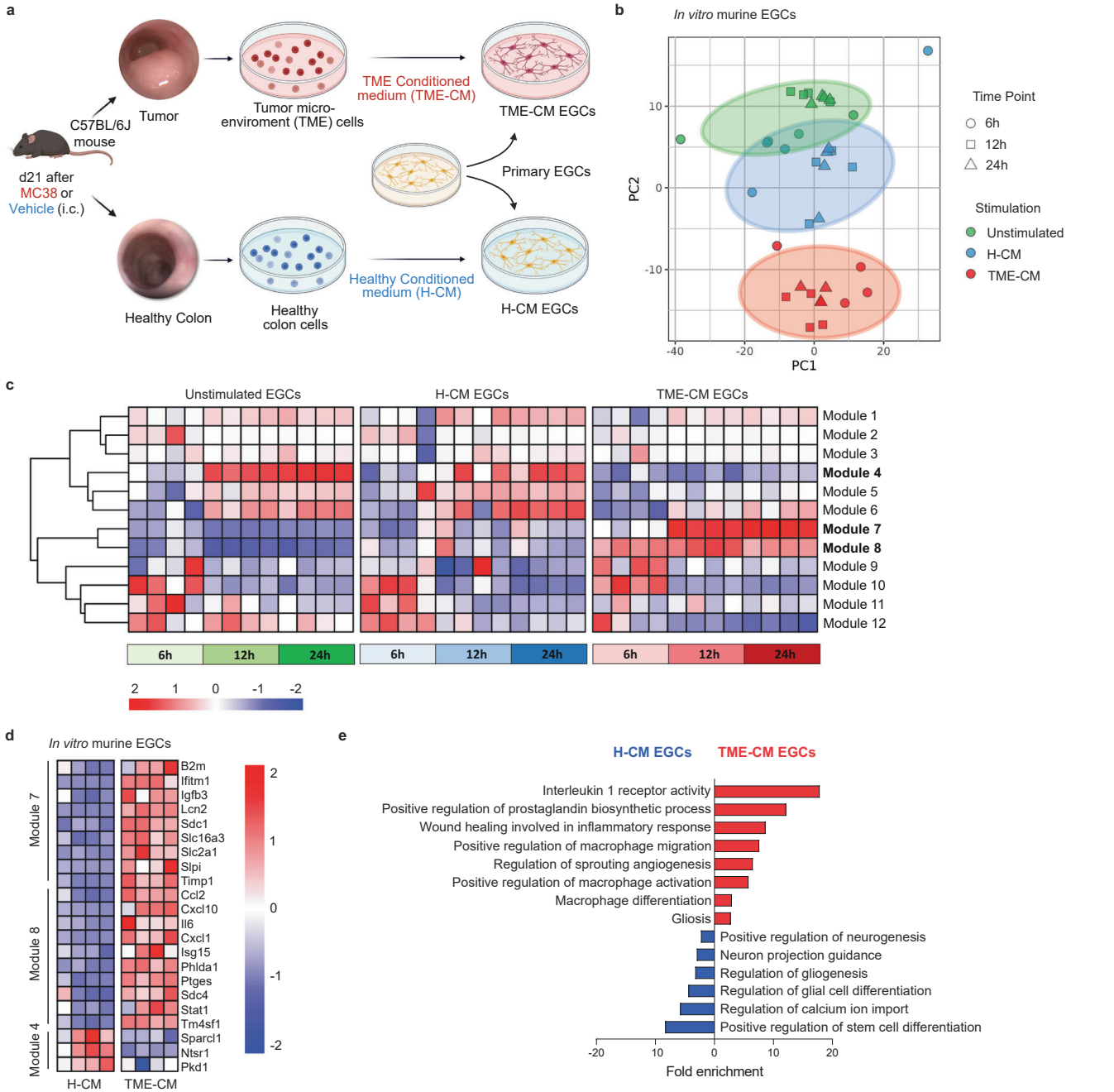


**Fig. 2 | EGCs display an activated and immunomodulatory phenotype in CRC.** Transcriptome analysis of in vitro primary embryonic neurosphere-derived EGCs alone or stimulated with healthy conditioned medium (H-CM) or tumor microenvironment conditioned medium (TME-CM) at different time points (6 h, 12 h, and 24 h, $n = 4$). **a** Schematic representation of the in vitro tumor EGCs model. **b** Principal component analysis (PCA) plot of EGCs gene signature identified by 3´mRNA bulk RNA-seq. Each dot represents an individual sample. **c** Heatmap showing the transcriptional modules identified by weighted gene correlation network analysis (WGCNA). **d** Heatmap of differentially expressed genes in modules 4, 7, and 8 of in vitro murine EGCs stimulated for 24 h with H- or TME-CM. **e** Gene set enrichment analysis for the differentially up- and down-regulated genes in TME-CM versus H-CM stimulated EGCs after 24 h ($n = 4$). Source data are provided as a Source Data file.

Taken together, upon exposure to the CRC TME, EGCs undergo a phenotypic switch associated with the activation of immunomodulatory programs related to macrophage interplay.

## Tumor EGC-derived IL-6 favors SPP1$^{+}$ TAM differentiation

Considering that tissue location and transcriptomic data suggest direct communication between EGCs and TAMs in the CRC microenvironment, we aimed to decipher the molecular mechanisms underpinning their interaction. Firstly, single-cell transcriptomic analysis was used to characterize the immune landscape of colorectal MC38 orthotopic tumors (Supplementary Fig. 4a). Interestingly, among the identified immune populations, monocytes and macrophages accounted for 60% of the tumor-infiltrating immune cells. Unsupervised clustering of the myeloid cells (*Lyz2, Cd68, H2-Ab1, Mrc1, C1qa, Ly6c2, Ccr2*, and *Fn1*) revealed 1 monocyte and 4 distinct macrophage sub-populations (Fig. 3a-b). The most abundant macrophage cluster was characterized by simultaneous marker gene expression for monocytes (*Ccr2* and *Ly6c2*) and for differentiated macrophages (*H2-*

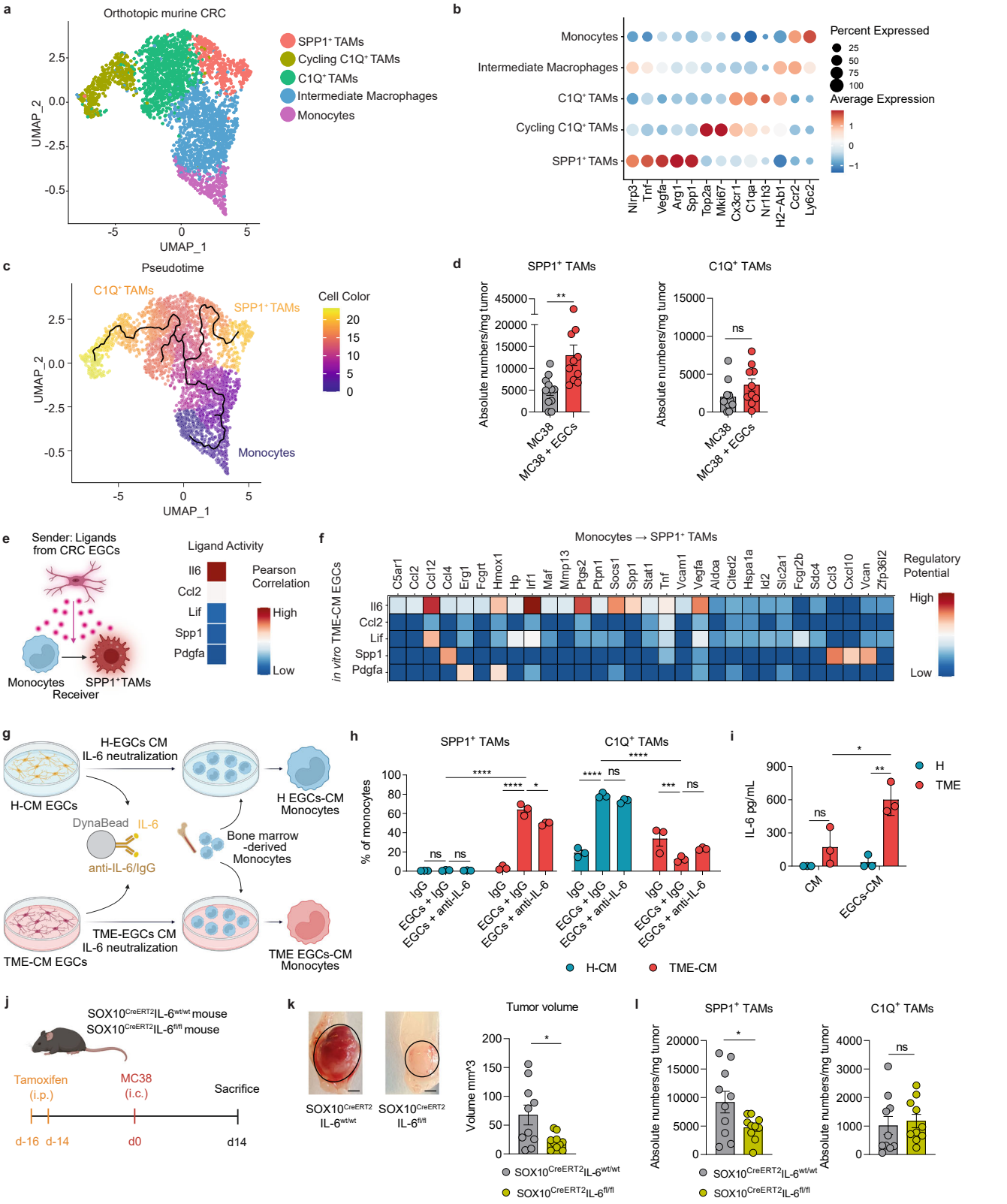


*Ab1* and *Nlrp3*), indicating a possible transitional cell state, which we termed "Intermediate Macrophages" (Fig. 3b). Additionally, we identified two clusters of TAMs, "SPP1$^+$ TAMs" and "C1Q+ TAMs". The "SPP1+ TAMs" co-express *Spp1* and *Arg1*, along with genes involved in angiogenesis (*Vegfa*) and extracellular matrix remodeling (*Spp1* and *Tnf*) (Fig. 3b and Supplementary Fig. 4b). The "C1Q+ TAMs" are characterized by genes involved in phagocytosis (*Nr1h3*), antigen presentation (*H2-Ab1*) and the complement cascade (*C1qa*). A second of C1Q$^+$ TAM cluster, distinguished by high expression of cell cycle genes such as *Mki67* and *Top2a*, was classified as 'Cycling C1Q$^+$ TAMs'.

Overall, our findings are in line with the study of Zhang et al., which reported very similar dichotomous functional phenotypes of TAMs in CRC patients[24]. Additionally, Zhang and colleagues predicted a dichotomic differentiation trajectory of monocytes towards SPP1$^+$

**Fig. 3 | Tumor EGC-derived IL-6 favors SPP1⁺ TAM differentiation. a-c** Analysis of monocytes and macrophages from the scRNA-seq data of orthotopic MC38 tumors in WT C57BL/6J mice, 21 days(d) after tumor induction ($n = 3$). UMAP of sub-clustering (**a**), dot plot of differentially expressed marker genes (**b**) and differentiation trajectory (**c**). **d** WT C57BL/6J mice were intracolonically injected with MC38 cells ± embryonic neurosphere-derived EGCs (1:1 ratio). SPP1⁺ TAMs and C1Q⁺ TAMs infiltration was assessed on d21. Data represent absolute numbers/mg tumor ($n = 11$ MC38, $n = 10$ MC38 + EGCs). **e**, **f** Nichenet analysis was performed considering ligands expressed by 24 h tumor microenvironment-conditioned medium (TME-CM) EGCs, (CRC EGCs bulk RNAseq; Fig. 2) and considering the differentially expressed genes between monocytes and SPP1⁺ TAMs as target genes (orthotopic murine CRC dataset; Fig. 3a). Pearson correlation of top TME-CM EGCs-released ligands predicted to induce monocytes to SPP1⁺ TAM differentiation (**e**). Heatmap showing regulatory potential scores between top EGC-released ligands and their target genes differentially expressed between monocytes and SPP1⁺ TAMs (**f**). **g**–**h** Supernatant of healthy (H)-CM, TME-CM, H EGCs-CM, and TME EGCs-CM were incubated with IgG or anti-IL-6 (both 5 μg/mL) along with Dynabeads™ Protein G followed by removal of the protein-antibody-bead complex. Murine monocytes were cultured for 48 h with the indicated supernatants ($n = 3$ H-CM and TME-CM). Experimental design (**g**). Percentages of SPP1⁺ and C1Q⁺ TAMs in monocyte cultures after stimuli (**h**). **i** IL-6 concentration in H-CM, TME-CM, H-EGCs-CM, and TME-EGCs-CM ($n = 3$ H-CM and TME-CM). After tamoxifen treatment were $SOX10^{CreERT2}IL\text{-}6^{wt/wt}$ and $SOX10^{CreERT2}IL\text{-}6^{fl/fl}$ mice intracolonic (i.c.) injected with MC38 cells. Tumor growth and immune infiltration were assessed at d14 ($n = 10$). Schematic representation (**j**), representative pictures (scale bar 2 mm) and comparison of tumor volume ($n = 10$) (**k**). Tumor-infiltrating TAM numbers/mg tumor ($n = 10$) (**l**). Data are presented as mean ± SEM (**d**, **h**, **i**, **k**, **l**). Statistical analysis: unpaired two-tailed Mann Whitney test (**d**), two-way ANOVA with correction for multiple comparisons (**h**, **i**), unpaired two-tailed t-test (**k**, **l**). $^{*}p < 0.05$, $^{**}p < 0.005$, $^{***}p < 0.0005$, $^{****}p < 0.00005$, ns not significant. Source data and exact $p$ values are provided as a Source Data file.

TAMs or C1QC⁺ TAMs in CRC patients. In line, we identified a strong directional flow from tumor-infiltrating monocytes towards intermediate macrophages, which in turn further branched into two opposite paths, ending either in SPP1⁺ TAMs or C1Q⁺ TAMs (Fig. 3c).

SPP1⁺ macrophages represent a significant cell population within the tumor immune cell compartment with negative prognostic value in CRC[24,25]. However, the current knowledge regarding microenvironmental cues, promoting the differentiation of tumor-infiltrating monocytes towards SPP1⁺ TAMs or C1Q⁺ TAMs, remains limited. Thus, we explored the possible role of EGCs in promoting monocyte to SPP1⁺ TAM or C1Q⁺ TAM differentiation using our EGC co-injection CRC model (Fig. 1e). Strikingly, supplementation of EGCs within the CRC TME resulted in more than a twofold increase in SPP1⁺ TAMs, while no significant difference was found for C1Q⁺ TAMs (Fig. 3d and Supplementary Fig. 4c).

Next, to identify key EGC-derived mediators accountable for SPP1⁺ TAM differentiation in CRC, we applied NicheNet, a computational tool designed to infer relationships between signaling molecules and their target gene expression[26]. By using the genes differentially expressed between SPP1⁺ TAMs and monocytes [data extracted from our single-cell RNA-seq (scRNAseq) murine orthotopic CRC dataset] as target genes, we prioritized candidate ligands derived from TME-CM EGCs (data extracted from bulk RNAseq in vitro CRC EGCs dataset) as potential drivers of this differentiation process (Fig. 3e). Here, TME-CM EGC-derived IL-6 was identified as the top predicted candidate factor involved in driving the SPP1⁺ TAM phenotype (Fig. 3e, f).

In line with this prediction, IL-6 neutralization in the TME-CM EGC supernatant attenuated the differentiation of monocytes into SPP1⁺ TAMs, further reflected by reduced *Spp1* and *Arg1* expression (Fig. 3g, h and Supplementary Fig. 4d). Of note, TME-CM EGCs did not promote C1Q⁺ TAM differentiation from monocytes. In contrast, H-CM EGCs had no effect on SPP1⁺ TAM polarization while they promoted C1Q⁺ TAM differentiation in an IL-6 independent fashion (Fig. 3h and Supplementary Fig. 4d). Consistent with this, high level of IL-6 could be measured only in the supernatant of TME-CM EGCs, with almost undetectable level in H-CM EGCs (Fig. 3i).

To finally investigate the effect of EGC-derived IL-6 on the SPP1⁺ TAM differentiation and tumor development in vivo, we orthotopically injected MC38 cells in the colonic mucosa of mice with a glial-specific deletion of IL-6 ($SOX10^{CreERT2}IL\text{-}6^{fl/fl}$) and their littermates ($SOX10^{CreERT2}IL\text{-}6^{wt/wt}$) (Fig. 3j). Strikingly, glial-specific IL-6 deletion led to a reduced tumor growth, which correlated with a reduction in SPP1⁺ TAMs while no effect was detected for C1Q⁺ TAMs (Fig. 3k-l). These results underline the importance of glial-derived IL-6 in both colonic tumor development and TAM differentiation in vivo. Glial reporter mouse line $SOX10^{CreERT2}Ai14^{fl/fl}$ showing co-localization of tdTomato signals together with GFAP immunostaining in glial cells, was used to confirm enteric glia targeting specificity (Supplementary Fig. 4e).

Altogether, our data reveal a significant and previously unknown interaction between EGCs and TAMs in the CRC TME, with EGC-derived IL-6 acting as a crucial regulator in driving SPP1⁺ TAM differentiation.

## Monocyte-derived IL-1 promotes the CRC EGC phenotype

Given the evidence that EGCs modulate their functions based on microenvironmental cues[12,15,19], we aimed to define the factors driving the EGC phenotypic switch in CRC. Considering the heavy infiltration of the colon TME by immune cells, which recent studies have pinpointed as sources of EGC-activating factors[12], we investigated the possibility of immune cells driving CRC EGC transition, potentially creating a reinforcing neuroimmune feedback loop. To investigate the cellular circuits coordinating this interaction we used again NicheNet, linking ligands derived from immune cells within the TME (from the scRNAseq murine orthotopic CRC dataset) to target genes differentially expressed between H-CM EGCs and TME-CM EGCs (data extracted from Bulk RNAseq in vitro CRC EGCs dataset) (Fig. 4a). In this analysis, IL-1β and IL-1α emerged as the top-ranked ligands driving the transcriptional transition from H-CM EGCs to TME-CM EGCs (Fig. 4a, b). Notably, we could confirm elevated levels of IL-1 in the TME samples compared to healthy colon cells, both at RNA and protein levels (Fig. 4c and Supplementary Fig. 5a). Next, we utilized primary EGC cultures derived from embryonic or adult neurospheres to analyze their response to IL-1 treatments. Of note, both EGC culture systems were characterized by strong enrichment of EGC markers (*Plp1*, *Sox10*, and *S100b*) with minimal expression of markers for other cell types such as epithelial cells (*Epcam* and *Cdh1*), smooth muscle cells (*Prkg1* and *Foxp2*), endothelial cells (*Cdh5* and *Pecam1*), neurons (*Nefl* and *Syp*), mesenchymal cells (*Pdgfra* and *Wt1*), and immune cells (*Ikzf1* and *Itgam*) (Supplementary Fig. 5b). Consistent with our prediction, treating primary EGCs with IL-1β markedly activated the CRC EGC phenotype, with induction of Lcn2 and Timp1, and immunomodulatory factors Ccl2 and Il6, both at RNA and protein level, highlighting a specific molecular EGC response independent of embryonic or adult neurosphere origin (Fig. 4d, e, Supplementary Fig. 5c, d and Supplementary Data 2). Conversely, inhibiting IL-1R signaling in EGCs during stimulation with the TME-CM, completely abrogated the induction of the CRC EGC key markers (Fig. 4f, g). Taken together, these findings underscore the pivotal role of IL-1 in the reprogramming of EGCs upon exposure to the colonic TME.

Next, to identify the cellular source of IL-1 within the TME, we quantified IL-1 expression across epithelial, stromal, and immune cells (Fig. 4h and Supplementary Fig. 5e–g). While Valès et al.[4] concluded that in vitro IL-1 is released by the tumor epithelial cells, we herein demonstrate that in vivo, in particular within the MC38 orthotopic model, the TME IL-1 secretion is restricted to myeloid cells, while no expression could be found in epithelial, nor in stromal cells (Fig. 4h and Supplementary Fig. 5g). Further analyses identified tumor monocytes

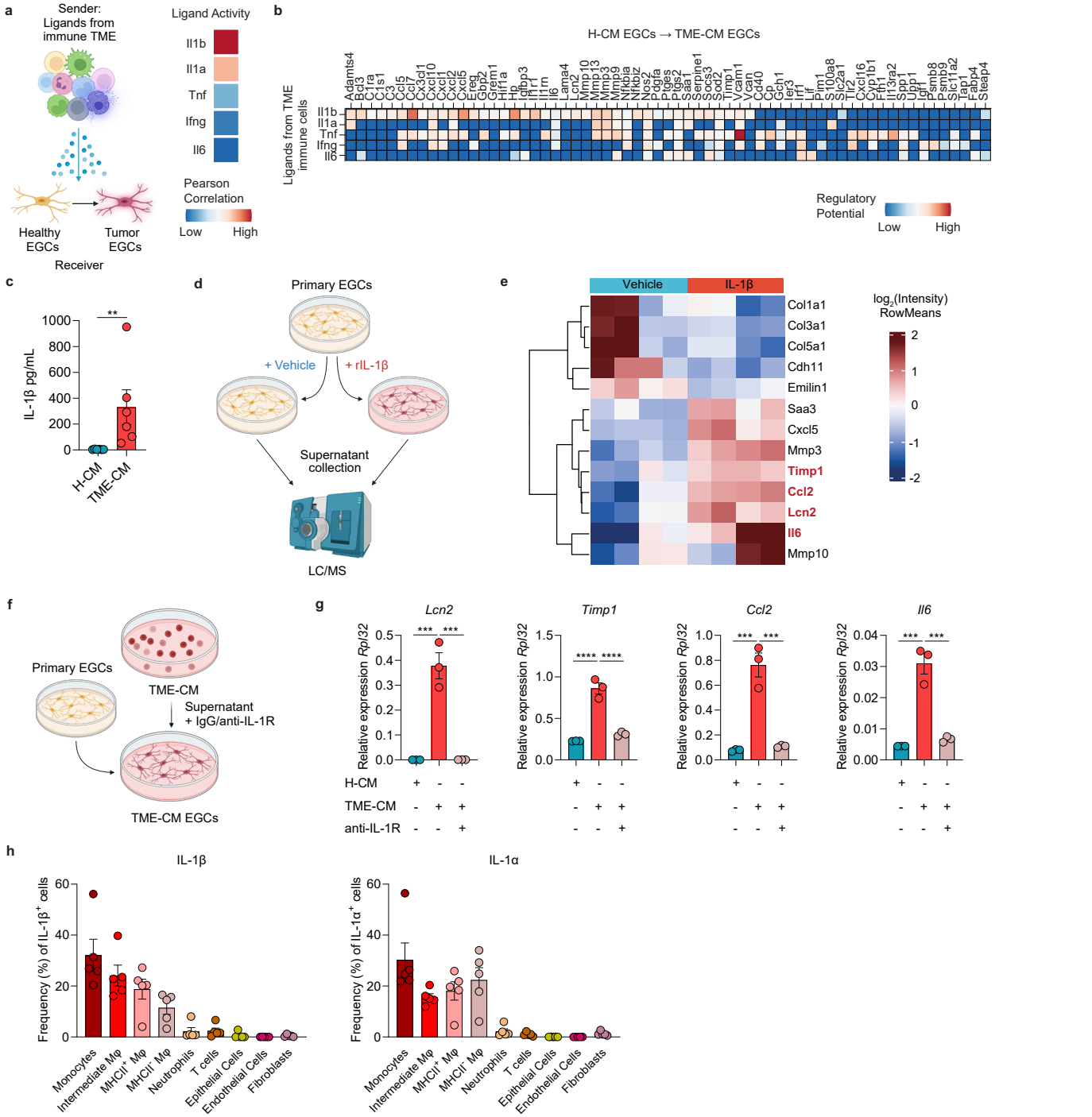


**Fig. 4 | IL-1R activation drives the CRC EGC phenotype. a**, **b** Top ligands from orthotopic CRC tumor-infiltrating immune cells predicted by NicheNet to be inducing CRC EGC signature. NicheNet analysis was performed considering the ligands expressed by murine orthotopic CRC tumor-infiltrating immune cells, data extracted from CRC orthotopic murine CRC dataset (see Supplementary Fig. 4a) and considering the differentially expressed genes between 24 h healthy conditioned medium (H-CM) EGCs and tumor microenvironment (TME)-CM EGCs as target genes, data extracted from in vitro CRC EGCs bulk RNAseq dataset (see Fig. 2). Schematic representation of TME-derived ligand-EGC interplay (left) and top 5 predicted ligands with their Pearson correlation (right) (**a**). Heatmap of ligand-target pairs showing regulatory potential scores between top ligands and target genes among the differentially expressed genes between in vitro H-CM EGCs and TME-CM EGCs (**b**). **c** Protein level of IL-1β in H-CM and TME-CM ($n = 6$ H-CM and TME-CM). **d**, **e** Primary adult neurosphere-derived EGCs were isolated from WT C57BL/6J mice and treated with or without recombinant (r)IL-1β (10 ng/mL) for 24 h. Protein concentration in the culture supernatants was determined by liquid chromatography/mass spectrometry ($n = 4$). Schematic experimental representation (**d**) and heatmap of differentially expressed proteins between vehicle and rIL-1β-treated EGCs (**e**). **f**, **g** Primary embryonic neurosphere-derived EGCs were stimulated for 24 h with H-CM or TME-CM in the presence or absence of IgG or anti-IL-1R (5 μg/mL each) ($n = 3$ H-CM and TME-CM). Schematic representation of experimental setup (**f**). Relative mRNA levels for *Lcn2, Timp1, Ccl2*, and *Il6* normalized to the housekeeping gene *Rpl32* (**g**). **h** WT C57BL/6J mice were intracolonically injected at day(d)0 with MC38 cells, and both stromal and immune cells were assessed for IL-1β and IL-1α expression at d21. Data are presented as the frequency of total live IL-1β$^+$ or IL-1α$^+$ cells ($n = 5$ mice). Data are represented as mean ± SEM (**c**, **g**, **h**). Statistical analysis: unpaired two-tailed Mann-Whitney test (**c**), unpaired one-way Anova test with multiple comparison correction (**g**). $^{**}p < 0.005$, $^{***}p < 0.0005$, $^{****}p < 0.00005$. Source data and exact *p* values are provided as a Source Data file.

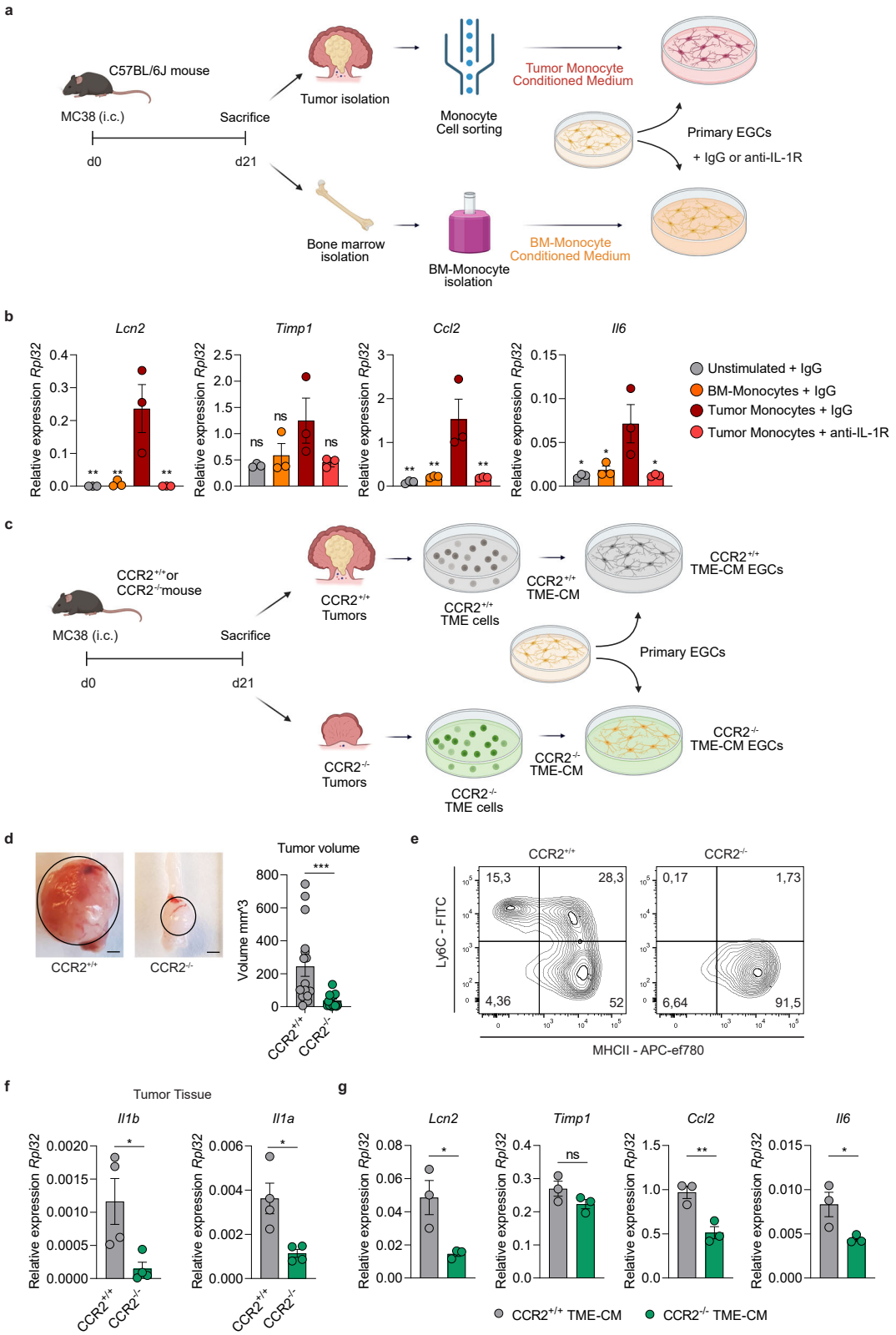


as the principal producers of both IL-1β and IL-1α at the RNA and protein levels (Fig. 4h and Supplementary Fig. 5h).

To define the possible effect of tumor monocyte-derived IL-1 on the immunomodulatory reprogramming of EGCs, we isolated tumor- and bone marrow (BM)-derived monocytes from mice bearing orthotopic colon tumors and exposed primary enteric glia to their supernatant with or without IL-1R blockade (Fig. 5a). Remarkably, the supernatant of tumor monocytes was able to induce a higher expression of CRC EGC marker genes (*Lcn2*, *Timp1*, *Ccl2*, and *Il6*) compared to control BM-derived monocytes in an IL-1R-dependent manner (Fig. 5b).

To further verify the monocyte origin of IL-1 signaling, we examined the effects on primary EGCs of orthotopic TME-CM, sourced from tumors induced in both monocyte-deficient [C-C chemokine receptor type 2 deficient ($CCR2^{-/-}$)] and monocyte-competent mice ($CCR2^{+/+}$)

**Fig. 5 | Monocyte-derived IL-1 promotes the CRC EGC phenotype. a**, **b** Primary embryonic neurosphere-derived EGCs were stimulated for 24 h with IgG or anti-IL-1R (5 μg/mL each) with or without the supernatant of sorted tumor monocytes or bone marrow (BM)-derived monocytes from WT C57BL/6J mice bearing orthotopic CRC tumors. Schematic representation of experimental setup (**a**). Relative mRNA levels of *Lcn2, Timp1, Ccl2*, and *Il6*, normalized to the housekeeping gene *Rpl32*, in primary embryonic neurosphere-derived EGCs were compared between EGCs stimulated with tumor monocyte supernatant + IgG and all other conditions ($n = 3$ primary EGC cultures and monocytes) (**b**). **c**–**g** $CCR2^{+/+}$ and $CCR2^{-/-}$ mice were intracolonically injected at day(d)0 with MC38 cells, tumor tissue was collected at d21. Then, in vitro embryonic neurosphere-derived EGCs were cultured for 24 h with the tumor microenvironment-conditioned medium (TME-CM) of $CCR2^{+/+}$ and $CCR2^{-/-}$ tumors. Schematic representation of experimental setup (**c**). Representative pictures (left, scale bar 2 mm) and quantitative comparison of tumor volume (right) ($n = 16$ $CCR2^{+/+}$, $n = 17$ $CCR2^{-/-}$) (**d**). Representative contour plots of tumor-infiltrating monocytes and macrophages gated on live-$CD45^+$-$CD11b^+$-$Ly6G^-$-$CD64^+$ cells (**e**). Relative mRNA levels of *Il1b* and *Il1a* normalized to the housekeeping gene *Rpl32* in $CCR2^{+/+}$ and $CCR2^{-/-}$ CRC tumors ($n = 3$ mice) (**f**). Relative mRNA levels of *Lcn2, Timp1, Ccl2*, and *Il6* in EGCs stimulated with TME-CM of $CCR2^{+/+}$ and $CCR2^{-/-}$ mice, normalized to the housekeeping gene *Rpl32* ($n = 3$ TME-CM) (**g**). Data represented as mean ± SEM (**b**, **d**, **f**, **g**). Statistical analysis: One-way ANOVA test with correction for multiple comparisons, compared to tumor monocyte supernatant + IgG condition (**b**), unpaired two-tailed Mann Whitney test (**d**) or unpaired two-tailed t-test (**f**, **g**). $^*p < 0.05$, $^{**}p < 0.005$, $^{***}p < 0.0005$, ns not significant. Source data and exact *p* values are provided as a Source Data file.

(Fig. 5c). Consistent with previous findings[27], the volume of orthotopic tumors grown in the colonic mucosa of $CCR2^{-/-}$ mice was significantly reduced (Fig. 5d) as a consequence of the lower number of monocytes and monocyte-derived macrophages in $CCR2^{-/-}$ tumors, as confirmed by flow cytometry (Fig. 5e). Consistently, *Il1b* and *Il1a* expressions were significantly decreased in the tumor tissue of CCR2-deficient mice compared to WT mice (Fig. 5f), further corroborating that monocytes and monocyte-derived macrophages are the major source of IL-1 ligands in the colon TME. As expected, TME-CM isolated from the $CCR2^{-/-}$ mice failed to induce CRC EGC reprogramming as reflected by the reduced expression of *Lcn2, Ccl2*, and *Il6* when compared with EGCs treated with $CCR2^{+/+}$ TME-CM (Fig. 5g). A similar trend, although not significant, was observed for *Timp1*. Overall, our findings strongly support the concept that IL-1, derived from tumor-infiltrating monocytes- and monocyte-derived macrophages, provides remodeling of the neighboring enteric glia into activated and immunomodulatory CRC EGCs.

## IL-1R signaling in EGCs promotes $SPP1^+$ TAM differentiation

Next, we assessed whether IL-1R blocking in CRC EGCs might directly affect TAM differentiation. For this purpose, EGC cultures were exposed to TME-CM or H-CM in the presence of an IL-1R blocking antibody and subsequently their supernatant was used to treat naive monocytes (Fig. 6a). To exclude any direct impact of anti-IL-1R antibody on monocytes, we removed the antibody from the EGC supernatant by using magnetic beads. Notably, the blockade of IL-1R led to a significantly reduced differentiation of monocytes into $SPP1^+$ TAMs with the supernatant of TME-CM EGCs. However, IL-1R blockade did not alter TAM polarization in the context of H-CM EGCs both at RNA and protein level (Fig. 6b, c and Supplementary Fig. 6a-b). As a result, IL-6 levels were markedly reduced in the supernatant of TME-CM-exposed EGCs following IL-1R inhibition (Fig. 6d). These findings further corroborated our hypothesis regarding the critical role of the IL-1R/IL-6 axis in CRC EGCs in directing monocyte differentiation towards the $SPP1^+$ TAM phenotype.

Then, to investigate the effect of IL-1R signaling inhibition on the immunomodulatory functions of EGCs in vivo, we co-injected WT or $IL\text{-}1R1^{-/-}$ EGCs and MC38 cells in C57/BL6J mice (Fig. 6e). Interestingly, co-injection of tumor cells with $IL\text{-}1R1^{-/-}$ EGCs resulted in lower tumor growth and reduced infiltration of $SPP1^+$ TAMs when compared with tumors co-injected with WT EGCs (Fig. 6f-g). Lack of IL-1R in co-injected EGCs had no impact on $C1Q^+$ TAMs.

Acknowledging the heterogeneity of CRC with regard to the immune compartment[28], we sought to investigate the glial-TAM crosstalk also in "immune cold" MSS-CRC like tumors, by injecting $villinCre^{ER}$ $Apc^{fl/fl}$ $Kras^{G12D/+}$ $Trp53^{fl/fl}$ $Trgfbrl^{fl/fl}$ (AKPT) tumor-derived cells orthotopically[29]. Indeed, while the MC38 model is representative of "immune hot" tumors, characterized by a large immune infiltrate[30], the AKPT model is characterized by a low tumor-immune compartment[30,31]. Thus, we injected AKPT cells in the colonic mucosa of mice with a glial-specific deletion of IL-1R1 ($GFAP^{Cre}IL\text{-}1R1^{fl/fl}$) and their littermates ($GFAP^{Wt}IL\text{-}1R1^{fl/fl}$) (Fig. 6h and Supplementary Fig. 6c). Notably, also in this model, deletion of IL-1R in EGCs impacted tumor growth and $SPP1^+$ TAM expansion (Fig. 6i, j), suggesting IL-1R triggered EGC-TAM crosstalk as a broad mechanism across independent orthotopic CRC subtypes.

In addition, we investigated the glia-TAM interaction also in a colitis-associated colorectal cancer model based on AOM/DSS administration[32] (Fig. 7a). Here, using the glia reporter mouse line $GFAP^{Cre}Ai14^{fl/fl}$ (Supplementary Fig. 6c), we confirmed spatial proximity of EGCs ($tdTomato^+$) and TAMs ($IBA1^+$) in the tumor regions (Fig. 7b), as we have previously observed in the orthotopic MC38 model. Transcriptomic analysis comparing AOM/DSS-induced tumors to naive tissue in wild-type mice supported the involvement of the IL-1R/IL-6 pathway in EGC-TAM crosstalk (Supplementary Fig. 6d, e, Supplementary Data 3). In particular, transcriptomic differences highlighted an increased expression of CRC EGC markers, as well as TAM signature genes together with increased IL-1 signaling. Consistent with the role of enteric glia in the orthotopic CRC model, the number of colonic tumors was diminished in AOM/DSS-treated $GFAP^{Cre}IL\text{-}1R1^{fl/fl}$ compared to littermate $GFAP^{Wt}IL\text{-}1R1^{fl/fl}$ mice, while no differences in weight loss or EGC network morphology were detectable between the two genotypes (Fig. 7c and Supplementary Fig. 6f, g). Interestingly, glial-specific IL-1R deficiency correlated with a decline in $SPP1^+$ TAMs, but $C1Q^+$ TAM levels remained unchanged (Fig. 7d). Importantly, glial-specific IL-1R deficiency was further associated with reduced *Il6* gene expression in tumor tissues of $GFAP^{Cre}IL\text{-}1R1^{fl/fl}$ compared to control $GFAP^{Wt}IL\text{-}1R1^{fl/fl}$ tumor lesions (Fig. 7e).

To further validate the expression of IL-6 in tumor EGCs, we performed fluorescence-activated cell sorting of enteric glia from healthy or tumor colonic mucosa of AOM/DSS-treated $GFAP^{Cre}Ai14^{fl/fl}$ mice. In line with our in vitro data, we detected a strong increase of *Il6* expression in tumor versus healthy $tdTomato^{pos}$ EGCs (Fig. 7f and Supplementary Fig. 6h-i). Consistently, IL-6 staining in tumor sections from the EGC reporter mouse line $Sox10^{CreERT2}Ai14^{fl/fl}$, revealed that IL-6 protein co-localized with $tdTomato^+$ cells in AOM/DSS tumors (Fig. 7g and Supplementary Fig. 6j).

In conclusion, these findings offer further in vivo evidence underscoring the IL-1-dependent interaction between EGCs and $SPP1^+$ TAMs within the CRC milieu.

## IL-1R induced-CRC EGC phenotype in patients with CRC

After identifying enteric glia-immune interactions in preclinical models of CRC, we investigated whether a similar process might influence disease progression in CRC patients. Initially, spatial tissue co-localization of EGCs and TAMs was confirmed in patient-derived CRC samples (Fig. 8a). Next, the possible contribution of EGCs in disease outcome was defined using the colon and rectal cancer datasets from The Cancer Genome Atlas (TCGA- COAD, and READ). Here, patients were hierarchically clustered into two groups based on the expression levels (high versus low) of the EGC transcriptomic signature, consisting of genes highly expressed by EGCs as defined in previously published

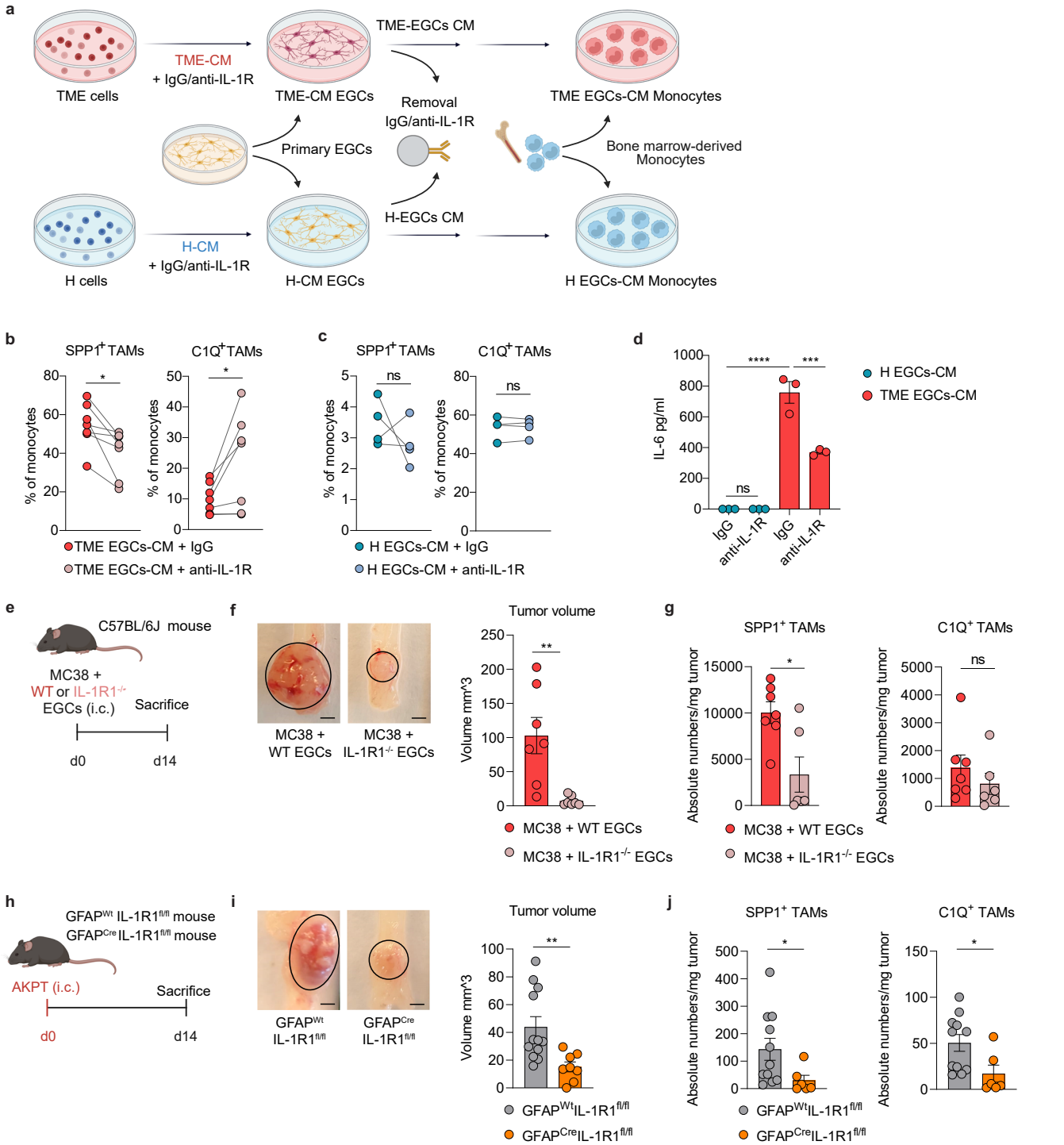


**Fig. 6 | IL-1R signaling in EGCs promotes SPP1⁺ TAM differentiation and tumor progression. a–c** Murine bone marrow-derived monocytes were cultured for 48 h with supernatant of primary embryonic neurosphere-derived EGCs, which were pre-incubated for 24 h with tumor microenvironment conditioned medium (TME-CM) or healthy-CM (H-CM) together with isotype IgG or anti-IL-1R (5 μg/mL each). Antibodies were removed from the CM through the application of Dynabeads™ Protein G prior to incubation with monocytes. Experimental design (**a**). Flow cytometry quantification of SPP1⁺ TAMs and C1Q⁺ TAMs after TME-EGCs ($n = 7$) (**b**) or H-EGCs ($n = 4$) (**c**) supernatant stimulation. **d** IL-6 concentration in the conditioned medium of H-EGCs and TME-EGCs pre-incubated with IgG or anti-IL-1R ($n = 3$ primary EGC cultures). **e–g** WT C57BL/6J mice were intracolonically (i.c.) injected with MC38 cells and embryonic neurosphere-derived WT EGCs or IL-1R1$^{-/-}$ EGCs (1:1 ratio). Tumor growth and immune infiltration were assessed on day (d)14. Schematic representation of EGCs co-injection mouse model (**e**) with representative pictures (scale bar 2 mm) and quantitative comparison of tumor volume ($n = 7$ mice) (**f**). Data show absolute tumor-infiltrating TAM cell numbers per mg tumor tissue ($n = 7$ MC38 + WT EGCs, $n = 6$ MC38 + IL-1R1$^{-/-}$ EGCs) (**g**). **h–j** GFAP$^{Wt}$IL-1R1$^{fl/fl}$ and GFAP$^{Cre}$IL-1R1$^{fl/fl}$ mice were i.c. injected with AKPT cells. Tumor growth and immune infiltration were assessed at d14. Schematic representation of orthotopic CRC mouse model (**h**) with representative pictures (scale bar 2 mm) and quantitative comparison of tumor volume ($n = 12$ GFAP$^{Wt}$IL-1R1$^{fl/fl}$, $n = 8$ GFAP$^{Cre}$IL-1R1$^{fl/fl}$) (**i**). Data show absolute tumor-infiltrating TAM cell numbers per mg tumor tissue ($n = 11$ GFAP$^{Wt}$IL-1R1$^{fl/fl}$, $n = 6$ GFAP$^{Cre}$IL-1R1$^{fl/fl}$) (**j**). Data are represented as mean ± SEM (**d**, **f**, **g**, **i**, **j**). Statistical analysis: paired two-tailed Wilcoxon test (**b**, **c**), two-way ANOVA test with correction for multiple comparisons (**d**) or unpaired two-tailed Mann-Whitney test (**f**, **g**, **i**, **j**). *$p < 0.05$, **$p < 0.005$, ***$p < 0.0005$, ****$p < 0.00005$, ns not significant. Source data and exact $p$ values are provided as a Source Data file.

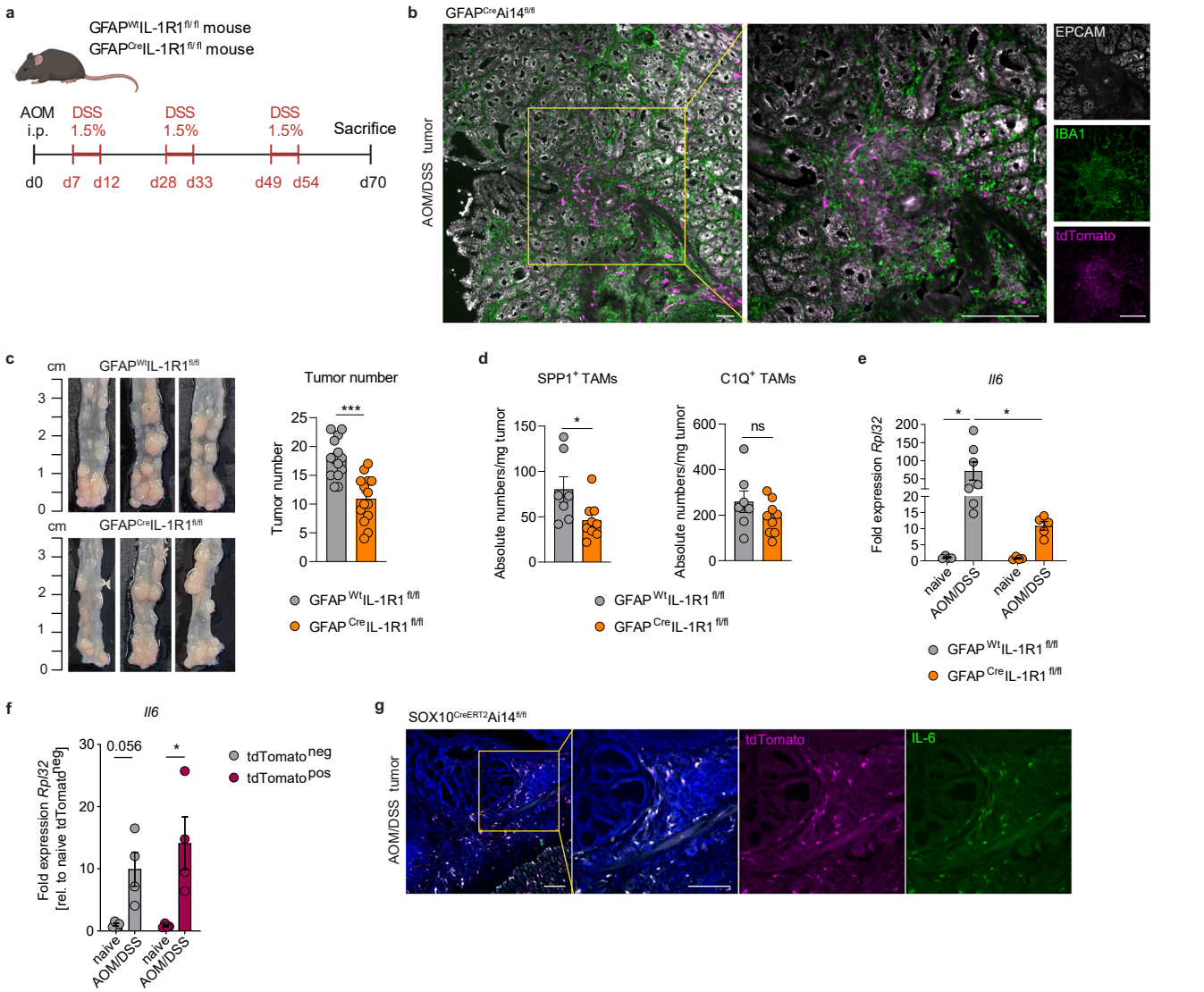


**Fig. 7 | IL-1R deficient EGCs impair tumor progression and SPP1$^+$ TAM differentiation in colitis-associated CRC. a** Schematic representation of the murine AOM/DSS CRC model. Mice were intraperitoneally (i.p.) injected with azoxymethane (AOM, 10 mg/kg body weight) at day(d)0. Starting from d7, mice underwent 3 repetitive cycles of 1.5% dextran sodium sulfate (DSS) in drinking water as indicated. **b** GFAP$^{Cre}$Ai14$^{fl/fl}$ mice were subjected to the AOM/DSS model (Fig. 7a) using 1% DSS per cycle. Representative images of EPCAM (white), IBA1 (green) and tdTomato (magenta) in tumor sections at d70 (scale bar 100 μm) ($n = 3$). **c-e** GFAP$^{Wt}$IL-1R1$^{fl/fl}$ and GFAP$^{Cre}$IL-1R1$^{fl/fl}$ mice were subjected to the AOM/DSS model (Fig. 7a). Tumors number and TAMs infiltration were assessed at d70. Tumor numbers of GFAP$^{Wt}$IL-1R1$^{fl/fl}$ and GFAP$^{Cre}$IL-1R1$^{fl/fl}$ littermates, representative images (left) and quantitative comparison of tumor numbers (right) ($n = 14$ mice per genotype) (**c**). Corresponding absolute numbers of SPP1$^+$ and C1Q$^+$ TAMs per mg tumor tissue ($n = 7$ GFAP$^{Wt}$IL-1R1$^{fl/fl}$, $n = 9$ GFAP$^{Cre}$IL-1R1$^{fl/fl}$) (**d**). Relative mRNA levels for *Il6*, normalized to the housekeeping gene *Rpl32* in naive ($n = 4$) and AOM/DSS treated mice ($n = 7$ GFAP$^{Wt}$IL-1R1$^{fl/fl}$, $n = 5$ GFAP$^{Cre}$IL-1R1$^{fl/fl}$) (**e**). **f** GFAP$^{Cre}$Ai14 $^{fl/fl}$ mice underwent the AOM/DSS model (Fig. 7a) using 1% DSS. Tumor or naive colon cells were isolated at d70 and FACS-sorted. *Il6* expression levels of sorted tdTomato$^{pos}$ glial cells versus remaining tdTomato$^{neg}$ cells of naive and AOM/DSS-treated GFAP$^{Cre}$Ai14$^{fl/fl}$ mice ($n = 4$). Expression displayed as fold to *Rpl32* and relative to naive tdTomato$^{neg}$ cells. **g** SOX10$^{CreERT2}$Ai14$^{fl/fl}$ mice were i.p. injected with Tamoxifen (1 mg in 100 μL sterile corn oil) on d−7, −6, and −5. Subsequently, mice were subjected to the AOM/DSS model (Fig. 7a) using 2% DSS per cycle. Representative image of tdTomato (magenta), IL-6 (green), and DAPI (blue) in tumor section at d70 (scale bar 100 μm) ($n = 3$). Data are represented as mean ± SEM (**c**–**f**). Statistical analysis: unpaired two-tailed t-test (**c**), unpaired two-tailed Mann-Whitney test (**d**), and two-way ANOVA with correction for multiple comparisons (**e**, **f**). $^*p < 0.05$, $^{***}p < 0.0005$, ns not significant. Source data and exact *p* values are provided as a Source Data file.

scRNA-seq datasets[22,33,34] (Supplementary Fig. 7a and Supplementary Table 3). Here, we observed that CRC patients with a higher enteric glia transcriptomic signature presented with a decreased overall survival probability compared to patients with low EGC signature (Fig. 8b and Supplementary Fig. 7b). Importantly, the correlation between the expression of the high EGC gene signature with worse survival probability in CRC patients was confirmed in a second independent CRC dataset, known as the Sidra-LUMC AC-ICAM cohort[35](Supplementary Fig. 7c, d).

In-depth characterization of the COAD-READ patients with high EGC gene signature revealed 79% of this group belonged to the mesenchymal consensus molecular subtype 4 (CMS4) (Supplementary Fig. 8a), defined by the stromal invasion phenotype, which is generally associated with the worst overall and relapse-free survival[36]. In comparison, only minor differences were identified when divided based on stage, microsatellite stability, or intrinsic CMS (iCMS). Interestingly, CRC patients with pronounced EGC involvement also exhibited higher expression of SPP1$^+$ TAM signature genes (Fig. 8c).

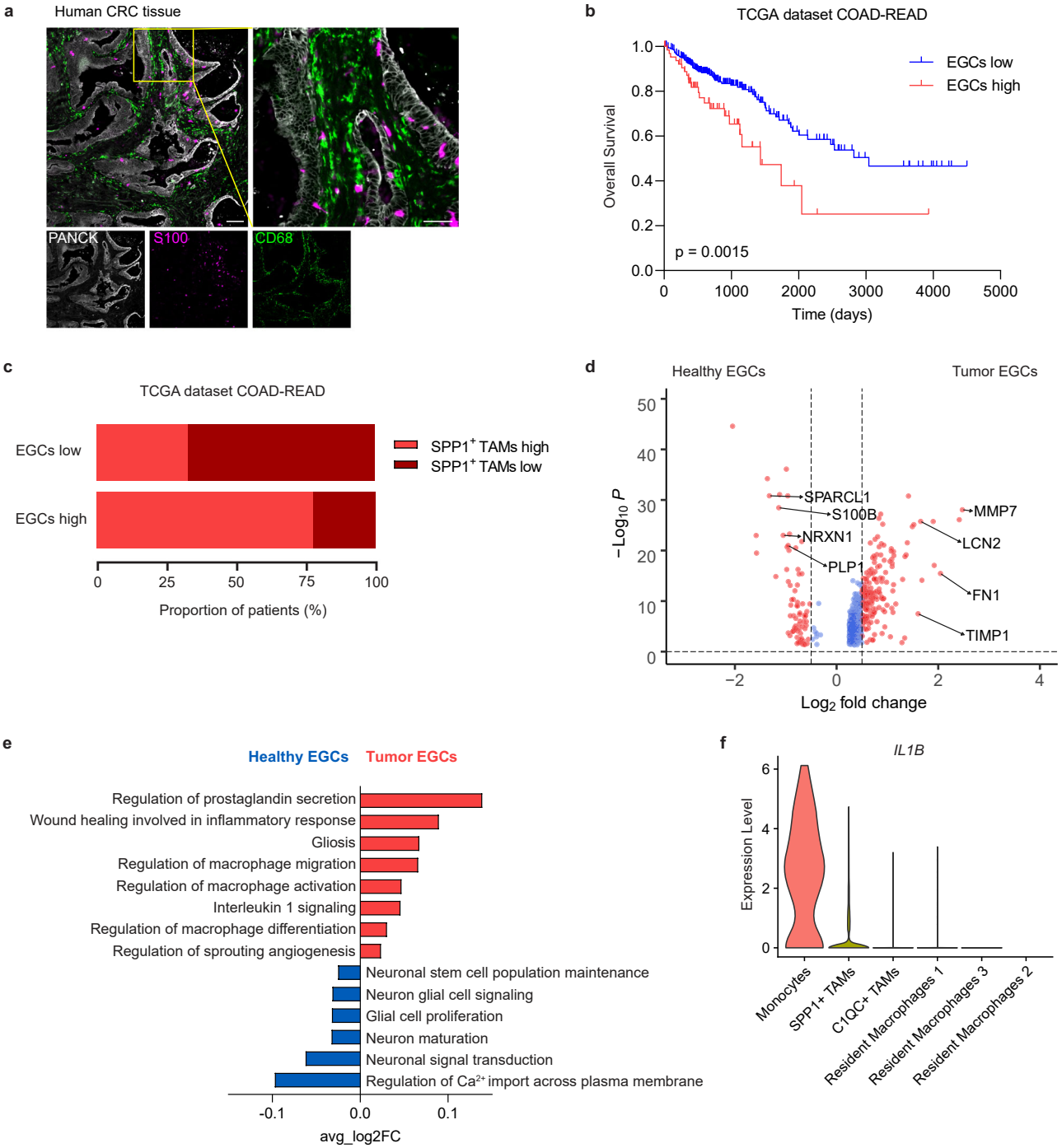


**Fig. 8 | IL-1R induced-CRC EGC phenotype in patients with CRC. a** Representative image showing S100 (magenta), CD68 (green) and Pancytokeratin (PANCK, white) in a human CRC tissue section (scale bar 200 μm and 50 μm). Image representative of ten stainings. **b, c** TCGA COAD and READ patients stratified based on their expression of the EGCs signature genes ($n = 309$ EGCs low, $n = 67$ EGCs high). Kaplan-Meier overall survival curve for EGCs high and low patients (**b**). The proportion of EGCs high and low patients classified based on high or low SPP1$^+$ TAMs gene signature expression (**c**). **d**, **e** Transcriptome analysis of tumor EGCs in CRC patients (KUL3 Dataset[33], $n = 5$). Volcano plot of differentially expressed genes between healthy and tumor EGCs (**d**), highlighting genes defining the tumor EGCs signature. Gene Set Enrichment Analysis presenting GO terms of interest (**e**). **f** Violin plot showing expression of *IL1B* in the tumor-infiltrating myeloid cell clusters of human CRC in the KUL3 Dataset[33] ($n = 5$). Statistical analysis: Mantel Cox test (**b**) and Wilcoxon test with Bonferroni correction using Seurat (**d**). Source data are provided as a Source Data file.

Finally, to assess if the murine CRC EGC transcriptional signature was conserved also in human CRC EGCs, we analyzed EGCs identified in a scRNA-seq dataset containing both CRC lesions and unaffected colonic tissues[33] (Supplementary Fig. 8b, c). By comparing gene expression profiles of tumor and healthy EGCs, we identified 589 genes specifically expressed in human CRC EGCs (Fig. 8d and Supplementary Data 2). Strikingly, among the top differentially expressed CRC EGC genes, we identified the two key murine CRC EGC marker genes *Lcn2* and *Timp1*. Using gene set enrichment analysis, we found that human EGC populations differentiate along the same homeostatic and tumor pathogenesis pathway transcriptomic signatures (Fig. 8e) as seen in our murine EGCs (Fig. 2e). Importantly, the significance of IL-1

signaling in the differentiation of patient CRC EGCs was further confirmed by the increased transcriptomic signatures for "*Interleukin-1 signaling*" as well as "*Regulation of macrophage differentiation, activation and migration*" compared to healthy colonic EGCs (Fig. 8e). In alignment with our preclinical findings, cell-population profiling of human CRC samples identified tumor-infiltrating monocytes as the primary source of IL-1β production (Fig. 8f and Supplementary Fig. 8d). Altogether, our data from mice and patients indicate the relevance of IL-1R induced glial-TAM interaction in CRC pathogenesis.

## Discussion

Using a variety of in vitro and in vivo models, we uncover a positive feedback loop between EGCs and TAMs in CRC. More specifically, we found that monocytes and monocyte-derived macrophages within the TME are the main producers of IL-1, inducing a pro-tumorigenic reactive phenotype in EGCs. IL-1-activated CRC EGCs via IL-6, in turn, directly promote the differentiation of tumor-infiltrating monocytes towards SPP1$^+$ TAMs. Importantly, the abundance of EGCs correlates with worse disease outcomes, as observed in both pre-clinical CRC mouse models and in patients with CRC.

EGCs are highly plastic cells that can rapidly adapt their functions under the influence of microenvironmental cues[7]. Recent studies have identified specific immunomodulatory factors, including IFN-γ, IL-1, and ATP, as triggers of enteric glia phenotypic and functional reprogramming in both homeostasis and diseased conditions[12,15,17]. In particular, IL-1-mediated EGC reactivity and its effects on immune cell modulation have been extensively studied in the context of intestinal inflammation[17,37]. However, the mechanisms underlying these processes in CRC were not yet understood. Using an unbiased approach combining murine bulk and human scRNA-seq, our investigation pinpointed TME-derived IL-1 as the principal initiator of EGC reactivity. Furthermore, we found that this IL-1-triggered EGC activation coincides with a profoundly immunomodulatory transcriptional signature in CRC EGCs. Of note, IL-1R signaling in EGCs may hold relevance for additional functions of CRC EGCs, as in vitro studies indicated the significance of IL-1 in EGC-cancer stem cell interactions[4]. Interestingly, we identified tumor-infiltrating monocytes and macrophages as the main source of IL-1 within the tumor. Nevertheless, although our in vivo data could not verify epithelial cells as a significant IL-1 source in CRC, tumor epithelial IL-1 might also contribute to EGC activation during CRC[4].

Our study utilizes single-cell and bulk RNA-seq techniques to better understand and predict the interactions between EGCs and TAMs within the colonic TME. In our murine orthotopic CRC model, we identified two distinct subsets of TAMs. The C1Q$^+$ TAMs, which preferentially express genes involved in phagocytosis and antigen presentation, coexist in the TME with SPP1$^+$ TAMs that are enriched for factors regulating angiogenesis and extracellular matrix, suggesting their key role in colon tumorigenesis. This dichotomy, recently also identified in patients with colorectal cancer[24] supports the relevance of our findings to human disease. In our research, we found that the two types of TAMs—SPP1$^+$ TAMs and C1Q$^+$ TAMs—are regulated by EGCs. Specifically, EGCs within tumors were effective in promoting the SPP1$^+$ TAM phenotype. In contrast, when monocytes were stimulated with healthy EGCs, the C1Q$^+$ TAM phenotype was induced. Importantly, while C1Q$^+$ macrophage differentiation was independent of IL-1R signaling in EGCs, we found that IL-1-activated tumor EGCs drive monocyte differentiation into pro-tumorigenic SPP1$^+$ macrophages via IL-6. Thereby, our findings underscore a bidirectional EGC-TAM interaction which was proven to influence tumor burden and SPP1$^+$ TAMs in three independent CRC mouse models. Of note, IL-6 can be produced by different cell types in the TME contributing to tumor development through direct and indirect pathways[38]. However, utilizing FACS-sorting and EGC-specific genetic IL-6 and IL-1R depletion models, we confirmed the critical role of IL-1-triggered EGC-IL-6 release as a regulator of tumor growth and SPP1$^+$ TAM differentiation. Thereby, our study identified EGCs as an additional important regulator of SPP1$^+$ TAM differentiation that, together with other cancer-associated stromal cells, may contribute to tumor progression[39,40]. Consistent with this, pan-cancer analysis has pinpointed SPP1$^+$ TAMs as the most pro-tumorigenic macrophage subset across various cancers[25,41].

Furthermore, our data also point to a functional association between CRC EGCs and monocyte migration, as reflected by increased *Ccl2* expression in CRC glia. Considering that the tumor monocyte population decreased upon EGC depletion, we speculate that CRC EGC-derived chemokines (i.e., CCL2 and CXCL5) could also promote the infiltration of monocytes in the colonic tumor site. This would be in line with our recent findings showing early expression of CCL2 by reactive EGCs in the context of intestinal inflammation[19]. However, further research will need to determine whether the pro-tumorigenic role of EGCs is exerted solely on the SPP1$^+$ TAMs or whether EGCs also affect other immune or stromal cells via glial-derived factors. Recent work by Progatzky et al. provides supportive evidence for this, demonstrating that EGCs are involved in a protective immune and stromal response to control parasitic insult in the gut[12].

Consistent with the identification of a pro-tumorigenic EGC phenotype in three independent CRC mouse models, we found that also in patients an increased EGC transcriptomic signature was associated with reduced overall survival in two independent CRC cohorts, the TCGA cohort and the Sidra-LUMC AC-ICAM cohort[35]. Therefore, we could speculate that the EGC gene signature might be used as a potential biomarker to predict disease outcomes. In line with the stromal nature of EGCs, we demonstrated that the vast majority of patients with high EGC involvement belonged to the CMS4, which is characterized by a mesenchymal-like phenotype, a strong stromal infiltration and the worst overall and relapse-free survival compared to the other CMS subtypes[36]. Gene ontology analysis revealed that also the human tumor glial cells were enriched for immunomodulatory transcriptional programs related to macrophage differentiation, leading to the assumption that CRC EGC-derived signals modulate TAMs also in patients. In line, human tumor EGCs also displayed enrichment for the GO term "Interleukin-1 signaling" hinting at a similar EGC activation in CRC as in our preclinical models. Moreover, various studies demonstrated increased IL-6 levels in both tumor tissues and serum samples of human CRC patients compared to healthy controls[42,43]. Consistently, immune-related pathways, including IL-6 signaling, were enriched in CRC EGCs in a human single-cell data set published by Qi et al.[39].

Our research elucidates the role of the IL-1/IL-6 axis in glial-immune communication in CRC, which could potentially be of relevance to various other tumors exhibiting neuronal infiltration, a feature often associated with less favorable disease outcomes[44–47]. Apart from EGCs, peripheral glial cells, including Schwann cells, are known to play a crucial role in cancer pathophysiology, as demonstrated in pancreatic ductal adenocarcinoma, lung cancer, and melanoma[48–50]. Consistent with the pro-tumorigenic functions of EGCs in CRC, studies in melanoma models have shown that tumor Schwann cells favor the differentiation of pro-tumorigenic macrophages enhancing tumor growth[50]. Therefore, glial-immune crosstalk might be an overlooked and conserved component of tumor pathophysiology in many cancer types beyond CRC.

In conclusion, our study reveals a critical role for IL-1R signaling in driving enteric glia-macrophage interactions in CRC pathogenesis. Our research provides insight into a complex neuroimmune mechanisms underlying CRC development, underscoring potential biomarkers and specific therapeutic targets that hold the promise of transforming the management of this devastating disease.

## Methods

### Animals

All experimental procedures were approved by the Animal Care and Animal Experiments Ethical Committee of KU Leuven (208/2018, 213/

2018 and 159/2021) or by the Regional Office for Nature, Environment and Consumer Protection of North-Rhine-Westphalia, Germany (81-02.04.2021.A424). WT C57BL/6J (JAX:000664), CCR2$^{-/-}$ (JAX: 004999), IL-1R1$^{-/-}$ (JAX:003245), PLP1$^{CreERT2}$iDTR (JAX:005975 and JAX:007900), PLP1$^{CreERT2}$Ai14$^{fl/fl}$ (JAX:005975 and JAX:007908), GFAP$^{Cre}$IL-1R1$^{fl/fl}$ (JAX:012886 and JAX:028398), GFAP$^{Cre}$Ai14$^{fl/fl}$ (JAX:012886 and JAX:007908) and SOX10$^{CreERT2}$Ai14$^{fl/fl}$ [SOX10$^{CreERT2}$ (kindly provided by Dr. Vassilis Pachnis[51], (Ai14$^{fl/fl}$ JAX:007908)], SOX$^{CreERT2}$IL-6$^{fl/fl}$ (SOX10$^{CreERT2}$ as mentioned previously and IL-6$^{fl/fl}$ were kindly provided by Juan Hidalgo's lab[52]) mice were originally purchased from Jackson Laboratory and bred in our animal facilities. All mice were housed in temperature-controlled specific pathogen–free facilities with ad libitum access to standard chow diet and water under 12-h light–dark cycles at the KU Leuven or University of Bonn. Criteria for euthanasia were >20% weight loss for AOM/DSS model (according to 81-02.04.2021.A424) and tumor growth that interferes with fecal evacuation (>50% of colonic lumen obstruction, Grade 5) for the orthotopic model. In cases where limits have been exceeded due to the natural variety of the models, animals were euthanized according to ethical regulations. In the case of GFAP$^{Cre}$IL-1R1$^{fl/fl}$ mice, following recommendation by The Jackson Laboratory (JAX:012886), we used a strict mating scheme using only Cre$^{+}$ carrying female with Cre$^{-}$ males to overcome any issues of germline Cre-expression and to produce only litters with a GFAP-promotor-driven Cre-expression. Specific GFAP$^{Cre}$ recombination was confirmed in the reporter mouse line GFAP$^{Cre}$Ai14$^{fl/fl}$ showing a strong overlap of tdtomato signal with immunolabelled GFAP and SOX10 cells in colonic tissue, confirming Cre activity exclusively in enteric glia (Supplementary Fig. 6c).

### In vitro tumor EGCs model

Both orthotopic tumors and healthy colons of C57BL/6J, CCR2$^{+/+}$ or CCR2$^{-/-}$ mice were digested for 30 min in DMEM with 2.5% FBS, 100 μg/mL Penicillin and Streptomycin, 200 U/mL collagenase IV (Gibco, ThermoFisher Scientific) and 125 μg/mL type II dispase (Gibco, ThermoFisher Scientific) to obtain a single-cell suspension. Tumor microenvironment conditioned medium (TME-CM) and healthy colon conditioned medium (H-CM) were generated by culturing $5 \times 10^5$ cells/mL in DMEM-complete medium overnight. Next, primary murine embryonic neurosphere-derived EGCs were stimulated with the TME-CM or H-CM for 6, 12, or 24 h. For IL-1R blocking experiments, primary embryonic neurosphere-derived EGCs were incubated for 24 h with TME-CM together with 5 μg/mL isotype IgG (BioXCell) or 5 μg/mL anti-IL-1R (BioXCell).

### Orthotopic CRC model

Orthotopic colonic sub-mucosal implantation of CRC cells was performed as previously described[20]. Briefly, MC38 cells[53] or AKPT cells[29,31] were intracolonically (i.c.) injected via endoscopy as a single-cell suspension containing between 75,000–750,000 cells/100 μL PBS depending on the susceptibility of the mouse strain. Both male and female mice were used for orthotopic tumor implantation. AKPT cells were received from Prof. Owen Sansom (UK). For the EGCs supplementation model, primary embryonic neurosphere-derived WT and IL-1R1$^{-/-}$ EGCs were isolated with 0.05% Trypsin-EDTA (Gibco, ThermoFisher Scientific) and treated with HBSS (Gibo, ThermoFisher Scientific) supplemented with 100 μg/mL DNAse I (Roche) and 5 mM $MgCl_2$ (Sigma-Aldrich) for 30 min at RT. Subsequently, EGCs were first washed with HBSS with 5 mM $MgCl_2$ and then with PBS. Finally, EGCs were resuspended in PBS together with MC38 cells in a ratio of 1:1 and orthotopically co-injected in C57BL/6J WT mice. Two weeks prior to the start of each experiment, PLP1$^{CreERT2}$iDTR mice, SOX$^{CreERT2}$IL-6$^{fl/fl}$ and SOX$^{CreERT2}$IL-6$^{wt/wt}$ were injected intraperitoneally (i.p.) 2 times every other day with 100 mg/kg Tamoxifen (Sigma-Aldrich) dissolved in 100 μL MIGLYOL®812 (Sigma-Aldrich). For EGCs in vivo depletion experiments, PLP1$^{CreERT2}$iDTR and C57BL/6J WT mice were injected i.c. with 2 mg/kg Diphtheria toxin (DT) (Merck, Sigma) dissolved in 100 μL of saline, three and five days prior to the start of the tumor implantation. Tumor volume was determined by caliper measurements and calculated based on the height ($h$), length ($l$) and width ($w$) of the tumor, according to the formula: $(\pi/6)*h*l*w$.

### AOM-DSS model

Female GFAP$^{Cre}$IL-1R1$^{fl/fl}$, GFAP$^{Wt}$IL-1R1$^{fl/fl}$ littermate and GFAP$^{Cre}$Ai14$^{fl/fl}$ mice (10–14 weeks of age) were injected i.p. with azoxymethane (AOM; 10 mg/kg; Sigma-Aldrich) a week prior starting three cycles of DSS colitis using 1.5% DSS in drinking water (MP Biomedicals) for 5 days followed by 16 days of recovery with normal drinking water[54]. On day 70, colonic tumor development was determined. For Sox10$^{CreERT2}$Ai14$^{fl/fl}$ mice subjected to the AOM/DSS model, slight adjustments were made to the protocol. Female Sox10$^{CreERT2}$Ai14$^{fl/fl}$ mice were i.p. injected with Tamoxifen (MP biomedicals, 1 mg in 100 μL sterile corn oil) on days −7, −6, and −5. On day 0, the AOM/DSS model was started as described above, but here mice were subjected to a DSS concentration of 2% in drinking water since this strain was less susceptible to DSS. On day 70, colons were harvested and cryo-embedded as Swiss rolls for immunohistochemistry.

### MC38 cell line

Murine colon adenocarcinoma cell line MC38 (NCI, ENH204-FP) was kindly provided by Prof. Max Mazzone (VIB - KU Leuven). The MC38 cell line was maintained in 5% $CO_2$ at 37 °C in high glucose Dulbecco's Modified Eagle Medium (DMEM) (Gibco, ThermoFisher Scientific) supplemented with 10% Fetal Bovine Serum (FBS) (Biowest), 100 μg/mL Penicillin and Streptomycin, 2 mM L- glutamine, 10 mM N-2-hydroxyethylpiperazine-N-2-ethane sulfonic acid (HEPES), 1 mM sodium pyruvate, 50 μM 2-Mercaptoethanol and 1X Non-Essential Amino Acids (all from Gibco, ThermoFisher Scientific).

### AKPT cell line

Murine small intestine villinCre$^{ER}$ Apc$^{fl/fl}$ Kras$^{G12D/+}$ Trp53$^{fl/fl}$ Trgfbrl$^{fl/fl}$ (AKPT) tumor-derived cells were kindly provided by Prof. Owen J. Sansom (Cancer Research UK Beatson Institute). The AKPT cells were maintained in 5% $CO_2$ at 37 °C in DMEM/F-12 (1:1) with L-glutamine and 2.438 g/L sodium bicarbonate (Gibco, ThermoFisher Scientific), 10% FBS (heat inactivation: 30 min at 56 °C, PAN Biotech) and Penicillin 100 U/ml and streptomycin 100 μg/ml (Gibco, ThermoFisher Scientific).

### Embryonic neurosphere-derived enteric glial cell culture

Embryonic neurosphere-derived EGCs were obtained as previously described[19]. Briefly, total intestines from E13.5 C57BL/6J mice were digested with collagenase D (10 mg/mL; Roche) and DNase I (0.08 mg/mL; Roche) in DMEM/F-12 (Gibco, ThermoFisher Scientific) for 1 h at 37 °C under gentle agitation. After digestion, tissue was filtered through a 70 μm cell strainer and cells were cultured in a $CO_2$ incubator at 37 °C in DMEM/F-12, 100 μg/mL Penicillin and Streptomycin, 2 mM L-glutamine, 10 mM HEPES, 1 mM sodium pyruvate, 50 μM 2-Mercaptoethanol supplemented with 1× B27 (Gibco, ThermoFisher Scientific), 40 ng/mL Epidermal Growth Factor (EGF) (Stemcell Technologies) and 20 ng/mL Fibroblast Growth Factors (FGF) (Invitrogen, ThermoFisher Scientific). After a minimum of 1 week of culture, neurospheres were treated with NeuroCult™ Chemical Dissociation Kit (Stemcell Technologies) according to the manufacturer's protocol and filtered through a 70-μm cell strainer. Cells were seeded on Poly-D-Lysine (PDL solution, 1.0 mg/mL, Sigma Aldrich) coated plates and differentiated in DMEM medium supplemented with 10% FBS, 100 μg/mL Penicillin and Streptomycin, 2 mM L- glutamine, 10 mM HEPES, 1 mM sodium pyruvate, 50 μM 2-Mercaptoethanol (DMEM complete medium) until confluence for 5 days to obtain primary EGCs. For IL-1 stimulation experiments, $5 \times 10^4$ neurosphere-derived EGCs/mL were

stimulated with or without recombinant murine 10 ng/mL IL-1α (Peptrotech) and/or 10 ng/mL IL-1β (Sigma Aldrich) for 24 h.

### Neurosphere-derived adult enteric glial cell culture

Neurosphere-derived adult EGC cultures were obtained as described previously[17]. Briefly, small intestines of 8–16 weeks old C57BL/6 mice were harvested, cleaned, cut into 3–5 cm long segments and kept in oxygenated Krebs-Henseleit buffer (126 mM NaCl; 2.5 mM KCl: 25 mM $NaHCO_3$; 1.2 mM $NaH_2PO_4$; 1.2 mM $MgCl_2$; 2.5 mM $CaCl_2$, 100 IU/mL Penicillin, 100 IU/mL Streptomycin and 2.5 µg/mL Amphotericin). For each segment, the muscularis layer was peeled and collected for digestion. Muscularis tissues were incubated for 15 min in DMEM containing Protease Type 1 (0.25 mg/mL, Sigma-Aldrich) and Collagenase A (1 mg/mL, Sigma-Aldrich) at 37 °C and 150 rpm. Digestion was stopped with DMEM containing 10% FBS (Sigma-Aldrich) and cells were cultured in proliferation medium (neurobasal medium with 100 IU/Penicillin, 100 µg/mL Streptomycin, 2.5 µg/mL Amphotericin (all ThermoFisher Scientific), FGF and EGF (both 20 ng/mL, Immunotools) at 37 °C, 5% $CO_2$ to promote neurosphere formation. After 1 week in culture, enteric neurospheres were dissociated with trypsin (0.25%, ThermoFisher Scientific) for 5 min at 37 °C and differentiated at 50% confluency on Matrigel (100 µg/mL, Corning) coated six well plates for 1 week in differentiation medium (neurobasal medium with 100 IU/Penicillin, 100 µg/mL Streptomycin, 2.5 µg/mL Amphotericin, B27, N2 (all Thermo Scientific) and EGF (2 ng/mL, Immunotools). For liquid chromatography/mass spectrometry (LC/MS) experiments, mature EGCs were treated with or without IL-1β (10 ng/mL, Immunotools) for 24 h. Conditioned media were collected and concentrated using Pierce™ Protein Concentrators, 3 K MWCO (ThermoFisher Scientific) according to the manufacturer's instructions. After denaturation at 95 °C for 5 min, samples were snap-frozen and kept at −80 °C until further processing.

### Bone marrow-derived monocyte isolation and stimulation

Murine bone marrow (BM)-derived monocytes were isolated from C57BL/6 mice. Briefly, the tibia and femur were dissected, and BM cells were flushed with DMEM high glucose supplemented with 10% FBS. After cells were collected and counted, monocytes were isolated with the EasySepTM Mouse monocyte isolation kit (Stemcell Technologies) according to the manufacturer's instructions. Next, $5 \times 10^5$ monocytes were stimulated for 48 h with 1 mL of H-CM, TME-CM, or with the supernatant of in vitro embryonic neurosphere-derived EGCs pre-incubated for 24 h with H-CM or TME-CM. For IL-1R blocking experiments, 5 µg/mL isotype IgG (BioXCell) or 5 µg/mL anti-IL-1R (BioXCell) was removed from the EGCs supernatant by using 20 µL/mL Dynabeads™ Protein G (ThermoFisher Scientific) according to the manufacturer's instructions. For IL-6 neutralization experiments, 20 µL/mL Dynabeads™ Protein G (ThermoFisher Scientific) together with 5 µg/mL anti-IL-6 (R&D Systems) or 5 µg/mL isotype IgG (R&D Systems) was added to the supernatant of H-CM EGCs and TME-CM EGCs and incubated for 2 h before removal by taking advantage of magnetization with the DynaMag™−2 Magnet (ThemoFisher Scientific).

### MILAN multiplex immunohistochemistry

Multiplex immunohistochemistry and analysis were performed according to a previously published method[55–57] and https://doi.org/10.21203/rs.2.1646/v5. Briefly, tissue sections (3 µm thickness) were prepared from formalin-fixed paraffin-embedded human CRC samples (collected at the UZ/KU Leuven biobank with informed consent from the patients according to protocol S66460, approved by the Ethics Committee Research UZ/KU Leuven). First, FFPE-tissue slides were deparaffinized by sequentially placing them in xylene, 100% ethanol and 70% ethanol. Following dewaxing, antigen retrieval was performed using PT link (Agilent) using 10 mM Ethylenediaminetetraacetic acid (EDTA) in Tris-buffer pH 8. Immunofluorescence staining was performed using Bond RX Fully Automated Research Stainer (Leica Biosystems) with the primary antibodies mouse anti-pan cytokeratin (1:500, Invitrogen, ThermoFisher Scientific), rabbit anti-S100B (1:500, Dako) or mouse anti-CD68 (1:100, Invitrogen, ThermoFisher Scientific). The sections were incubated for 4 h with the primary antibodies, washed several times and afterwards stained for 30 min with fluorescently labeled secondary antibodies (1:800, Alexa fluor 647 donkey anti-rabbit and 1:800, Alexa Fluor 488 goat anti-mouse respectively). Slides were then incubated for 10 min with a buffer containing 4,6-diamidino-2-phenylindole (1:1000, DAPI), after which mounting medium (50% glycerol; 584 mM C12H22O11; 10 mM Phosphate, 154 mM NaCl; pH 7,5) and a coverslip (Agilent, ref. CR12230-7) were manually applied to the slides. Then the slides were scanned using a Zeiss Axio Scan Z.1 (Zeiss) at 10x magnification. After completion of the staining procedure, the coverslips were manually removed after 30 min soaking in the washing buffer. Consecutive washing steps were thereafter performed using TBS. Stripping of the antibodies was performed in a buffer containing 1% SDS and β-mercaptoethanol for 30 min at 56 °C. After this stripping process, the slides were washed in a washing buffer for 45 min with frequent changes in the buffer. The staining procedure was repeated until all markers were stained and scanned on each of the slides. Utilize ImageJ (1.53T) and Qu path (0.3.2) were used for the region selection and to subtract background and tissue autofluorescence. Further analysis was performed by using ImageJ.

### Immunohistochemistry and Immunofluorescence

Orthotopic tumors were fixed overnight (ON) at 4 °C in Periodate-Lysine-Paraformaldehyde (PLP) buffer consisting of Milli-Q Water supplemented with 1% paraformaldehyde, 0.075 M lysine (pH 7.4), 0.037 M sodium phosphate (pH 7.4) and 0.01 M $NaIO_4$ (all from Sigma-Aldrich). Samples were washed three times with Milli-Q Water supplemented with 0.037 M sodium phosphate (pH 7.4), followed by a minimum of 4 h incubation in 30% sucrose (VWR chemicals) in PBS. Then, samples were embedded in OCT (Scigen) and stored at −80 °C until usage.

Preceding immunohistochemical staining, 7-µm orthotopic tumor tissue sections on SuperFrost Plus™ Adhesion slides (Epredia) were exposed to two washes with HistoChoice Cleaning Agent for 2 min each (Sigma-Aldrich) and subsequent hydration with Ethanol 100% for 2 min each (Merck) followed by deionized water. Then haematoxylin and eosin (both from Leica) staining was performed using standard procedures. Imaging was performed with Nikon Marzhauser Slide Express2, processed and analyzed using ImageJ.

Preceding immunofluorescent staining, tissues were sectioned to 7-µm thickness on SuperFrost Plus™ Adhesion slides (Epredia) and blocked with blocking buffer consisting of PBS containing 0.02% Sodium azide (Sigma-Aldrich), 0.3% donkey serum (Jackson), and 3% Bovine Serum Albumin (BSA, Serva) for 2 h at room temperature (RT). Subsequently, samples were incubated ON at 4 °C with the following primary antibodies: rat anti-F4/80, (1:500, BioRad) and rabbit anti-GFAP (1:300, Dako) or chicken anti-IBA1 (1:400, Synaptic Systems), rat anti-CD326 (EPCAM) (1:1000, Biolegend) and rabbit anti-Ki67 (1:400, Abcam) in staining buffer consisting of blocking buffer supplemented with 0.3% Triton X-100 (ThermoFisher, Scientific). Then, samples were washed in PBS and incubated with DAPI (4′,6-Diamidine-2′-phenylindole dihydrochloride; Sigma-Aldrich) combined with the secondary antibodies: donkey anti-rat AF488 (1:1000, Invitrogen, ThermoFisher Scientific), and donkey anti-rabbit Cy5 (1:400, Jackson) or donkey anti-chicken Cy3 (1:800, Invitrogen, Thermo Fisher Scientific), donkey anti-rat 488 (1:800, Invitrogen, Thermo Fisher Scientific) and donkey anti-rabbit AF647 (1:800, SouthernBiotech) in staining buffer for 2 h at RT. Finally, samples were rinsed three times in PBS and mounted with SlowFade Diamond Antifade mounting (Invitrogen, ThermoFisher Scientific). Imaging was performed on the ZEISS LSM 880 confocal

microscope or the Nikon ECLIPSE Ti2 microscope using NIS-Elements AR software (version 5.41.01). Pictures were analyzed using ImageJ.

For immunofluorescent staining of AOM/DSS or naive Swiss rolls of GFAP$^{Cre}$Ai14$^{fl/fl}$, GFAP$^{Cre}$IL-1R1$^{fl/fl}$, and SOX10$^{CreERT2}$Ai14$^{fl/fl}$ mice were fixed ON at 4 °C in 4% PFA. Samples were washed once with PBS followed by ON incubation at 4 °C in 30% sucrose (Sigma) in PBS. Subsequently, swiss rolls were embedded in Tissue-Tek® O.C.T.™ Compound (Sakura) and stored at −80 °C until usage.

Prior to immunofluorescent staining, AOM/DSS or naive GFAP$^{Cre}$Ai14$^{fl/fl}$, GFAP$^{Cre}$IL-1R1$^{fl/fl}$, and SOX10$^{CreERT2}$Ai14$^{fl/fl}$ samples were sectioned to 14 μm thickness on SuperFrost Plus™ Adhesion slides (Epredia). Slides were washed three times in PBS and blocked with blocking buffer (PBS containing 3% donkey serum and 0.1% Triton X-100) for 1 h at RT. Subsequently, primary antibody staining was performed ON at 4 °C in staining buffer (blocking buffer diluted with PBS in a 1:1 ratio) using the following antibodies: rabbit anti-IBA1 (1:400, Abcam), chicken anti-IBA1 (1:400, Synaptic Systems) and rat anti-CD326 (EPCAM) (1:1000, Biolegend), or rabbit anti-IL-6 (1:100, Abcam), or chicken anti-GFAP (1:1000, Biolegend). For IgG control staining, rabbit IgG (Dianova) was used in the same antibody concentration as rabbit anti-IL6. Slides were washed three times in PBS and secondary antibody staining was performed for 2 h at RT with donkey anti-rabbit FITC (1:800, Dianova), donkey anti-chicken CF633 (1:800, Sigma), donkey anti-rat 488 (1:800, Invitrogen, Thermo Fisher Scientific), or donkey anti-chicken FITC (1:800, Jackson) in staining buffer. After three more washes with PBS, slides were incubated with DAPI (Sigma-Aldrich) for 5 min at RT. After a final wash with PBS, slides were mounted with Shandon™ Immu-Mount™ (Epredia). Imaging was performed on the Nikon ECLIPSE Ti2 microscope using NIS-Elements AR software (version 5.41.01) or a Leica SP8 with LAS AF v3.x software for confocal images. Pictures were analyzed using ImageJ.

For whole-mount samples of PLP1$^{CreERT2}$Ai14$^{fl/fl}$ mice and GFAP$^{Cre}$Ai14$^{fl/fl}$ mice, the terminal colon was opened longitudinally, fixed with 4% PFA for 30 min, and washed with PBS. Muscularis externa was peeled off the colonic tissue and blocked with blocking buffer consisting of PBS containing 0.02% Sodium azide (Sigma-Aldrich), 0.3% donkey serum (Jackson), and 3% BSA (Serva) for 2 h at RT. Subsequently, samples were incubated 2 ONs at 4 °C in staining buffer consisting of blocking buffer supplemented with 0.3% Triton X-100 (ThermoFisher, Scientific) with following primary antibodies for PLP1$^{CreERT2}$Ai14$^{fl/fl}$ mice: rabbit anti-GFAP (1:300, Dako) and goat anti-SOX10 (1:300, R&D Systems), and for GFAP$^{Cre}$Ai14$^{fl/fl}$ mice: chicken anti-GFAP (1:1000, Biolegend) and goat anti-SOX10 (1:1000, custom-made aliquot kindly provided by Prof. Wegner, University of Erlangen[58]. Then, samples were washed in PBS and incubated with DAPI (Sigma-Aldrich) combined with the secondary antibodies in staining buffer ON at 4 °C. Secondary antibodies used for PLP1$^{CreERT2}$Ai14$^{fl/fl}$ mice; donkey anti-rabbit Cy5 (1:400, Jackson) and donkey anti-goat AF488 (1:500, Invitrogen, ThermoFisher Scientific) and for GFAP$^{Cre}$Ai14$^{fl/fl}$ mice: donkey anti-chicken FITC (1:800, Jackson) and donkey anti-goat CF647 (1:800, Sigma). Lastly, samples were rinsed three times in PBS and mounted with SlowFade Diamond Antifade mounting (Invitrogen, ThermoFisher Scientific). Imaging was performed on the ZEISS LSM 880 confocal microscope (PLP1$^{CreERT2}$Ai14$^{fl/fl}$) or Leica SP8 with LAS AF v3.x software (GFAP$^{Cre}$Ai14$^{fl/fl}$) and the pictures were analyzed using ImageJ.

### Enzyme-linked immunosorbent assay (ELISA)

Healthy and tumor-conditioned medium EGCs supernatants were collected and analyzed for IL-6 and IL-1β content using sensitive commercial ELISA kits (R&D Systems, Minneapolis, MN and V-Plex Pro-inflammatory panel Meso Scale Discovery; MSD respectively) according to the manufacturer's instructions. The data were analyzed with the Discovery Workbench 4.0 software (MSD).

### Western blot

Total proteins were extracted from mouse colonic tissues in T-PER buffer (ThermoFisher, Scientific) supplemented with 1 mM dithiothreitol, 10 mg/mL aprotinin, 10 mg/mL leupeptin, 1 mM phenylmethylsulfonyl fluoride, 1 mM Na3VO4 and 1 mM NaF (all from ThermoFisher, Scientific), by homogenization for 1 minute at 30 Hz (TissueLyser II, Qiagen). Lysates were clarified by centrifugation at 4 °C, 12,000 *g* for 30 min and separated on sodium dodecyl sulfate (SDS)-polyacrylamide gel electrophoresis. Blot was incubated with the GFAP antibody (1:500, Cell Signaling) followed by a secondary antibody conjugated to horseradish peroxidase (HRP) (1:5000; Dako Agilent Technologies). HRP was detected using the SuperSignal West Dura Extended Duration Substrate kit (ThermoFisher Scientific). To ascertain equivalent loading of the lanes, the blot was stripped and incubated with an anti-vinculin antibody (1:5000, Sigma-Aldrich) followed by a secondary antibody conjugated to horseradish peroxidase (1:5000; Dako Agilent Technologies) and HRP detection as described above. Computer-assisted scanning densitometry (GE Healthcare ImageQuant LAS 4000 Luminscent Image Analyzer) was used to analyze the intensity of the immunoreactive bands.

### Liquid chromatography/mass spectrometry (LC/MS)

LC/MS analysis of adult neurosphere-derived EGC supernatants treated with or without IL-1β was performed by the Core Facility Analytical Proteomics of the University of Bonn as described in the following. All chemicals from Sigma unless otherwise noted. For LC/MS sample preparation, 70 μg of protein per sample was subjected to in-solution preparation of peptides with the iST-NHS 96x sample preparation kit (Preomics GmbH, Martinsried, Germany) according to the manufacturer's recommendations. 0.4 mg TMT10plex isobaric Mass Tag Labeling reagent (Thermo Scientific) was added to each sample and incubated at room temperature for 1 h. 10 μL 5% hydroxylamine was used to quench the reaction. The preparation procedure was continued according to the iST-NHS kit instructions. Peptide concentration was determined with a colorimetric peptide assay (Thermo Scientific). Equal amounts of peptides were pooled and dried in a vacuum concentrator, dissolved in 20 mM ammonium formate (pH 10) and fractionated by reversed phase chromatography at elevated pH with a Reprosil100 C18 column (3 μm 125 ×4 mm, Dr. Maisch GmbH, Ammerbuch-Entringen, Germany). 60 fractions were combined into 6 pools and dried in a vacuum concentrator.

Before measurement, peptides were re-dissolved in 0.1% formic acid (FA) to yield a 1 g/L solution and separated on a Dionex Ultimate 3000 RSLC nano HPLC system (Dionex GmbH, Idstein, Germany). The autosampler was operated in μL-pickup mode. 1 μL was injected into a C18 analytical column (self-packed 400 mm length, 75 μm inner diameter, ReproSil-Pur 120 C18-AQ, 1.9 μm, Dr. Maisch). Peptides were separated during a linear gradient from 5% to 35% solvent B (90% acetonitrile, 0.1% FA) at 300 nL/min during 150 min. The nano-HPLC was coupled online to an Orbitrap Fusion Lumos Mass Spectrometer (Thermo Fisher Scientific, Bremen, Germany). Peptide ions between 330 and 1600 m/z were scanned in the Orbitrap detector every three seconds with a resolution of 120,000 (maximum fill time 50 ms, AGC target 100%). From MS3-based quantification, peptides were subjected either to collision-induced dissociation for identification (CID: 0.7 Da isolation, normalized energy 30%) and fragments analyzed in the linear ion trap with AGC target 50% and a maximum fill time 35 ms, rapid mode. Fragmented peptide ions were excluded from repeat analysis for 30 s. The top 10 fragment ions were chosen for synchronous precursor selection and fragmented with higher energy CID (HCD: 3 Da MS2 isolation, 65% collision energy) for detection of reporter ions in the Orbitrap analyzer (range 100–180 m/z, resolution 50,000, maximum fill time 86 ms, AGC target 200%). Alternatively, peptides were only fragmented by HCD and fragment ions and reporter ions were analyzed in the same spectrum (Orbitrap resolution 50,000).

Raw data processing and database search were performed with Proteome Discoverer software 2.5.0.400 (Thermo Fisher Scientific). Peptide identification was done with an in-house Mascot server version 2.8.1 (Matrix Science Ltd, London, UK). LC/MS data were searched against the Uniprot reference proteome mouse database (2022/05, 63628 sequences) and contaminants database (cRAP1)[59]. Precursor Ion m/z tolerance was 10 ppm, fragment ion tolerance 0.5 Da (CID). Tryptic peptides with up to two missed cleavages were searched. C6H11NO-modification of cysteines (delta mass of 113.08406) and TMT10plex on N-termini and lysines were set as static modifications. Oxidation was allowed as dynamic modification of methionine. Mascot results were evaluated by the Percolator algorithm version 3.02.12 as implemented in Proteome Discoverer[60]. Spectra with identifications above 1% *q* value were sent to a second round of database search with semi-tryptic enzyme specificity (one missed cleavage allowed). Protein N-terminal acetylation, methionine oxidation, TMT10plex, and cysteine alkylation were then set as dynamic modifications. Actual false discovery rates (FDR) values were 0.2% (peptide spectrum matches) and 0.9% (peptides). Reporter ion intensities (most confident centroid) were extracted from the MS3 level, with SPS mass match >65%.

The statistical analyses of the peptide-spectrum match (PSM) level data were done by the Core Unit for Bioinformatics Data Analysis of the University of Bonn. Analyses were carried out in R environment (R version 4.2) using an in-house developed workflow. Non-unique peptides and single-hit proteins (proteins identified/quantified by only one peptide) were filtered-out prior to the statistical analysis. From all available fractions, only those with the least number of missing values per feature and maximum average intensity across all TMT labels were selected. The PSM-level data were then log-transformed and scaled such that all the samples have the same median values (median normalization method). Next, the normalized data was aggregated to protein-level by applying the Tukey's median polish method. The statistical analysis was performed using the R package limma[61]. For each statistical contrast, the resulting *P* values were adjusted for multiple testing. The FDR were calculated by the Benjamini-Hochberg method.

### Isolation of tumor-infiltrating cells

Tumor-bearing mice were sacrificed at the described time points. After peeling off the muscularis layer from the orthotopic tumors, tissues were first cut into 1 mm pieces and then went under mechanical and enzymatic digestion for 30 min in DMEM with 2.5% FBS, 100 µg/mL Penicillin and Streptomycin, 200 U/mL collagenase IV (Gibco, ThermoFisher Scientific) and 125 µg/mL type II dispase (Gibco, ThermoFisher Scientific). AOM/DSS-induced tumors and healthy colon samples were peeled off the muscularis layer and underwent epithelial removal by vigorous shaking in Hanks' balanced salt solution (HBSS) with phenol red (Gibco, ThermoFisher Scientific) containing 1% FBS, 100 µg/mL Penicillin and Streptomycin, 1 mM EDTA (Invitrogen, ThermoFisher Scientific) and 1 mM dithiothreitol (DTT) (Sigma-Aldrich) for 8 min at 37 °C. A second incubation step was performed for 8 min at 37 °C in the same medium without DTT. After washing in wash medium (DMEM with 2.5% FBS and 100 µg/mL Penicillin and Streptomycin), the remaining tissue was cut into small pieces and digested for 30 min at 37 °C in pre-warmed alpha Minimum Essential Medium (MEM) (Lonza) containing 5% FBS, 100 µg/mL Penicillin and Streptomycin, 5 U/mL DNase (Roche), 1 mg/mL dispase (Gibco, ThermoFisher Scientific), 1.25 mg/mL Collagenase D (Roche) and 0.85 mg/mL Collagenase V (Sigma-Aldrich). For FACS sorting of tdTomato$^{pos}$ and tdTomato$^{neg}$ cells, tumors of AOM/DSS-treated mice were cut out and collected, while non-tumorous tissue was excluded. Naive and tumor tissues were enzymatically digested with 0.15 U/ml Liberase™ TH (Roche) and 0.15 mg/ml DNase (DN25, Sigma) in HBSS for 35 min at 37 °C in a shaking water bath. Independent of tumor origin, cells were then filtered through a 70-µm cell strainer (BD Falcon), washed with PBS, and stained with fluorophore-conjugated antibodies.

### FACS staining and analysis

Single-cell suspensions (obtained as described above) were incubated for 15 min with mouse FcR Blocking Reagent (1:100 BD Pharmingen) at 4 °C. Next, cells were stained for surface markers (see Supplementary Table 1 for antibodies list) and incubated for 20 min incubation at 4 °C. Then cells were washed with FACS buffer (0.5% FBS and 2 mM EDTA in PBS) and resuspended in FACS buffer containing the viability marker 7-AAD (1:100 BD Pharmingen) before filtering through a 70-µm strainer.

For the intracellular measurement of IL-1α and IL-1β, single-cell suspensions were pre-cultured in DMEM with 2.5% FBS, 100 µg/mL Penicillin and Streptomycin and stimulated with BD GolgiStop™ (1:1000, BD Biosciences) for 4 h in 5% $CO_2$ at 37 °C followed by a pre-incubation with the viability dye eFluor 506 (1:400 eBioscience) for 20 min at 4 °C. Then cell suspensions were washed, blocked with FcR Blocking Reagent (1:100 BD Pharmingen) and stained with surface antibodies (see Supplementary Table 1 for antibodies list) as described above. After a washing step with FACS buffer, cells were incubated for 45 min in Fix/Perm buffer (eBioscience, Invitrogen, ThermoFisher Scientific), followed by 5 min incubation in 1X Permeabilization buffer (eBioscience, Invitrogen, ThermoFisher Scientific). Next, the cells were stained for a minimum of 1 h in 1X Permeabilization buffer containing FcR Blocking Reagent (1:600 BD Pharmingen) and intracellular markers (see Supplementary Table 1 for antibody details). Cells were subsequently washed and resuspended in a Permeabilization buffer before filtering through a 70-µm strainer.

For cell counting goals, counting beads (1:100 Spherotech) were added per sample. Flow cytometry analyses were performed on a BD Symphony A5 Cell Analyzer (BD Biosciences) and subsequently analyzed using FlowJo v.10.6.1.

### FACS sorting of EGCs

FACS-sorting of tdTomato$^{pos}$ and tdTomato$^{neg}$ cells was performed on a BD FACSAria III cell sorter using BD FACSDiva 9.0.1 software (both BD Biosciences). A non-fluorescent sample was used as negative control to determine background fluorescence. Sorted cells were collected, centrifuged and pellets were snap frozen. RNA isolation was done using TRIzol™ reagent (Thermo Fisher Scientific) and the RNeasy Micro Kit (Qiagen) according to the manufacturers' instructions.

### Tumor-infiltrating monocyte sorting for EGCs stimulation

Tumor-infiltrating monocytes were sorted from orthotopic tumors based on the expression of the viability marker 7-AAD, CD45, CD64, Ly6C, MHCII, SiglecF and Ly6G (see Supplementary Table 1 for antibodies details) using a Sony MA9000 sorter. Next, $1 \times 10^5$ tumor or BM-derived monocytes were cultured in a complete DMEM medium overnight in 5% $CO_2$ at 37 °C. The conditioned medium of these monocytes was collected and used to stimulate primary embryonic neurosphere-derived EGCs ($5 \times 10^4$ cells/mL) in the presence of 5 µg/mL IgG (BioXCell) or 5 µg/mL anti-IL-1R (BioXCell) for 24 h in 5% $CO_2$ at 37 °C.

### RNA extraction and gene expression

RNA was isolated using the innuPREP RNA Mini Kit (Analytik Jena) or RNeasy Mini Kit (Qiagen) for tissue and high cell numbers or RNeasy Plus Micro Kit (Qiagen) for low cell numbers according to the manufacturer's instructions. Dependent on RNA concentrations, total RNA was transcribed into cDNA by the qScript™ cDNA SuperMix (QiantaBio) or the High-Capacity cDNA Reverse Transcription Kit (ThermoFisher Scientific) according to manufacturer's instructions. qRT-PCR was performed with the LightCycler 480 SYBR Green I Master (Roche) on the Light Cycler 480 (Roche) or with the PowerSYBR Green PCR

Master Mix (Thermo Fisher Scientific) on the QuantStudio5 cycler (Thermo Fisher Scientific) (primers listed in Supplementary Table 2). Results were quantified using the $2^{-\Delta Ct}$ method or were applicable to the $2^{-\Delta\Delta Ct}$ method, usage stated by "relative to". The expression levels of the genes of interest were normalized to the expression levels of the reference gene *Rpl32*.

### Bulk RNA sequencing

For Bulk RNA-seq of the in vitro tumor EGCs model, total RNA from in vitro generated unstimulated, H-CM and TME-CM primary embryonic neurosphere-derived EGCs was provided to the Genomics core (KU Leuven). QuantSeq 3′ mRNA libraryprep (015, Lexogen) was used to generate cDNA libraries, followed by sequencing on the HiSeq4000 system. Quality control of raw reads was performed with FastQC v0.11.7 (Andrews S. FastQC: a quality control tool for high throughput sequence data. Available online at: http://www.bioinformatics.babraham.ac.uk/projects/fastqc, 2010.). Adapters were filtered with ea-utils fastq-mcf v1.05 (Erik Aronesty. ea-utils: Command-line tools for processing biological sequencing data. Available online at: https://github.com/ExpressionAnalysis/ea-utils, 2011.). Splice-aware alignment was performed with HISAT2[62] against the reference genome mm10 using the default parameters. Reads mapping to multiple loci in the reference genome were discarded. Resulting BAM alignment files were handled with Samtools v1.5[63]. Quantification of reads per gene was performed with HT-seq Count v0.10.0, Python v2.7.14[64]. Count-based differential expression analysis was done with R-based (The R Foundation for Statistical Computing, Vienna, Austria) Bioconductor package DESeq2[65]. Reported *p* values were adjusted for multiple testing with the Benjamini-Hochberg procedure, which controls FDR. Data visualization was prepared using ggplot2 R package (v3.4.1) or pheatmap (v1.0.12).

For 3′mRNA sequencing of naive and AOM/DSS-treated mice, isolated RNA was provided to the Genomics Core Facility of the University Hospital Bonn, which performed library preparation using QuantSeq FWD 3′mRNA-Seq kit (Lexogen) according to the manufacturer's instructions. Sequencing was performed on the NovaSeq6000 with a sequencing depth of 10 M raw reads. Data were analyzed using PartekFlow software (V10.0.23.0720) available from https://www.partek.com/partek-flow/#features with the Lexogen12112017 pipeline and Ensemble transcripts release 102 for mm10 mouse alignment. Briefly, two adapter-trimming steps and one base-trimming step were performed before alignment was done by star2.5.3a. Post-alignment QC was performed and reads were quantified to the annotation model. Gene counts were normalized and data were further analyzed by gene-specific analysis. Visualization was done with PartekFlow software (V10.0.23.0720) and GraphPad Prism 6 (V6.07).

To quantify the transcripts per million (TPM) values from the bulk RNA-seq data of adult derived EGCs (previously published in refs. 15,17, PartekFlow software (V10.0.23.0720) available from https://www.partek.com/partek-flow/#features. The TPM values for bulk RNA-seq of embryonic neurosphere-derived EGCs were obtained by processing fastq files using nf-core/rnaseq pipeline (nf-co.re/rnaseq/3.12.0) where GRCh37 was used as reference genome and Salmon was used for quantification[66].

### Weighted gene correlation network analysis (WGCNA)

First, variance stabilizing transformation was performed on the bulk RNA-seq data generated from unstimulated, H-CM and TME-CM primary neurosphere-derived EGCs using the DESeq2[65] package in R (v4.2.2). PCA was performed after variance stabilizing transformation using DeSeq2 package by selecting samples stimulated for 24 h. The function prcomp() was used for obtaining the gene strength towards each PC. Next, WGCNA[67] was performed using the R package WGCNA (v1.72.1). To distinguish the modules with different expression patterns, a soft threshold power of 12, which was the lowest power for the scale-free topology fit index of 0.85, was selected to produce a hierarchical clustering tree (dendrogram). The function "blockwiseModules" was used for automatic block-wise network construction and module identification. The number of modules was detected automatically by the algorithm, with the number of genes in a module limited to between 30 and 5000 genes. The co-expression networks were created based on the similarity of expression patterns of genes and the networks were established by merging genes with similar co-expression patterns into modules. The clusterProfiler[68] package was used to implement enrichGO() for gene ontology over-representation test using the genes of modules 4, 7, and 8.

### Single-cell RNA sequencing of orthotopic murine tumors

Cell suspensions of orthotopic murine tumors were processed with a 10x Chromium Next GEM Single Cell 5′ kit and loaded on a 10x chromium controller to create Single Cell Gel beads in Emulsion (GEM). A cDNA library was created using a 10 × 5′ library kit and was then paired-end sequenced on an Illumina Novaseq device following 10x's guidelines (https://www.10xgenomics.com/support/single-cell-immune-profiling/documentation/steps/sequencing/sequencing-requirements-for-single-cell-v-d-j). Sample demultiplexing and data analysis was performed using 10x's Cellranger suite (https://support.10xgenomics.com/single-cell-vdj/software/pipelines/latest/using/vdj) using the standard parameters.

### scRNA-seq clustering and dimensionality reduction

The count matrices obtained after pre-processing with Cellranger were concatenated to obtain a combined raw count matrix which was then analyzed using the Seurat R package (v3.1.3). Cells with less than 300 or more than 6000 genes and cells with more than 15% mitochondrial genes were discarded from the analysis. Normalization and scaling were done with default variables with top variable genes identified using FindVariableFeatures function. After principal component analysis, 1st 39 principal components were used based on the elbow plot for creating a nearest neighbor graph using FindNeighbours function in Seurat. After clustering at a resolution of 1, clusters were classified into immune and non-immune clusters. Six small doublet clusters with markers of two or more distinct cell types were removed. Also, two clusters with low nUMI and lacking distinguishing markers of any cell types were removed. A subset of Seurat Object with immune clusters alone was created and the same pipeline was followed from Normalization to Clustering (number of principal components used = 32). After clustering at resolution 1, the clusters were manually annotated following Zhang et al.[24]. Clusters annotated as monocytes or macrophages were re-clustered similarly to identify the subclusters. These sub-clusters were annotated manually based on the expression of Ly6c2, Ccr2, H2-Ab1, Spp1, C1qa, Cx3cr1, and Mki67. Further to learn potential differentiation trajectory, Monocle-3 was used. (Parameters: *n* center = 300, minimal branch length = 10, nn.k = 20). Genes upregulated or downregulated in $SPP1^+$ TAMs compared to $C1Q^+$ TAMs were functionally annotated using universal enrichment function "enricher" from the "ClusterProfiler" package (v4.6.0) with a gene annotation database aggregation containing all terms from Human Phenotype, Transcription factor, and Hallmark from Molecular Signature Database (MSigDB), BIOCARTA, REACTOME, GO and KEGG Markers for different clusters were determined using a Wilcoxon rank sum test with FindMarkers or FindAllMarkers functions in Seurat.

### Inferring cell–cell communication using NicheNet

NicheNet (nichenetr R package; v1.1.0) was used to study the interactions between EGCs and tumor-infiltrating monocytes. To identify TME EGC-derived ligands potentially inducing the differentiation of monocytes into $SPP1^+$ TAMs, bulk RNA-seq data from in vitro TME-CM EGCs was used. Ligands were identified after filtering for genes upregulated in 24 h time point TME-CM EGCs with respect to 24 h

timepoint H-CM EGCs (adjusted $p$ value < 0.05). Genes differentially expressed between SPP1$^{+}$ TAMs and monocytes (adjusted $p$ value < 0.05) were considered as the gene set of interest.

NicheNet was also used to study the interaction between tumor-infiltrating immune cells and EGCs. To identify immune cell-derived ligands potentially inducing differentiation of 24 h time point H-CM EGCs into 24 h time point TME-CM EGCs, scRNA-seq data of the immune compartment of the in vivo murine orthotopic CRC model was used. Using get_expressed_genes function from NichenetR, genes expressed in at least 5 % of immune cell clusters were considered as potential ligands. Genes differentially expressed between TME-CM EGCs and H-CM EGCs (adjusted $p$ value < 0.001) were considered as the gene set of interest.

### Bio-informatic analysis: KUL3 dataset

Bio-informatic analysis of the CRC tumor microenvironment of patients with CRC was performed making use of the published KUL3 dataset[33]. Integration of the data, dimensionality reduction, unsupervised clustering and differential gene expression analysis was performed in R using Seurat with SCTransform - Integration pipeline. For downstream analysis, "border" and "tumor" samples were taken together and considered as tumor samples. Patient KUL31 was excluded from all EGCs analysis, due to extremely low cell numbers. Pathway enrichment analysis was done using Ingenuity pathway Analysis (IPA, Qiagen). Modules identified using WGCNA on mouse bulk RNA-seq data was converted to one-to-one human orthologs and then used for single-sample Gene Set Enrichment Analysis GSEA as implemented in single-cell Gene Set Variation Analysis R package (v0.0.11).

### Bio-informatic analysis: TCGA and LUMC AC-ICAM dataset

The processed gene expression RNA-seq (IlluminaHiSeq) data of the Cancer Genome Atlas (TCGA) colorectal adenocarcinoma (COAD-READ) was downloaded from the University of California SantaCruz (UCSC) Xena using the UCSCXenaTools (https://doi.org/10.21105/joss.01627) R library. The details of data integration and processing are described in UCSC-Xena browser (https://xenabrowser.net/). The clinical information and overall survival (OS) data of the patients were also obtained using UCSCXenaTools (data subtype: "phenotype"). According to their age, the patients were classified as above 65 years (>=65) and below 65 years. Patients with tumor stage I and IA were clustered as stage I, patients with stage II, IIA, IIB as stage II, patients with stage III, IIIA, IIIB, IIIC as stage III, and patients with stage IV, IVA, IVB as stage IV. Patients with microsatellite stability were classified as MSS and patients with microsatellite instability high and low as MSI. The consensus molecular subtypes (CMS) were predicted using the R package CMSClassifier (v1.0.0) and the iCMS classification of the patients was performed as previously described[69]. The 376 patients with CRC were hierarchically clustered according to the high and low expression patterns of the specific gene signatures (Supplementary Table 3) in the tumor samples which resulted in 2 patient categories (EGC high and EGC low). The R packages survival (v3.5.5) and survminer (v0.4.9) were used for survival analysis and plotting the Kaplan-Meier (KM) survival curve. A statistically significant difference in survival was indicated by a log-rank test p-value of $p < 0.05$. Survival analysis with univariate and multivariate proportional hazards regression models (Cox regression) was performed to adjust for age, gender, radiation therapy, stage and EGC signature expression. The R packages pheatmap, gtsummary, and ggplot2 were used for visualization.

The second CRC cohort used was the Sidra-LUMC AC-ICAM dataset, published by Roelands et al.[35]. The 348 patients were hierarchically clustered and survival analysis was performed as described above.

### Reporting summary

Further information on research design is available in the Nature Portfolio Reporting Summary linked to this article.

## Data availability

The scRNA-seq (related to Fig. 3 and Supplementary Fig. 4) and bulk RNA-seq (related to Fig. 2 and Supplementary Fig. 3 and 5b) data generated for this study are deposited in the Gene Expression Omnibus (GEO) database under the GEO accession code GSE231804. The bulk RNA-seq (related to Supplementary Fig. 6), data generated for this study are deposited in the Gene Expression Omnibus (GEO) database under the GEO accession code GSE231709. The mass spectrometry proteomics data generated for this study (related to Fig. 4) have been deposited to the ProteomeXchange Consortium via the PRIDE partner repository with the dataset identifier PXD045911. Bulk RNA-seq data (related to Supplementary Fig 5b) were published previously[15,17] and can be accessed via GSE205610 and GSE134943. The remaining data are available within the Article, Supplementary Information or Source Data file. Source data are provided in this paper.

## References


1. Kuipers, E. J. et al. Colorectal cancer. *Nat. Rev. Dis. Prim.* **1**, 1–25 (2015).
2. AlMusawi, S., Ahmed, M. & Nateri, A. S. Understanding cell-cell communication and signaling in the colorectal cancer microenvironment. *Clin. Transl. Med.* **11**, e308 (2021).
3. Albo, D. et al. Neurogenesis in colorectal cancer is a marker of aggressive tumor behavior and poor outcomes. *Cancer* **117**, 4834–4845 (2011).
4. Valès, S. et al. Tumor cells hijack enteric glia to activate colon cancer stem cells and stimulate tumorigenesis. *EBioMedicine* **49**, 172–188 (2019).
5. Yuan, R. et al. Enteric glia play a critical role in promoting the development of colorectal cancer. *Front. Oncol.* **10**, 1–12 (2020).
6. Neunlist, M. et al. Enteric glial cells: Recent developments and future directions. *Gastroenterology* **147**, 1230–1237 (2014).
7. Seguella, L. & Gulbransen, B. D. Enteric glial biology, intercellular signalling and roles in gastrointestinal disease. *Nat. Rev. Gastroenterol. Hepatol.* **18**, 571–587 (2021).
8. Thomasi, B. & Gulbransen, B. Mini-review: Intercellular communication between enteric glia and neurons. *Neurosci. Lett.* **806**, 137263 (2023).
9. Prochera, A. & Rao, M. Mini-Review: Enteric glial regulation of the gastrointestinal epithelium. *Neurosci. Lett.* **805**, 137215 (2023).
10. Bohórquez, D. V. et al. An enteroendocrine cell - Enteric glia connection revealed by 3D electron microscopy. *PLoS One* **9**, e89881 (2014).
11. Ibiza, S. et al. Glial-cell-derived neuroregulators control type 3 innate lymphoid cells and gut defence. *Nature* **535**, 440–443 (2016).
12. Progatzky, F. et al. Regulation of intestinal immunity and tissue repair by enteric glia. *Nature* **599**, 125–130 (2021).
13. Grubišić, V. et al. Enteric glia modulate macrophage phenotype and visceral sensitivity following inflammation. *Cell Rep.* **32**, 108100 (2020).
14. Grubišić, V. et al. Enteric glial adenosine 2B receptor signaling mediates persistent epithelial barrier dysfunction following acute DSS colitis. *Mucosal Immunol.* **15**, 964–976 (2022).
15. Schneider, R. et al. A novel P2X2-dependent purinergic mechanism of enteric gliosis in intestinal inflammation. *EMBO Mol. Med.* **13**, 1–20 (2021).
16. Brown, I. A. M., McClain, J. L., Watson, R. E., Patel, B. A. & Gulbransen, B. D. Enteric glia mediate neuron death in colitis through purinergic pathways that require connexin-43 and nitric oxide. *Cmgh* **2**, 77–91 (2016).

17. Schneider, R. et al. IL-1-dependent enteric gliosis guides intestinal inflammation and dysmotility and modulates macrophage function. *Commun. Biol.* **5**, 1–16 (2022).
18. Rosenbaum, C. et al. Activation of myenteric glia during acute inflammation in vitro and in vivo. *PLoS One* **11**, 1–20 (2016).
19. Stakenborg, M. et al. Enteric glial cells favor accumulation of anti-inflammatory macrophages during the resolution of muscularis inflammation. *Mucosal Immunol.* **15**, 1296–1308 (2022).
20. Zigmond, E. et al. Utilization of murine colonoscopy for orthotopic implantation of colorectal cancer. *PLoS One* **6**, 1–7 (2011).
21. Clarke, L. E. et al. Normal aging induces A1-like astrocyte reactivity. *Proc. Natl Acad. Sci. USA* **115**, E1896–E1905 (2018).
22. Drokhlyansky, E. et al. The human and mouse enteric nervous system at single-cell resolution. *Cell* **182**, 1606–1622 (2020).
23. Baghdadi, M. B. et al. Enteric glial cell heterogeneity regulates intestinal stem cell niches. *Cell Stem Cell* **29**, 1–15 (2021).
24. Zhang, L. et al. Single-cell analyses inform mechanisms of myeloid-targeted therapies in colon cancer. *Cell* **181**, 442–459 (2020).
25. Matusiak, M. et al. Spatially segregated macrophage populations predict distinct outcomes in colon cancer authors. *Cancer Discov.* https://doi.org/10.1158/2159-8290.CD-23-1300 (2024).
26. Browaeys, R., Saelens, W. & Saeys, Y. NicheNet: modeling intercellular communication by linking ligands to target genes. *Nat. Methods* **17**, 159–162 (2020).
27. Afik, R. et al. Tumor macrophages are pivotal constructors of tumor collagenous matrix. *J. Exp. Med.* **213**, 2315–2331 (2016).
28. Borràs, D. M. et al. Single cell dynamics of tumor specificity vs bystander activity in CD8+ T cells define the diverse immune landscapes in colorectal cancer. *Cell Discov.* **9**, 114 (2023).
29. Jackstadt, R. et al. Epithelial NOTCH signaling rewires the tumor microenvironment of colorectal cancer to drive poor-prognosis subtypes and metastasis. *Cancer Cell* **36**, 319–336.e7 (2019).
30. Efremova, M. et al. Targeting immune checkpoints potentiates immunoediting and changes the dynamics of tumor evolution. *Nat. Commun.* **9**, 32 (2018).
31. Beach, C. et al. Improving radiotherapy in immunosuppressive microenvironments by targeting complement receptor C5aR1. *J. Clin. Investig.* **133**, e168277 (2023).
32. Parang, B., Barret, C. W. & Williams, C. S. AOM/DSS model of colitis-associated cancer. *Methods Mol. Biol.* **1422**, 297–307 (2016).
33. Lee, H. O. et al. Lineage-dependent gene expression programs influence the immune landscape of colorectal cancer. *Nat. Genet.* **52**, 594–603 (2020).
34. Kinchen, J. et al. Structural remodeling of the human colonic mesenchyme in inflammatory bowel disease. *Cell* **175**, 372–386 (2018).
35. Roelands, J. et al. An integrated tumor, immune and microbiome atlas of colon cancer. *Nat. Med.* **29**, 1273–1286 (2023).
36. Guinney, J. et al. The consensus molecular subtypes of colorectal cancer. *Nat. Med.* **21**, 1350–1356 (2015).
37. Stoffels, B. et al. Postoperative ileus involves interleukin-1 receptor signaling in enteric glia. *Gastroenterology* **146**, 176–187 (2014).
38. Grivennikov, S. I. & Karin, M. Inflammatory cytokines in cancer: Tumour necrosis factor and interleukin 6 take the stage. *Ann. Rheum. Dis.* **70**, i104–i108 (2011).
39. Qi, J. et al. Single-cell and spatial analysis reveal interaction of FAP+ fibroblasts and SPP1+ macrophages in colorectal cancer. *Nat. Commun.* **13**, 1742 (2022).
40. Luo, H. et al. Pan-cancer single-cell analysis reveals the heterogeneity and plasticity of cancer- associated fibroblasts in the tumor microenvironment. *Nat. Commun.* **13**, 6619 (2022).
41. Cheng, S. et al. A pan-cancer single-cell transcriptional atlas of tumor infiltrating myeloid cells. *Cell* **184**, 792–809 (2021).
42. Komoda, H. et al. Interleukin-6 levels in colorectal cancer tissues. *World J. Surg.* **22**, 895–898 (1998).
43. Galizia, G. et al. Prognostic significance of circulating IL-10 and IL-6 serum levels in colon cancer patients undergoing surgery. *Clin. Immunol.* **102**, 169–178 (2002).
44. Magnon, C. et al. Autonomic nerve development contributes to prostate cancer progression. *Science* **341**, 1236361 (2013).
45. Albergotti, W. G. et al. Defining the prevalence and prognostic value of perineural invasion and angiolymphatic invasion in human papillomavirus-positive oropharyngeal carcinoma. *JAMA Otolaryngol. Head. Neck Surg.* **143**, 1236–1243 (2017).
46. Hayakawa, Y. et al. Nerve growth factor promotes gastric tumorigenesis through aberrant cholinergic signaling. *Cancer Cell* **31**, 21–34 (2017).
47. Renz, B. W. et al. β2 Adrenergic-neurotrophin feedforward loop promotes pancreatic cancer. *Cancer Cell* **33**, 75–90 (2018).
48. Deborde, S. et al. Reprogrammed Schwann cells organize into dynamic tracks that promote pancreatic cancer invasion. *Cancer Discov.* **12**, 2454–2473 (2022).
49. Zhou, Y., Li, J., Han, B., Zhong, R. & Zhong, H. Schwann cells promote lung cancer proliferation by promoting the M2 polarization of macrophages. *Cell. Immunol.* **357**, 104211 (2020).
50. Shurin, G. V. et al. Melanoma-induced reprogramming of Schwann cell signaling aids tumor growth. *Cancer Res.* **79**, 2736–2747 (2019).
51. Laranjeira, C. et al. Glial cells in the mouse enteric nervous system can undergo neurogenesis in response to injury. *J. Clin. Investig.* **121**, 3412–3424 (2011).
52. Quintana, A. et al. Astrocyte-specific deficiency of interleukin-6 and its receptor reveal specific roles in survival, body weight and behavior. *Brain Behav. Immun.* **27**, 162–173 (2013).
53. Corbett, T. H., Griswold, D. P., Roberts, B. J., Peckham, J. C. & Schabel, F. M. Tumor induction relationships in development of transplantable cancers of the colon in mice for chemotherapy assays, with a note on carcinogen structure. *Cancer Res.* **35**, 2434–2439 (1975).
54. Parang, B., Barrett, C. W. & Williams, C. S. AOM/DSS model of colitis-associated cancer. *Methods Mol. Biol.* **1422**, 297–307 (2016).
55. Pombo Antunes, A. R. et al. Single-cell profiling of myeloid cells in glioblastoma across species and disease stage reveals macrophage competition and specialization. *Nat. Neurosci.* **24**, 595–610 (2021).
56. Bosisio, F. M. et al. Functional heterogeneity of lymphocytic patterns in primary melanoma dissected through single-cell multiplexing. *Elife* **9**, 1–28 (2020).
57. Naulaerts, S. et al. Multiomics and spatial mapping characterizes human CD8+ T cell states in cancer. *Sci. Transl. Med.* **15**, eadd1016 (2023).
58. Wüst, H. M. et al. Egr2-guided histone H2B monoubiquitination is required for peripheral nervous system myelination. *Nucleic Acids Res.* **48**, 8959–8976 (2020).
59. Mellacheruvu, D. et al. The CRAPome: a contaminant repository for affinity purification-mass spectrometry data. *Nat. Methods* **10**, 730–736 (2013).
60. The, M., MacCoss, M. J., Noble, W. S. & Käll, L. Fast and accurate protein false discovery rates on large-scale proteomics data sets with percolator 3.0. *J. Am. Soc. Mass Spectrom.* **27**, 1719–1727 (2016).
61. Ritchie, M. E. et al. Limma powers differential expression analyses for RNA-sequencing and microarray studies. *Nucleic Acids Res.* **43**, e47 (2015).
62. Kim, D., Paggi, J. M., Park, C., Bennett, C. & Salzberg, S. L. Graph-based genome alignment and genotyping with HISAT2 and HISAT-genotype. *Nat. Biotechnol.* **37**, 907–915 (2019).
63. Li, H. et al. The sequence alignment/map format and SAMtools. *Bioinformatics* **25**, 2078–2079 (2009).
64. Anders, S., Pyl, P. T. & Huber, W. HTSeq-A Python framework to work with high-throughput sequencing data. *Bioinformatics* **31**, 166–169 (2015).

65. Love, M. I., Huber, W. & Anders, S. Moderated estimation of fold change and dispersion for RNA-seq data with DESeq2. *Genome Biol.* **15**, 1–21 (2014).
66. Ewels, P. A. et al. The nf-core framework for community-curated bioinformatics pipelines. *Nat. Biotechnol.* **38**, 271–278 (2020).
67. Langfelder, P. & Horvath, S. WGCNA: an R package for weighted correlation network analysis. *BMC Bioinforma.* **9**, 1–13 (2008).
68. Yu, G., Wang, L. G., Han, Y. & He, Q. Y. ClusterProfiler: an R package for comparing biological themes among gene clusters. *OMICS J. Integr. Biol.* **16**, 284–287 (2012).
69. Joanito, I. et al. Single-cell and bulk transcriptome sequencing identifies two epithelial tumor cell states and refines the consensus molecular classification of colorectal cancer. *Nat. Genet.* **54**, 963–975 (2022).

## Acknowledgements

We acknowledge all members of Prof. Matteoli's laboratory and Prof. Wehner's laboratory for the support and scientific discussions. We would like to thank Tine Gomers and Karlien Vranken (TARGID, KU Leuven) and Patrik Efferz and Bianca Schneiker (Department of Surgery, University Hospital Bonn) for technical assistance during experiments. Furthermore, we would like to thank Ally Peddle and Yourae Hong (Molecular Digestive Oncology, Department, KU Leuven), Lukas Ferreira Maciel (Laboratory for Molecular Cancer Biology, VIB-KU Leuven) and Florent Petitprez (MRC Centre for Reproductive Health, University of Edinburgh) for their scientific support on bio-informatic analysis. Within KU Leuven we would like to acknowledge the following core facilities: FACS Core, Genomics Core (UZ Leuven), LiMoNe VIB Bioimaging Core and VIB Center for Brain & Disease Research. We would like to thank the Cell and Tissue Imaging Cluster (KU Leuven) for the usage of the Zeiss LSM 880 – Airyscan (supported by Hercules AKUL/15/ 37_GOH1816N and FWO G.0929.15 to Prof. Pieter Vanden Berghe). We would like to thank the support from the Core Facilities of the Medical Faculty, University of Bonn, specifically, the Analytical Proteomics Core, funded by the Deutsche Forschungsgemeinschaft (DFG)—project 386936527, the Bioinformatics Data Analysis Core, the Microscopy Core funded by the DFG – project 266686698, the Flow Cytometry Core funded by the DFG —project 216372545, and the Next Generation Sequencing Core. We thank Dr. Vassilis Pachnis for sharing the SOX10$^{CreERT2}$ mice, Prof. Juan Hidalgo for sharing the IL-6$^{fl/fl}$ mice and Prof. Michael Wegner for sharing the Sox10 antibody. Figures 1a, 1b, 1e, 2a, 3e, 3g, 3j, 4a, 4d, 4f, 5a, 5c, 6a, 6e, 6h, 7a, S1f, S1o, created with BioRender.com, released under a Creative Commons Attribution-NonCommercial-NoDerivs 4.0 International license. We would like to acknowledge Prof. Owen Sansom for providing us with the AKPT CRC cell lines. V.D.S. was supported by a Stichting Tegen Kanker postdoctoral fellowship. S.S. was supported by KU Leuven-University of Melbourne Global PhD (GPUM/22/020). F.B. was supported by KU LEUVEN INTERNAL FUNDS KU Leuven Global PhD Partnerships with the University of Edinburgh (GPUE/20/003). B.K. was supported by the Taiwan - KU Leuven PhD Scholarship. M.V. was supported by a Fonds voor Wetenschappelijk Onderzoek Vlaanderen (FWO, 11L0822N) PhD fellowship. G.B. is funded by ERC Advanced grant no. 833816-NEUMACS. S.I. was supported by an MSCA-IF (79756–GLIAMAC) and a fellowship from the European Crohn's and Colitis Organization (ECCO). S.V. and S.T. were supported by the FWO grant G067821N and Stichting tegen Kanker grant F/2020/1512. Research in ADG lab is supported by Research Foundation Flanders (FWO) (Fundamental Research Grant, G0B4620N), KU Leuven (C3 grant, C3/21/037 or C3/23/067), and VLIR-UOS (iBOF grant, iBOF/21/048, for 'MIMICRY' consortium). R.S.L. is supported by FWO-SB PhD Fellowship (1S44123N). G.M.'s lab was supported by FWO grants G0D8317N, G0A7919N, G086721N, G088816N, S008419N and W001620N, KU Leuven Internal Funds (C12/15/016 and C14/17/097). S.W. and L.S. were supported by the DFG-funded Immunosensation$^2$ cluster of excellence EXC2151-190873048. S.W. and R.S. received funding from BONFOR. B.G.R. received funding from the Deutsche Krebshilfe through a Mildred Scheel Nachwuchszentrum Grant (70113307).

## Author contributions

Conceptualization, L.V.B., V.D.S., L.S., R.S., S.W. and G.M.; Methodology, L.V.B., V.D.S., L.S., S.W. and G.M.; Software, S.S., S.A., Z.H., J.H., L.V.B. and L.S.; Validation, L.V.B., V.D.S. and L.S.; Formal Analysis, L.V.B., V.D.S., L.S., S.S. and S.A.; Investigation, L.V.B., V.D.S., L.S., S.S., S.A., F.B., L.Z., S.V., B.K., B.G.R., M.T., M.V., R.S.D.M., N.S., R.S.L. and S.I.; Resources, G.M., S.W., S.T., G.B, A.D.G. and F.D.S.; Data Curation, L.V.B., V.D.S., L.S., S.S., S.A., S.V., Z.H. and J.H.; Writing—original draft, L.V.B., V.D.S. and L.S.; Writing—review & editing, all; Visualization, L.V.B., V.D.S., L.S., S.S., S.A., and Z.H.; Supervision, G.M., S.W., S.T., F.D.S., R.S., M.S. and V.D.S.; Project administration, L.V.B., V.D.S., L.S., R.S., S.W. and G.M.; Funding acquisition, V.D.S., S.I., G.M. and S.W.

## Competing interests

The authors declare no competing interests.

## Additional information

**Supplementary information** The online version contains supplementary material available at https://doi.org/10.1038/s41467-024-50438-2.

**Correspondence** and requests for materials should be addressed to Sven Wehner or Gianluca Matteoli.

**Peer review information** *Nature Communications* thanks the anonymous reviewer(s) for their contribution to the peer review of this work. A peer review file is available.

[1]Laboratory of Mucosal Immunology, Department of Chronic Diseases and Metabolism (CHROMETA), Translational Research Center for Gastrointestinal Disorders (TARGID), KU Leuven, Leuven, Belgium. [2]Department of Surgery, University Hospital Bonn, Medical Faculty, Bonn, Germany. [3]Department of Anatomy and Physiology, University of Melbourne, Parkville, VIC, Australia. [4]Centre for Inflammation Research, University of Edinburgh, Edinburgh, UK. [5]Department of Biology and Biotechnology "L. Spallanzani", University of Pavia, Pavia, Italy. [6]Digestive Oncology, Department of Oncology, KU Leuven, Leuven, Belgium. [7]Laboratory for Intestinal Neuro-Immune Interaction, Department of Chronic Diseases and Metabolism (CHROMETA), Translational Research Center for Gastrointestinal Disorders (TARGID), KU Leuven, Leuven, Belgium. [8]Cell Stress and Immunity (CSI) Lab, Department of Cellular and Molecular Medicine, KU Leuven, Leuven, Belgium. [9]Mildred Scheel School of Oncology, Aachen Bonn Cologne Düsseldorf (MSSO ABCD), University Hospital Bonn, Medical Faculty, Bonn, Germany. [10]Department of Pathology, University Hospital Bonn, Medical Faculty, Bonn, Germany. [11]Translational Cell and Tissue Research Unit, Department of Imaging & Pathology, Laboratory for Precision Cancer Medicine, KU Leuven, Leuven, Belgium. [12]Leuven Institute for Single-Cell Omics (LISCO), KU Leuven, Leuven, Belgium. [13]Laboratory of Cell Biology & Histology, Department of Veterinary Sciences, University of Antwerp, Antwerp, Belgium. [14]These authors contributed equally: Lies van Baarle, Veronica De Simone, Linda Schneider. [15]These authors jointly supervised this work: Sven Wehner, Gianluca Matteoli. ✉e-mail: sven.wehner@ukbonn.de; gianluca.matteoli@kuleuven.be

# 4. Discussion

Over the past two decades, the focus on EGCs and unraveling their role in intestinal homeostasis and disease has risen. Several studies already identified EGCs as important mediators of intestinal inflammation and their active contribution to disease outcomes through the secretion of cytokines and chemokines as well as their interaction with other cells [1]. My thesis advanced the current knowledge about EGCs by identifying novel molecular pathways of glial homeostasis and activation involving the ECM [2], adrenergic signaling [3], and IL-1 signaling [4, 5]. Utilizing *in vitro* studies, we optimized EGC primary cultures and identified Matrigel and laminin as superior coating substrates to advance enteric glial yield, network formation, and immune reactivity [2]. Furthermore, we used our glial culture system and the postoperative gut inflammation model of POI to define the role of adrenergic [3] and IL-1-mediated [4] activation of EGCs during acute inflammation of the *musclaris externa*. Finally, we studied the role of reactive EGCs in CRC development [5]. Thereby, we unraveled a pro-tumorigenic reactive glial phenotype in CRC and a bidirectional signaling cascade between EGCs and macrophages that drives disease progression [5].

## 4.1 Activation of EGCs in acute intestinal inflammation

Previously, our group and others identified several inducers of enteric glial reactivity in acute intestinal inflammation [6–10], with the first evidence of molecular interactions being derived from *in vitro* studies. EGC primary cultures are a valuable tool widely used to study the interplay of EGCs with other cell types or their distinct reaction to specific molecular stimuli. However, the culture conditions differ strongly between groups, varying in isolation protocols, media composition, or cell culture coating substrates. Surface coating, used to facilitate cell adhesion, is usually done with proteins that naturally occur in the cells' ECM. However, the ECM also serves as an important regulator of cellular properties in the intestine, as shown for monocyte differentiation [11], transmigration [12], or immunosuppression [13]. Therefore, we speculated on the involvement of ECM substrates in glial reactivity. Notably, comparing different ECMs to improve EGC culture purity and quality is not new. Previous studies showed that laminin promotes the expression of glial markers over neuronal markers in ENS cultures [14] and identified the differentiation-driving

effects of ECM substrates on ENS progenitors *in vitro* [15]. However, none of these studies addressed the impact of ECM substrates on potential changes in glial network formation and the immune response and reactivity of EGCs. In our work, we demonstrated Matrigel and laminin as superior coating substrates in EGC purity and network formation and investigated the differential influence of ECM compounds on glial reactivity after IL-1β treatment [2], a stimulus well-known in glial activation [4, 16]. When looking at the IL-1β-induced gene expression, pathways related to myeloid differentiation and macrophage activation were induced in glia on Matrigel and laminin. This aligns with the herein-characterized glia-macrophage interactions after IL-1β stimulus [4, 5]. Furthermore, previous works described the close proximity of EGCs and macrophages [17] and a glial-induced differentiation of the latter [16], hinting at a bidirectional communication of those cell types. Conversely, poly-L-ornithine coating resulted in GO term enrichment related to lymphocytes in EGC cultures. While interactions between EGCs and lymphocytes are mostly unexplored, a few studies have suggested T cell-EGC interactions in Crohn's disease [18], EGC-mediated T cell activation via antigen presentation [19], or EGC-mediated control of cytokine release by innate lymphoid cell type 3 [20]. Nevertheless, the changes in glial immune function, at least on the transcriptional level, were less pronounced than the effects of ECM substrates on cell numbers and network formation capacity. On this base, we identified Matrigel and laminin as superior coatings, which we will use in future EGC *in vitro* studies. A shortcoming of this study is the lack of double-coatings, which other studies have already used for ENS cultures [14, 21–23]. As Matrigel, similar to the ECM *in vivo*, is a mixture of ECM proteins, including laminin, collagen IV, and entactin [24], it is likely that combinatorial coating approaches might further advance EGC network formation and reactivity. Additionally, we did not address the ECM protein agrin, which was recently described as part of a specific ECM composition surrounding enteric ganglia and implicated to be important in intestinal inflammation and neural cell migration [17, 25]. Future work is needed to decipher the effect of ECM molecules on glial-immune interactions *in vivo*.

While *in vitro* cell culture models greatly help to get mechanistic insight into cellular functions, *in vivo* models are necessary to study the role of EGC reactivity in the context of inflammation-driven diseases and disorders. A common *in vivo* model to study acute intestinal inflammation is the model of small bowel manipulation. Sterile manipulation of

the intestine, mimicking the surgeons' handling and surgical trauma to the gut surface, results in acute inflammation of the *tunica muscularis*, which finally results in transient motility disturbances [26], clinically known as POI [27]. In a previous study, our group investigated the transcriptional changes of EGCs during those inflammatory processes and introduced the term "enteric gliosis", a reactive enteric glial phenotype [6] identifying EGCs as important contributors to disease outcomes. Continuing to analyze the enteric glial tissue microenvironment as a potential inducer of glial reactivity, we next focused on mediators of the SNS, known to control homeostasis and inflammatory conditions. Therein, neurotransmitters of the SNS can bind to adrenergic receptors (AR) on EGCs [28, 29]. Additionally, the SNS has recently been shown to influence immune cell infiltration into the muscle layer of the intestine [30]. However, the direct effect of adrenergic activation of EGCs on intestinal inflammation was unknown. In our recent work, we performed a time course analysis using glial-specific transcriptomes [31] at different time points during POI. Thereby, SNS-mediated glial activation was identified as an early trigger during intestinal trauma, already induced by the first surgical skin incision and even more pronounced by intestinal manipulation [3]. We demonstrated that the neurotransmitter norepinephrine (NE) induces glial reactivity and pinpointed adrenergic signaling via β1- or β2-ARs, or both, as responsible for NE-induced glial activation *in vitro*. Of note, an immunomodulatory function of adrenergic pathways has been described before: NE is already known to regulate motility [32] and immune responses of a variety of immune cells in the gut [33], which express the β2-ARs [34], too. Interestingly, NE has rather anti-inflammatory effects on immune cells [35], while here, we found proinflammatory cytokine release by EGCs activated via the same mechanism. However, since the direct impact of NE on EGCs was tested *in vitro*, we can only speculate on its influence on disease outcomes *in vivo*. Potentially, longer NE exposure might have other effects on EGC reactivity, allowing them to contribute to the beneficial impact of the SNS during chronic diseases [36–38]. In addition, in a colitis model that was aggravated by psychological stress, increased NE levels were detected, and abrogation of adrenergic signaling worsened the disease outcome [39], further hinting at a rather beneficial involvement of adrenergic signaling during chronic inflammation. However, prolonged activation of β-ARs resulted in desensitization, phosphorylation, or even internalization of β-ARs [40, 41], which we did not assess in this context. Future work

with glial-specific knockouts in adrenergic pathways needs to determine if and when EGC activation via NE aggravates or resolves intestinal inflammation *in vivo*.

With acute intestinal inflammation forming a dynamic and fast-changing tissue microenvironment in the gut, we aimed to identify additional mediators contributing to POI progression. IL-1 is a well-known and strong immune modulator in several inflammatory processes. IL-1, alone or together with inflammasomes as its activators, has been widely discussed [42, 43], and increased IL-1 levels were found in IBD patients [44–47]. However, IL-1 can have both inflammatory and pro-resolving effects dependent on the phase and time of the disease [48]. Our group previously showed that a systemic deficiency of IL-1R1 protected mice from POI. Interestingly, IL-1R1 was also co-expressed with glial markers in immunohistochemistry [10]. Moreover, IL-1 expression has directly been correlated with the production of inflammatory cytokines, such as IL-6 and CCL2 [49]. An earlier study by Rühl *et al.* already demonstrated IL-1 as an important trigger of glial activity in EGC cultures [50]. However, the role of IL-1-induced glial reactivity in POI has not yet been fully investigated. Therefore, we expanded this knowledge using glial-specific IL-1R1-deficient mice and glial-specific transcriptomic analysis after intestinal manipulation in early (3h) and peak (24h) disease time points. We identified gliosis gene signatures in both IL-1-treated EGC cultures and glial-specific transcriptomes 3h after intestinal manipulation. At the peak of the disease, the recruitment of intestinal macrophages, previously demonstrated as key regulators of intestinal inflammation [51–53], was significantly reduced in glial-IL-1R1-deficient mice [4]. Comparing the gene expression of glial IL-1R1-deficient versus glial IL-1R1-competent mice, we found significantly reduced expression levels of inflammatory mediators, such as *Csf1*, *Ccl2*, *Il6*, or *Cxcl2* [4]. The direct influence of these mediators on macrophages and their recruitment [54, 55] underlines the importance of IL-1-activated EGCs as immune regulators in intestinal inflammation. Of note, different macrophage subpopulations have been identified in the intestine [52, 56], and glial activation was correlated to specific pro-resolving macrophages in POI [16], underlining the relevance of glial-macrophage interactions.

Interestingly, IL-1-induced gene expression in EGCs shared transcriptomic similarities with activated EGCs after infection [57] and during colitis [58]. Although this hints at an overarching gliosis signature of EGCs during different intestinal inflammatory conditions,

the described analyses used different intestinal regions and transcriptomic methods, underlining the need for a more in-depth analysis in the future to evaluate the transferability between approaches.

## 4.2 Potential interactions of different glial activators in the inflammatory environment

Having identified ECM compounds, adrenergic signaling, and IL-1β as potent regulators of glial biology and reactivity, we were intrigued by the possible interconnections of those pathways. Literature screening for potential interactions of ECM and the SNS revealed that ECM collagens were affected by sympathectomy [59] and that NE led to increased collagen expression via β-ARs [60] in the vascular system, hinting at a requirement of SNS signaling for the production of ECM proteins. Additionally, the ECM compound laminin was postulated to be critical for cell proliferation and differentiation in the SNS [61]. On the other hand, neurons and glia were shown to synthesize proteoglycans [62], which are major components of the ECM, and Schwann cell-derived ECM even serves as a treatment for peripheral axon regeneration [63], suggesting important bidirectional pathways between ECM and the SNS in periphery organs.

Similarly, dual effects were described for the connection of the SNS and IL-1. In several early studies, IL-1β suppressed the release of NE in rodents, being potentially involved in neurogenic dysfunctions [64–66]. Conversely, sympathectomy significantly reduced IL-1β and IL-6 levels in a study of lung inflammation [67], which aligns with our work, showing reduced inflammatory mediators after sympathectomy [3]. This indicates that the SNS greatly affects cytokine release during inflammation and, potentially, vice versa.

Previous studies have also reported bidirectional signaling in the interplay of IL-1 and the ECM. On the one hand, fibroblast-derived cytokines, such as IL-1β and IL-6, decreased the synthesis of the ECM molecules glycosaminoglycans and collagen in the skin [68], and similar IL-1β-mediated ECM impairment was found for articular cartilage cells [69]. This hints at an inflammation-induced ECM dysfunction, as shown for ECM remodeling [70, 71]. IL-1β-treatment also stimulated ECM protein production in fibroblasts [72] related to fibrogenesis [73]. On the other hand, ECM-derived fragments but not intact ECM molecules were reported to trigger monocyte/macrophage secretion of inflammatory cytokines,

including IL-1 [74], indicating the involvement of ECM-mediated inflammation during tissue damage. In a model of acute brain injury, IL-1-triggered endothelial activation was significantly influenced by ECM compounds [75]. Moreover, attachment to ECM substrates *in vitro* was described to significantly impact IL-1-mediated astrocyte activation [76], which strongly resembles the differential outcomes from our IL-1β-treated reactive EGC cultures on different ECM substrates [2].

Taken together, we identified three major components of the intestinal tissue microenvironment and their individual effects on EGC homeostasis and reactivity, as well as their effects on intestinal inflammation. The following literature screening exposed distinct connections between the individual pathways, leading to the hypothesis that EGCs are regulated by a well-orchestrated signaling network, including ECM compounds, adrenergic signaling, IL-1 signaling, and others during intestinal inflammation. However, we did not test the connection of those pathways *in vivo*, leaving their sequential order and potential phase-dependent actions that might change over the disease course undiscovered. Future work is needed to unravel the dynamics of this complex signaling network involved in glial activation.

### 4.3 IL-1-mediated, tumor-promoting signaling cascade between EGCs and macrophages in colorectal cancer

So far, EGCs have been discussed as inflammatory mediators in different intestinal diseases, but their potential role in CRC is just emerging. Initial studies showed that EGC depletion reduces tumor burden, identifying them as important regulators of tumor formation [77]. However, the underlying molecular mechanisms remained unknown. Another study then used tumor stem cell cultures treated with an EGC-conditioned medium or vice versa and recognized IL-1 as a promising trigger for the tumor-promoting phenotype of EGCs [78]. Nevertheless, *in vivo* evidence and the molecular mechanisms of tumor promotion by IL-1-triggered EGCs remained elusive.

Using orthotopic CRC models, we confirmed IL-1 as the main activator of EGC reactivity in CRC *in vivo* and identified tumor-infiltrating monocytes and macrophages as its cellular source within the TME. While we here described an IL-1R1-dependent glia-macrophage interaction, IL-1R1-activated EGCs might also exert additional tumor-promoting functions,

as previous *in vitro* work suggested the interaction of EGCs and cancer stem cells via IL-1 [78]. Furthermore, we confirmed the tumor-promoting effect of IL-1-activated EGCs via the secretion of inflammatory cytokines that regulate TAM phenotypes in orthotopic and AOM/DSS-induced murine CRC models. We classified two distinct macrophage subsets coexisting in the CRC TME: C1Q$^+$ TAMs associated with phagocytosis and antigen presentation and SPP1$^+$ TAMs related to angiogenesis and the ECM. Similar TAM subsets have recently been described by transcriptomic analysis in human CRC [79]. While C1Q$^+$ TAMs were found in the colonic mucosa of healthy and ulcerative colitis patients, SPP1$^+$ TAMs were almost exclusively present in cancerous tissues, suggesting their key role in the CRC TME [79]. SPP1$^+$ TAMs have recently been described as a tumor-promoting macrophage subset in the CRC TME [80] and have also been shown to interact with other stromal cells in the TME [81]. Importantly, SPP1$^+$ TAMs are currently understood as the most tumor-promoting TAM subset across multiple cancers [82].

The present study pinpointed IL-6 as the main trigger of SPP1$^+$ macrophage differentiation among EGC-secreted cytokines after glial IL-1 stimulation. The importance of IL-6 in CRC has been shown previously, as IL-6 expression in tissue samples correlated with poor survival, metastasis formation, and advanced disease stages in CRC [83]. Since then, several studies focused on cell-specific roles of IL-6 in the CRC TME, identifying IL-6-mediated inhibition of dendritic cell maturation, blockade of CD8$^+$ T cell effector functions, obstruction of anti-PD-L1 treatment in mice, and TAM-induced cancer cell chemoresistance [84, 85]. Herein, we expanded this knowledge and described a bidirectional interaction of EGCs and TAMs in the CRC TME, with tumor-infiltrating monocytes secreting IL-1, which triggers EGC reactivity and cytokine secretion. Then, among those EGC-secreted cytokines, IL-6 promotes monocyte differentiation towards tumor-promoting SPP1$^+$ TAMs.

EGC-secreted cytokines might also be involved in monocyte recruitment to the CRC TME. Among the EGC-secreted factors, we found increased expression of *Ccl2*, known as a potent chemoattractant for monocytes [86] in CRC, suggesting that EGCs not only drive the differentiation of tumor-infiltrating monocytes towards TAMs but also contribute to their recruitment.

The herein-identified neuro-immune interaction might also be relevant for other cancer types, as strongly innervated organs, such as the pancreas, are the current focus of cancer research. Various cancers exhibit neuronal infiltration, often correlated with worse disease outcomes [87–90]. Another peripheral glial cell type, namely Schwann cells, was described as an important contributor to cancer progression in pancreatic ductal adenocarcinoma, melanoma, breast cancer, or lung cancer [91–94]. Schwann cells were also shown to promote a malignant type of cancer-associated fibroblasts in the pancreatic TME [95]. Interestingly, some studies highlighted glial-induced factors as responsible for the polarization of macrophages towards a pro-tumorigenic phenotype across several types of cancer [91, 93, 96], which is consistent with the EGC actions in our study. Of note, a recent study using a breast cancer mouse model correlated glial-induced macrophage modulation with cancer pain, further highlighting the potential of glial-immune interactions in cancer pathophysiology [94].

Overall, our study revealed a tumor-promoting IL-1-induced glia-macrophage interaction in CRC. Thereby, we unraveled important molecular mechanisms of CRC pathogenesis, presenting potential therapeutic targets for disease treatment.

### 4.4 Clinical translation and potential therapeutic targets

Although animal models are relevant tools for gaining mechanistic insights *in vivo*, the translation to other species, let alone humans, remains challenging [97, 98]. Latest technologies, such as single cell [99] or single nuclei sequencing [100], might help to identify the role of the hard-to-isolate EGC population [101]. However, isolating the fragile glial cell networks will remain challenging considering the complex tissue microenvironment, in which epithelial cells and fibroblasts are the most numerous cell types. Therefore, it is crucial to substantiate the murine findings and the identified molecular mechanisms with human data via human specimens or human datasets. Our group's previous work introduced the term "enteric gliosis" to describe the reactive glial phenotype observed during acute intestinal inflammation [6]. Transferring this phenotype to human specimens, we verified comparable enteric gliosis signatures in humans [6]. Similarly, in the herein-presented work, the IL-1-activation of EGCs and corresponding cytokine release could be confirmed in human primary EGCs [4], and EGC-macrophage co-localization was verified

in human intestinal specimens. This proximity was also confirmed in patient samples of CRC [5]. Additionally, high expression of the EGC gene signature correlated with worse patient survival, and tumor EGCs were enriched in GO terms related to IL-1 signaling, gliosis, and macrophage activation. This high expression of EGC gene signatures also correlated with the high expression of $SPP1^+$ TAM genetic signatures in 75 % of CRC patients. We further analyzed the correlation of EGC signatures and consensus molecular subtypes (CMS), a gene expression-based classification of CRC patients. Interestingly, patients with high EGC signatures were classified as CMS4, which is described to correlate with the worst overall survival and shows strong stromal infiltration [102]. Given the stromal nature of EGCs, this underlines the involvement of EGCs in human CRC development as well. These data hint at a conserved glia-immune mechanism in CRC and, potentially, also in other intestinal diseases.

Consistent with the bidirectional communication found in murine CRC models, the enrichment of IL-1 signaling in human CRC EGCs, together with increased IL-6 levels detected in serum and tissue samples of CRC patients [103, 104], hint at a conserved role of IL-1/IL-6 signaling in CRC pathogenesis. Glial IL-1 signaling or IL-6 release might serve as potential therapeutic targets in immunotherapy, a currently studied treatment option for intestinal inflammatory diseases targeting specific immune pathways. The IL-1 antagonist anakinra has already been studied in the context of POI [4, 10] and was applied in clinical trials [105]. A case report recently described the successful application of anakinra in ulcerative colitis treatment [106]. Moreover, its use has been reported in treating several types of cancer [107], including breast cancer [108–110], pancreatic ductal adenocarcinoma [111, 112], and CRC [113]. Interestingly, anakinra treatment was correlated with reduced IL-6 levels in myeloma patients [114], hinting at the potential of the IL-1/IL-6 axis in human carcinogenesis. However, most signaling pathways, including IL-1 signaling, are not solely detrimental but fulfill additional functions, potentially resulting in adverse immunotherapy- induced side effects [115]. Furthermore, the relevance of glial-restricted IL-1 signaling and IL-6 release might only be part of a complex puzzle. Therefore, it is crucial to gain detailed molecular insights into immune-related signaling pathways, such as their cellular specificities and clinical relevance, to develop more restricted treatment options, potentially targeting individual cell populations or specific cell-cell interactions.

Another avenue for potential clinical interventions in intestinal diseases is the herein-identified adrenergic signaling via β1/2 receptors on EGCs. With only a limited number of studies exploring the use of β-blockers, the results are rather controversial between acute and chronic inflammation: while β1-blockade reduced acute inflammation after abdominal surgery in rodents [116], it is also correlated with higher relapse risk in IBD patients [117]. For CRC, on the other hand, the effects of β-blocker usage seem to depend on the disease state: while the risk of developing CRC could not be reduced by β-blockers [118], they improved the prognosis of CRC patients, especially in patients with advanced cancer stages [119]. Similar to IL-1 or IL-6 signaling, future work using cell-specific and time-restricted β-blocker treatments must provide further insights into their potential in clinical interventions.

### 4.5 Overall impact

This work refined the knowledge about EGC reactivity in intestinal diseases, specifically characterizing new interaction partners and corresponding signaling molecules in intestinal immunity. Before, EGCs were described as contributors to gut inflammation, shaping the tissue microenvironment. Herein, we identified specific players of the intestinal tissue microenvironment, such as ECM proteins, the SNS, and intestinal macrophages, as important interaction partners for EGCs. We improved primary EGC culture conditions by comparing different ECM substrates and their impact on EGC reactivity, allowing us to recommend Matrigel and laminin as preferred substrates for EGCs *in vitro* studies. Additionally, we determined NE and IL-1 as triggers of EGC reactivity, providing new molecular mechanisms of this activated glial phenotype in acute intestinal inflammation.

The clinically most interesting novelty of this study is the identification of the pro-tumorigenic role of EGCs in CRC. We identified a bidirectional signaling cascade between EGCs and macrophages, in which EGCs switch into a reactive phenotype triggered by IL-1 signaling and, in turn, secrete IL-6 as an inflammatory cue to promote pro-tumorigenic $SPP1^{+}$ macrophage differentiation. This previously unknown cellular interaction and the corresponding molecular pathways not only promise further research of glial functions in CRC but also indicate that they might be potential novel targets for

clinical intervention or useful diagnostic tools. From the latter perspective, EGC presence in CRC is associated with poorer outcomes, and future studies could focus on whether glial presence or reactivity might be used as a stratification marker for different treatment regimes.

## 4.6 References


1. Santhosh S, Zanoletti L, Stamp LA, Hao MM, Matteoli G. From diversity to disease: unravelling the role of enteric glial cells. *Front Immunol*, 2024; 15:1408744. doi:10.3389/fimmu.2024.1408744
2. Schneider L, Schneider R, Hamza E, Wehner S. Extracellular matrix substrates differentially influence enteric glial cell homeostasis and immune reactivity. *Front. Immunol.*, 2024; 15. doi:10.3389/fimmu.2024.1401751
3. Leven P, Schneider R, Schneider L, Mallesh S, Vanden Berghe P, Sasse P, et al. β-adrenergic signaling triggers enteric glial reactivity and acute enteric gliosis during surgery. *J Neuroinflammation*, 2023; 20:255. doi:10.1186/s12974-023-02937-0
4. Schneider R, Leven P, Mallesh S, Breßer M, Schneider L, Mazzotta E, et al. IL-1-dependent enteric gliosis guides intestinal inflammation and dysmotility and modulates macrophage function. *Commun Biol*, 2022; 5:811. doi:10.1038/s42003-022-03772-4
5. van Baarle L, Simone V de, Schneider L, Santhosh S, Abdurahiman S, Biscu F, et al. IL-1R signaling drives enteric glia-macrophage interactions in colorectal cancer. *Nat Commun*, 2024; 15:6079. doi:10.1038/s41467-024-50438-2
6. Schneider R, Leven P, Glowka T, Kuzmanov I, Lysson M, Schneiker B, et al. A novel P2X2-dependent purinergic mechanism of enteric gliosis in intestinal inflammation. *EMBO Mol Med*, 2021; 13:e12724. doi:10.15252/emmm.202012724
7. Liñán-Rico A, Turco F, Ochoa-Cortes F, Harzman A, Needleman BJ, Arsenescu R, et al. Molecular Signaling and Dysfunction of the Human Reactive Enteric Glial Cell Phenotype: Implications for GI Infection, IBD, POI, Neurological, Motility, and GI Disorders. *Inflamm Bowel Dis*, 2016; 22:1812–1834. doi:10.1097/MIB.0000000000000854
8. Rosenbaum C, Schick MA, Wollborn J, Heider A, Scholz C-J, Cecil A, et al. Activation of Myenteric Glia during Acute Inflammation In Vitro and In Vivo. *PLoS One*, 2016; 11:e0151335. doi:10.1371/journal.pone.0151335
9. Boyen GB von, Steinkamp M, Reinshagen M, Schäfer K-H, Adler G, Kirsch J. Nerve growth factor secretion in cultured enteric glia cells is modulated by proinflammatory cytokines. *J Neuroendocrinol*, 2006; 18:820–825. doi:10.1111/j.1365-2826.2006.01478.x
10. Stoffels B, Hupa KJ, Snoek SA, van Bree S, Stein K, Schwandt T, et al. Postoperative ileus involves interleukin-1 receptor signaling in enteric glia. *Gastroenterology*, 2014; 146:176-87.e1. doi:10.1053/j.gastro.2013.09.030
11. Li L, Song J, Chuquisana O, Hannocks M-J, Loismann S, Vogl T, et al. Endothelial Basement Membrane Laminins as an Environmental Cue in Monocyte Differentiation to Macrophages. *Front Immunol*, 2020; 11:584229. doi:10.3389/fimmu.2020.584229

12. Nighot M, Ganapathy AS, Saha K, Suchanec E, Castillo EF, Gregory A, et al. Matrix Metalloproteinase MMP-12 Promotes Macrophage Transmigration Across Intestinal Epithelial Tight Junctions and Increases Severity of Experimental Colitis. *J Crohns Colitis*, 2021; 15:1751–1765. doi:10.1093/ecco-jcc/jjab064

13. Au KM, Wilson JE, Ting JP-Y, Wang AZ. An injectable subcutaneous colon-specific immune niche for the treatment of ulcerative colitis. *Nat Biomed Eng*, 2023. doi:10.1038/s41551-023-01136-9

14. Veríssimo CP, Da Carvalho JS, da Silva FJ, Campanati L, Moura-Neto V, Coelho-Aguiar Jd. Laminin and Environmental Cues Act in the Inhibition of the Neuronal Differentiation of Enteric Glia in vitro. *Front Neurosci*, 2019; 13:914. doi:10.3389/fnins.2019.00914

15. Raghavan S, Gilmont RR, Bitar KN. Neuroglial differentiation of adult enteric neuronal progenitor cells as a function of extracellular matrix composition. *Biomaterials*, 2013; 34:6649–6658. doi:10.1016/j.biomaterials.2013.05.023

16. Stakenborg M, Abdurahiman S, Simone V de, Goverse G, Stakenborg N, van Baarle L, et al. Enteric glial cells favor accumulation of anti-inflammatory macrophages during the resolution of muscularis inflammation. *Mucosal Immunol*, 2022; 15:1296–1308. doi:10.1038/s41385-022-00563-2

17. Dora D, Ferenczi S, Stavely R, Toth VE, Varga ZV, Kovacs T, et al. Evidence of a Myenteric Plexus Barrier and Its Macrophage-Dependent Degradation During Murine Colitis: Implications in Enteric Neuroinflammation. *Cell Mol Gastroenterol Hepatol*, 2021; 12:1617–1641. doi:10.1016/j.jcmgh.2021.07.003

18. Pabois J, Durand T, Le Berre C, Filippone RT, Noël T, Durieu E, et al. Role of ICAM-1 in the Adhesion of T cells to Enteric Glia: Perspectives in the Formation of Plexitis in ’”” ’Crohn’s disease. *Cell Mol Gastroenterol Hepatol*, 2024. doi:10.1016/j.jcmgh.2024.02.016

19. Chow AK, Grubišić V, Gulbransen BD. Enteric Glia Regulate Lymphocyte Activation via Autophagy-Mediated MHC-II Expression. *Cell Mol Gastroenterol Hepatol*, 2021; 12:1215–1237. doi:10.1016/j.jcmgh.2021.06.008

20. Ibiza S, García-Cassani B, Ribeiro H, Carvalho T, Almeida L, Marques R, et al. Glial-cell-derived neuroregulators control type 3 innate lymphoid cells and gut defence. *Nature*, 2016; 535:440–443. doi:10.1038/nature18644

21. Smith TH, Ngwainmbi J, Grider JR, Dewey WL, Akbarali HI. An in-vitro preparation of isolated enteric neurons and glia from the myenteric plexus of the adult mouse. *J Vis Exp*, 2013. doi:10.3791/50688

22. Lowette K, Tack J, Vanden Berghe P. Role of corticosterone in the murine enteric nervous system during fasting. *Am J Physiol Gastrointest Liver Physiol*, 2014; 307:G905-13. doi:10.1152/ajpgi.00233.2014

23. Wang Z, Ocadiz-Ruiz R, Sundaresan S, Ding L, Hayes M, Sahoo N, et al. Isolation of Enteric Glial Cells from the Submucosa and Lamina Propria of the Adult Mouse. *J Vis Exp*, 2018. doi:10.3791/57629

24. Zhang Y, Hu W. Mouse enteric neuronal cell culture. *Methods Mol Biol*, 2013; 1078:55–63. doi:10.1007/978-1-62703-640-5_6

25. Mueller JL, Stavely R, Guyer RA, Soos Á, Bhave S, Han C, et al. Agrin Inhibition in Enteric Neural Stem Cells Enhances Their Migration Following Colonic Transplantation. *Stem Cells Transl Med*, 2024. doi:10.1093/stcltm/szae013

26. Kalff JC, Carlos TM, Schraut WH, Billiar TR, Simmons RL, Bauer AJ. Surgically induced leukocytic infiltrates within the rat intestinal muscularis mediate postoperative ileus. *Gastroenterology*, 1999; 117:378–387. doi:10.1053/gast.1999.0029900378

27. Vather R, Trivedi S, Bissett I. Defining Postoperative Ileus: Results of a Systematic Review and Global Survey. *Journal of Gastrointestinal Surgery*, 2013; 17:962–972. doi:10.1007/s11605-013-2148-y

28. Nasser Y, Ho W, Sharkey KA. Distribution of adrenergic receptors in the enteric nervous system of the guinea pig, mouse, and rat. *J Comp Neurol*, 2006; 495:529–553. doi:10.1002/cne.20898

29. Gulbransen BD, Bains JS, Sharkey KA. Enteric glia are targets of the sympathetic innervation of the myenteric plexus in the guinea pig distal colon. *J Neurosci*, 2010; 30:6801–6809. doi:10.1523/JNEUROSCI.0603-10.2010

30. Mallesh S, Schneider R, Schneiker B, Lysson M, Efferz P, Lin E, et al. Sympathetic Denervation Alters the Inflammatory Response of Resident Muscularis Macrophages upon Surgical Trauma and Ameliorates Postoperative Ileus in Mice. *Int J Mol Sci*, 2021; 22. doi:10.3390/ijms22136872

31. Leven P, Schneider R, Siemens KD, Jackson WS, Wehner S. Application of a RiboTag-based approach to generate and analyze mRNA from enteric neural cells. *Neurogastroenterol Motil*, 2022; 34:e14309. doi:10.1111/nmo.14309

32. Lomax AE, Sharkey KA, Furness JB. The participation of the sympathetic innervation of the gastrointestinal tract in disease states. *Neurogastroenterology Motil*, 2010; 22:7–18. doi:10.1111/j.1365-2982.2009.01381.x

33. Sharma D, Farrar JD. Adrenergic regulation of immune cell function and inflammation. *Semin Immunopathol*, 2020; 42:709–717. doi:10.1007/s00281-020-00829-6

34. Nance DM, Sanders VM. Autonomic innervation and regulation of the immune system (1987-2007). *Brain Behav Immun*, 2007; 21:736–745. doi:10.1016/j.bbi.2007.03.008

35. Ağaç D, Estrada LD, Maples R, Hooper LV, Farrar JD. The β2-adrenergic receptor controls inflammation by driving rapid IL-10 secretion. *Brain Behav Immun*, 2018; 74:176–185. doi:10.1016/j.bbi.2018.09.004

36. Willemze RA, Welting O, van Hamersveld P, Verseijden C, Nijhuis LE, Hilbers FW, et al. Loss of intestinal sympathetic innervation elicits an innate immune driven colitis. *Mol Med*, 2019; 25:1. doi:10.1186/s10020-018-0068-8

37. Willemze RA, Welting O, van Hamersveld HP, Meijer SL, Folgering JH, Darwinkel H, et al. Neuronal control of experimental colitis occurs via sympathetic intestinal innervation. *Neurogastroenterology Motil*, 2018; 30. doi:10.1111/nmo.13163

38. Deng L, Guo H, Wang S, Liu X, Lin Y, Zhang R, et al. The Attenuation of Chronic Ulcerative Colitis by (R)-salbutamol in Repeated DSS-Induced Mice. *Oxid Med Cell Longev*, 2022; 2022:9318721. doi:10.1155/2022/9318721

39. Schneider KM, Blank N, Alvarez Y, Thum K, Lundgren P, Litichevskiy L, et al. The enteric nervous system relays psychological stress to intestinal inflammation. *Cell*, 2023; 186:2823-2838.e20. doi:10.1016/j.cell.2023.05.001

40. Hausdorff WP, Caron MG, Lefkowitz RJ. Turning off the signal: desensitization of β-adrenergic receptor function. *FASEB j.*, 1990; 4:2881–2889. doi:10.1096/fasebj.4.11.2165947

41. January B, Seibold A, Whaley B, Hipkin RW, Lin D, Schonbrunn A, et al. beta2-adrenergic receptor desensitization, internalization, and phosphorylation in response to full and partial agonists. *J Biol Chem*, 1997; 272:23871–23879. doi:10.1074/jbc.272.38.23871

42. McEntee CP, Finlay CM, Lavelle EC. Divergent Roles for the IL-1 Family in Gastrointestinal Homeostasis and Inflammation. *Front Immunol*, 2019; 10:1266. doi:10.3389/fimmu.2019.01266

43. Chan AH, Schroder K. Inflammasome signaling and regulation of interleukin-1 family cytokines. *J Exp Med*, 2020; 217. doi:10.1084/jem.20190314

44. Reinecker HC, Steffen M, Witthoeft T, Pflueger I, Schreiber S, MacDermott RP, et al. Enhanced secretion of tumour necrosis factor-alpha, IL-6, and IL-1 beta by isolated lamina propria mononuclear cells from patients with ulcerative colitis and ’”” ’Crohn’s disease. *Clin Exp Immunol*, 1993; 94:174–181. doi:10.1111/j.1365-2249.1993.tb05997.x

45. Mahida YR, Wu K, Jewell DP. Enhanced production of interleukin 1-beta by mononuclear cells isolated from mucosa with active ulcerative colitis of ’”” ’Crohn’s disease. *Gut*, 1989; 30:835–838. doi:10.1136/gut.30.6.835

46. McAlindon ME, Hawkey CJ, Mahida YR. Expression of interleukin 1 beta and interleukin 1 beta converting enzyme by intestinal macrophages in health and inflammatory bowel disease. *Gut*, 1998; 42:214–219. doi:10.1136/gut.42.2.214

47. Reimund JM, Wittersheim C, Dumont S, Muller CD, Baumann R, Poindron P, et al. Mucosal inflammatory cytokine production by intestinal biopsies in patients with ulcerative colitis and ’”” ’Crohn’s disease. *J Clin Immunol*, 1996; 16:144–150. doi:10.1007/BF01540912

48. Kaneko N, Kurata M, Yamamoto T, Morikawa S, Masumoto J. The role of interleukin-1 in general pathology. *Inflamm Regen*, 2019; 39:12. doi:10.1186/s41232-019-0101-5

49. Hupa KJ, Stein K, Schneider R, Lysson M, Schneiker B, Hornung V, et al. AIM2 inflammasome-derived IL-1β induces postoperative ileus in mice. *Sci Rep*, 2019; 9:10602. doi:10.1038/s41598-019-46968-1

50. Rühl A, Franzke S, Collins SM, Stremmel W. Interleukin-6 expression and regulation in rat enteric glial cells. *Am J Physiol Gastrointest Liver Physiol*, 2001; 280:G1163-71. doi:10.1152/ajpgi.2001.280.6.G1163

51. Wehner S, Behrendt FF, Lyutenski BN, Lysson M, Bauer AJ, Hirner A, et al. Inhibition of macrophage function prevents intestinal inflammation and postoperative ileus in rodents. *Gut*, 2007; 56:176–185. doi:10.1136/gut.2005.089615

52. Enderes J, Mallesh S, Schneider R, Hupa KJ, Lysson M, Schneiker B, et al. A Population of Radio-Resistant Macrophages in the Deep Myenteric Plexus Contributes to Postoperative Ileus Via Toll-Like Receptor 3 Signaling. *Front Immunol*, 2020; 11:581111. doi:10.3389/fimmu.2020.581111

53. Wehner S, Engel DR. Resident macrophages in the healthy and inflamed intestinal muscularis externa. *Pflugers Arch*, 2017; 469:541–552. doi:10.1007/s00424-017-1948-4

54. Bain CC, Bravo-Blas A, Scott CL, Perdiguero EG, Geissmann F, Henri S, et al. Constant replenishment from circulating monocytes maintains the macrophage pool in the intestine of adult mice. *Nat Immunol*, 2014; 15:929–937. doi:10.1038/ni.2967

55. Takada Y, Hisamatsu T, Kamada N, Kitazume MT, Honda H, Oshima Y, et al. Monocyte chemoattractant protein-1 contributes to gut homeostasis and intestinal inflammation by composition of IL-10-producing regulatory macrophage subset. *J Immunol*, 2010; 184:2671–2676. doi:10.4049/jimmunol.0804012

56. Schepper S de, Verheijden S, Aguilera-Lizarraga J, Viola MF, Boesmans W, Stakenborg N, et al. Self-Maintaining Gut Macrophages Are Essential for Intestinal Homeostasis. *Cell*, 2018; 175:400-415.e13. doi:10.1016/j.cell.2018.07.048

57. Progatzky F, Shapiro M, Chng SH, Garcia-Cassani B, Classon CH, Sevgi S, et al. Regulation of intestinal immunity and tissue repair by enteric glia. *Nature*, 2021; 599:125–130. doi:10.1038/s41586-021-04006-z

58. Delvalle NM, Dharshika C, Morales-Soto W, Fried DE, Gaudette L, Gulbransen BD. Communication Between Enteric Neurons, Glia, and Nociceptors Underlies the Effects of Tachykinins on Neuroinflammation. *Cell Mol Gastroenterol Hepatol*, 2018; 6:321–344. doi:10.1016/j.jcmgh.2018.05.009

59. Dab H, Hachani R, Hodroj W, Sakly M, Bricca G, Kacem K. Differential control of collagen synthesis by the sympathetic and renin-angiotensin systems in the rat left ventricle. *Auton Neurosci*, 2009; 151:106–110. doi:10.1016/j.autneu.2009.07.014

60. Dab H, Kacem K, Hachani R, Dhaouadi N, Hodroj W, Sakly M, et al. Physiological regulation of extracellular matrix collagen and elastin in the arterial wall of rats by noradrenergic tone and angiotensin II. *J Renin Angiotensin Aldosterone Syst*, 2012; 13:19–28. doi:10.1177/1470320311414752

61. Reichardt LF, Tomaselli KJ. Extracellular matrix molecules and their receptors: functions in neural development. *Annu Rev Neurosci*, 1991; 14:531–570. doi:10.1146/annurev.ne.14.030191.002531

62. Melrose J, Hayes AJ, Bix G. The CNS/PNS Extracellular Matrix Provides Instructive Guidance Cues to Neural Cells and Neuroregulatory Proteins in Neural Development and Repair. *Int J Mol Sci*, 2021; 22. doi:10.3390/ijms22115583

63. Jiang M, Chen M, Liu N. Interactions between Schwann cell and extracellular matrix in peripheral nerve regeneration. *Front Neurol*, 2024; 15:1372168. doi:10.3389/fneur.2024.1372168

64. Hurst S, Collins SM. Interleukin-1 beta modulation of norepinephrine release from rat myenteric nerves. *Am J Physiol*, 1993; 264:G30-5. doi:10.1152/ajpgi.1993.264.1.G30

65. Xia Y, Hu HZ, Liu S, Ren J, Zafirov DH, Wood JD. IL-1beta and IL-6 excite neurons and suppress nicotinic and noradrenergic neurotransmission in guinea pig enteric nervous system. *J Clin Invest*, 1999; 103:1309–1316. doi:10.1172/JCI5823

66. Takahashi H, Nishimura M, Sakamoto M, Ikegaki I, Nakanishi T, Yoshimura M. Effects of interleukin-1 beta on blood pressure, sympathetic nerve activity, and pituitary endocrine functions in anesthetized rats. *Am J Hypertens*, 1992; 5:224–229. doi:10.1093/ajh/5.4.224

67. Grebe KM, Takeda K, Hickman HD, Bailey AL, Embry AC, Bennink JR, et al. Cutting edge: Sympathetic nervous system increases proinflammatory cytokines and exacerbates influenza A virus pathogenesis. *J Immunol*, 2010; 184:540–544. doi:10.4049/jimmunol.0903395

68. Bodo M, Becchetti E, Giammarioli M, Baroni T, Bellucci C, Pezzetti F, et al. Interleukin-1 and interleukin-6 differentially regulate the accumulation of newly synthesized extracellular matrix components and the cytokine release by developing chick embryo skin fibroblasts. *Int J Dev Biol*, 1994; 38:535–542.

69. Frischholz S, Berberich O, Böck T, Meffert RH, Blunk T. Resveratrol counteracts IL-1β-mediated impairment of extracellular matrix deposition in 3D articular chondrocyte constructs. *J Tissue Eng Regen Med*, 2020; 14:897–908. doi:10.1002/term.3031

70. Piterina AV, Cloonan AJ, Meaney CL, Davis LM, Callanan A, Walsh MT, et al. ECM-based materials in cardiovascular applications: Inherent healing potential and augmentation of native regenerative processes. *Int J Mol Sci*, 2009; 10:4375–4417. doi:10.3390/ijms10104375

71. Marangio A, Biccari A, D'Angelo E, Sensi F, Spolverato G, Pucciarelli S, et al. The Study of the Extracellular Matrix in Chronic Inflammation: A Way to Prevent Cancer Initiation? *Cancers (Basel)*, 2022; 14. doi:10.3390/cancers14235903

72. Vesey DA, Cheung C, Cuttle L, Endre Z, Gobe G, Johnson DW. Interleukin-1beta stimulates human renal fibroblast proliferation and matrix protein production by means of a transforming growth factor-beta-dependent mechanism. *J Lab Clin Med*, 2002; 140:342–350. doi:10.1067/mlc.2002.128468

73. Gomes I, Mathur SK, Espenshade BM, Mori Y, Varga J, Ackerman SJ. Eosinophil-fibroblast interactions induce fibroblast IL-6 secretion and extracellular matrix gene expression: implications in fibrogenesis. *J Allergy Clin Immunol*, 2005; 116:796–804. doi:10.1016/j.jaci.2005.06.031

74. Adair-Kirk TL, Senior RM. Fragments of extracellular matrix as mediators of inflammation. *Int J Biochem Cell Biol*, 2008; 40:1101–1110. doi:10.1016/j.biocel.2007.12.005

75. Summers L, Kangwantas K, Rodriguez-Grande B, Denes A, Penny J, Kielty C, et al. Activation of brain endothelial cells by interleukin-1 is regulated by the extracellular matrix after acute brain injury. *Mol Cell Neurosci*, 2013; 57:93–103. doi:10.1016/j.mcn.2013.10.007

76. Summers L, Kangwantas K, Nguyen L, Kielty C, Pinteaux E. Adhesion to the extracellular matrix is required for interleukin-1 beta actions leading to reactive phenotype in rat astrocytes. *Mol Cell Neurosci*, 2010; 44:272–281. doi:10.1016/j.mcn.2010.03.013

77. Yuan R, Bhattacharya N, Kenkel JA, Shen J, DiMaio MA, Bagchi S, et al. Enteric Glia Play a Critical Role in Promoting the Development of Colorectal Cancer. *Frontiers in Oncology*, 2020; 10:595892. doi:10.3389/fonc.2020.595892

78. Valès S, Bacola G, Biraud M, Touvron M, Bessard A, Geraldo F, et al. Tumor cells hijack enteric glia to activate colon cancer stem cells and stimulate tumorigenesis. *EBioMedicine*, 2019; 49:172–188. doi:10.1016/j.ebiom.2019.09.045

79. Zhang L, Li Z, Skrzypczynska KM, Fang Q, Zhang W, O'Brien SA, et al. Single-Cell Analyses Inform Mechanisms of Myeloid-Targeted Therapies in Colon Cancer. *Cell*, 2020; 181:442-459.e29. doi:10.1016/j.cell.2020.03.048

80. Matusiak M, Hickey JW, van IJzendoorn DG, Lu G, Kidziński L, Zhu S, et al. Spatially Segregated Macrophage Populations Predict Distinct Outcomes in Colon Cancer. *Cancer Discov*, 2024; 14:1418–1439. doi:10.1158/2159-8290.CD-23-1300

81. Qi J, Sun H, Zhang Y, Wang Z, Xun Z, Li Z, et al. Single-cell and spatial analysis reveal interaction of FAP+ fibroblasts and SPP1+ macrophages in colorectal cancer. *Nat Commun*, 2022; 13:1742. doi:10.1038/s41467-022-29366-6

82. Cheng S, Li Z, Gao R, Xing B, Gao Y, Yang Y, et al. A pan-cancer single-cell transcriptional atlas of tumor infiltrating myeloid cells. *Cell*, 2021; 184:792-809.e23. doi:10.1016/j.cell.2021.01.010

83. Chung Y-C, Chaen Y-L, Hsu C-P. Clinical significance of tissue expression of interleukin-6 in colorectal carcinoma. *Anticancer Res*, 2006; 26:3905–3911.

84. Toyoshima Y, Kitamura H, Xiang H, Ohno Y, Homma S, Kawamura H, et al. IL6 Modulates the Immune Status of the Tumor Microenvironment to Facilitate Metastatic Colonization of Colorectal Cancer Cells. *Cancer Immunol Res*, 2019; 7:1944–1957. doi:10.1158/2326-6066.CIR-18-0766

85. Yin Y, Yao S, Hu Y, Feng Y, Li M, Bian Z, et al. The Immune-microenvironment Confers Chemoresistance of Colorectal Cancer through Macrophage-Derived IL6. *Clin Cancer Res*, 2017; 23:7375–7387. doi:10.1158/1078-0432.CCR-17-1283

86. McClellan JL, Davis JM, Steiner JL, Enos RT, Jung SH, Carson JA, et al. Linking tumor-associated macrophages, inflammation, and intestinal tumorigenesis: role of MCP-1. *Am J Physiol Gastrointest Liver Physiol*, 2012; 303:G1087-95. doi:10.1152/ajpgi.00252.2012

87. Magnon C, Hall SJ, Lin J, Xue X, Gerber L, Freedland SJ, et al. Autonomic nerve development contributes to prostate cancer progression. *Science*, 2013; 341:1236361. doi:10.1126/science.1236361

88. Albergotti WG, Schwarzbach HL, Abberbock S, Ferris RL, Johnson JT, Duvvuri U, et al. Defining the Prevalence and Prognostic Value of Perineural Invasion and Angiolymphatic Invasion in Human Papillomavirus-Positive Oropharyngeal Carcinoma. *JAMA Otolaryngol Head Neck Surg*, 2017; 143:1236–1243. doi:10.1001/jamaoto.2017.2019

89. Hayakawa Y, Sakitani K, Konishi M, Asfaha S, Niikura R, Tomita H, et al. Nerve Growth Factor Promotes Gastric Tumorigenesis through Aberrant Cholinergic Signaling. *Cancer Cell*, 2017; 31:21–34. doi:10.1016/j.ccell.2016.11.005

90. Renz BW, Takahashi R, Tanaka T, Macchini M, Hayakawa Y, Dantes Z, et al. β2 Adrenergic-Neurotrophin Feedforward Loop Promotes Pancreatic Cancer. *Cancer Cell*, 2018; 33:75-90.e7. doi:10.1016/j.ccell.2017.11.007

91. Zhou Y, Li J, Han B, Zhong R, Zhong H. Schwann cells promote lung cancer proliferation by promoting the M2 polarization of macrophages. *Cellular Immunology*, 2020; 357:104211. doi:10.1016/j.cellimm.2020.104211

92. Deborde S, Gusain L, Powers A, Marcadis A, Yu Y, Chen C-H, et al. Reprogrammed Schwann Cells Organize into Dynamic Tracks that Promote Pancreatic Cancer Invasion. *Cancer Discov*, 2022; 12:2454–2473. doi:10.1158/2159-8290.CD-21-1690

93. Shurin GV, Kruglov O, Ding F, Lin Y, Hao X, Keskinov AA, et al. Melanoma-Induced Reprogramming of Schwann Cell Signaling Aids Tumor Growth. *Cancer Res*, 2019; 79:2736–2747. doi:10.1158/0008-5472.CAN-18-3872

94. Zhang Y, Sang R, Bao J, Jiang Z, Qian D, Zhou Y, et al. Schwann cell-derived CXCL2 contributes to cancer pain by modulating macrophage infiltration in a mouse breast cancer model. *Brain Behav Immun*, 2023; 109:308–320. doi:10.1016/j.bbi.2023.02.004

95. Xue M, Zhu Y, Jiang Y, Han L, Shi M, Su R, et al. Schwann cells regulate tumor cells and cancer-associated fibroblasts in the pancreatic ductal adenocarcinoma microenvironment. *Nat Commun*, 2023; 14:4600. doi:10.1038/s41467-023-40314-w

96. Zhang B, Guo X, Huang L, Zhang Y, Li Z, Su D, et al. Tumour-associated macrophages and Schwann cells promote perineural invasion via paracrine loop in pancreatic ductal adenocarcinoma. *Br J Cancer*, 2024; 130:542–554. doi:10.1038/s41416-023-02539-w

97. Agoston DV. How to Translate Time? The Temporal Aspect of Human and Rodent Biology. *Front Neurol*, 2017; 8:92. doi:10.3389/fneur.2017.00092

98. Radermacher P, Haouzi P. A mouse is not a rat is not a man: species-specific metabolic responses to sepsis - a nail in the coffin of murine models for critical care research? *Intensive Care Med Exp*, 2013; 1:26. doi:10.1186/2197-425X-1-7

99. Jovic D, Liang X, Zeng H, Lin L, Xu F, Luo Y. Single-cell RNA sequencing technologies and applications: A brief overview. *Clin Transl Med*, 2022; 12:e694. doi:10.1002/ctm2.694

100. Fischer J, Ayers T. Single nucleus RNA-sequencing: how ”” ‘’it’s done, applications and limitations. *Emerg Top Life Sci*, 2021; 5:687–690. doi:10.1042/ETLS20210074

101. Guyer RA, Stavely R, Robertson K, Bhave S, Mueller JL, Picard NM, et al. Single-cell multiome sequencing clarifies enteric glial diversity and identifies an intraganglionic population poised for neurogenesis. *Cell Reports*, 2023; 42:112194. doi:10.1016/j.celrep.2023.112194

102. Guinney J, Dienstmann R, Wang X, Reyniès A de, Schlicker A, Soneson C, et al. The consensus molecular subtypes of colorectal cancer. *Nat Med*, 2015; 21:1350–1356. doi:10.1038/nm.3967

103. Komoda H, Tanaka Y, Honda M, Matsuo Y, Hazama K, Takao T. Interleukin-6 levels in colorectal cancer tissues. *World J Surg*, 1998; 22:895–898. doi:10.1007/s002689900489

104. Galizia G, Orditura M, Romano C, Lieto E, Castellano P, Pelosio L, et al. Prognostic significance of circulating IL-10 and IL-6 serum levels in colon cancer patients undergoing surgery. *Clin Immunol*, 2002; 102:169–178. doi:10.1006/clim.2001.5163

105. Wardill HR, Mooij CE de, Da Silva Ferreira AR, Havinga H, Harmsen HJ, van der Velden WJ, et al. Supporting the gastrointestinal microenvironment during high-dose chemotherapy and stem cell transplantation by inhibiting IL-1 signaling with anakinra. *Sci Rep*, 2022; 12:6803. doi:10.1038/s41598-022-10700-3

106. Truyens M, Hoste L, Geldof J, Hoorens A, Haerynck F, Huis In 't Veld D, et al. Successful treatment of ulcerative colitis with anakinra: a case report. *Acta Gastroenterol Belg*, 2023; 86:573–576. doi:10.51821/86.4.11246

107. Xie J, Zhang Y, Jiang L. Role of Interleukin-1 in the pathogenesis of colorectal cancer: A brief look at anakinra therapy. *Int Immunopharmacol*, 2022; 105:108577. doi:10.1016/j.intimp.2022.108577

108. Holen I, Lefley DV, Francis SE, Rennicks S, Bradbury S, Coleman RE, et al. IL-1 drives breast cancer growth and bone metastasis in vivo. *Oncotarget*, 2016; 7:75571–75584. doi:10.18632/oncotarget.12289

109. Wu T-C, Xu K, Martinek J, Young RR, Banchereau R, George J, et al. IL1 Receptor Antagonist Controls Transcriptional Signature of Inflammation in Patients with Metastatic Breast Cancer. *Cancer Res*, 2018; 78:5243–5258. doi:10.1158/0008-5472.CAN-18-0413

110. 'O'Shaughnessy J, Young RR, Levin MK, Baisch J, Timis R, Muniz LS, et al. Safety and immunologic activity of anakinra in HER2-negative metastatic breast cancer (MBC). *JCO*, 2016; 34:e14565-e14565. doi:10.1200/JCO.2016.34.15_suppl.e14565

111. Becerra C, Paulson AS, Cavaness KM, Celinski SA. Gemcitabine, nab-paclitaxel, cisplatin, and anakinra (AGAP) treatment in patients with localized pancreatic ductal adenocarcinoma (PDAC). *JCO*, 2018; 36:449. doi:10.1200/JCO.2018.36.4_suppl.449

112. Whiteley A, Becerra C, McCollum D, Paulson AS, Goel A. A pilot, non-randomized evaluation of the safety of anakinra plus FOLFIRINOX in metastatic pancreatic ductal adenocarcinoma patients. *JCO*, 2016; 34:e15750-e15750. doi:10.1200/JCO.2016.34.15_suppl.e15750

113. Isambert N, Hervieu A, Rébé C, Hennequin A, Borg C, Zanetta S, et al. Fluorouracil and bevacizumab plus anakinra for patients with metastatic colorectal cancer refractory to standard therapies (IRAFU): a single-arm phase 2 study. *Oncoimmunology*, 2018; 7:e1474319. doi:10.1080/2162402X.2018.1474319

114. Lust JA, Lacy MQ, Zeldenrust SR, Witzig TE, Moon-Tasson LL, Dinarello CA, et al. Reduction in C-reactive protein indicates successful targeting of the IL-1/IL-6 axis resulting in improved survival in early stage multiple myeloma. *Am J Hematol*, 2016; 91:571–574. doi:10.1002/ajh.24352

115. Kichloo A, Albosta M, Dahiya D, Guidi JC, Aljadah M, Singh J, et al. Systemic adverse effects and toxicities associated with immunotherapy: A review. *World J Clin Oncol*, 2021; 12:150–163. doi:10.5306/wjco.v12.i3.150

116. Tan S, Zhou F, Zhang Z, Wang J, Xu J, Zhuang Q, et al. Beta-1 blocker reduces inflammation and preserves intestinal barrier function after open abdominal surgery. *Surgery*, 2021; 169:885–893. doi:10.1016/j.surg.2020.11.004

117. Willemze RA, Bakker T, Pippias M, Ponsioen CY, Jonge WJ de. β-Blocker use is associated with a higher relapse risk of inflammatory bowel disease: a Dutch retrospective case-control study. *Eur J Gastroenterol Hepatol*, 2018; 30:161–166. doi:10.1097/MEG.0000000000001016

118. Jansen L, Below J, Chang-Claude J, Brenner H, Hoffmeister M. Beta blocker use and colorectal cancer risk: population-based case-control study. *Cancer*, 2012; 118:3911–3919. doi:10.1002/cncr.26727

119. Wang J, Lu S, Meng Y, Fu W, Zhou X. Beta adrenergic blockade and clinical outcomes in patients with colorectal cancer: A systematic review and meta-analysis. *Eur J Pharmacol*, 2022; 929:175135. doi:10.1016/j.ejphar.2022.175135

## 5. Acknowledgements

I would like to express my sincere gratitude to my supervisor, Prof. Sven Wehner, for his invaluable mentorship, feedback, and guidance throughout my studies. I am deeply grateful for the opportunity to grow as a scientist, drive my career, and be part of his unique working group.

Similarly, I am extremely grateful to Dr. Reiner Schneider for his scientific advice and constructive feedback, which promoted me throughout my PhD. With his sense of humor and positive attitude, he combines scientific expertise with unwavering moral support in the best possible way.

I would like to express my gratitude to the members of my dissertation committee, Prof. Nicolas Schlegel, Prof. Dagmar Wachten, and Prof. Jörg C. Kalff, for their valuable insights and thoughtful suggestions for my work. Furthermore, I would like to thank the Cluster of Excellence ImmunoSensation² of the University of Bonn for funding my research. I am also thankful for our collaborators from Prof. Gianluca Matteoli's group in Leuven, Belgium, with whom we achieved a great publication.

Special thanks to the whole team of AG Wehner for creating a kind and supportive working atmosphere. I am grateful to our technicians for their unconditional support, which I could always count on, and to our postdocs for sharing their expertise and providing valuable feedback. I thank my fellow PhD candidates, students, and technicians in training for our lively discussions about science and beyond, which brightened even the longest lab hours. I am happy to have met many nice people over the years and made some really good friends. I am proud to have been part of this amazing team.

Next, I want to thank my former colleagues and supervisors of the Institute of Reconstructive Neurobiology and the Department of Neurology for contributing to the earlier stages of my academic path. I enjoyed diving into the world of science at their side and got the chance to grow rapidly in both scientific and personal ways.

I thank all my friends and family members for their unconditional support. Especially my parents always ensured me in my decisions and helped me stay grounded.

Their belief in me has kept my spirits and motivation high during this journey. Lastly, I want to thank my partner, Florian, for his tremendous understanding and encouragement. He always provided me with spontaneous emotional support food, and he took care of our cat, Lilly, who kept him company during the most demanding phases of my dissertation.

## Publications and conference contributions

### Publications

Bresser, M.*, Siemens, K.*, **Schneider, L.** *et al.* (2025). Macrophage-induced enteric neurodegeneration leads to motility impairment during gut inflammation. *EMBO Mol Med*, 17(2), 301-335.

Schneider, R., **Schneider, L.** *et al.* (2024). The role of reactive enteric glia-macrophage interactions in acute and chronic inflammation. *Neurogastroenterology & Motility.* 00:e14947.

**Schneider, L.** *et al.* (2024). Extracellular matrix substrates differentially influence enteric glial cell homeostasis and immune reactivity. *Frontiers in Immunology*, 15, 1401751.

van Baarle, L.*, De Simone, V.*, **Schneider, L.*** *et al.* (2024). IL-1R signaling drives enteric glia-macrophage interactions in colorectal cancer. *Nature Communications*, 15(1), 1-22.

Leven, P.*, Schneider, R.*, **Schneider, L.** *et al.* (2023). β-adrenergic signaling triggers enteric glial reactivity and acute enteric gliosis during surgery. *J Neuroinflammation*, 20, 255.

Schneider, R., Leven, P., Mallesh, S., Breßer, M., **Schneider, L.** *et al.* (2022). IL-1-dependent enteric gliosis guides intestinal inflammation and dysmotility and modulates macrophage function. *Commun Biol.* 5, 811.

Nitsch, L., Petzinna, S., Zimmermann, J., **Schneider, L.** *et al.* (2021). Astrocyte-specific expression of interleukin 23 leads to an aggravated phenotype and enhanced inflammatory response with B cell accumulation in the EAE model. *J Neuroinflammation* 18, 101.

Nitsch, L., **Schneider, L.** *et al.* (2021). Microglia-Derived Interleukin 23: A Crucial Cytokine in Alzheimer's Disease? *Front Neurol.* 12, 639353.

Sheng, C., Jungverdorben, J., Wiethoff, H., Lin, Q., Flitsch, L. J., Eckert, D., Hebisch, M., Fischer, J., Kesavan, J., Weykopf, B., **Schneider, L.** *et al.* (2018). A stably self-renewing adult blood-derived induced neural stem cell exhibiting patternability and epigenetic rejuvenation. *Nature Communications,* 9, 4047.

### Conference contributions

Annual meeting of the German Society for Neurogastroenterology and Motility (DGNM) 2024, Freising – Conference talk

ImmunoSensation² Cluster Science Days 2023, Bonn – Conference talk

From Paradigms to Paradoxes in Immunity and Immunopathology 2022, Freiburg – Poster presentation

ImmunoSensation² Cluster Science Days 2020-2022, Bonn – Poster presentation and Poster prize 2020